An Algorithm For The Selection Of A Method For The Modelling Of Direct-On-Line Starting Of Cage Induction Motors From Finite Supplies

by

John Michael Arneaud, BSc, MSc

in the Department of Electrical and Electronic Engineering

Submitted in fulfilment of the requirements for the degree of

Doctor of Philosophy

UNIVERSITY OF TASMANIA

HOBART

December, 1995

I declare that this thesis does not contain anything that has been accepted for the award of a degree or diploma in any other university, and also that , to the best of my knowledge and belief, the thesis does not contain a copy or a paraphrase of material written or published by anyone else except where due reference to it is made in the text of the thesis.

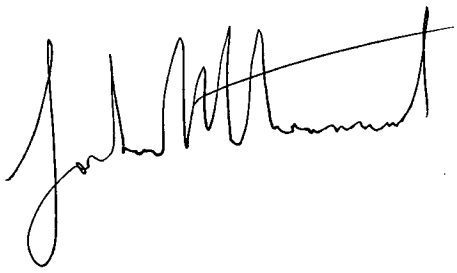

An Algorithm For The Selection Of A Method For The Modelling Of Direct-On-Line Starting Of Cage Induction Motors From Finite Supplies

[Selecting An Induction Motor Model]

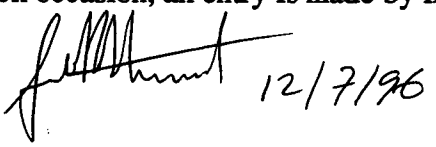

Name of Borrower	Company/Department Affiliation or Contact Address	Date borrowed

CKNOWLEDGEMENTS

I would like to express sincere thanks to the following people for their help :

My supervisors : Dr Richard Langman, (University of Tasmania) for his continual encouragement and Dr Anthony Parker, (University of Adelaide) for his support in the early stages of the work.

Mr Glen Mayhew, Technical Support Manager in the Department of Electrical and Electronic Engineering who designed much of the electronic hardware used for the data acquisition so that it did what I required of it. The workshop staff of the Department of Electrical and Electronic Engineering who put Glen's designs into a useable form.

Mr Russell Twining, Computing Officer, (Network & Hardware) for his assistance with the operation of the PC systems and in particular with the transfer of textual material between different software packages.

The staff of Hobart Technical College who allowed me to have access to their Siemens motor for test purposes.

Mr John Liddell, (Neurosurgeon) and Ms Margaret Stewart, (Physiotherapist) who, each in their own way, tried to help me avoid back surgery during the final phase of the work and to the staff at the Royal Hobart Hospital who did a great job when it became unavoidable. Special thanks to Mr Guy Corkhill, (Neurosurgeon).

Finally to my loving wife, Petula and my sons, Tim, Nick, Christopher and Simon who put up with my strange obsession for so long, with a special thank you to Christopher for the  . (Unfortunately the rest of the thesis cannot live up to medieval standards of illumination).

An Algorithm For The Selection Of A Method For The Modelling Of Direct-On-Line Starting Of Cage Induction Motors From Finite Supplies

Summary

The objective of the study was the derivation of an algorithm for the selection of a numerical simulation method for the direct-on-line starting of induction motors from power supplies whose voltage and frequency may vary during the simulation period.

A major part of the work consisted of an evaluation of methods for treating the variation of motor parameters under different conditions and the relative effect of these variations on predicted output. Two new methods were introduced for predicting the variation of leakage reactance with current and a new method was developed for deriving the rotor parameter variation with slip for bars of arbitrary, but known, cross-section.

An existing method was modified to derive model parameters from manufacturer's quoted performance data. The results are given of an investigation into the effect on the derived parameters and consequently on the predicted performance, of allowing the quoted performance data to vary within the tolerances permitted by Australian Standard 1359.

A set of descriptive measures for simulation output were defined. This enabled the motor's starting performance to be quantified in terms of a small number of variables. The factorial method of experimental design was used to calculate relative coefficients of performance. These related the effect of changes in program input data to the resultant variation in program output and thus allowed numerical measures to be placed on the significance of data uncertainty and model complexity as they affected the simulated performance.

PC-based data acquisition and processing techniques were used to take measurements from two laboratory motors which confirmed the results of numerical simulation work.

The broad general conclusion of the thesis was that in most situations, the total system data needs to be included in the model if the uncertainty is to be improved beyond that obtainable with simple non-recursive calculations. An expert system shell was used to present an algorithm for the selection of a method of modelling appropriate to the quality of the data, the type of system, the purpose of the study and the availability of computational tools.

Contents

INDEX OF VARIABLES

Page numbers refer to first appearance of symbol.

Symbol	Description	pg.
A_c	Area of core through which magnetic flux passes.	9
B	Magnetic flux density	98
B_E	Index used for Lee's method of saturation modelling.	61
B_m	Maximum value of magnetic flux density.	9
B_L	Index used for Logarithmic method of saturation modelling.	60
B'_L	Index used for IEE of Japan's method of saturation modelling.	60
B''_L	Index used for IEE of Japan's method of saturation modelling.	60
{C}	Set of rotor parameters for DCC model of rotor.	85
CP1	pu peak transient line current	45
CP2	pu RMS line current when speed is at 0.5 pu.	140
d	Equivalent depth of rotor bar derived from R_{st}/R_{dc} ratio.	17
d'	Value of d derived from X_{dc}/R_{dc} ratio.	19
del_star	Data in Pereira's method for motor connection type.	
DF	Describing function (for modelling of leakage path saturation)	12
DF_s	Value of DF at rated voltage	13
DF_u	Value of DF at reduced voltage, ie current < Isat	13
E_f	Generator excitation voltage in simple supply model.	39
E_{rms}	RMS value of induced EMF	9
f	Frequency, of supply or rotor currents.	9
H	Inertia constant $H = \frac{1}{2} J\omega^2 / (ratedVA)$	176
$H_{gen.}$	The inertia constant (s) of the total generator capacity + connected motor loads	37
I_1	Current into stator or stator-referred per-phase equivalent circuit	7
I_2	Referred rotor current in per-phase equivalent circuit	7
i_{as}	Current in phase 'a' of stator	34
$I_{b,r,y}$	Currents in blue, red and yellow phases	149
i_{bs}	Current in phase 'b' of stator	34
I_c	Current in core loss branch of per-phase equivalent circuit	7
i_{cs}	Current in phase 'c' of stator	34
i_{dr}	current in direct axis of rotor	30
i_{ds}	current in direct axis of stator	30
i_{qr}	current in quadrature axis of rotor	30
i_{qs}	current in quadrature axis of stator	30
I_m	Current in shunt form of magnetising branch of per-phase equivalent circuit	7
I_{red}	Starting current with reduced stator voltage., V_{red}	13
I_{sat}	Per-unit stator current at which locked rotor saturation curve departs from the linear.	12
I_{st}	Per-unit stator current at starting.	19
IT1	number of positive-going zero crossings on the transient torque/speed curve.	144

Symbol	Description	pg.
J	Current density	15
J	Polar moment of inertia of motor or/and load	22
kt_1 kt_2 kt_3 kt_4	Load torque representation as a polynominal : function of per-unit speed, N with T_{base} defined in terms of rated power and synchnonous speed. $T_{load} = T_{base}\left[kt_1 + kt_2(1-N)^{kt4} + kt_3N^2\right]$	176
Kz	Impedance factor (See also Appendix 1)	39
Kj	Inertia factor	39
Ke	Excitation factor	39
Kt	Prime mover torque factor	39
k_e	Eddy current loss constant of proportionality.	9
k_h	Hysteresis loss constant of proportionality.	9
Ks	Ratio of unsaturable leakage reactance to total leakage reactance, Xt0 / Xtl	237
L_1	Leakage-inductance per phase of the rotor winding	30
L_2	Leakage-inductance per phase of the rotor winding	30
L_{dr}	Self inductance of rotor phase in direct axis.	30
L_{ds}	Self inductance of stator phase in direct axis.	30
L_{qr}	Self inductance of rotor phase in quadrature axis.	30
L_{qs}	Self inductance of stator phase in quadrature axis	30
L_m	Mutual inductance between stator and rotor phases.	30
L_r	Self inductance of rotor phase.	31
L_s	Self inductance of stator phase.	31
		30
$\overline{M}$	Peak fundamental of the mutual inductance between stator and rotor	31
$\overline{M}_1$	Mutual inductance between stator windings	31
$\overline{M}_2$	Mutual inductance between rotor windings	31
m	Double cage rotor design ratio	86
m_1	Value of m derived from ratio of resistance/reactance changes.	91
m_2	Value of m derived from DCC model directly.	91
n	Rotor/stator transformation ratio.	30
N	Number of turns in a coil.	9
p	Differential operator.	30
p_1	Rated power of motor in kW. (See Pout below)	122
P_{core}	Core loss in kW.	9
P_e	Eddy curent loss in kW.	9
pf	Power factor of motor.	122
pf_1	Power factor at rated load, (as nameplate).	122
P_{FWC}	loss in kW	122
P_h	Hysteresis loss in kW.	9
Pout	Rated power output in watts. (See p1 above)	237
pp	Number of pole pairs in stator winding.	34
PHI	Phase angle at which starting occurs.	237

Symbol	Description	pg.
R_1	Stator AC resistance per phase.	7
R_2	Rotor effective AC resistance per phase referred to the stator.	7
R_c	Shunt resistor representing core loss in equivalent circuit.	7
R_a	Resistance of rotor upper cage referred to stator.	16
R_{ac}	Ac resistance of rotor.	105
rat	Per-unit rating for load condition. (Used in Pereira's method).	122
R_b	Resistance of lower rotor cage referred to stator.	16
R_c	Shunt resistor (referred to stator) representing total core loss per phase.	7
r_c	Series form of R_c.	152
R_{cold}	Cold value of resistance.	21
R_{dc}	Referred resistance of rotor at low slip; eg near rated speed.	15
R_e	Effective rotor circuit resistance per phase referred to stator	16
R_{e0}	Value of R_e at low slip.	138
R_{e1}	Value of R_e at starting.	138
R_e'	Value of R_e derived from depth d.	90
R_e''	Value of R_e derived from depth d'..	90
R_f	Value of R_e at any frequency, f derived using UDB model.	16
R_{hot}	Hot value of resistance.	21
R_{s0}	Resistive part of input impedance at terminals at low slip	153
R_{s1}	Resistive part of input impedance at terminals at high slip	153
R_{st}	Referred rotor resistance at starting, slip = 1 pu	12
R_{th}	Resistive part of Thevenin equivalent impedance.	22
{S}	Set of rotor parameters for UDB model.	85
s	Induction motor per-unit slip.	7
s_1	Per unit slip at rated condition; ie as nameplate.	22
s_m	Value of slip at which maximum torque, T_m occurs.	22
Sm	pu maximum speed	140
SP3	pu speed at which TPS occurred	140
t	Time as independent variable.	23
t1	time for TPM	45
t2	time for TP1	45
t3	time for TPS	45
t4	time for CP1	45
t5	time for the pu speed to settle between 0.95 and 1.05 pu	45
t6	time for current to fall below 1 pu	140
t7	time at which the last torque zero-crossing occurred	140
t8	time at which Sm occurred	140
t9	time for speed to rise to 0.5 pu.	140
T_a	Torque available to accelerate motor.	34
T_{cold}	Temperature of cold winding (See R_{cold}).	21
T_e	Gross electromagnetic torque produced by motor.	22
T_{hot}	Temperature of hot winding (See R_{hot}).	21
T_{load}	Load torque.	23
TP1	First peak transient torque.	45

Symbol	Description	pg.
TPM	Per unit peak positive transient torque, (See also pg 23)	45
TPN	Per unit peak negative transient torque.	144
TPS	Per unit peak torque after decay of electrical transients (pull-out torque) as determined from model including transients.	45
T_m	Per unit peak torque (pull-out torque) as determined from steady-state equivalent circuit model.	22
T_{st}	Per unit starting torque as nameplate or steady-state equivalent circuit model.	18
TST	Per unit starting torque as mean of TPM and TPN.	140
V_1	Voltage per phase at terminals of motor or equivalent circuit	7
$V_{b,r,y}$	Voltage applied to blue, red and yellow phases	149
V_{bus}	Voltage at finite bus from which motor is started.	36
Vll	Rated line voltage of motor.	122
V_{red}	Reduced voltage for locked rotor test for determining the unsaturated leakage reactances.	13
V_{th}	Thevenin equivalent voltage source behind stator impedance and magnetising branch of equivalent circuit, Figure 2.3.1.	
v_{dr}	Voltage applied to direct axis winding of rotor	30
v_{ds}	Voltage applied to direct axis winding of stator	30
v_{qr}	Voltage applied to quadrature axis winding of rotor	30
v_{qs}	Voltage applied to quadrature axis winding of stator	30
w	circumferential width of rotor slot.	99
w_1	Width at the top (airgap) of trapezoidal rotor slot.	100
w_2	Width at the bottom (towards shaft) of rotor slot.	100
W_{fw}	Power losses due to friction and windage.	119
x	Position radially from bottom of rotor slot towards airgap	98
X_1	Per phase leakage reactance of stator at specified or implied freqency and current.	7
X_2	Per phase leakage reactance of rotor referred to stator under stated or implied conditions of supply voltage, frequency, slip and current.	7
X_a	Leakage reactance of rotor upper rotor cage referred to stator.	16
X_{ab}	Mutual reactance between upper and lower cages.	16
X_b	Leakage reactance of lower rotor cage referred to stator.	16
X_{dc}	Referred reactance of rotor at low slip.	15
X_e	Effective referred rotor circuit reactance.	16
X_{e0}	Value of X_e at low slip.	138
X_{e1}	Value of X_e at starting.	138
X_e'	Value of X_e derived from d	90
X_e''	Value of X_e derived from d'	90
X_f	Value of X_e derived from UDB model.	16
X_m	Magnetising reactance referred to the stator per phase equivalent circuit.	7
$\overline{\cdot\cdot}$	Mutual reactance between phases stator/rotor referred to stator.	7
x_m	Series form of magnetising reactance.	152

Symbol	Description	pg.
X_r	Self reactance of rotor per phase referred to stator.	7
X_{r0}	Unsaturable part of rotor leakage reactance	127
X_{rs}	Saturable part of rotor leakage reactance	127
X_s	Self reactance of stator per phase at specified frequency.	7
X_{s0}	Reactive part of input impedance at terminals at low slip	153
X_{s0}	Unsaturable part of stator leakage reactance (See also above)	127
X_{s1}	Reactive part of input impedance at terminals at high slip	153
X_{ss}	Saturable part of stator leakage reactance	127
X_{st}	Referred reactance of rotor at starting; slip = 1.	15
X_{t0}	Component of total leakage reactance which is regarded as unsaturable, ie invariant with current.	13
X_{tl}	Total leakage reactance	13
X_{tls}	Value of X_{tl} derived at test voltage equal to rated voltage.	13
X_{tlu}	Value of X_{tl} derived at reduced test voltage V_{red}.	13
X_{ts}	Maximum value of the component of total leakage reactance which is regarded as saturable, ie variable with current.	13
X_{th}	Reactive part of Thevenin equivalent impedance.	22
X_{tu}	Unsaturated value of total leakage reactance.	13
y	Distance radially from bottom of rotor slot towards airgap.	98
Ze	Complex impedance of rotor at any slip, (See Xe and Re)	16
Z_{line}	Impedance in line between motor and bus, (IEEE Brown Book)	36
Z_{motor}	Impedance of motor, (IEEE Brown Book method)	36
α	Reciprocal of skin depth	17
α_c	Value of α when cold, (See text for actual temperature)	115
α_h	Value of α when hot	115
γ	Arbitrary constant which determines split of total leakage reactance between stator and rotor.	7
ΔP	The power taken from the power system by the motor during starting (pu on generator base).	37
ε	Error term in calculation of starting current.	65
η	Per unit efficiency of motor	124
η'	Modified efficeiency, Rogers and Shirmohammadi's method.	124
ϕ_1	Angle between stator current and voltage phasors.	125
Φ	Magnetic flux	98
φ_{dr}	Flux linkages in rotor direct axis.	33
φ_{ds}	Flux linkages in stator direct axis.	33
φ_{qr}	Flux linkages in rotor quadrature axis.	33
φ_{qs}	Flux linkages in stator quadrature axis.	33
ρ	Resistivity of material used in rotor conductor or laminations.	9
ω	Angular frequency of supply	31
ω_e	Angular velocity of freely rotating reference frame.	30
ω_r	Angular velocity of rotor in electrical radian per second.	30
ω_r'	Actual angular velocity of motor shaft (mechanical radian per second).	32

1. INTRODUCTION AND OVERVIEW

1.1. Development Of The Initial Perspective On The Problem

The work which is the subject of this thesis took place between 1987 and 1995 but the motivation for selecting the topic arose from much earlier experiences whilst I was a design engineer at GEC Large Machines at Rugby in England. At that time I was faced with the problem of determining the voltage dip experienced in offshore power systems due to the starting of large pump motors. I was aware of the difficulty of predicting accurately the sub transient and transient reactances of the solid-pole synchronous machines. The computational models available at that time did not always give results which compared well with those obtained from sudden short circuit tests. I began to wonder if the induction motor loads were subject to the same inaccuracies and inconsistencies and if the advantages gained by using a sophisticated simulation method were outweighed by the additional data that such methods seemed to require.

Whilst at the Whyalla campus of the (then) South Australian Institute of Technology, I began to look seriously at the use of numerical simulation of induction motor performance. At that stage I developed a model for the induction motor based on differential equations in fixed axes. This was an early version of the program IM_SIM.PAS, the current version of which is documented in Chapter 3. The manufacturer's quoted motor equivalent circuit parameters were used as a starting point with the simulation yielding graphs of current and torque. The values of the equivalent circuit parameters were held constant during the simulation. I became concerned with the extent to which predicted performance was dependent on small changes in the input data. For example, variation in the actual supply voltage or frequency from the nominal value would contribute to a difference between the simulated performance and that of the actual motor. This may seem obvious but most published simulation work seemed to proceed on the basis that all the required input data was available with zero uncertainty. This will be discussed further in Chapters 6 and 8.

The factorial method of experimental design was used to establish relative coefficients of performance which related the effect of changes in program input data to the resultant variation in simulated motor performance (program output). This allowed a numerical measure to be placed on the significance of the uncertainty in each program input data item as it affected the predicted output; eg the effect of leakage reactance on peak transient torque. This work is reported on in Chapter 4. As a result of this study it was concluded that for constant parameter models, the most significant data items were supply system voltage and frequency. This means that an assessment of the proposed model prior to simulation should include an estimate of the degree of finiteness of the supply bus. It also became clear that where the equivalent circuit parameters do vary during the simulation, this variation needs to be modelled fairly accurately. This point was reinforced by some useful discussions with Dr Colin Grantham (of the University of New South Wales) on the subject of motor modelling and parameters.

Consideration of a variable parameter model led to doubts about using the circuit parameters quoted by manufacturers as a starting point for simulation work. It was

found that manufacturer's quoted motor parameters are sometimes based on rated load conditions and consequently may not give realistic results when used in models designed to calculate starting or pull-out conditions. This led to a re-appraisal of the project's objectives.

1.2. Redefinition Of The Problem Of Formulating An Algorithm

The problem was redefined in terms of using the performance parameters as a starting point and adopting inverse modelling techniques to derive a set of parameters for a specified equivalent circuit, such that the error over the known performance range was minimised. The simulation exercise was then seen as an extrapolation in the performance space defined by the set of terminal vector quantities {voltage, current, speed and torque}. The problem was examined from the point of view of a project consulting engineer rather than that of a motor designer. Consequently, it was assumed that the motor itself was not available to the algorithm user. Data for the numerical model could only be obtained from either type tests or from manufacturer's quoted performance data, ie access to design data was precluded.

The determination of a pathway from the performance data to the induction motor circuit model had largely been performed by Rogers and Shirmohammadi, [1987]. The method was available as a commercial computer program, [Rogers, 1993] but this often gave a close fit only to the starting and pull-out conditions and was prone to fail completely with small motors. Substantial email/fax discussions ensued between the author and Mr. Rogers which led to a revised version of the software being produced in mid-1995. In the interim, the program PARAM.PAS was developed by the author and this is discussed in Chapter 6.

The relative performance of different models was of primary concern in the formulation of the algorithm. It was recognised that a review of available models would have to be conducted. It was noted at an early stage that many sophisticated computer models existed, that all of these were claimed to work, that in general, there was little cross-referencing between published work and almost no comparison of different models using the same data. The issue of data uncertainty due to the reluctance of manufacturers to reveal design information or to include wide tolerances in performance data (as permitted by AS1359) was recognised. The objective of the study was then formulated.

1.3. Goals Of The Thesis

The goal of the project was stated to be the development of an algorithm for the selection of a suitable method for the simulation of the dynamic performance of the induction motor under direct-on-line starting conditions taking into account the uncertainty created in simulation output by data un-availability or uncertainty. This required :

- The development of a thorough understanding of the detailed models for modelling motor parameter variation; described in Chapter 5.
- An appreciation of the relative significance of the effect of finite power systems on supply voltage and frequency; demonstrated in the simulation work of Chapters 4 and 8.
- An assessment of the usefulness of the parameter determination method (as modified) in the light of permitted tolerances in data; Chapters 6 and 7.

- An assessment of the relative importance of all the various simulation program input data items; developed as a result of the simulation work of Chapter 8.
- An appreciation of the effect of being forced to use a simpler model due to lack of motor or system data; Chapter 8.

1.4. Exclusions From The Scope Of The Algorithm

The parameters derived were to be used in models of the induction motor operating from sinusoidal, balanced 3-phase mains operating close to rated frequency. The motor parameters were required to be valid over the slip range from starting to rated slip and over the operating current range from the rated-voltage starting current down to below rated current. The modelling of the performance of power electronic variable speed drives (VSDs) is excluded from the study. However, if the harmonic content of the drive may be ignored, then little error may result from the use of parameters derived using the algorithm described, provided that the action of drive feedback-control modules is incorporated into the simulation model.

The simulation of bus transfer, cyclic load shedding or the effect of transient disturbances to the supply, other than those caused by the motor itself, were not the prime focus of the study. The algorithm was initially designed to give guidance to the selection of a model for direct-on-line starting only. In the course of the literature survey additional knowledge was accumulated pertaining to problems other than simple starting. This arose naturally from the consideration of the effect on motors already running, of starting the motor which is the prime subject of the simulation. For these other motors, the starting of the new motor appears as a transient supply disturbance. The bus transfer problem may be regarded as an extreme form of the supply disturbance situation. Many of the guiding principles were found to be common to all types of numerical simulation work with induction motors. The algorithm was formulated in terms of an Expert System which was extended to include some advice regarding the simulation of problems other than starting. Formal validation of the Expert System was restricted to the case of direct-on-line starting only.

1.5. Development And Use Of The Complete Simulation Model

Although the presentation given here is sequential, the actual work described in the thesis proceeded in an iterative manner. As various elements were investigated they were incorporated into earlier developments. The path to achieving the objectives of the thesis was somewhat tortuous and the subjects inter-related so that at times it became difficult to see the overall picture because of the detail. As a result it was decided in the writing of the thesis to give the reader an early overview of the work done that is somewhat longer than that allowed in a formal synopsis.

1.5.1. Development Of The Software

Generally, commercial software does not allow modification of the computational algorithms within the simulation process in order to include or exclude certain effects or compare different methods of modelling. Because of this, the program, IM_SIM.PAS referred to earlier was re-written to include parameter variation within the Runge-Kutta solution of the system's differential equations. It was felt that although this would be expensive in terms of time, it would prove to be the best choice in the long run due to its flexibility and ability to control the way in which things were done. For example, there were found to be small, but sometimes

significant, differences between the method suggested by Rogers and Shirmohammadi in the paper referred to earlier and the commercial program.

By writing my own software I was able to incorporate the Turbo-Pascal procedures, which were used within the Runge-Kutta method for parameter variation, into a similar program based on the steady-state equivalent circuit. This guaranteed that any differences were due to the motor equations rather than to different treatments of parametric variation. Chapter 3 discusses the programs in detail and gives instructions for using default versions which produce graphs and text files for the simulated response for six selected motors.

1.5.2. Variation Of Circuit Parameters

A major part of the work consisted of an evaluation of methods for treating the variation of motor parameters under different conditions and the relative effect of these variations on predicted output.

1.5.2.1. Leakage path saturation

The variation of stator and rotor leakage reactances due to leakage path saturation was investigated. Statistical analysis was performed of the errors introduced by using several different methods for predicting the variation of leakage reactance with current. Two new methods were introduced which have the advantage of requiring less data than the established best method whilst retaining reasonable accuracy.

1.5.2.2. Skin effect in the rotor

The uniform-deep-bar (UDB) and double-cage-circuit (DCC) methods used for modelling rotor parameter variation due to skin effect were compared. Both models are based on the values of the referred rotor reactance and resistance at zero and unity slip. It was shown that given the parameters of the UDB model, an exact equivalent DCC model can be derived but not always conversely. For some double cage rotors, the derived UDB model, gave the correct rotor impedance at zero and unity slip but was grossly in error for slip values in-between. The analysis of the uniform bar was extended to develop a new method for deriving the rotor parameter variation with slip for bars of arbitrary, but known, cross-section.

1.5.3. Obtaining Data For The Model

Various methods for obtaining the equivalent circuit parameters were assessed. The method finally adopted is discussed and justified in Chapter 6. It is emphasised that the circuit parameters as quoted by manufacturers are not to be trusted to give a reliable prediction of performance over the complete operating range of the motor.

1.5.4. Use Of The Simulation Model

Simulated performance was compared using models with a range of complexity and the relative effects of model complexity and data uncertainty were assessed. This work is presented in Chapter 8 which includes a systematic study of the effect of varying some of these features.

1.6. Experimental Confirmation Of Results

Two small laboratory machines were used to verify the results of simulation work. One of these motors had a single-cage rotor and the other was of the double-cage rotor type. The test data was recorded by a new test procedure based on fast data acquisition using a PC. This work is discussed in Chapter 7.

Initially, the main reason for performing the tests on these motors was to gain some direct experience in the measurement of motor parameters using PC-based methods.

Later a comparison was made between the set of parameters obtained from tests and those derived from the performance specification. The comparison between the two sets of performance data for each motor; one based on test results and the other derived from quoted performance data is considered to be more significant. These results are given in Chapter 8. It was recognised that tests on a larger range of motors would be desirable so such data was willingly utilised whenever available.

Advantage was taken of the availability of locked-rotor test results performed by the IEE of Japan, [1980] for 52 motors. Some starting information for a 660 kW motor was supplied by Comalco Aluminium (Bell Bay). Comparisons were also made between simulation results using the author's simulation program and simulation/test results published by Rogers and Shirmohammadi for a 8.2 MW motor, [1987].

1.7. The Structuring Of The Knowledge As An "Expert System"

The goal of the work described in this thesis has always been to present the experience gained in the form of an algorithm : a structured set of rules for attaining an objective. The use of an Expert System shell was not considered in the early stages. Since most of the simulation and experimental work involved numerical programming it seemed initially that the algorithm would take the form of a program, probably written in the Turbo Pascal language, which would evaluate the available data in terms of the simulation objectives. This was finally rejected in favour of an Expert System, mainly because this allowed forward and backward chaining through a rule set which could be added to as knowledge increased. The expert system also allowed easy communication to the user; for example, of the implications of lack of requested data.

One of the main advantages of the choice to use an expert system was that it forced the codification of the information which required the development of a deeper understanding of the relationship between the system variables. This process is summarised in Chapter 9.

1.8. The Verification Of The Expert System

The documentation of the verification of the expert system is based on four test cases. This represents a small subset of the many test runs that were performed using the software. The comments and predictions of the algorithm were assessed in the light of the experience reported in the earlier chapters of the thesis. Where errors of "judgement" were made by the algorithm during the verification process, the program was stopped and the reason for the false conclusion identified and rectified. Notes were made regarding helpful comments or references so that these could be added to the algorithm to be brought to the attention of the user.

The end product is an algorithm which detects gross errors in a user specified motor data file, is tolerant of redundant or non-essential data and arrives at an assessment of the available simulation model for the system under consideration. The algorithm concludes by presenting a summary of the available and ideal models for various parts of the system and advises the user on appropriate action.

2. CIRCUIT MODELS AND PARAMETERS

This chapter includes a review of the standard and some less well known circuit models of the induction motor so that material found in disparate undergraduate texts and some quite old publications would be brought together in one place. Whilst I had some reservations about this, I recognised that most of the material would be unfamiliar to many readers since it is not introduced into current undergraduate courses and is unfashionable at postgraduate level. The chapter therefore serves as a critical review of the approximations, assumptions and methods used in induction motor modelling. By including such a review I hoped to assist those beginning work in the area of induction machine modelling.

An appreciation of the relative importance of the various motor parameters under different circumstances and the ways in which they vary during machine operation was developed by the author gradually over the whole period of the study and in some ways this paralleled the historical development of induction motor modelling. For example, the first application (described in Chapter 4) of the Runge-Kutta method to solve the differential equation model, was based on a constant circuit parameter model. This led to the detailed investigation into parameter variation described in Chapter 5 and the use of performance rather than circuit parameters as the starting point for the simulation processes, (Chapter 6). These three chapters form an essential background to the developments introduced in later chapters

In this work, the focus is on models which use a limited amount of design data since, in the experience of the author, complete data is often unwillingly given by manufacturers and when supplied, may include estimates or large unspecified tolerances. This situation precluded the use of hybrid circuits, [Göl, 1986]; finite element models for the determination of reactance, [Belmans et al, 1990], or core loss, [Zhu and Ramsden, 1993] and the use of detailed design information such as the dimensions of radial ventilation slots, [Williamson and Flack, 1994]. This restriction meant that when leakage path saturation was considered in Chapter 5, an empirical method was used because the design approach could not be adopted, [Agarwal and Alger, 1960].

The commonly used equivalent circuit model is expected to represent the machine. To do this, the circuit and machine must have the same appearance to an observer throughout the operating range. This means that the stator voltage and current, shaft torque and speed must be the same, and consequently, so will power factor and total losses. There are three operating conditions which are usually of interest namely; starting, near rated load and run-up from rest to close to the no-load speed. Test data will not normally be available for the whole region of interest. If it were, then there would be little point in doing the simulation. The main purpose of numerical simulation is to enable interpolation or extrapolation from a few known points in the machine's operating space to any other required operating condition. As in all work of this sort, the accuracy of the curve fitting is expected to increase with the number of available data points. Some of the methods, discussed in Chapter 6 which are used to fit a set of parameters to the motor model, require complete data curves of torque, power-factor and current against slip at rated voltage and frequency. It is to be expected that such models will give accurate modelling of steady-state behaviour since the model is fairly well constrained in this mode of operation by the input data to

the modelling process. The challenge is to obtain information about the machine's performance over as wide a range of operating conditions as possible with a small amount of readily available data.

In order to determine the equivalent circuit parameters, measurements are usually taken at slip values of 1 and close to zero giving Locked-Rotor (LR) and No-Load (NL) test results respectively, [IEEE, 1988]. These tests yield two complex impedances. The stator resistance is measured separately. The circuit model which is derived from these tests is not the machine. This statement may sound trite but failure to appreciate it is the source of much error. In particular, it will be shown in Chapters 5 and 8 that it is dangerous to assign reactance values to the machine when these are properties of a particular circuit used as a model. In other words, a value for a circuit parameter cannot be quoted unless the form of the circuit is specified. There are several possible circuits which may adequately model a given machine in the steady state. In the absence of a circuit specification, the only impedance which may be assigned to the machine with complete lack of ambiguity is that derived from the voltage/current relationship at its terminals. All the others are dependent on conceptual models which the observer brings to the test results and assigns parameter values in order to conform with the behaviour measured at the machine's terminals.

2.1. The Classical Equivalent Circuit

The classical equivalent circuit of Figure 2.1.1 has 6 parameters. The standard test data obtained as above yields five real numbers. The circuit therefore contains one degree of freedom so that, in practice, several versions of the steady-state equivalent circuit exist, all of which will match the given test data. In particular, in the absence of design data it is impossible to separate the stator and rotor components of leakage reactance with any degree of accuracy from measurements made at the motor terminals, [Jones, 1967] and [Grantham, 1985].

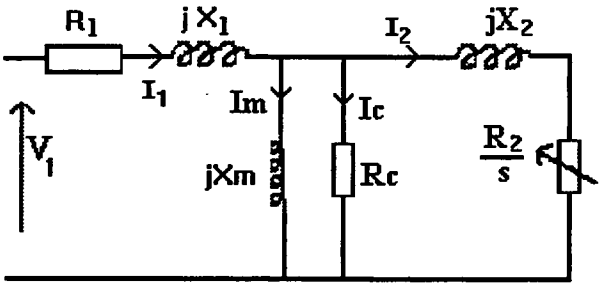

Figure 2.1.1 : Classical "exact " equivalent circuit

With many small machines, where the variation in rotor parameters with slip may be ignored, it is unnecessary to separate the leakage reactances. Jones showed that the equivalent circuit may be represented (in terms of self and mutual reactances, $X_s, X_r, \overline{X}_m$) generally in the form of Figure 2.1.2 in which γ cannot be determined from NL and LR tests. If $\gamma = X_s / \overline{X}_m$ then the circuit becomes that of Figure 2.1.3. All the leakage reactance is then assigned to the rotor. Similar circuits have been used by Gosbell and Dalton, [1991] in the determination of parameters for variable speed drive (VSD) modelling. Although this may seem an extreme approach, it has been supported by a factorial design by Smith and Hamil, [1973] which showed that the predicted performance of the single-cage induction motor was insensitive to the allocation of leakage reactance.

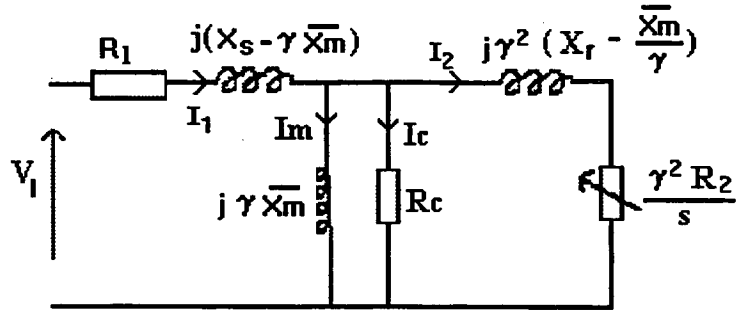

Figure 2.1.2 : General form of the equivalent circuit in terms of self and mutual reactances

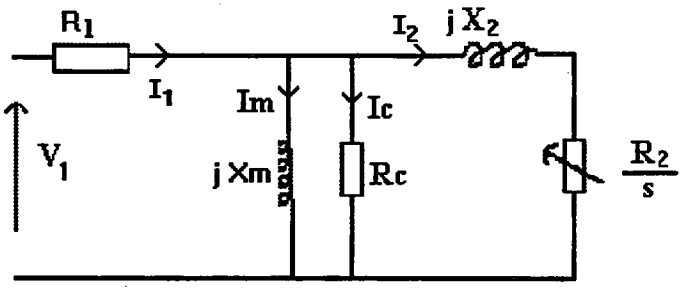

Figure 2.1.3 : Equivalent circuit of Figure 2.1.2 with $\gamma = X_s / \overline{X}_m$

In cases where the rotor reactance is known to vary with the frequency of the currents induced in the rotor, it becomes conceptually difficult to combine the stator and rotor reactances into a total leakage reactance. The question then arises of how to divide the total reactance into its frequency-sensitive and frequency-insensitive parts. Simulated machine performance is then highly dependent on the allocation of total leakage reactance between the rotor (taken as variable with slip) and stator (taken as invariant with slip).

Three of the circuit parameters (R_1 , X_m and R_c) are shown in Chapter 4 to have relatively little influence on the predicted dynamic performance of the motor during direct-on-line starting. This agrees with the work of Smith and Hamil mentioned previously. It is interesting, however, to examine the effect of errors in R_1 on the derived value for Rc. If a slightly smaller value of R_1 were used in the analysis of the locked-rotor test results then the effect would be to produce a slightly larger value for the referred rotor resistance, R_2 and to marginally affect the value deduced for R_c from the no-load test. Given a particular set of test results at low-slip and locked-rotor respectively, the derived equivalent circuit will match the input impedance at these slip extremities. The effect of the error in the measurement of R_1 will be to create discrepancies in total circuit input impedance in the mid-slip region and to allocate losses within the machine in a slightly different way at all slip values. The importance of this will depend on the reasons for performing the numerical simulation study.

2.2. Discussion of Circuit Model Parameters

2.2.1. Stator Resistance, R_1

Strictly, the value used should be the ac resistance which allows for skin effect in the stator conductors. Unlike the rotor, these are usually stranded. This is done partly in order to minimise the deep-bar effect. This effect is usually allowed for by multiplying the measured dc resistance by a factor of approximately 1.1 to derive the ac resistance, [Gosbell and Dalton, 1991]. The dc resistance is commonly measured directly using one of four methods.

1) Direct measurement using a hand-held multimeter
2) The Ware test, [Bourne, 1969]
3) As the slope of a curve of dc supply voltage against current
4) Using a four-terminal bridge circuit.

The last two methods seem preferable but as mentioned, the accuracy is not critical. In any case, it would be pointless to measure the dc resistance accurately and then multiply it by a factor whose value could lie between 1.05 and 1.15.

The effect of errors in the assigned value of R_1 is to change the value of referred rotor resistance, R_2 derived from locked-rotor test results. The most sensitive indicator of the low-slip value of rotor resistance is the slip at which maximum electrical torque occurs (See Section 9.2.3). This is difficult to measure with any accuracy.

2.2.2. Core Loss Resistor, R_c

Hysteresis loss is usually modelled by $P_h = k_h f B_m^x$ (2.2.1)

where B_m is maximum flux density and $0.8 \le x \le 2.3$.
(usually close to 2 for modern core material).

Similarly, the eddy current loss is given by $P_e = \left[k_e t^2 f^2 B_m^2\right] / \rho$ (2.2.2)

The induced EMF, $E_{rms} = \sqrt{2}\pi f N A_c B_m$ (2.2.3)

If the ratio of E_{rms} to frequency, f is kept constant, then the flux density will be constant. This condition will be approximately satisfied if the power system is such that the frequency and voltage do not change much, (ie. an infinite-bus system).
Core loss is then given as $P_{core} = P_h + P_e \approx kV_1^2$ (2.2.4)
Here k represents some constant of proportionality and the applied voltage and induced back EMF are taken as approximately equal. This is reasonable if, as is usual in practical motors and transformers, the voltage drop due to leakage reactance is small. This loss can then be represented by a constant resistance in parallel with the magnetising reactance.

Measurements with an Epstein frame in the rage of 50 to 2000 Hz over a temperature range of 20 to 220 ^{0}C have suggested that the core loss is proportional to the cube of the flux density, [Mouillet et al, 1994] but this has not been supported by measurements on actual motors. If the relationship were a cubic, then this would then require a variable resistor for the representation of core loss. This would not be particularly difficult but has not been pursued in view of the difficulties associated

with accurate measurement of core loss under dynamic conditions and the uncertainty in total losses.

In practice, other (stray) machine losses are also present and the uncertainty due to these is usually combined with the core loss uncertainty to result in an overall uncertainty in energy flow within the motor. The author's experience is that the measured frictional torque may vary between motors of the same nominal design due to manufacturing inconsistencies. These uncertainties add to those which might arise from inadequacies in system modelling, particularly if variable voltage or frequency conditions are encountered. For example, in marine systems, where frequency dips of 5% may be combined with voltage dips of 25% during the starting of large motors. These factors may lead to inaccuracy in the prediction of net shaft torque. This sets limits on the degree of precision that should be sought in modelling the "constant losses".

For a given motor, the friction and windage (F&W) loss is constant at constant operating speed. For induction motors at fixed frequency, the speed is approximately constant over the normal operating range. During starting, the F&W loss is reduced at lower speeds but there are additional core losses in the rotor due to the fact that the rotor flux during starting is at a higher frequency than under rated load operation. In practice the extra rotor core loss compensates for the reduced F&W loss and the assumption of constant core loss remains valid to a reasonable degree of approximation. For VSD modelling this method breaks down as low rotor frequency and reduced rotational friction losses can co-exist. However, the overall loss may well be of a similar order since the harmonic losses will be greater (but not precisely known) due to the non-sinusoidal VSD supply.

Another approach to core loss modelling is to recognise that the loss is associated with the total stator flux linkage (leakage as well as mutual flux) and to place the resistor used to represent core loss as in Figure 2.2.1, [Andria, Dell'Aquila, Salvatore and Savino, 1987]. In theory this seems reasonable but it assumes that accurate allocation of stator leakage can be done. From a circuit point of view it is possible to derive a combination of parameter values for Figure 2.2.1 which has the same input impedance at a given slip as Figure 2.1.1

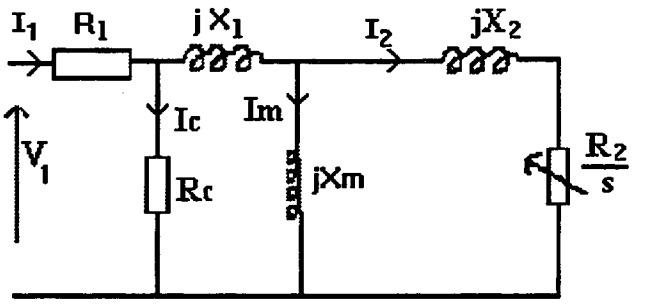

Figure 2.2.1 : Non-conventional core loss representation

Rogers and Shirmohammadi, [1987] ignored core loss altogether and compensated for it by increasing the mechanical losses. This results in adjustments being made to the other circuit parameters in order to match the required power factor.

In the derivation of R_c from NL test results, it is usually assumed that the slip is zero. Actual slip on no-load is non-zero, being just sufficient to generate enough torque to

overcome mechanical no-load losses so that a small amount of power is used in the rotor circuit. The effect of assuming that the input impedance on no-load is given by the circuit of Figure 2.1.1 with slip set equal to zero, is discussed in Chapter 5.

It seems more precise to represent the mechanical losses by a speed dependent loss, to make R_c variable with frequency and flux level and to measure core losses with the machine driven at synchronous speed. In practice, if data which would allow the accurate separation and modelling of friction and windage losses over the region of interest is not available, then it seems inappropriate to be overly concerned about the accurate representation of core loss.

Usual practice is to separate the friction and windage loss from the core loss by performing the NL test over a range of stator voltages [IEEE, 1988, Section 5.6.2]. The input power (less stator copper loss) is plotted against voltage squared as shown in Figure 2.2.2. At low voltages, the slip rises and the results are ignored. A straight line extrapolated back to the power axis has an intercept equal to the friction and windage loss ie. the input power (less stator copper loss) with core loss reduced to zero.

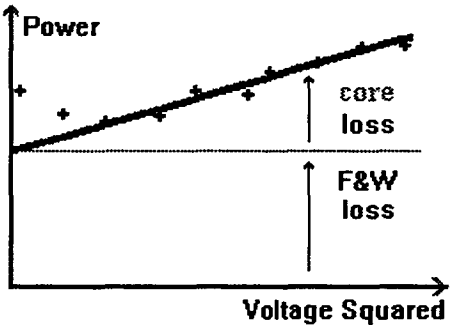

Figure 2.2.2 - Loss separation

2.2.3. Magnetising Reactance, X_M

Magnetising current is dependent on flux level, so it seems reasonable that the value of X_m selected for inclusion in a model is based on tests done at an appropriate level of main-flux ie at the same level as would occur under the condition to be simulated, [de Mello and Walsh, 1961]. With infinite-bus mains supplies, this means at rated voltage less the voltage drop in the stator. In the simulation of induction motor starting, the voltage dip may be up to 25% in mining or offshore systems and the level of the dip is unknown until the simulation is done. Under these conditions, the motor magnetising reactance may vary from the normal (slightly saturated) condition to the unsaturated (as the voltage dips) then to a condition of greater than usual saturation (as the frequency falls and the automatic voltage regulator increases excitation) and then back to normal saturation as the frequency returns to normal (the governor regains control). The level of magnetising path saturation may also vary from the nominal design condition if a motor designed for use at one voltage level is in fact used on a system of a slightly different voltage. This situation is likely to occur more often with moves to broaden permitted tolerances on supply voltages; eg. 415/240V or 380/220V motors operating on 400/230V supplies.

Saturation along the main flux path has been shown to have little influence on the starting condition, [Sivokobylenko and Kostenko, 1980]. The usual practice is to determine X_m from the NL test. Like R_c ,the effect of assuming that the NL slip is zero is to generate an inaccurate value for X_m. However since, as will be shown in Chapter 4, the predicted motor dynamic performance during starting is relatively insensitive to variation in X_m , the NL test results may be used in such studies without too much concern as to saturation level or non-zero NL slip.

Stability at an operating point may be significantly affected by saturation in the main flux path, especially where the system has a limited amount of natural damping, [He and Lipo, 1984]. This means that the modelling of the effect of transient voltage disturbances on a lightly loaded motor may need to allow for the effect of main flux saturation on X_m (and on the leakage inductances due to the self-inductances being under saturated conditions).

2.2.4. Leakage Reactance Variation With Magnetic Saturation

The total referred leakage reactance is the most important machine parameter in that the predicted performance is highly dependent on it, (See Chapter 4). The total leakage reactance decreases with increased current due to saturation of leakage flux paths. For some machines with complex slot shapes this can occur at relatively low currents due to a deliberate attempt by designers to improve starting torque/ampere. This is especially true of smaller machines with cast aluminium rotors and can make the prediction of full-voltage starting current difficult. Considerable work has been done to allow starting currents to be predicted based on the results of up to three reduced-voltage locked rotor tests, [Lee, 1989]. Two methods are introduced here with a detailed comparison being left until Chapter 5.

It is noted that since the measurement of LR voltages and currents takes place during steady-state tests after the decay of the electrical transients, these methods give the steady-state reactance. The starting currents derived from them will not include transient dc offsets which may need to be taken into account when setting overcurrent protection relays. This is confirmed in Chapter 8.

2.2.4.1. Describing function method

One approach that is sometimes used to model leakage path saturation is the describing function. A variant of this is given by Chalmers and Mulki, [1970]. The method outlined here is that of Rogers and Shirmohammadi, [1987] which is similar to that used in the INSPEC/INSTART package discussed in Chapter 3. The notation agrees with that work. Define a describing function parameter, DF such that

for any stator current, I<Isat, $DF = 1$ (2.2.5)

and for I>Isat, $$DF = \frac{2}{\pi}\left[\xi + \frac{1}{2}\sin(2\xi)\right]$$

$$\text{where } \xi = \sin^{-1}\left(\frac{Isat}{I}\right)$$

At starting, we can neglect the magnetising branch so the total leakage reactance, X_{tl} is given by,

$$X_{tl} = \sqrt{\left(\frac{V_1}{I_1}\right)^2 - (R_1 + R_{st})^2} \qquad (2.2.6)$$

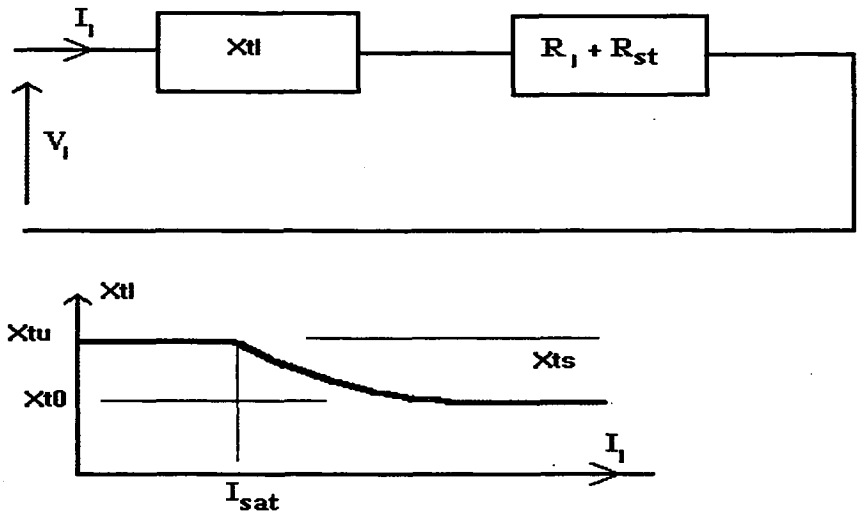

Figure 2.2.3 : Describing Function Method for Saturation

Two data points are needed from locked rotor tests, one at full voltage and the other at reduced voltage, Vred as shown in Table 2.2. These allow saturated (subscript, s) and unsaturated (subscript, u) values of the total leakage reactance, Xtl and describing function, DF to be calculated.

Test Voltage, V_1	V_1 = 1pu	Vred
Test Current, I_1	Ist	Ired
Derived Reactance, Xtl	Xtls	Xtlu
DF	DFs	DFu

Table 2.2 : Data needed for describing function method

Since Xtlu and Xtls are given by

Xtlu = Xt0 + DFu Xts and Xtls = Xt0 + DFs Xts

the saturated and unsaturated parts of the total leakage reactance as shown in Figure 2.2.3 may be separated as :

Xts = (Xtlu-Xtls)/ (DFu-DFs) and Xt0 = (Xtls DFu - Xtlu DFs)/(DFu -DFs)

The leakage reactance, Xtl at any current, I can then be determined by using an appropriate value of DF derived from equation (2.2.5) and from

Xtl = Xt0 + DF Xts (2.2.7)

For this method it is assumed that the onset of saturation occurs at a particular value of stator current, I_{sat}. The describing function method is compared with other methods in Chapter 5 and with experimental results in Chapter 7.

A similar describing function was used by Smith, Rogers and Buckley, [1979] but in this case allowance was made for the fact that saturation affects the different components of leakage reactance by differing amounts. This method has not been considered further because it requires a considerable amount of design data.

2.2.4.2. Logarithmic least-squares method

This method and the example given are taken from Melik, [1987].
Let the RMS starting current, I at any RMS line voltage, V be given by $I = A V^B$

Hence ln(I) = ln(A) + B ln(V) {where ln(x) is natural log of x}

Writing ln(A)=a gives ln(I) = a + B ln(V) to which a least-squares fit yields constants A and B. e.g. for

I	67	87	168
V	1752	2170	3640

we get A=0.005468 and B=1.26.

At rated voltage of 6600 V, the predicted starting current is then 355 A
(The actual test starting current given in the paper by Melik was 357 A)

Assuming a star circuit model, the total input impedance per phase at starting is given by $Z = \frac{V}{\sqrt{3}I}$. Since the magnetising current is usually much less than the starting current the magnetising branch may be neglected to give the total leakage reactance as

$$X_{ll} = \sqrt{\left[\frac{I^{\left(\frac{1}{B}-1\right)}}{\sqrt{3}k^{\frac{1}{B}}}\right]^2 - \left(R_1 + R_2\right)^2} \qquad (2.2.8)$$

Melik's method is the logarithmic proportional method with the curve-fit constants determined as a least-squares fit based on three data points. The direct proportional method is a special case of the logarithmic proportional method where B=1 and A=Ired/Vred.

In Chapter 5, two other modified forms of the logarithmic method in which the values of constants A and B are assigned based on statistical analysis of 52 tested motors are discussed and two new methods are introduced. All four of these methods are shown to be improvements on the logarithmic least-squares method described above.

2.2.5. Rotor Resistance Variation With Leakage Path Saturation

It may seem at first sight that leakage path saturation cannot affect the rotor resistance. For example, Klaes, [1993] states that the physical stator and rotor winding resistances 'solely depend on temperature'. The referred rotor resistance can be seen to depend on the stator/rotor transformation ratio which in turn depends on stator flux. In addition, where the rotor bars are deep enough to cause current displacement effects, the changing flux paths due to differential saturation in various parts of the rotor teeth, will also affect the current distribution in the rotor bars. The net effect is to cause a marginal dependence of rotor resistance on both stator and rotor flux levels which has been measured by Grantham, [1987], reported by Smith, Rogers and Buckley, [1979] and appears to be confirmed by the measurements on the 2.2 kW motor presented in Chapter 7.

Rotor resistance has a considerable influence on the motor's dynamic and steady-state performance. Apart from steady-state operation, the value used significantly affects the predicted peak transient torque and the time taken to run up to speed.

The relative significance of the three factors (temperature, frequency and magnetic saturation) which affect rotor resistance, depends on the size on the machine and type of rotor. The relative effects of frequency and temperature are discussed in Section 5.4 using calculated reactances based on different bar shapes. This is discussed further when the results from practical tests are presented in Chapter 7.

2.2.6. Rotor Impedance Variation With Frequency

The frequency of the supply is usually constant to within 2% and therefore the stator leakage reactance is essentially constant at constant current. The referred rotor impedance varies from $R_{dc} + j X_{dc}$ at low slip to $R_{st} + j X_{st}$ at starting. Typical simulated results of such variation are shown in Sections 5.2 and 5.3 with experimental confirmation being given in Chapter 7.

Analysis of the magnetic field can be used to derive the relationship between rotor impedance and frequency. Typically this may be done using finite element methods as Silvester [1968] or by piece-by-piece calculation of eigen vectors as Rogers and Benaragama, [1976]. Both of these methods require a large amount of, usually unavailable, design data. This is particularly true if an attempt is made to include non-slot components of leakage reactance. In addition, it is conceptually difficult to assign particular components of reactance to separate parts of the machine. It would be extremely tedious to have to include finite element methods within a numerical simulation routine, although use of a look-up table with pre-calculated values might help.

If the magnetic flux is assumed to go straight across the slot, the slot component of rotor leakage reactance may be calculated from the slot dimensions, [Say, 1976] and [Alger, 1951]. This method suffers from the disadvantage that it requires these dimensions which may not be readily available. The effect of finite permeability of the steel (such as would occur under conditions of saturation) is to change the magnetic reluctance. This could in theory be allowed for by modification of the slot width in the saturated regions to increase the MMF required at that part of the slot. A further problem arises since the current density, J is assumed to be uniform so that the current giving rise to the magnetic flux, Φ is taken to be proportional to the area of the conductor below the small segment. In general, if J is a function of radial depth into the slot and frequency, then the analysis is more complicated and the leakage and mutual inductances will depend on rotor frequency. This method is adopted in Chapter 5 and used to determine the impedance of non-uniform width rotor bars.

Variation of rotor circuit impedance with rotor frequency is more usually modelled using one of two different methods. The more common method uses a double-cage form of the "exact" equivalent circuit (DCC) as shown in Figure 2.2.4. An alternative method is based on an equivalent-deep-bar of uniform width (UDB). Both of these are performance rather than design models and do not necessarily represent the actual flux paths in the real motor. For example, the UDB method is based on an analysis of the rotor slot portion only and ignores end effects. Similarly, when the method introduced in Chapter 6 is used to derive its parameters, the DCC method is

forced to neglect the leakage flux which links only with the upper double-cage section. These models are justified if they give adequate predictions of motor performance over the full slip range.

There seems to be no agreed basis for selection of either the UDB or the DCC model and it might be assumed that they give equally good results. In the simulation work done by the author, the UDB model was used at first but this was not always successful and the DCC model was adopted as more generally useful. The two models are introduced here with a detailed comparison and guidelines for the selection of a method being left until chapter 5.

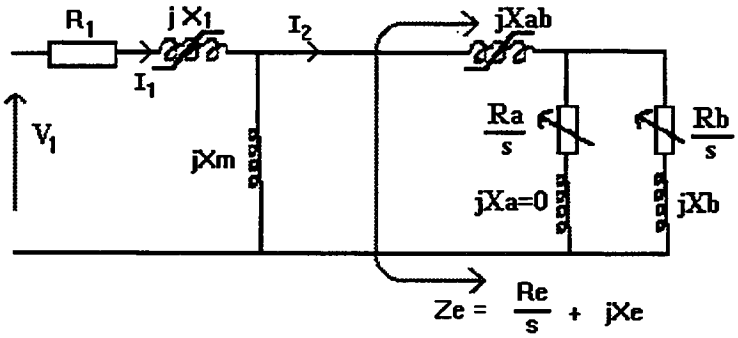

Figure 2.2.4 : Double cage equivalent circuit model

2.2.6.1. The double-cage circuit (DCC) model

A bar with non-uniform width may be represented as segmented, with each segment being considered to have uniform current density distribution. Each segment may then be represented as a branch of a ladder circuit, with the branch impedances for the nth branch being determined by the segment geometry and the appropriate current density, J_n at that depth [Klingshirn and Jordan, 1970]. When there are only two distinct rotor bar sections, the ladder circuit reduces to the double cage circuit of Figure 2.2.4.

At any slip, the total effective rotor circuit impedance referred to the stator is given by circuit analysis as

$$Z_e = \frac{R_e}{s} + jX_e \qquad (2.2.9)$$

where

$$R_e = \frac{R_a R_b \left(R_a + R_b\right) + s^2 \left(R_a X_b^2 + R_b X_a^2\right)}{\left(R_a + R_b\right)^2 + s^2 \left(X_a + X_b\right)^2} \qquad (2.2.10)$$

and

$$X_e = X_{ab} + \frac{R_a^2 X_b + R_b^2 X_a + s^2 X_a X_b \left(X_a + X_b\right)}{\left(R_a + R_b\right)^2 + s^2 \left(X_a + X_b\right)^2} \qquad (2.2.11)$$

This allows the rotor referred impedance to be calculated at any slip value once the circuit parameters are known. In the absence of design information, the method adopted for the estimation of the circuit parameter values was that of Rogers and Shirmohammadi, [1987] which is discussed in Chapter 6.

2.2.6.2. The uniform deep bar (UDB) model

The effect of variation in penetration depth with frequency has been analysed by Field, [1905]. Alger, [1965] showed that for a deep bar of uniform width, the effective referred rotor resistance, R_f is given by :

$$R_f = \frac{\alpha d[\sinh(2\alpha d)+\sin(2\alpha d)]}{\cosh(2\alpha d)-\cos(2\alpha d)} R_{dc} \qquad (2.2.12)$$

where $\alpha^2 = \frac{\pi f \mu_0}{\rho}$

and that the referred rotor reactance , X_f is given as :

$$X_f = \frac{f_s}{f}\frac{\alpha d[\sinh(2\alpha d)-\sin(2\alpha d)]}{\cosh(2\alpha d)-\cos(2\alpha d)} R_{dc} \qquad (2.2.13)$$

An alternative formula (in terms of X_{dc}) was given by Kostenko and Piotrovsky [undated] as :

$$X_f = \frac{3}{2\alpha d}\frac{[\sinh(2\alpha d)-\sin(2\alpha d)]}{[\cosh(2\alpha d)-\cos(2\alpha d)]} X_{dc} \qquad (2.2.14)$$

An examination of equations (2.2.13) and (2.2.14) shows that if $\frac{X_{dc}}{R_{dc}} = \frac{2\alpha^2 d^2}{3}$ then they are equivalent.

This is shown to be true in Section 5.3.3.1.

Equation (2.2.14) may also be derived directly from equation (2.2.13) as in Section 2.6 by considering

$$\lim_{f\to 0}\left|\frac{2\alpha d[\sinh(2\alpha d)-\sin(2\alpha d)]}{[f\{\cosh(2\alpha d)-\cos(2\alpha d)\}]}\right|.$$

Since both Field and Alger performed their analysis with truly uniform width slots with no slot bridge, these authors both omit the additional term which was given by Swann and Salmon, [1963] as equation (2.2.15).

$$\frac{8d}{\delta^2}\sum_{n=1}^{N}\frac{\sin\frac{\pi n l}{\omega}}{\left(\frac{\pi n l}{\omega}\right)}\frac{[u_n\sin(2dv_n)+v_n\sinh(2du_n)]}{(u_n^2+v_n^2)[\cosh(2du_n)-\cos(2dv_n)]} \qquad (2.2.15)$$

with u_n being given by $u_n = \pm\frac{\sqrt{2}n\pi}{\alpha}\sqrt{\left[\sqrt{1+\left(\frac{\alpha a}{2n\pi}\right)^4}+1\right]}$ and

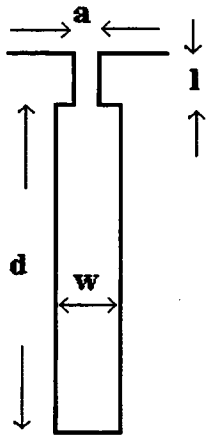

and v_n given by

$$v_n = \pm\frac{\sqrt{2}n\pi}{\alpha}\sqrt{\left[\sqrt{1+\left(\frac{\alpha a}{2n\pi}\right)^4}-1\right]}$$

Figure 2.2.5
Slot with bridge

In practice, large machines have uniform rotor bars for ease of manufacture although they may have semi-closed rotor slots. For small machines, bar widths are deliberately made non-uniform to improve performance. This gives rise to a wide range of slot cross-sections as shown in Figure 2.2.6. Even though the actual rotor bar is non-uniform it is possible to postulate that a uniform bar model exists which, at all frequencies, will have the same effective referred impedance as the actual bar. This is what those authors who use the UDB model are implicitly doing and is what I did initially. The examination of this hypothesis forms the basis of Section 5.2 in Chapter 5.

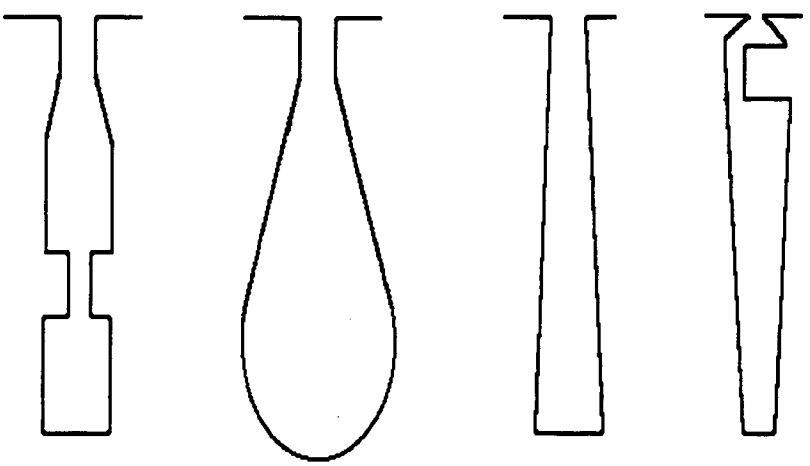

Figure 2.2.6. Typical cross-sections for rotor slots

The postulated equivalent uniform bar will have constant width and a depth which is referred to as the equivalent bar depth, d. The advantage of using this single parameter is that the rotor quantities may be related to the rotor dc resistance which may be easily calculated from performance data as shown below.

If it is possible to calculate d, then equation (2.2.12) and either equation (2.2.13) or (2.2.14) may be used to determine the rotor impedance at any value of slip as part of a numerical simulation of induction machine performance. Iterative methods have been used to determine the value of d. Lindsay and Barton, [1973] assigned values for the case of a particular trapezoidal bar until there was close agreement with unspecified input data. Melik, [1987] used an iterative method based on re-calculation of torque at the rated slip point.

Two other methods are given here which are new and based on motor performance data which is readily obtainable. The first uses the set $\{T_{st}\ I_{st}\ I_1\ s_1\}$ to derive the ratio of starting and rated slip values of rotor resistance and hence the bar depth. The second method derives the depth from the ratio of rotor reactance and resistance at rated slip.

2.2.6.2.1. Depth, d, from R_{st} and R_{dc}

The referred rotor resistances R_{st} and R_{dc} may be measured experimentally as in Chapter 7 or alternatively their ratio determined from manufacturer's performance data as done by Rogers and Shirmohammadi, [1987] and outlined in Chapter 6.

$$\frac{R_{st}}{R_{dc}} = \frac{T_{st}}{s_1}\left(\frac{I_1}{I_{st}}\right)^2 \qquad (2.2.17)$$

Equation (2.2.17) may be used, together with equation (2.2.12), to determine αd at slip = 1 and hence αd at other frequencies. Since the impedance ratio is independent of the effective stator/rotor turns ratio, the referred quantities R_f and X_f may be determined from equations (2.2.12) and (2.2.14). If the resistivity of the rotor bar material is assumed (either copper or aluminium) then equivalent depth, d may also be calculated from the definition of α.

2.2.6.2.2. Depth, d', from Xdc and Rdc

The ratio X_{dc}/R_{dc} may be determined experimentally or from manufacturer's data as outlined in chapter 6.

The alternative bar depth is then given by $$d' = \sqrt{\frac{3\rho X_{dc}}{2\mu_0 \pi f_s R_{dc}}} \qquad (2.2.18)$$

This value for the UDB depth may be compared with the value of d calculated in the previous section.

2.2.6.2.3. Limitations of the UDB method

The above analysis is based on the primary leakage flux path shown in Figure 2.2.7. [Kostenko and Piotrovsky, undated], [Alger, 1951]. Clearly, the secondary and zigzag leakage components would need a different analysis. Both authors cited suggest that, to a first approximation, slot -impedance dominates rotor impedance since these methods derive per-unit-length values for the slot portion of bar impedance at any value of slip neglecting other components. The hypothesis is that that these (slot-based) models give the correct variation in rotor impedance over the slip range.

It seems reasonable to assume that the primary leakage reactance component is the major variable reactance for the following reasons :

- For most practical industrial motors, the axial length is greater than the diameter; ie the "sausage" rather than the "pancake" shape is the norm. The slot portion of the windings is relatively longer than the endwinding region. This means that whatever happens to the slot portion dominates the behaviour of the total leakage reactance.
- The endwinding magnetic leakage flux paths are mainly in air and are therefore less affected by changes in rotor frequency. (The permeability of the surrounding medium affects the value of α).

Any constant parts of the rotor reactance may be absorbed into the slip-insensitive stator reactance component of the equivalent circuit. The separation of reactance into its different forms is not particularly useful to those engaged in performance simulation as opposed to design work. In most cases, insufficient data is usually available to enable detailed calculation of separate reactances. Since there are field phenomena involved, the use of a circuit model with separate reactances allocated to different parts of the machine will always be a pragmatic approach to modelling the externally observed behaviour. In assigning values to a DCC model for performance simulation, it may be better to think of "reactance which varies with slip" rather than "rotor reactance".

More seriously than the above, equations (2.2.12) and (2.2.13) were derived assuming that the width of the bar is independent of radial height. As mentioned previously, modern induction motor rotors contain extruded sections of aluminium (or less commonly, copper) which have cross-sectional geometries optimised for performance and have anything but uniform width. The extension of Alger's method to non-uniform width bars is discussed in Section 5.3.

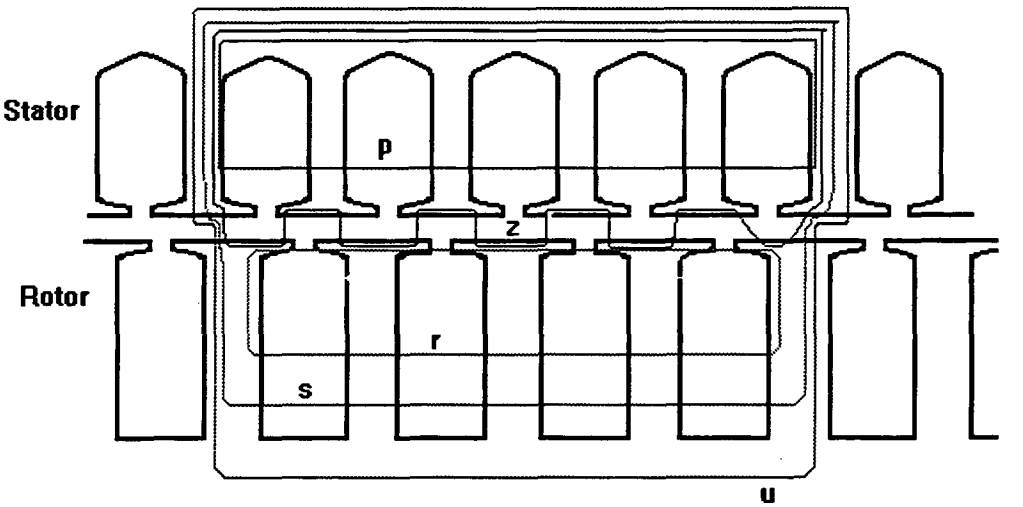

Figure 2.2.7 Primary, secondary and zigzag leakage flux paths

2.2.7. Rotor Impedance Variation With Temperature

The variation of leakage reactance with temperature is a minor effect that has been reported by Grantham, [1985] whose results are supported by simulation as shown in Chapter 5. It is due to the resistivity of the stator and rotor conductors affecting the flux distribution at high frequency and hence the reactance variation. This needs to be considered when designing the test method used for the determination of leakage reactance. The fast PC-based method described in Chapter 7 avoids temperature variation during the reactance measurement.

Significantly different results are obtained when motors are started hot compared with cold starting due to an increase in the effective referred rotor resistance. The problem with rotor resistance variation with temperature is not so much the manner in which it varies (which is well known, [IEEE, 1988]) but rather the estimate of rotor temperature itself. Once the temperature is known, the dc resistance, R_{hot} at elevated temperature, T_{hot} is given by the equation :

$$R_{hot} = R_{cold}\left(\frac{234.5 + T_{hot}}{234.5 + T_{cold}}\right). \qquad (2.2.19)$$

where R_{cold} is the cold resistance at temperature, T_{cold} .

It is difficult for an electrical model to take this effect into consideration, depending as it does on flow-rate of coolant, ambient temperatures and duty history. Whilst a sophisticated hybrid model containing much design data could be made to represent rotor temperature variations it seems more practical for an estimate of temperature to be based on a I^2t model of temperature rise. No work has been done by the author on developing either form of model. The simulation of temperature effects presented in Chapter 8 assumes that the machine is at a constant operating temperature during the simulation of starting performance.

2.3. Reduced Forms Of The Equivalent Circuit

In these forms of the circuit model the magnetising branch is transferred to the terminals of the equivalent circuit by circuit reduction without approximation. The circuit below achieves the computational simplicity of the approximate equivalent circuit whilst retaining the accuracy of the exact circuit.

2.3.1. Thevenin Equivalent Circuit

Here the stator and magnetising branch components are combined using Thevenin's theorem to arrive at Figure 2.3.1.

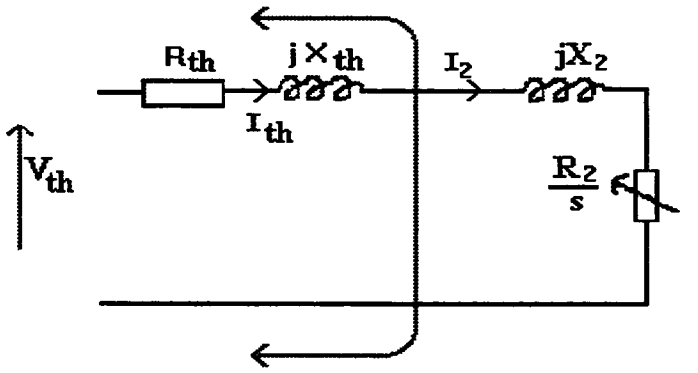

Figure 2.3.1 : Thevenin equivalent circuit

2.3.2. Other Modified Circuits

Several other circuits have been used mainly with the aim of reducing the complexity of the computation in complex numbers. Notable examples of this are the "exact equivalent L" circuit of Kostenko and Piotrovsky [undated, pp 429-433] and the circuit summarised by Slemon, [1983]. From a computational point of view, these have lost much of their significance due to the ease with which calculations can now be done. As far as the external behaviour is concerned, this equivalent circuit is identical with that of Figure 2.1.1. The circuit of Figure 2.1.1 is used in all subsequent work with the addition of a second rotor circuit in Chapter 5.

2.4. Models For The Simulation Of Dynamic And Transient Performance

2.4.1. Starting Time

The Thevenin equivalent circuit of Figure 2.3.1 has been used to derive an expression for the time taken for a motor to accelerate with an inertial load from slip, s_1 to s_2, [Section 5.8, pg 97of Daniels, 1976]. Defining the pull-out torque as T_m and the slip at which it occurs as s_m, the derivation starts from the expression for electromagnetic torque, T_e derived from Figure 2.3.1

ie
$$T_e = \frac{2T_m\left[s_m^2 R_{th} / R_2 + s_m\right]}{\left[s + s_m^2 / s + 2s_m^2 R_{th} / R_2\right]}$$

to arrive at the time, t_1 to accelerate from rest to slip, s_1 as :

$$t_1 = \left[\frac{J\omega_s^2}{3V_{th}^2}\right]\left[2R_{th}(1-s_1) - R_2\ln(s_1) + \frac{(1-s_1^2)\left\{R_{th}^2 + (X_{th}+X_2)^2\right\}}{2R_2}\right] \qquad (2.4.1)$$

It should be pointed out here that the expression given by Sen Gupta and Lynn, [1980] is incorrect as can be shown by substituting $s_1 = 1$ (with the expected answer of zero). The derivation contains a fundamental error. Two expressions are written with the first valid at low slip and the second at slip =1. These are then combined into a single expression even though they cannot both be true at the same time.

Equation (2.4.1) can be modified to include friction, windage and/or load torque but the analytical solution is lost and a numerical integration method must be used. The load curve must be entered into the calculation in terms of a polynominal or spline fit.

The time, t_1 taken to reach speed, ω_1 is then given by $t_1 = J\int_0^{\omega_1} \frac{1}{T_a} d\omega$

where the accelerating torque, T_a is given by $T_a = T_e - T_{load}$.

The loss of an analytical solution does not really matter in practice since the computation would probably be done on a PC and the acquisition of the correct input data will take longer than the solution of the problem.

Simulation results for a program based on the double-cage steady-state equivalent circuit including leakage path saturation are given in Chapter 8.

2.4.2. Transient Torque And Current

Some work has been done to predict the transient torque and current by analytical methods. Three methods were studied in detail and are mentioned here for completeness with the numerical comparison being left until Chapter 8.

Slater and Wood, [1967] used a constant-speed solution to evaluate the first transient torque peak. This was given as

$$T_{p1} = T_{st}\left(1 + \sqrt{\left(1 + [\omega\tau]^2\right)\left(\cos^2\alpha + \sin^2[\alpha + \beta]\right)}\right) \qquad (2.4.2)$$

Where $\tau = L_{LR} / (R_1 + R_2)$

α = switching angle at which the first line is connected

β = delay in connecting the third line

T_{st} = steady-state, locked rotor torque

A method by Smith and Sriharan, [1966] based on Laplace transform analysis, produced equations for the transient current and torque at slip=1 (and also equations for these quantities at slips of 0.5 pu and close to zero). These equations are not quoted here since they are rather long and are expressed in terms of non-dimensional parameters which would need to be defined.

Natarajan and Misra, [1991] considered the prediction of transient starting current; i_1 and derived equation (2.4.3).

$$i_1(t) = A_1 e^{m_1 t} + A_2 e^{m_2 t} + A_3 \cos\omega t - jA_4 \sin\omega t \qquad (2.4.3)$$

Terms m_1, m_2, A_1, A_2, A_3 and A_4 are non-linear functions of the motor circuit parameters and the supply angular frequency, ω. As expressed, the notation in the equation is confusing since it uses the phasor notation for the forced response and instantaneous values for the natural response. The graphs in the reference show the current envelope decreasing with time after switching on the motor. On closer

examination this is seen to be wholly due to the variation of the circuit impedance with slip which is assumed to reduce linearly to zero within a known run-up time. This produces an appropriate-looking current decrement. In reality, the equation can only be of value in determining the initial current transient. An attempt was made to reproduce this work but the constants derived did not give zero current at time = 0 as expected from the de-energised initial condition of the motor. It is impossible to confirm that the current waveform shown by Natarajan and Misra originates at zero because the scale of the graph in the 1991 paper is condensed to show the full slip range. Although this looks impressive and superficially matches the experimental curve given by the authors, the results over this speed range are based on an assumed impractical linear variation in slip. For a linear slip variation, the net accelerating torque would have to be constant. Given the shape of the induction motor torque/speed curve, this would be difficult to arrange. After some time spent checking the method and the program code used to implement it, it was abandoned.

Although none of the above authors said so, it is clear that, in general, reasonable results could only be expected from all these equations if the values of motor parameters are appropriate to conditions of high current and high slip. These methods were included in a version of the circuit-based simulation program. The equations for each method were programmed as Turbo Pascal procedures to enable easy checking. It will be shown in Chapter 8 that the first two methods give good results for torque and current transients for the larger motors (above about 100 kW).

2.5. Concluding Review Of Chapter 2

The main purpose of Chapter 2 was to collect together several ideas which will form the basis for subsequent developments in the thesis. Since the material is not normally available in one place the reader would otherwise be required to search out several sources. The initial reservations about including a chapter which consisted of existing information, were overcome as it was realised that the collection of the material into a single inter-related whole, was a useful contribution in itself.

A further advantage of reviewing and discussing the several complications and approximations, is that the development of the detailed investigations in Chapters 5, 6 and 7 will not be hampered by continual sidetracking to clarify small points.

2.6. Equivalence Of Alger and Kostenko/Piotrovsky Formulae

This section is in the nature of an Appendix to Chapter 2. It is shown that the equations (2.2.1.3) and (2.2.1.4) are equivalent. Acknowledgment is given to help from my colleague Dr. Sergio Montes who took an interest this topic until we had three alternative proofs of which the following is the most succinct. In parallel with this, a proof from consideration of current density distribution and flux linking turns was developed by the author on his own and this is presented in Section 5.3.3.1 as part of the verification of the variable width bar method for determining leakage reactance.

Starting from Alger's formula, (2.2.13) and considering the value of X_f as the rotor frequency tends to zero. $X_{dc} = \lim_{f \to 0} |X_f|$

$$= \frac{R_{dc} f_s}{2} \lim_{f \to 0} \left| \frac{2\alpha d[\sinh(2\alpha d) - \sin(2\alpha d)]}{[f\{\cosh(2\alpha d) - \cos(2\alpha d)\}]} \right| \qquad (2.6.1)$$

Writing $\frac{2\alpha d}{f} = \frac{1}{2\alpha d}\frac{(2\alpha d)^2}{f} = \frac{1}{2\alpha d}\frac{4\mu_0 \pi f d^2}{\rho f}$ in equation (2.6.1)

gives $X_{dc} = \frac{2\pi\mu_0 d^2}{\rho} R_{dc} f_s \lim_{f \to 0} \left| \frac{[\sinh(2\alpha d) - \sin(2\alpha d)]}{[2\alpha d\{\cosh(2\alpha d) - \cos(2\alpha d)\}]} \right| \qquad (2.6.2)$

let $2\alpha d = A$.

To derive (2.2.14) it is required to show that $\lim_{A \to 0} \left\langle \frac{[\sinh(A) - \sin(A)]}{A[\cosh(A) - \cos(A)]} \right\rangle = \frac{1}{3}$

writing $\sin A = A - \frac{A^3}{3!} + \frac{A^5}{5!} + ..$ $\qquad \sinh A = A + \frac{A^3}{3!} + \frac{A^5}{5!} + \frac{A^7}{7!} .+...$

$\cos A = 1 - \frac{A^2}{2!} + \frac{A^4}{4!} - \frac{A^6}{6!} + ...$ $\qquad \cosh A = 1 + \frac{A^2}{2!} + \frac{A^4}{4!} + \frac{A^6}{6!} + ...$

$$\lim_{A \to 0} \left\langle \frac{\left(A + \frac{A^3}{3!} + \frac{A^5}{5!} + \frac{A^7}{7!} .+..\right) - \left(A - \frac{A^3}{3!} + \frac{A^5}{5!} + ..\right)}{A\left\{\left(1 + \frac{A^2}{2!} + \frac{A^4}{4!} + \frac{A^6}{6!} + .\right) - \left(1 - \frac{A^2}{2!} + \frac{A^4}{4!} - \frac{A^6}{6!} + .\right)\right\}} \right\rangle$$

$$= \lim_{A \to 0} \left\langle \frac{\frac{2A^3}{3!} + \frac{2A^7}{7!} + ..}{A\left(\frac{2A^2}{2!} + \frac{2A^6}{6!} + ..\right)} \right\rangle \quad = \lim_{A \to 0} \left\langle \frac{\frac{1}{3}\left(1 + \frac{6A^4}{7!} + ..\right)}{1 + \frac{2A^4}{6!} + ..} \right\rangle \quad = \quad \frac{1}{3}$$

Inserting this into (2.6.2) gives $X_{dc} = \frac{2\pi\mu_0 d^2}{3\rho} R_{dc} f_s$.

This can be used to substitute for R_{dc} in the original equation (2.2.14) to give the alternative formula (in terms of X_{dc}) as given by Kostenko and Piotrovsky, namely :

$$X_f = \frac{f_s}{f} \frac{\alpha d[\sinh(2\alpha d) - \sin(2\alpha d)]}{\cosh(2\alpha d) - \cos(2\alpha d)} X_{dc} \frac{3\rho}{2\pi\mu_0 d^2 f_s}$$

$$= \frac{3}{2\alpha d} \frac{[\sinh(2\alpha d) - \sin(2\alpha d)]}{[\cosh(2\alpha d) - \cos(2\alpha d)]} X_{dc}$$

3. PC-BASED NUMERICAL SOLUTIONS

The systematic analysis of electrical machines in terms of coupled circuits began with a paper by R H Park, which focussed on the synchronous machine, [Park, 1929]. This was followed by induction motor studies by Levine, [1935] and Stanley, [1938]. The rigorous work of Gabriel Kron, [Kron, 1934] was dismissed by many at the time as being too academic since it was expressed in terms of tensor notation. This work however laid the ground for later developments in the field. The key advance of Kron was to recognise that most electrical machines could be represented by one matrix equation with the different forms being obtained by suitable transformations.

By 1944, analogue simulation work was being done using an early differential analyser, [Maginniss and Schultz, 1944]. This involved simulation of conditions such as direct-on-line and resistance starting, voltage disturbances and plugging and was based on Stanley's equations. By the 1960s the unified theory, as it became to be known, had developed to become subject matter in some undergraduate degree courses, [Jones, 1967]. Later the trend reversed and undergraduate degree teaching focussed on the separate machine types with the generalised theory being left to postgraduate work. The Development of the ElectroMagnetic Transients Program (EMTP) by Bonneville Power in the USA led to its adoption as an industry standard, [Lauw and Scott-Meyer, 1982]. Subsequent development has focussed on the inclusion of effects such as parameter variation and the development of simulation software that is more user-friendly than the EMTP.

Several commercial computer programs are now available with different levels of induction motor model sophistication. A formal comparison of ten of these was presented by Bengiamin and Holcomb, [1992] with particular emphasis on load-flow and fault-analysis problems. That work treated the induction motor as a minor component within the power system and on the user interface. No discussion was presented concerning the detailed induction motor model which is the main concern of this work.

3.1. A Review Of Some Commercial Packages

The focus of this thesis is on the selection of an appropriate model for the simulation of induction motor performance with particular emphasis on motor starting direct-on-line. The original plan for the thesis topic was that several simulation packages would be run and the results compared. As the work progressed it became apparent that such a comparison would not be particularly useful because all of the available packages used different motor models and required different data as starting points. The various packages were designed for different purposes and it is therefore important to define clearly the purpose of the simulation exercise and identify which of the simulation yields is of greatest significance. This approach was incorporated into the Expert System developed in Chapter 9.

It was decided to concentrate on the development of the programs IM_SIM.PAS and IM4.PAS which incorporated the differential equation and equivalent circuit models respectively. The advantage of this approach was that the source code could be modified to include or exclude various effects. The results of this process are described in Chapter 8. The use of the program IM_SIM.PAS is described in Section

3.4 of this chapter. The rest of this section discusses some commercial packages with which the author has had operating experience.

3.1.1. INSPEC And INSTART

The main feature of interest in this software is its implementation of the algorithm for the derivation of motor double-cage equivalent circuit parameters including leakage path saturation as described by Rogers and Shirmohammadi, [1987].

The INSPEC/INSTART programs were written by Graham Rogers after his retirement from Ontario Hydro and marketed under the name of "Cherry Tree Scientific Software", [Rogers, 1993]. The author was introduced to the packages as a result of queries raised with Mr. Rogers regarding the above paper. The software was purchased and evaluated during 1994 by the author with the assistance of Ms J. Foulkes, an undergraduate student. A lively communication developed by email and FAX and several shortcomings of the software were identified. Most of these were in the area of programming rather than technical aspects of the model. A report on the program's technical accuracy and user friendliness was made to Mr. Rogers at the end of 1994, [Foulkes, 1994]. In 1995 a modified version of the software was released which was much more user-friendly but still contained no formal optimisation procedure to ensure that the motor parameters determined gave the best fit to the quoted performance data.

In spite of its negative aspects, the INSPEC package is considered to be useful in that, with experience, the optimisation can be performed interactively from the keyboard. The INSPEC package was used by the author in the work presented in Chapter 6. Its main deficiency is that it sometimes fails to converge with smaller motors due to an approximation in the treatment of leakage reactance saturation. It assumes that the reactance may be split into equal saturable and unsaturable parts rather than as derived from reduced voltage test data as outlined in Section 2.2.4.1. This approximation reduces the data input requirement but requires an arbitrary value for the saturation current, Isat.; ie not the same as the true departure from the linear locked-rotor saturation curve. The result is a slightly different curve for the leakage reactance variation with current. In large motors, the discrepancy can be made up by adjustments to the double cage circuit model so that the net effect on total rotor impedance is the same during starting. (ie in going from a high-current, high slip condition to a low-current , low-slip state the variation of rotor impedance in time is the same). With smaller motors, the bar size is small, the scope for these adjustments is reduced and the algorithm may fail.

The INSTART program is based on the solution of the machine's differential equations in Kron's freely rotating axes with currents as state variables. It accepts circuit parameter data directly from the INSPEC program. The program uses a simple single impedance model for the supply system. This cannot include the modelling of the behaviour of motors already running. In some circumstances it may be appropriate to run more than one model so that both overall system and local motor performance may be modelled with sufficient detail. In the original 1994 version of INSTART it interfaced poorly with other packages, with no ability to import graphical output into documents or analysis programs. This made its use for investigative research somewhat limited. It appeared to give the same results as the IM_SIM.PAS program but precise numerical comparison was impossible.

3.1.2. CAPTOR And DAPPER

The CAPTOR/DAPPER software, is based on a steady-state motor model and accepts machine impedances as data input unlike the INSPEC/INSTART program which has the performance data as a starting point. However the INSPEC program may be used to generate input data for CAPTOR. Further information can be found in the operation manual, [SKM, Systems Analysis Inc, 1991] or perhaps more readily in an article by Healy and Lang, [1992].

The main advantage of this package is that it allows the simultaneous simulation of up to ten motors in various stages of stopping, starting or responding to load changes. As such, it is extremely useful for system studies. Care must be taken to use appropriate reactance data since the program does not allow for reactance variation due to changing saturation conditions in either the main or leakage flux paths. This deficiency is one of its main weaknesses. The CAPTOR program manual refers the user to Waters and Willoughby, [1983] as a method for determining the circuit impedance parameters. The main problem with this method is that it always generates a motor model which neglects leakage path saturation and ascribes all the change in leakage reactance to skin effect in the rotor. This method was therefore rejected by the author in favour of that of Rogers and Shirmohammadi as discussed in Section 6.1.

3.1.3. ATP4 (A Version Of The EMTP)

The author has had a limited amount of experience with the alternative version of the electromagnetic transients program. The main deficiency of this software is its extreme user unfriendliness and high cost both in terms of capital outlay and staff training. This contrasts sharply with CAPTOR/DAPPER and the new version of INSPEC/INSTART. Technically the motor and system models are sophisticated and the effects of interaction between several motors may be modelled. The main reasons for using this software would be that staff might already be familiar with it and the strong interaction between the motor and other parts of the system would require simultaneous modelling of electrical transients in more than one motor.

3.1.4. Questions To Be Asked When Selecting Commercial Software

Assessment of a given simulation package can be assisted by identifying the models used by the software for particular aspects of the system behaviour. How can the user know what kind of internal model is used by a particular package? In order to apply successful modelling to a particular feature, the program must request certain data items. The absence of a request for such information means that the simulation program under evaluation uses an approximate method or ignores the phenomenon.

Supply Bus

Frequency

Inertia of generation plant and governor characteristics

Voltage

Impedance between motor and system infinite bus.
Generator field winding time constants
AVR constants

Load On The Motor

Polynominal constants for load torque/speed curve.
Inertia of load

Motor Model

Leakage path saturation

Starting current data from reduced voltage locked rotor tests

Skin effect in the rotor

Double-cage form of rotor equivalent circuit.
(See Section 5.2 for rejection of uniform bar model)

Temperature of operation

Thermal data such as winding temperatures and possibly longer term thermal behaviour such as cooling medium temperature and heat transfer model.

It may be important to identify whether the current and torque output includes the fast electrical transients. When a multi-bus power network must be considered, these may have to be neglected due to the difficulty of modelling individual motors in a complex system in complete detail. It is shown in Chapter 8 that the equivalent circuit model, when modified to allow for parameter variation, may be as accurate as the differential equation model for most simulation yields. Chapter 8 also demonstrates that the modelling of the interaction of motors being started, with the power system to which they are connected, is usually more significant than the sophistication of the motor model. When considering the use of reduced order models for predicting the stability of motors already running, the guidelines given by Skvarenina and Krause, [1979] may be useful.

The limitations of some packages may be overcome by careful selection of input data values. For example, the PSS/E program, [Power Technologies, Inc, 1994] has no facility for including leakage path saturation but if saturated reactance values are used then reasonable predictions can be made over a restricted range of operation. Alternatively, an unsaturable motor model may be used which fits the known performance data at all points. This last technique is demonstrated in Chapter 8 where it is shown to give some error, particularly in predicted run-up times.

The choice of a model for numerical simulation of a particular condition may be determined by several factors. The simulation model ultimately chosen may not be the theoretically ideal one. In practice, the choice may be dictated by constraints such as availability of system data, software, computing power, and engineering familiarity with the package. The discussion of the relative significance of these components and the circumstances in which each of them is significant is presented in Chapter 9 in the form of an expert system. This algorithm, seeks appropriate data, summarises the choices and describes the performance costs associated with adopting a less than ideal simulation model.

3.2. Induction Machine Free Axis Model

Several good texts are now available which give the detailed derivation of the differential equations for the induction motor. The most helpful of these was found to be that by Jones, [1967] which contains some extremely useful practical measurements and discusses many of the basic ideas in some detail. The text by Adkins and Harley, [1975] extended the work of Jones with emphasis on practical applications. The text by Krause, [1987] which incorporates many of the newer developments in this area was also valued highly. One of the problems encountered during the whole work on which this thesis is based, was the use of different notations by the several authors who have published on the subject of induction machine

modelling. As a result of this, it was decided to include the following section so that all the terms used here would be well defined and these would be related to the variable names used in the subsequent simulation program, IM_SIM.PAS. The section also highlights some modifications to existing models to allow inclusion of both leakage path and main flux saturation.

Equations are expressed in terms of flux linkages as state variables and also in terms of rotor current and rotor flux linkages. Some discussion is included regarding the theoretical differences between these two approaches with numerical comparison of the effect on simulation output being left to Chapter 8.

3.2.1. General Equations And Nomenclature

The general matrix equation for a symmetrical, 3-phase, 3-wire induction machine in axes d and q rotating at an arbitrary electrical angular velocity, ω_e is given , in terms of currents as state variables :

$$\begin{bmatrix} v_{ds}^e \\ v_{qs}^e \\ v_{dr}^e \\ v_{qr}^e \end{bmatrix} = \begin{bmatrix} R_1 + L_{ds}p & -\omega_e L_{qs} & L_m p & -\omega_e L_m \\ \omega_e L_{ds} & R_1 + L_{qs}p & \omega_e L_m & L_m p \\ L_m p & -(\omega_e - \omega_r)L_m & R_2 + L_{dr}p & -(\omega_e - \omega_r)L_{qr} \\ (\omega_e - \omega_r)L_m & L_m p & (\omega_e - \omega_r)L_{qr} & R_2 + L_{qr}p \end{bmatrix} \begin{bmatrix} i_{ds}^e \\ i_{qs}^e \\ i_{dr}^e \\ i_{qr}^e \end{bmatrix} \qquad (3.2.1)$$

This matrix equation may be interpreted in conjunction with Figure 3.2.1 which shows the relationship between the rotating dq axes and the (abc) phase axes of the machine with rotor angular velocity of ω_r relative to the stator.

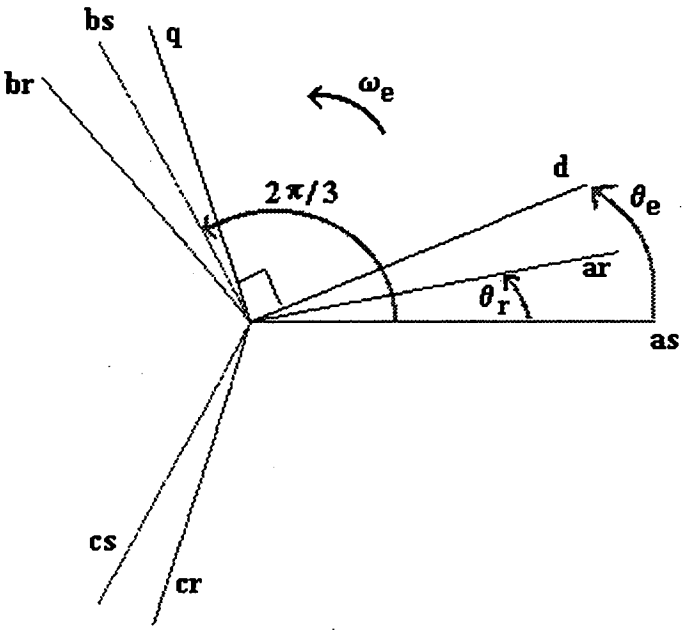

Figure 3.2.1 : Trigonometric relations between the axes.

The machine parameters are defined as :

R_1, R_2	Stator and rotor resistances per phase (equal on d and q axes)
L_{ds} , L_{qs}	Stator direct and quadrature axis self-inductances.
L_{dr} L_{qr}	Rotor direct and quadrature axis self-inductances.
L_m	Mutual inductance between stator and rotor d and q axis windings

Because of the symmetry of the induction machine it is possible to say that the direct and quadrature axis self inductances are equal; ie that

$$L_{qs} = L_{ds} = L_s \qquad \text{and} \qquad L_{qr} = L_{dr} = L_r$$

In practice, if the measureable mutual inductances of the actual phase windings are defined as :

the peak fundamental of the mutual inductance between stator and rotor	$\overline{M}$
the mutual inductance between stator windings	$\overline{M}_1$
the mutual inductance between rotor windings	$\overline{M}_2$
and the stator/rotor transformation ratio as	n

then the magnetising and leakage inductances are derived as

$$L_m = \tfrac{3}{2}\overline{M}$$

$$L_2 = n^2\left[L_r - \overline{M}_2\right] \qquad L_1 = L_s - \overline{M}_1$$

In practice, these leakage inductances are more accurately measured directly rather than derived from the difference between self and mutual inductances, [Jones, 1967].

The inductances may be related to the leakage and magnetising reactances referred to the stator in the steady-state equivalent circuit of Figure 2.1.1 as follows :

$$X_1 = 2\pi f L_1 \qquad X_2 = 2\pi f L_2 n^2 \qquad X_m = 2\pi f L_m$$

Where f is the frequency of the stator supply.

Voltages v_{ds} and v_{qs} are impressed on the d and q axis windings and are given by

$$v_{ds} = \sqrt{\tfrac{3}{2}}V\sin(\omega t - \theta_e) \qquad \text{and} \qquad v_{qs} = -\sqrt{\tfrac{3}{2}}V\cos(\omega t - \theta_e)$$

where V is the peak supply phase voltage eg $v_a = V\sin(\omega t)$.

The magnitude of v_{ds} is therefore equal to the RMS line voltage if a star-connected equivalent circuit is assumed.

If ω_e is made equal to zero then the equation is referred to the stationary reference frame, [Stanley, 1938]. Similarly, Park's equation, [Park, 1929] is arrived at by making $\omega_e = \omega_r$. This generality of the equation is the main reason for selecting it as a basis for the simulation program.

Figure 3.2.2 shows a model, derived by the author, of the cage induction motor referred to stationary axes. This clearly shows the induction of voltage, e_{qr} in the rotor quadrature axis winding due to flux, φ_{dr} in the direct axis and vice versa. This is not the classical steady state equivalent circuit since it is derived directly from equation 3.1.1 without the usual procedure of replacing the p operator by $j\omega$. One significant difference between them is the representation of power in the rotor. The variable rotor resistance has been replaced with an active voltage source.

Zero phase sequence components have been neglected since the 3-wire connection is assumed for the stator and the rotor is a cage. Iron loss is not included in the model though the addition of a small resistor in series with the magnetising inductance would achieve this. Alternatively, the iron loss may be included with the friction and windage losses as discussed in Chapter 2.

The rotor speed, ω_r in electrical radian per second is related to the mechanical speed, ω_r' as , $\omega_r = \omega_r' *$ (pole pairs)

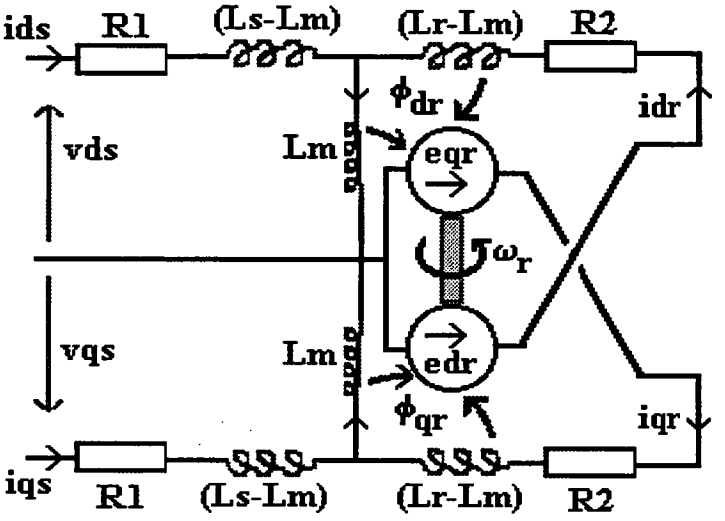

Figure 3.2.2 : Exact transient equivalent circuit.

3.2.1.1. Effect of variations in parameters

In equation (3.2.1) the inductances are assumed constant so that there are no voltages induced in the windings due to parametric variation. For example, in general, the component of voltage induced in the stator direct axis winding due to current in the direct axis is $(R_1 + pL_{ds})i_{ds} = R_1 i_{ds} + L_{ds} p i_{ds} + i_{ds} p L_{ds}$. The last term is absent from equation (3.2.1). This was the model adopted in Chapter 4.

The variation of impedance parameters has been outlined in Chapter 2 but will be discussed further in Chapter 5. When parameter variation due to saturation or skin effect is considered, the induced voltages due to this effect are seen to be non-zero. In the consideration of saturation in the main flux path this introduces complications due to the presence of "cross saturation" terms, [Brown, Kovacs and Vas, 1982] and [Melkebeek, 1983]. One possible approach is to assume that the equations remain valid and to include for parameter variation by recalculating the new parameter values at each step of the RK4 procedure.

It is shown in Chapter 8 that the relative magnitudes of the voltages induced due to time variation of the leakage inductance are small in comparison with the other elements of voltage, even the resistive term. Due to system inertia, the variation of rotor impedance with slip, (rotor frequency) is slow and there is no problem with the step-by-step approach. When equations based on currents as state variables are used for modelling of motor starting and the variation of leakage reactance with current

due to leakage path saturation is included, care must be taken to avoid numerically induced oscillations.

Equation (3.2.1) includes stator transients in the rotating reference frame. These may be neglected in order to save computational time. This work considers simulation of the performance of only a single induction motor and the speed of computing was not a problem so this was not done. It is important to note that care must be taken in the neglecting of these terms. Krause et al, [1979] showed that if these stator transients are neglected in the synchronously rotating reference frame then it is equivalent to both neglecting flux linkage and setting the speed, in the speed voltage terms in the voltage equations, equal to synchronous speed.

The most direct method of solving for the currents as state variables is to re-write equation (3.2.1) with the $p\psi$ terms as the subject of the matrix equation. Solution requires the inversion of the impedance matrix. If the parameters are treated as variable, then this should be inverted at each step of the RK4 procedure. This was not done. Instead, the method described below in Section 3.2.2 was adopted at first. Then a second version of the program was created in terms of flux linkages as state variables. This "second version" really only required re-writing the dozen lines of code used for the state equations.

3.2.2. Differential Equations In Terms Of Rotor Quantities

From the definition of inductance, the stator and rotor flux linkages are given by :

$$\begin{bmatrix} \varphi^e_{ds} \\ \varphi^e_{qs} \\ \varphi^e_{dr} \\ \varphi^e_{qr} \end{bmatrix} = \begin{bmatrix} L_s & - & L_m & - \\ - & L_s & - & L_m \\ L_m & - & L_r & - \\ - & L_m & - & L_r \end{bmatrix} \begin{bmatrix} i^e_{ds} \\ i^e_{qs} \\ i^e_{dr} \\ i^e_{qr} \end{bmatrix} \qquad (3.2.2)$$

Substituting for the stator currents in the d and q axes from (3.2.1) yields for the first row of (3.2.1)

$$v^e_{ds} = (R_1 + L_s p)\left(\frac{1}{L_m}\left\{\varphi^e_{dr} - L_r i^e_{dr}\right\}\right) - \omega_e L_s\left(\frac{1}{L_m}\left\{\varphi^e_{qr} - L_r i^e_{qr}\right\}\right) + L_m p i^e_{dr} - \omega_e L_m i^e_{qr}$$

which may be expanded and rearranged to give

$$i^e_{dr} = \omega_e i^e_{qr} + \frac{\left[R_1\varphi^e_{dr} - R_1 L_r i^e_{dr} + L_s p\varphi^e_{dr} - L_m v^e_{ds} - \omega_e L_s \varphi^e_{qr}\right]}{\left[L_s L_r - L_m^2\right]} \qquad (3.2.3)$$

Similarly by substitution for i_{ds} and i_{qs} into the second row of (3.2.1) gives

$$i^e_{qr} = -\omega_e i^e_{qr} + \frac{\left[R_1\varphi^e_{qr} - R_1 L_r i^e_{qr} + L_s p\varphi^e_{qr} - L_m v^e_{qs} + \omega_e L_s \varphi^e_{dr}\right]}{\left[L_s L_r - L_m^2\right]} \qquad (3.2.4)$$

Expanding the third row of (3.2.1) gives

$$v_{dr}^e = L_m p i_{ds}^e + (R_2 + L_{dr} p) i_{dr}^e - (\omega_e - \omega_r)(L_m i_{qs}^e + L_{qr} i_{qr}^e)$$

which can be written as $$v_{dr}^e = R_2 i_{dr}^e - (\omega_e - \omega_r)\varphi_{qr}^e + p\varphi_{dr}^e$$

and since the rotor is a cage rotor this gives $$p\varphi_{dr}^e = (\omega_e - \omega_r)\varphi_{qr}^e - R_2 i_{dr}^e \quad (3.2.5)$$

similarly $$p\varphi_{qr}^e = -(\omega_e - \omega_r)\varphi_{dr}^e - R_2 i_{qr}^e \quad (3.2.6)$$

3.2.2.1. Deriving the stator currents

Once the rotor currents and flux linkages in the dq axes are known the stator dq axes currents may be found from equation (3.2.2) as :

$$i_{ds}^e = \left[\varphi_{dr}^e - L_r i_{dr}^e\right] / L_m \quad \text{and} \quad i_{qs}^e = \left[\varphi_{qr}^e - L_r i_{qr}^e\right] / L_m$$

These may be transformed to give the stator phase currents

$$i_{as} = \sqrt{\tfrac{2}{3}}\left[i_{ds}^e \cos(\theta_e) - i_{qs}^e \sin(\theta_e)\right]$$
$$i_{bs} = \sqrt{\tfrac{2}{3}}\left[i_{ds}^e \cos(\theta_e - \tfrac{2\pi}{3}) - i_{qs}^e \sin(\theta_e - \tfrac{2\pi}{3})\right]$$
$$i_{cs} = \sqrt{\tfrac{2}{3}}\left[i_{ds}^e \cos(\theta_e + \tfrac{2\pi}{3}) - i_{qs}^e \sin(\theta_e + \tfrac{2\pi}{3})\right]$$

It can be seen that the RMS phase current is given as $I_1 = \sqrt{(i_{ds}^2 + i_{qs}^2)} / \sqrt{3}$

3.2.2.2. Torque and acceleration

The expression for electromagnetic torque is given by $T_e^e = pp\left[i_{dr}^e \varphi_{qr}^e - i_{qr}^e \varphi_{dr}^e\right]$ and so the fifth differential equation can be written in terms of the angular velocity in electrical radian per second rather than in terms of actual shaft speed as

$$p\omega_r = \frac{pp}{J}\left[T_e^e - T_{load}\right] \quad (3.2.7)$$

3.2.3. Differential Equations In Terms Of Flux Linkages

Osama, Sakkoury and Lipo, [1993] have pointed out that "cross saturation" can be avoided if the equations are derived wholly in terms of flux linkages.

Writing the equations in a form suitable for solution by the RK4 method.

$$p\varphi_{dr}^e = v_{dr}^e + (\omega_e - \omega_r)\varphi_{qr}^e - R_2 i_{dr}^e$$

$$p\varphi_{qr}^e = v_{qr}^e - (\omega_e - \omega_r)\varphi_{dr}^e - R_2 i_{qr}^e \quad (3.2.8)$$

$$\varphi_{ds}^e = v_{ds}^e + \omega_e \varphi_{qs}^e - R_1 i_{ds}^e$$

$$\varphi_{qs}^e = v_{qs}^e + \omega_e \varphi_{ds}^e - R_1 i_{qs}^e$$

The stator and rotor currents referred to the freely rotating axes are given by equations (3.2.9) to (3.2.12).

$$i_{ds} = \frac{L_m \varphi_{dr} - L_r \varphi_{ds}}{L_m^2 - L_s L_r} \tag{3.2.9}$$

$$i_{dr} = \frac{\varphi_{ds} - L_s i_{ds}}{L_m} = \frac{\varphi_{ds}}{L_m} - \frac{L_s \left(L_m \varphi_{dr} - L_r \varphi_{ds} \right)}{L_m \left(L_m^2 - L_s L_r \right)} \tag{3.2.10}$$

$$i_{qs} = \frac{L_m \varphi_{qr} - L_r \varphi_{qs}}{L_m^2 - L_s L_r} \tag{3.2.11}$$

$$i_{qr} = \frac{\varphi_{qs} - L_s i_{qs}}{L_m} = \frac{\varphi_{qs}}{L_m} - \frac{L_s \left(L_m \varphi_{qr} - L_r \varphi_{qs} \right)}{L_m \left(L_m^2 - L_s L_r \right)} \tag{3.2.12}$$

These could be algebraically substituted into the set of equations (3.2.8) but were instead computed within each step of the RK4 procedure. This was done to allow access to the axis currents and hence the phase currents. Although this includes currents in the numerical process it is quite different from treating them as state variables since it avoids the differentiation of inductances that arises in that case.

In the work by Osama et al cited above, the leakage inductances are treated as constants even though simulation results are presented for direct on line starting. It is significant that the comparison given in the work by Osama et al is between two different methods of simulation rather than between simulated and test results. As such, the problem of leakage path saturation is avoided by excluding it from both models. The method will not give accurate results when used to simulate starting performance of motors with significant leakage path saturation. The significance of this is discussed in detail in the first part of Chapter 5 where it is shown that the mean errors caused by neglecting leakage path saturation in the prediction of starting current was 20% (based on a population of 52 motors). In contrast, the magnetising reactance value is shown in Chapter 4 to have little effect on the outcome of the simulation of starting conditions. (Although it has been shown to affect the accuracy of behaviour in the region of normal operation, [He and Lipo, 1984].)

It seems therefore that both types of saturation need to be included in a general model so that the complete range of motor performance may be modelled accurately for different motor designs.

3.2.4. Conclusion Of Section 3.2

It is suggested that the general model for induction motor studies should be based on machine equations in terms of flux linkages rather than currents to avoid "cross saturation". The variation of parameters is discussed in detail in Chapter 5. This variation should be included within the RK4 solution of these equations by applying :

the double-cage rotor model to allow for skin-effect,
the main flux saturation model [Osama et al, 1993] and
the describing function method to allow for leakage path saturation.

The circumstances in which each of these should be applied, and where they may be neglected, are discussed in Chapter 9 based on the simulation work done in Chapter 8.

3.3. Simple Model For The Supply System

In this section several ways of representing the motor supply will be reviewed. It will be shown in Chapter 8 that the use of an infinite-bus approximation for the supply is to be avoided in the simulation of motor starting. The simple approximate models described here are shown to give adequate representation of the starting performance except in extreme cases. Guidelines are given in Chapter 9 for the selection of an appropriate model for the system bus.

3.3.1. Rejection of the Infinite bus model

This simply assumes that the motor terminal voltage will remain constant during the starting period. The IEEE "Brown Book" [1980] stresses that the use of accurate values for utility and generator transient impedances is important. Clearly this is so since the presence of a small voltage drop will reduce starting current and torque and prolong the run-up time. It is difficult to imagine a situation in which a numerical simulation is to be conducted and the use of an infinite bus approximation for the supply is justified. Even the simplest estimate of starting current and torque require the voltage drop due to line impedance to be considered. The Brown Book's impedance method indicates that for an infinite bus voltage of V_{bus} connected to the motor through a line of impedance Z_{line} as shown in the circuit model of Figure 3.1, the voltage, V_1 at the motor will be given by equation (3.3.1).

$$V_1 = V_{bus}\frac{Z_{motor}}{Z_{motor}+Z_{line}} \qquad (3.3.1)$$

Another way of expressing this is in terms of starting kVA and system fault level :

$$pu\_Voltage\_Droop = \frac{Starting\_kVA}{Starting\_kVA + Fault\_Level\_kVA} \qquad (3.3.2)$$

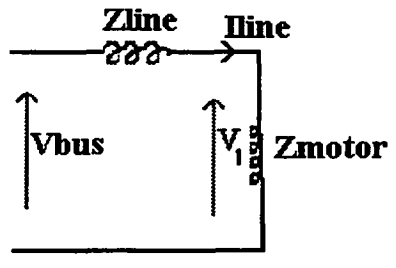

Figure 3.1 : Simple model for voltage dip during starting

Taking the effective rotor-circuit resistance as R_e and assuming that during starting, the magnetising current is negligible so that the rotor current, I_r equals the line current, then the electromagnetic torque produced, T_e is given by :

$$T_e = 3\frac{V_{bus}^2 R_e}{(Z_{bus}+Z_{motor})^2 s\omega_s} \qquad (3.3.3)$$

Simple error analysis will show that the torque produced is twice as sensitive to voltage variation as it is to frequency and that the total impedance of the motor and bus is also significant. If run-up times are required then the errors will be integrated over the run-up period. However in this case, the effect of errors in the describing function for the load on the motor and the correct modelling of motor parameter variation also become significant. This is discussed further in Chapter 8 and guidelines are given in Chapter 9.

3.3.2. Simple Approximate Models

The following simple models are recommended as initial checks on the system before running a detailed simulation. As indicated they do not give definitive results. They are used within the expert system algorithm in Chapter 9 to assist the selection of more sophisticated models or clarify the need for additional data.

3.3.2.1. Minimum generator size

Private correspondence with consultant engineers at Kennedy and Donkin (in the UK) has suggested the following rule of thumb may be used to determine the minimum generation kVA required to start a motor satisfactorily :

$$\text{kVA\_Required} = \frac{(motor\_starting\_kVA)(0.98 - \delta V)}{(Fault\_Level\_kVA)(\delta V - 0.02)} \qquad (3.3.4)$$

This yields for a system fault level of 5 pu (on a motor kVA base), a motor starting kVA of 6 pu and voltage drop of 0.15, a value for the generator kVA of 7.7 times the motor kVA, which seems reasonable. This agrees roughly with the author's experience with generators for offshore oil platforms. In that application, voltage dips of 25% are often tolerated during the starting of selected large motors. A generator rating of five times the rating of the largest motor is about as small as I would recommend without a detailed multi-bus study; ie generator kVA approximately equal to the motor starting kVA at rated voltage. The main problem with such simple rules of thumb is that they do not allow for motor load torque characteristics which may cause the motor to fail to run-up to speed in a reasonable time. The effect of increased current drawn by any motors already running is also neglected.

It has been suggested, [Barber, 1982] that for a single large motor starting from an unloaded diesel-engine-driven generating set, the generator kVA may only need to be of the order of 0.56 times the motor starting kVA (ie about 3 times the motor rating). This seems a little optimistic. It assumes a 10% overload capacity on the engine (standard) and leads to a voltage dip of the order of 25% which is assumed to have been compensated for by the time the maximum power demand occurs. The example given was based on a motor with a maximum torque of 2.8 pu occurring at 0.18 pu slip. This implies a maximum motor power (output) of less than 2.5 pu. Since half the power during acceleration is going into stored energy in the rotating masses, the power input could be up to 5 times motor rating.

3.3.2.2. Frequency droop

The rate of frequency decrease, (Hz/s) during motor starting, may be taken simply as

$$\frac{df}{dt} = \frac{f\Delta P}{2H_{gen}} \qquad (3.3.5)$$

where

H_{gen} is the inertia constant (s) of the total generator capacity
+ connected motor loads,

f is the system frequency (Hz),

ΔP is the power taken from the power system by the motor during starting
(pu on generator base).

Using the IEEE "Brown Book" estimate of starting power factor of 0.2 and assuming a ratio of starting kVA to kW rating of 5.8 it can be seen that a frequency droop of

4% (to 48 Hz on 50 Hz systems) will be reached after a starting time, t_{start} given by equation (3.3.6).

$$t_{start} = \frac{2H_{gen}(pu\_freq\_droop)}{0.2 * 5.8 * motor\_Rating} = \frac{0.07H_{gen}}{Motor\_kw} \qquad (3.3.6)$$

where the motor rating is expressed on a base of total generator power.

3.3.2.3. Other motors

In many motor starting studies, the behaviour of motors already running, contributes to the system disturbance. The main problem with these motors is the gathering of appropriate data and the ability of the available simulation program to accommodate multi-machine studies. If the motors are old it may be difficult to persuade manufacturers to provide data which would have been more readily available at the time the motor was purchased. This emphasises the need to keep a file on each large motor in a system for use in future simulation studies, eg prior to the next upgrade of plant.

In the extreme, each motor may be represented in detail in the manner suggested by section 3.2. This would not normally be the case unless a small number of large motors were to be supplied from a small generation system and the cost of a detailed study could be justified. This might be the case if the minimum generation size mentioned above were approached and detailed data was available to allow full representation of the actual governor and AVR characteristics as well as individual load curves and full representation of motor parameter variation during run-up. It is however, likely that gains sought from the more detailed representation of the system would be lost in data inaccuracy. It is the experience of the author that, all too often, data items are provided with large tolerances to cover manufacturing variation and this provides a limit which is as significant as the errors caused by using approximate models for motors not actually being started.

The simplest approximation is that motors already running continue to behave as constant kVA loads throughout the run-up of the motor being started. Adequate representation of these running motors will usually be achieved by equivalent circuit models as Figure 2.1.1. These should use appropriate low frequency values for the motor impedances and unsaturated values for leakage reactance. The use of a model which includes the effect of voltage depression on the magnetising reactance of running motors is also implied by the work of Osama, Sakkoury and Lipo, [1993] discussed in Section 3.2. It will be shown in Chapter 8 that a reliable load characteristic and accurate impedance data for each motor and its connection to the bus is more important than differential equation representation of the running motors. Operation of protective circuits may also need to be simulated.

3.3.3. Representation of AVR and Governor Action

Once the initial 0.5 s of starting has elapsed, the effect of system voltage regulation may be experienced. The neglect of this will lead to an over-estimate of starting time. The detailed modelling of the effect of voltage regulator characteristics on synchronous generator performance is well established, [Concordia, 1944]. Standard models exist for the representation of voltage regulator response, [IEEE, 1968]. The work of Abu-Elnaga and Alden, [1988] was reviewed and considered but ultimately not used. This was because it was found that the reduced simple model for the system bus successfully reproduced the order of magnitude of the voltage and frequency

deviations required for the purposes of this thesis which concentrated on the motor model.

Fairly early on in the work associated with this thesis it was recognised that uncertainties in the motor model would be the main focus and that modelling of the power system and motor load would be restricted to reproducing just sufficiently realistic a response to enable an assessment to be made of the effect of neglecting various factors in the supply model and mechanical load. As a consequence, sophisticated modelling of the synchronous machine(s) acting as the supply was not attempted. Such modelling is allowed for by the EMTP-type programs but requires a significant amount of data before it can approach a realistic prediction of the detailed system response. This approach has been vindicated by the simulation results of Chapter 8 which show that first order approximations to the modelling of voltage dip are the most critical feature.

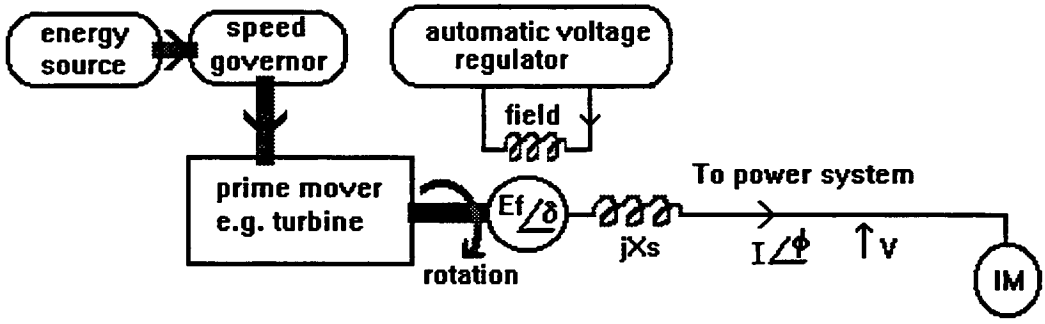

Figure 3.2 : Simple model for power system showing components to be included in terms of their basic first-order responses.

3.3.3.1. Simple model for AVR and governor

The AVR action was represented by a simple first order model

$$\frac{dE_f}{dt} = K_e f\left[\sqrt{\tfrac{2}{3}}V_{line} - V_{peak}\right] \qquad (3.3.7)$$

An exciter ceiling was added to ensure that the excitation voltage, E_f did not exceed 1.5 pu. The peak phase voltage, V_{peak} was determined from

$$V_{peak} := E_f - Z_{line} * Z_{base} * \text{Average line current.} \qquad (3.3.8)$$

Where Z_{line} is the pu line impedance (real part ignored)

The prime mover speed, ω_g was influenced by $\frac{d\omega_g}{dt} = \left[T_{pm} - T_g\right]/\left[K_j J_m\right]$ (3.3.9)

where

T_{pm} is the torque produced by the prime mover

T_g is the torque exerted on the prime mover by the motor.
(T_g was calculated from the input power to the motor and the prime mover speed)

K_j is the ratio of prime mover inertia to inertia of the motor and load

J_m is the polar moment of inertia of the motor and connected load.

The governor action was simulated by another first-order response with a limit on the maximum torque of 1.1 times the maximum torque based on a prime mover rating K_j times the motor rating.

$$\frac{dT_{pm}}{dt} = K_j K_t\left(\omega_{ref} - \omega_g\right) \qquad (3.3.10)$$

These approximate models for the generator control, and in fact the representation of the system by a single generator, are shown to have the desired result of producing a realistic looking voltage and frequency response which can be tailored to suit the starting studies which are the focus of this thesis. It is noted that such simple models would not be as effective in the determination of transient stability limits or long-term bus transfer problems.

3.3.4. Conclusion of Section 3.3

It is recommended that a staged approach be adopted to the representation of power systems in motor starting studies. In the preliminary stage of the study, the rules of thumb and simple single-reactance representation of the motor should be applied before equivalent circuits are used. At this stage it is more important that the parameter values are correct than that the models are sophisticated.

The simple models used for representing the AVR and governor response have been outlined and these will be shown in Chapter 8 to be adequate for the purposes of this study.

3.4. Summary Of The Turbo-Pascal Program IM_SIM.PAS

The production of this program was expensive in terms of time but was nevertheless important because without it, the ability to modify the code to effect changes in the models used for the representation of particular phenomena would be absent.

IM_SIM.PAS was written in Turbo Pascal and uses four Turbo Pascal units called PART1, PART3, PART5, and PART7 as well as HGRAPH units for graphical output. A version of the program has been created called IM0_SIM.PAS which does not produce screen graphics and does not use HGRAPH units. This is because for some systems it may be more convenient to run the program to produce the output text files and use another program package to display the graphs, eg if the HGRAPH software is unavailable.

The independent variable for the simulation was time in seconds and the system state variables were stator and rotor flux linkages. To avoid ambiguity arising out of the choice of different power bases for the pu system, the calculations were expressed in terms of SI units. When comparison between the results of this program and other programs (such as INSPEC/INSTART) was necessary, care was taken to ensure that they were expressed using the same base convention.

IM_SIM.PAS is faster than INSTART and produces graphs on the screen during the run-time. Exceptions to this are when either the No_Graphs option is selected or the files are saved in archive format (see later). Selected saved variables are written to a sequential text data file with a name unique to the motor and the model used. They are not necessarily the state variables. This output file may be accessed by other

applications for graph plotting. In addition, the program searches for numerical measures of the simulation output, called yields and writes these to an output file defined in the CONST declaration of the main program segment, IM_SIM.PAS. These yields are defined in Chapters 4 and 6 where they are used to assess the relative the effect of various factors on the simulated output.

Each modification made to the original program was compared with the previous version so that gradually a picture was built up of the significance of each included variation; for example,

- the effect of temperature on the simulated output (Section 5.4)
- the effect on the simulation output of using a UDB model (Alger's formulae) as opposed to the DCC rotor model, (Section 5.2).
- the various ways of modelling leakage path saturation.

This would have been impossible without the ability to modify source code.

The program uses a control file, defined in the CONST statement at the start of the main program unit, which defines the motor data file and the motors to be simulated. This makes the program more flexible. Because the source code is available, it may be modified to suit particular purposes, eg. control of selected plotted data to create the space phasor plots shown in Chapter 8. However the default version of the program may be run without any knowledge of its internal working. This version is described in Appendix 1 at the end of the thesis.

4. FACTORIAL ANALYSIS WITH FIXED PARAMETERS

In this chapter the method of factorial analysis of experimental design is introduced and applied to the analysis of the output of the program used for the numerical simulation of the direct-on-line starting of induction motors. The results of a preliminary study done by the author in 1988 using a constant parameter RK4-based simulation are given. The constant parameter model was used at this stage of the work because the investigation into the effects of parameter variation was done later. An earlier version of the program simulation model discussed in Chapter 3 was used. This did not include the procedures for modelling leakage path saturation nor for skin-effect in the rotor. The conclusions of the work are nevertheless valuable since they confirm in a rigorous way that the equivalent circuit parameters such as stator and core-loss resistance and magnetising reactance have little effect on the dynamic performance of motors. The unimportance of the proportional split of total leakage reactance between stator and rotor was also confirmed. Attention is directed towards the supply system which is often neglected in the discussion of accurate models.

It is shown that, where model parameter variation during the simulation can be neglected, errors in values used for the system voltage and frequency will have more effect on the predicted performance than similarly sized errors in other input data items. Adequate modelling of supply system variation is shown to be more significant than accurate determination of some of the motor equivalent circuit parameters. For some motors, there are gross variations in the total leakage reactance and rotor resistance during the simulation period. It is shown that, when this occurs, careful attention must be paid to the modelling of these variations.

The material in this Chapter was presented at the 1991 AUPEC Conference, [Arneaud, 1991].

4.1. Description Of The Factorial Method

Factorial design studies have been found to be useful where the outcome of an experiment is determined by several independent factors; [National Bureau of Standards, 1957]. The first wide use of the method was in agricultural research and the terminology reflects these origins.

In general, a given combination of factors, (a **treatment**) is applied to a **plot** and the outcome measured as a **yield**. For each of the yields, a **coefficient of performance** is evaluated which relates a change in yield attributable to each of the variable factors. If there are L factors applied in N combinations to produce M yields then the COP which measures the influence of the Kth factor to the Ith yield is given by :

$$COP_{IK} = \frac{1}{N}\sum_{J=1}^{N} Y_{JI} T_{JK} \qquad (4.1.1)$$

Where Y and T are the arrays of yields and treatments. Negative COPs indicate that an increase in the particular factor leads to a decrease in the corresponding yield.

The COP defined above relates to "main effects" ie. the effect of factors acting alone. The effect of simultaneous variations in two factors may also be computed in a similar way. In general, two factor interactions are usually smaller than the main effects and

in this study, this was found to be so. However this cannot be taken for granted and for this reason the factorial method was preferred to a simple sensitivity analysis which would have yielded the main effects only.

Some definitions are given below :

Factor

A parameter, the value of which may influence the outcome of an experiment. Factors are assumed to be independent of one another in so far as the process is concerned. For the machine simulations this means that altering one data item in the program input data file does not affect the others. (It does not mean that two parameters nominated as factors are independent of one another in the motor design process).

Treatment

A given combination of factors each at a given level constitutes a treatment, eg. in an experiment to investigate the influence of four factors A,B,C,D; a particular treatment may consist of high levels of A and D together with low levels of B and C. Such a treatment is referred to as the treatment 'ad'.

Plot

An experimental unit to which the treatment is applied. In some experimental work it is necessary to either assume that all the plots are identical or to group treatments in blocks which may be completely or partially randomised.

Yield

A measurable outcome of an experimental process.

Coefficient of Performance (COP)

A signed parameter which is a measure of the extent to which a yield is affected by the level of a particular factor

Main Effect

The effect of a factor acting alone. These are usually the most significant effects.

Interaction

The effect of two or more factors acting together. In some circumstances, this can be larger than the effect of either acting on its own

4.1.1. Fractional Factorial Designs

A complete factorial design study having n factors each at two levels requires 2^n measurements for all the combinations of the n factors. A fractional replicate that uses a subset of 2^{n-p} measurements from the original 2^n is known as a $1/2^p$ replicate. The reduction in the number of measurements needed is obtained at the cost of losing (confounding) some information on main effects and/or higher order interactions. Standard fractional experimental plans with the extent of confounding for each main effect and/or interaction are given in tabular form in the US National Bureau of Standards publication referenced above.

The fractional factorial method was later applied to determine the effect of manufacturers' tolerances (to AS 1359.69 Table 69.1) on the motor's equivalent circuit parameters derived from quoted performance data. This work is described in Chapter 6. A complete factorial analysis was used in Chapter 8 to assess the effect of various system variables on the simulated output.

4.2. Application To RK4 Model Simulation

Factorial design methods have been used in cases other than in agricultural studies. They may be used in any situation where the outcome of a process depends on a number of independent factors. The method may be applied to numerical simulations by considering the input data as the factors and the program output as the yields. The COPs relate the sensitivity of yields to variations in single input data items or groups of items acting together.

4.2.1. Previous Work

The method of factorial analysis was applied by Kopilov, Ilyinski and Kutnezov, [1970] to the starting of induction motors and this was extended by Smith and Hamil, [1973] to include switching, reconnection and plugging. The latter work is a rare and interesting example of the application, by researchers outside the USSR, of experimental planning techniques to the simulation of rotating machine performance. However, as a result of the experience gained during the whole of the work reported on in this thesis, it can be said with some confidence, that for the switching, re-connection, and most certainly for the plugging, the motor models used were inadequate.

In both of these studies the supply voltage and frequency as well as the total inertia were assumed to be known and constant. No account was taken of leakage path saturation or motor parameter variation with slip. The computing process (hardware and software) constituted a plot, with defined data items being factors. The result of each computer simulation was a set of graphs of electromagnetic torque, current and speed against time for the period of run-up.

4.2.2. The Constant Parameter Study

During the study reported on in this chapter, the constant parameter motor model was also used but the supply bus was assumed to be finite so that system voltage and frequency were considered to be variable factors. For the purposes of numerical comparison, specific quantities were defined as yields. The plots were assumed to be identical, ie each run of the program with the same data is assumed to give the same output. (Whenever this was checked, it was found to be so).

The simulation was based on a fourth order Runge-Kutta (RK4) solution of the six simultaneous differential equations for the induction motor expressed in terms of rotor quantities as described in Section 3.2.2 but referred to stationary dq axes. Supply voltage and frequency were taken as factors affecting the yield, as was total inertia of motor and load. Total leakage reactance was considered rather than separate stator and rotor components.

In the present case, the seven data items can be applied to the RK4 simulation program in $2^7 = 128$ combinations. A fractional factorial design was used to reduce this to only 32 treatments. Each treatment constituted a program run with an appropriate combination of data items as defined by a standard experimental plan. The 1/4 fractional experimental plan for seven factors (US National Bureau of Standards, Plan 4.7.4) was used. This defines the combinations of data items which are to be applied to the simulation. For example, the first four treatments are given below in Table 4.2.1 . This means that for the first program run, all data items were set at their nominal values (zeros in Table). For the second run, all items except R1 and J were increased by a given percentage increase.

A	B	C	D	E	F	G
R1	Lm	J	Ll	R2	f	V
0	0	0	0	0	0	0
0	1	0	1	1	1	1
1	1	1	1	1	1	0
1	0	1	0	0	0	1

Table 4.2.1 : First four treatments of US National Bureau of Standards plan 4.7.4

With this plan, second order interactions between factors AB, CA, CB, EA EB and EC are confounded and hence not measurable. By selecting the designation of factors carefully it was possible to render this less important. By assigning factors as in Table 4.2.1, the effect of the following pairs of factors acting together were not measurable:

R1, Lm R1, J Lm, J R2, R1 R2, Lm R2, J

R1, Lm and J will be seen to have little effect on the dynamic simulation and it was thought that their second order effects would be smaller still. There was some concern about the last pair as it was thought that R2 and J might interact. A trial run was made with one set of machine data with the designation of the factors re-ordered so that R2 was swapped with f, making any R2, J interaction available. The interaction was found to be negligibly small. It is noted that in some experimental situations this is not the case; eg where the presence of two chemicals together is required to initiate a reaction.

4.2.3. Definition of Numerical Simulation Yields

In order to be able to assess the effect of varying the program data, the graphical output was defined in terms of yields as Figures 4.2.1 and 4.2.2 and Table 4.2.2. Additional yields are defined in Chapter 6 where factorial analysis is applied to the effect of tolerances in quoted performance data on the predicted performance during starting.

TPM	pu peak positive transient torque.
TPS	pu peak torque after decay of electrical transients (pull-out torque).
t3	time for TPS
TP1	first peak transient torque.
CP1	pu peak transient line current
t1	time for TPM
t5	time for the pu speed to settle between 0.95 and 1.05 pu
t2	time for TP1
t4	time for CP1

Table 4.2.2 : Definition of the nine numerical simulation yields which are used in Chapter 4

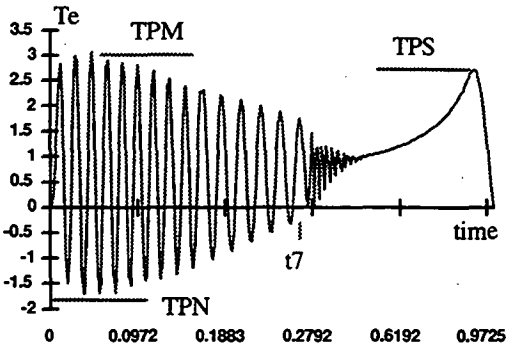

Figure 4.2.1 : pu Torque against Time in seconds

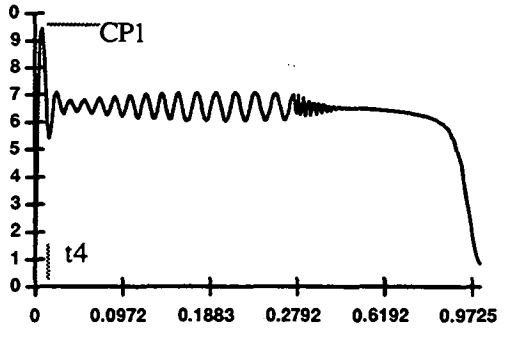

Figure 4.2.2 : pu Stator Current against Time in seconds

During the simulation the yields were determined by a search routine within the RK4 procedure. A visual check on the torque, current and time graphs against speed (plotted on the PC's screen) was also made to ensure that the simulations were well behaved. Mean COPs were calculated for a range of 15 machines whose data was taken from work done by the following authors :

1) Cathey, Cavin & Ayoub, [1973],
2) Sastry and Burridge, [1976];
3) Smith I R and Hamil B, [1973]
4) Sen Gupta and Lynn, [1980].

This set of motor data is reproduced in Table 4.2.2 at the end of this chapter.

4.2.4. Results of the study

The calculation of the COPs was computationally intensive and no attempt is made to present the mass of data used in the process. A few cases were done by hand as a check, using equation 4.1.1. Confidence was obtained in the results by random visual checks on the algorithm used for evaluation of the yields as defined in Section 4.2.3. This was done using graphs plotted on the PC's screen during the simulation. Similarly, the program used for calculating the mean COPs was checked using dummy data. The method was then applied to all 15 motors in the data-base using an early version of the simulation program described in Chapter 3. Data for the experimental plan was contained in a data file as a seven-bit binary word as shown in Table 4.2.1. The original input data to the RK4 simulation program was then modified by an appropriate amount. This process was also checked by dumping the modified data into a diagnostic output file and checking it against the variation required by the experimental plan designated 4.7.4 by the US Bureau of Standards.

The percentage variation of the nominated factors was varied from 5% to 30% in steps of 5%. This meant that there were 32 cases for each fractional experimental plan and each plan was performed 6 times for each of 15 motors. This gave a total of 2880 Runge-Kutta simulations of the six simultaneous differential equations based on full dq representation of the motor. Step sizes were set within the RK4 procedure in an automatic manner as described in Chapter 3. Stator transients were not ignored. The simulations took a long time (on an AT PC at that time) but this was unimportant since they were done by the PC while the author was doing something else.

For each of the nine defined yields, the mean percentage COPs for each of the seven factors were calculated for the fifteen machines studied and for the six levels of factor variation. The results are shown in Figures 4.2.3 to 4.2.11 as graphs of mean COP for each yield as a function of percentage factor variation. The standard deviation of the population of COPs was also determined to justify the use of the mean as a statistical measure. An assessment of the statistical significance of the means was made using the Students t distribution, [Dally , Riley and McConnell , 1984]. This means that the lines shown in the graphs can be imagined to have a width which is proportional to the coefficient of variation, C_V where

$$C_V = \text{Standard Deviation / Mean} \qquad (4.2.1)$$

For example, for the Figure 4.2.3, the mean COP shown is accurate to within $\pm 3\%$ of the true mean with a reliability of 95% for all points on the curve for frequency, f . Such a narrow tolerance band and good reliability of the computed mean was typical of all the uppermost curves in the Figures 4.2.3 to 4.2.11.

Standard deviations increased with level of factor variation. This meant that, in general, the greater uncertainties in the calculated means were associated with lower absolute values of the mean COPs. For example, for the curve for inertia, J shown in Figure 4.2.3, the means are not statistically significant. More precisely, the true mean COP is known with a 90% reliability to be within about $\pm 20\%$ of the line shown, a fairly broad tolerance. Since the main purpose of the exercise was to establish an order of importance of the factors and not to quantify precisely the mean COPs of the factors of lesser importance, this vagueness for some mean COPs does not pose a problem .

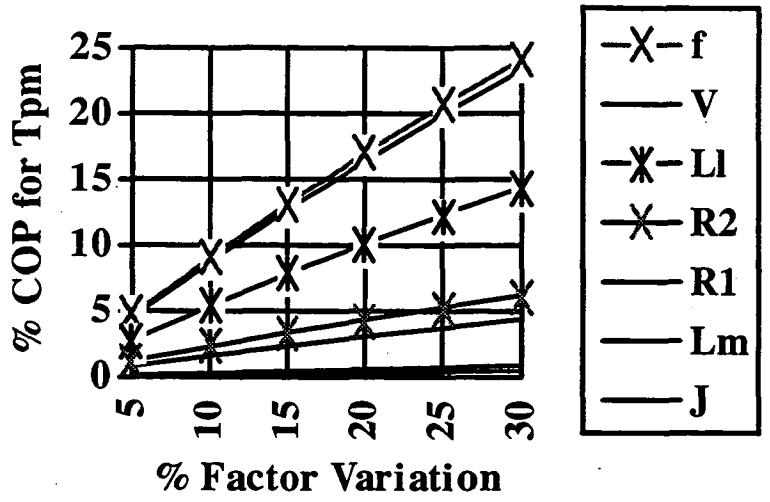

Figure 4.2.3 : TPM, Peak positive transient torque

Figure 4.2.3 shows the graph for TPM. This was found to be mainly dependent on the voltage and frequency of the supply, ie on the flux level. A 30% increase in leakage reactance had as much effect as about 18% change in supply voltage.

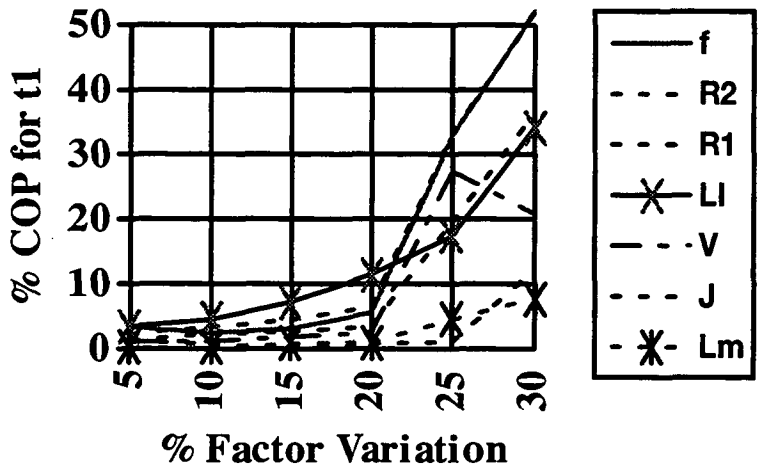

Figure 4.2.4 : t1, time for TPM

The results for t1 were inconclusive, especially for large increases in the factors where the standard deviation across the range of motors was too large to make the results significant.

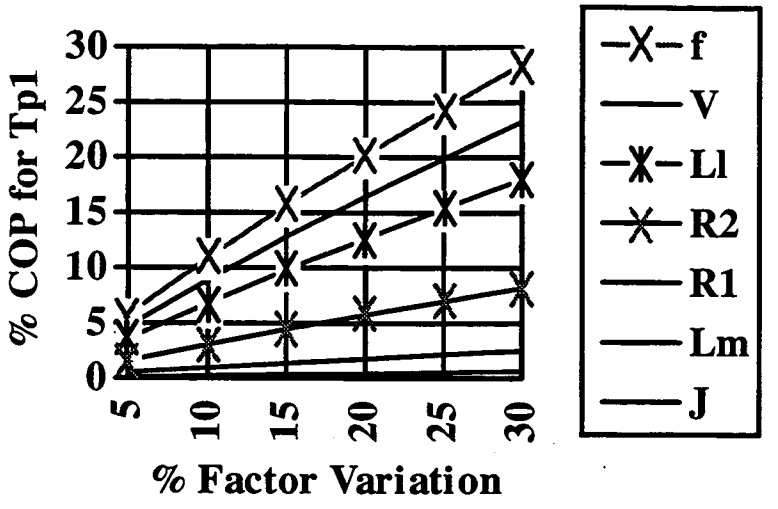

Figure 4.2.5 : TP1, first peak transient torque

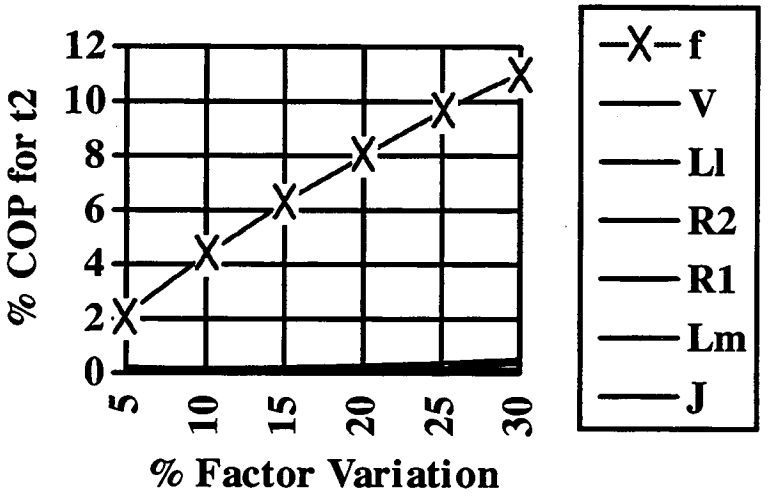

Figure 4.2.6 : t2, time for TP1

The graph for t2 shown in Figure 4.2.6 and for t4 in Figure 4.2.10 are perhaps obvious results but at least they confirm that the method performed sensibly. In practice, the frequency variation would not be large relative to the voltage depression unless a very small motor was started on a system with low supply reactance.

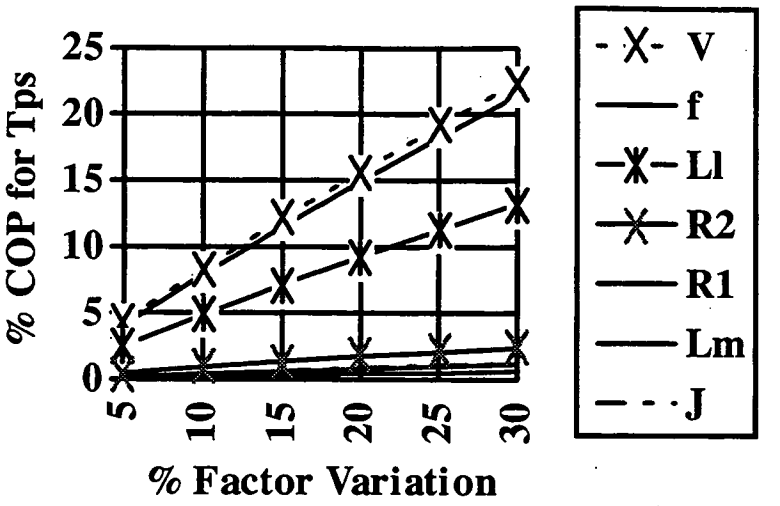

Figure 4.2.7 : TPS, Peak torque after decay of electrical transients.

Again, this result is not surprising except that it underlines the importance of not assuming an infinite bus supply when modelling motor starting. In this simple study the load was assumed to be purely inertial. If the load torque was modelled as a polynominal function of speed then it is possible that for sufficiently reduced voltage, the motor might fail to start in a reasonable time due to reduced net accelerating torque.

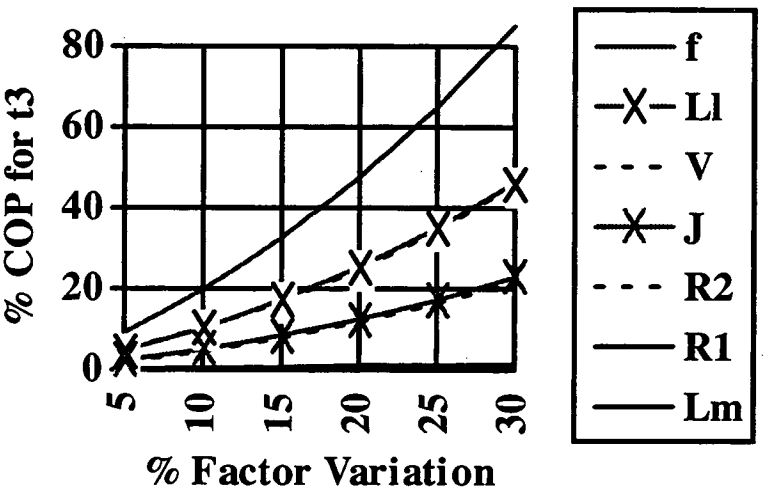

Figure 4.2.8 : t3, time for TPS

Figure 4.2.8 shows that the time at which TPS occurred was primarily dependent on the supply frequency and then on the leakage reactance and supply voltage to an equal extent. The load inertia and rotor resistance were also of equal influence. This result may be compared with the simulated performance given in Chapter 8 for a variable parameter motor model.

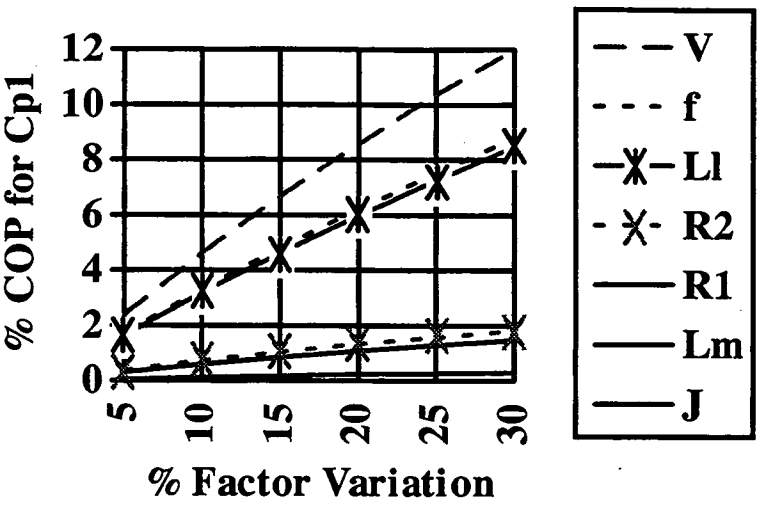

Figure 4.2.9 : CP1, pu peak transient line current

This graph indicates that the simple methods outlined in Section 2.4.2 for the prediction of transient current (and torque) cannot be relied on unless an accurate value is available for the supply voltage during the switching operation. Due to line impedance, the current and voltage affect one another. This interaction can be made more complex due to leakage path saturation affecting the value of motor leakage reactance. This is shown in Section 8.2 where all these effects are considered.

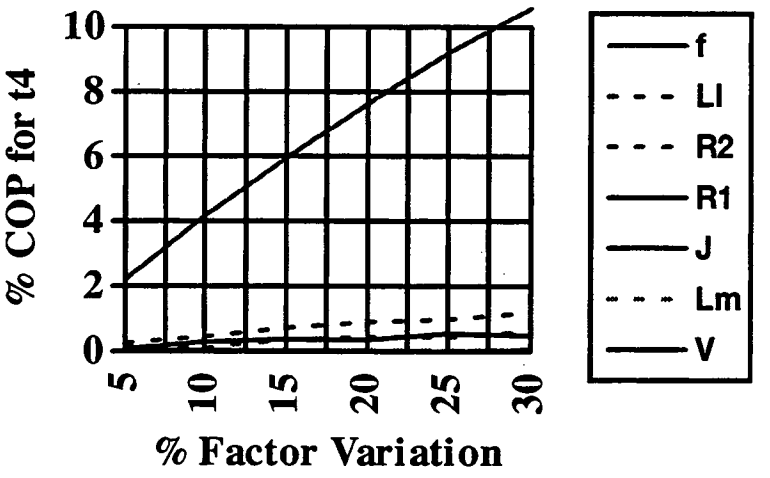

Figure 4.2.10 : t4, time for CP1

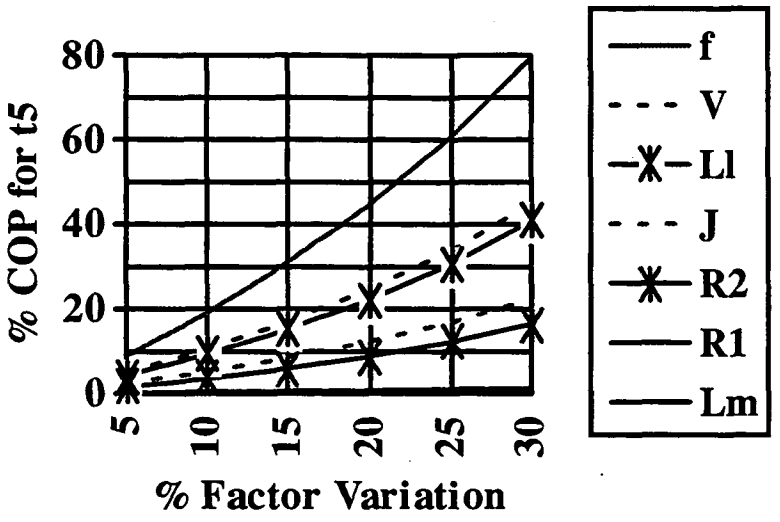

Figure 4.2.11 : t5, time for the pu speed to settle between 0.95 and 1.05 pu

4.2.5. Discussion of Results

The results for each Main Effect are shown in Figures 4.2.3 to 4.2.11. As expected, all mean COPs increased with the percentage factor variation. In general, it was seen that the variations in voltage and frequency were more significant than variations in the other factors. Total leakage inductance was of next importance. The system inertia was of relatively minor significance affecting only the times t3 and t5 and even then not being as significant as frequency, voltage or leakage reactance.

Typically, the mean percentage COPs for f and V were about 1.5 times that of the most significant machine parameter, Ll. For example, with TPM, a response coefficient of 10% was achieved with about 12% variation in f and V compared with a required variation of 10% in Ll for the same effect. COPs for R2 and J were usually less than half those of Ll. Variations of less than 20% in R1 and Lm produced relatively small coefficients.

For the yield, t1, at levels of factor variation greater than 25% the standard deviations were too large for the means to be considered statistically valid for the population of 15 motors. By examination of the simulation graphs it was seen that for some machines, at a particular treatment, the 'first-peak' and 'maximum-peak' torques ceased to be coincident at a particular treatment level and this led to a discontinuity in the t1 value. This was not pursued further. This time, t1 was included as a yield in an attempt to define the shape of the transient torque curve. In practice, it is not usually of great significance, though the magnitude of the transient torque is.

The two-factor interactions were seen to be of relatively minor significance compared with the main effects and have not been plotted but are shown in Table 4.2. It is noted that they need not have been of minor importance. If for example the changes in V and f had been taken in opposite directions then this would have led to a change in the flux level. As it was, the voltage and frequency were assumed to change in the same direction and this had a marginal effect on the simulated performance. The dominant effect of variations in V and f can be seen in Table 4.2 which shows the effect of pairs of factors acting together. Only yields t3 and t5 were found to have mean COPs greater than 10%. These were to combinations of V, f and Ll.

Yield	Mean % Coefficient of Performance with 30% Factor Variation		
	>10%	5% to 10%	1% to 5%
t3	[f,Ll]; [V,f]	[V,Ll]; [f,J]; [f,R2]	[V,J]; [Ll,J]; [V,R2]; [R2,Ll]
t5	[V,f]; [f,Ll]	[f,J]; [V.Ll]; [f,R2]	[V,J]; [Ll,J]; [R2,Ll]; [V,R2]
Tp1		[V,f]; [f,Ll]	[f,Ll]; [V,Ll]; [f,R2]; [V,R2]; [R2,Ll]
Tpm		[V,f]	[f,Ll]; [V,Ll]; [f,R2]; [V,R2]
Tps			[V,f]; [V,Ll,]; [f,Ll]
Cp1			[V,f]; [V,Ll,]

Decreasing significance ----->>

Table 4.2 : Major Two-Factor Interactions

4.3. Conclusions From This Initial Factorial Analysis

The results of this preliminary study show that for machines where the machine parameters do not vary during the simulation period, it is more important to consider the deviation of the system frequency and voltage from their nominal values than to obtain accurate machine parameters. If, for example, the system voltage and/or frequency are expected to deviate by 10% then this will have as much effect on simulation yields as an error of 20% in leakage reactance. For example the work of Ansuj et al, [1989] claims that motor performance may be calculated to less than 1%. This is based on the assumption that the supply is at its nominal value. Over a period of time, the value of the supply voltage is distributed over a tolerance range. The simulation of critical functions may need to take this into account.

Chapter 5 will consider the changes in rotor parameters which occur with current and slip. For machines where saturation or deep-bar effects are significant, machine parameter changes of the order of 200% can occur. Bus voltage dips are usually restricted to 6% in domestic and commercial situations and to within 20-25% for marine or offshore installations. The system frequency is usually held to within 5% even during "Black-Start" operations on offshore platforms. In such cases, accurate modelling of the power bus voltage and frequency deviations is likely to be less important than including the variation of leakage reactance and rotor resistance during starting.

Even though the results of the work reported on in this chapter are strictly applicable to constant-parameter motors, they were useful in that they acted as a guide to future work. In particular, the study focussed attention on the leakage reactance and rotor resistance variation and led on to the work of Chapter 5.

In addition, the work was a first application of a method which is used in Chapter 6 to determine the sensitivity of derived circuit parameters and simulated performance to tolerances in quoted performance data. It is noted that similar work could be performed using dimensional and material parameters as input data to a factorial design study based on a motor design algorithm. Such work is outside the scope of the present thesis which focusses on performance modelling.

Table 4.4 : Data Used For Fractional Factorial Design Study (All SI Units, not per-unit)

R1	Lm	J	L1	R2	f	Vll	Pout	PP	Machine ID	Data Source
0.435E+00	0.693E-01	0.445E-01	0.200E-02	0.816E+00	60.	220.0	0.224E+04	2.	A	1
0.404E+00	0.526E-01	0.312E+00	0.290E-02	0.626E+00	60.	208.0	0.224E+04	3.	B	2
0.146E+00	0.267E-01	0.379E+00	0.160E-02	0.206E+00	60.	208.0	0.560E+04	3.	C	2
0.245E+01	0.420E+00	0.102E+00	0.170E-01	0.245E+01	50.	400.0	0.560E+04	3.	D	3
0.100E+00	0.257E-01	0.100E+01	0.800E-03	0.100E+00	50.	173.2	0.100E+05	3.	E	4
0.249E+00	0.587E-01	0.277E+00	0.150E-02	0.536E+00	60.	460.0	0.187E+05	2.	F	1
0.870E-01	0.347E-01	0.831E+00	0.800E-03	0.228E+00	60.	460.0	0.373E+05	2.	G	1
0.310E-01	0.189E-01	0.222E+01	0.400E-03	0.134E+00	60.	460.0	0.746E+05	2.	H	1
0.681E+00	0.228E+00	0.346E+01	0.650E-02	0.401E+00	60.	2300.0	0.187E+06	2.	I	1
0.262E+00	0.143E+00	0.553E+01	0.320E-02	0.187E+00	60.	2300.0	0.373E+06	2.	J	1
0.131E+00	0.957E-01	0.106E+02	0.190E-02	0.940E-01	60.	2300.0	0.597E+06	2.	K	1
0.112E+00	0.144E+00	0.149E+02	0.160E-02	0.740E-01	60.	2300.0	0.746E+06	2.	L	1
0.560E-01	0.527E-01	0.223E+02	0.100E-02	0.370E-01	60.	2300.0	0.112E+07	2.	M	1
0.290E-01	0.346E-01	0.319E+02	0.600E-03	0.220E-01	60.	2300.0	0.168E+07	2.	N	1
0.220E-01	0.589E-01	0.337E+03	0.800E-03	0.220E-01	60.	4160.0	0.448E+07	2.	O	1

The data from reference number [4] above is unlikely to be a real motor since the voltage and rating data is not standard.)
The reference numbers relate to the following sources :

[1] Cathey, Cavin & Ayoub, [1973]
[2] Sastry and Burridge, [1976]
[3] Smith I R and Hamil B, [1973]
[4] Sen Gupta and Lynn, [1980]

5. MODELLING PARAMETER VARIATION

In this chapter the variation of motor parameters with slip and current is investigated. The work was prompted by a realisation that the circuit parameters as quoted by manufacturers often relate to rated load conditions only and that for correct modelling of the motor performance over the complete range of slip and current a proper understanding of the parameter variation was required.

The original model used in Chapter 4 was a constant parameter model. Once it was established that the yields of the computation process were more strongly influenced by the rotor impedance than by most other input data items, it became apparent that effort should be concentrated on accurate modelling of the variation of this impedance with slip. At that stage it was not clear whether the UDB or DCC model should be used. It was assumed that since both had been used in published work that they were both useful. The data for the machines in Table 4.4 is given in terms of a single cage circuit and hence the UDB model seemed to be the most appropriate model. At that stage of the work, it was not clear to the author how the bar depth could be assigned other than by estimating a depth appropriate to the motor's rating and iterating until reasonable performance was obtained. The problem with this is that no starting performance data was given for the motors of Table 4.4 and so the iteration about the starting torque point could not be done. In addition, the work of Section 5.1 shows that for many motors it would be impossible to re-calculate the starting torque with any accuracy without allowing for leakage path saturation. The rotor parameter values given in Table 4.4 are those based on the unsaturated, low-slip equivalent circuit which is only appropriate for a restricted operating range. This made it impossible to use the rated torque points as done by Melik, [1987] because the data was already given in terms of the low frequency rotor impedances rather than taken from locked rotor tests. The UDB method was tried with assigned bar depths ranging from 15 to 60 mm; it being assumed that the depth always increased with rating. This resulted in very low starting torques for some machines which raised some doubts about the validity of assuming a UDB model for the wide range of machines in Table 4.4.

With hindsight, the poor starting torque can be seen to be due to the fact that, for some motors, the assigned equivalent bar depths were too large in comparison with the depths obtained from equation 2.18 and confusion existed about the determination of the variation of bar impedance with slip. The failure of the first attempt to model parameter variation stimulated a thorough investigation into the whole subject and led to the work described in Chapters 5 and 6.

Section 5.1 deals with the effect of leakage path saturation on the prediction of leakage reactance. Several methods are compared and criteria are given for the selection of an appropriate method for modelling leakage path saturation. In the second section of Chapter 5 the two main methods for the modelling of skin effect in the rotor are compared. It is shown that these two models may be inter-related. For practical bar sizes, the double-cage circuit is shown to be a super-set of the uniform-width deep bar. In Section 5.3 a new method for determining the impedance of a rotor bar of any specified cross-sectional profile is described and applied to several practical bar shapes. The last two sections deal with the effects of temperature and magnetising path saturation.

5.1. Comparison Of Models For Leakage Path Saturation.

Two papers based on the work discussed in this chapter were presented in September 1995 to the Electric Energy Conference in Adelaide and to the Australian Universities Power Engineering Conference in Perth, [Arneaud and Langman, 1995] and [Arneaud, 1995].

5.1.1. Introduction

In this section it is shown that if the effect of leakage path saturation is neglected then large errors may occur in the prediction of current under locked-rotor conditions. Several methods are discussed for the estimation of leakage reactance and starting current. Two of these methods are new and have been developed in an attempt to cope with the lack of test or design data that often arises in practical situations. It is important for an engineer to know if it is worth while spending the rest of the afternoon trying to locate additional data, ie if doing so will help to improve the accuracy of the computer model to the degree needed for the problem in hand. In order for the accuracy of the predictions generated by a model to increase it appears that the amount of data required to establish the model must also increase. It will be shown that the decrease in uncertainty in predicted starting current, as achieved by the more sophisticated saturation models, depends on this additional data.

Based on the analysis of the relative magnitudes of the errors in estimated current, guidelines are given for the selection of a predictive method appropriate to the amount of test or design data available. The work discussed in this section (5.1) is based on data from 52 machines taken from a paper by Lee, [1989]. Lee's data relates to the same motors as used by the IEE of Japan in a study conducted between 1972 and 1980, [IEE of Japan, 1980].

Four sets of locked rotor test results are defined with starting currents and applied voltages as shown in Table 5.1.1 below. It is noted that, in this Chapter, the usual notation for of V_1 and I_1 as rated terminal quantities is suspended and replaced by V_N and I_N . This is so as to be consistent with the source material of Lee and the Turbo Pascal code segments used by the author in this work.

V_N = rated voltage	I_N = rated current			
Applied locked-rotor voltage	$V_1 < V_2$	$V_2 < V_3$	$V_3 < V_N$	V_N
Measured starting current	$I_1 \cong I_N$	$I_2 \cong 1.5I_N$	$I_3 \cong 2I_N$	I_{st}

Table 5.1.1 : Definition of Data for Methods in this Section

A figure for the rated-voltage starting current, I_{st} is usually readily available from manufacturers and, as discussed in Section 6.3, must be within a tolerance given by AS1359 as +20% of the quoted starting current. This is a fairly broad tolerance range and is probably set by the need to allow variation between machines manufactured to the same nominal specification. (No negative tolerance is stipulated). The locked-rotor test on large motors is often done at reduced voltage because the full-voltage starting current is generally between four and nine times greater than rated current, I_N (Tables 5.1.2 and 5.1.3). It is suspected that the figure for I_{st} quoted by some manufacturers is derived from a single reduced-voltage locked-rotor test with a correction factor applied, based on previous test results. It is shown in Section 5.1.6 that if actual locked-rotor test data is available, then the starting current may be predicted to a much closer tolerance than this. Since manufacturers do not routinely perform locked rotor tests at more than one current, the starting currents at a range of

reduced voltages is often not available. The probability of increasing the error in predicted full-voltage starting current due to lack of sufficient test data is discussed in section 5.1.7.

The determination of starting current at any given voltage is an important test of the ability of various computer modelling methods to include for the effect of leakage path saturation. Available data may be restricted to the quoted I_{st} value or may include at least one additional set of locked-rotor test results. Two of the commercially available induction motor models do not include the leakage path saturation effect explicitly. Several recently published works include either leakage saturation or skin effect (but not both of them). It is noted that leakage path saturation may be included accidentally within the skin effect model if all the starting data used is based on full-voltage starting, [Grantham, 1985, pg 247]. This means that the model will work reasonably well as long as the saturation effect occurs together with high slip conditions. As long as the conditions being simulated are not very different from those of the tests upon which the parameter derivation was based, the model will give good results. A more demanding test is the prediction of maximum torque (a low slip, high current condition) or reduced-voltage starting (low current, high slip). The data from Lee's paper was used to assess the ability of several models for leakage reactance saturation to accurately predict starting currents I_2 and I_3 which occur at reduced voltages as defined in Table 5.1.1.

5.1.2. Outline Of Work Done In This Section

The first situation which was investigated, and which is discussed in Sections 5.1.3 to 5.1.7, is the prediction of rated-voltage starting current based on data from locked-rotor tests at reduced voltages V_1 , V_2 and V_3 . This would be primarily of interest to manufacturers and those with access to reliable data from reduced-voltage locked-rotor tests. It will be shown that using two locked rotor tests significantly reduces the mean error compared with an estimate of starting current based on a single test at reduced voltage. It is also shown that using results from three locked rotor tests reduces the error still further. Guidelines are given for the likelihood of reducing the error in predicted starting current by including additional test or design data.

If results from a locked-rotor test at rated voltage are available, then there is no need to predict the value of Ist but in some situations, knowing this steady-state current may not be adequate. The presence of a transient DC component which depends on the instant of switching may need to be considered for the setting of protection relays. Such transients are not considered in this chapter but are discussed in Chapters 7 and 8. However, the accurate simulation of this behaviour may require inclusion of leakage path saturation in the induction motor model.

The second situation which was investigated was the use of locked rotor test results at voltages V_1 and V_N to predict leakage reactance over the full range of motor currents. At voltages V_2 and V_3 , the accurate representation of leakage reactance would result in small errors in the predicted locked-rotor currents I_2 and I_3 . The method used to determine the estimates for I_2 and I_3 and the corresponding errors, is discussed in Section 5.1.9. Guidelines are given in Section 5.1.10 for the selection of a method for the representation of leakage path saturation in simulation programs.

In order to implement the above predictions and error comparisons, several short Turbo Pascal programs where written. In order to keep track of these and their associated input and output data files the Table 5.10.1 was produced. This was found

to be an essential part of the documentation since without it, it was impossible to remember which data files were required for each program. Each program's individual procedures were checked with known data and it is unlikely that errors exist in the developed versions which are on a floppy disc in the pocket at the end of the thesis.

5.1.3. Existing Methods For Predicting Starting Current at Rated Voltage

In this section, five methods which are commonly used for the prediction of starting current, are discussed and the errors in predicted starting current compared. This comparison is based on data from four sets of actual locked-rotor tests. The use of reduced-voltage test results to compute the, already known, full-voltage starting current forms a useful evaluation of the different methods. In the case of the methods of Lee and the IEE of Japan, knowledge of the rotor slot type is required.

In addition, the describing function method outlined in Section 2.2.4.1 was modified so that it may be used to predict starting current at rated voltage. This new Reversed Describing Function method is outlined in Section 5.1.5.1.

Two modified forms of Lee's method which take into account the possible lack of data were also developed as part of this work. The first of these (referred to as ML) requires only two sets of locked-rotor tests instead of three as required by the methods of Lee and the IEE of Japan. The second (referred to as UNS) also needs only two sets of locked rotor data and in addition does not require the rotor slot type to be known. It is shown in Section 5.1.7 that the additional error caused by using these methods is not large.

5.1.3.1. Range of stator currents

The machines studied had actual full-voltage, per-unit starting currents distributed as shown in Tables 5.1.2 and 5.1.3 and Figure 5.1.1. The starting currents of the 52 machines were processed using programs PROBDA.PAS and MNDVA.PAS.

The coefficients of variation, C_V (Standard Deviation/Mean) were low and therefore in the total absence of other data these tables can be used as a rough guide for the estimation of starting current. The likely uncertainty is given by the Range. It can be seen that in the worst case error would be 47% for the closed-slot motor and 23% for a semi-closed slot. (Based on assuming a starting current equal to the mean value with actual starting current equal to the minimum or maximum).

Closed Slots	Min.	Max.	Range	Mean	RMS	Std.Dev	Cv	R
	4.72	9.08	4.35	6.94	7.02	1.03	0.148	95

Range	4.5	5.1	5.7	6.4	7.0	7.6	8.2	8.9	9.5
Rel. freq.	0.03	0.06	0.16	0.32	0.16	0.13	0.10	0.03	

Table 5.1.2 : Distribution of per-unit starting currents for closed slots

Semi-closed	Min.	Max.	Range	Mean	RMS	Std.Dev	Cv	R
	4.30	7.80	3.50	6.04	6.10	0.83	0.137	90

Range	4.0	4.5	5.0	5.5	6.0	6.5	7.0	7.5	8.0
Rel freq.	0.05	0.00	0.24	0.19	0.14	0.33	0.00	0.05	

Table 5.1.3 : Distribution of per-unit starting currents for semi-closed slots

Based on the coefficients of variation of 0.148 and 0.137 with sample sizes of 31 and 21 respectively, it is possible to say that the probability of the increase in mean current from 6.04 to 6.94 being not due to pure chance is better than 99.5%. This can be used to justify the separation of the two sub-populations of closed and semi-closed slots. It is noted, however that the ranges overlap considerably. Whilst it is impossible to identify the rotor slot type from the quoted starting current on an individual machine, it can be done on the basis of a sufficiently large sample taken from a group of machines all with the same type of rotor slot.

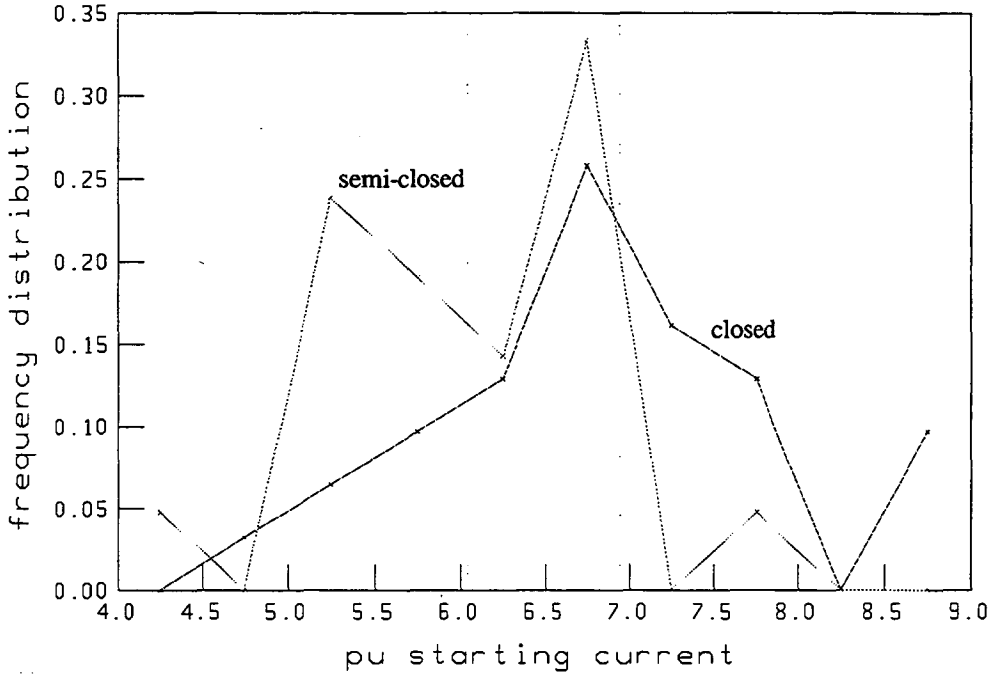

Figure 5.1.1 Distribution of quoted per-unit starting currents

The true mean for the population of all closed slot motors may be estimated by using the Student's t distribution, [Dally, Riley and McConnell, 1984]. From the computed reliability it may be said that the likelihood that the true mean is within ± 5% of 6.94 pu is better than 95 %. Similarly, for semi-closed slots, the probability that the true mean lies within a confidence interval of ± 5% is greater than 90 %. The reduced confidence in the semi-closed slot mean reflects the smaller sample size.

In practice, some locked-rotor test data will usually be available and at least one of the following methods may be used :

5.1.3.2. Corrected proportional method (Cprop)

This method neglects saturation and derives a value for the starting current, I_{stp} which is proportional to applied voltage but is modified by a correction factor. Without this correction, the method always predicts a current lower than the actual value. A correction factor of 1.2 was used since this is midway between the mean errors of 22.25% and 18.05% calculated by simple proportion based on the data for the 31 closed slot and 21 semi-closed slot machines; ie

$$I_{stp} = 1.2 I_1 \frac{V_N}{V_1} \qquad (5.1.1)$$

5.1.3.3. Logarithmic proportional method (Lprop)

This assumes that the starting current, I_{stl} may be related to starting voltage, V by an expression of the form $I_{stl} = AV^{B}$, where A and B are constants.
The method defines

$$I_{stl} = I_1\left(\frac{V_N}{V_1}\right)^{B_L} \tag{5.1.2}$$

$$\text{where } B_L = \frac{\log(I_3 / I_1)}{\log(V_3 / V_1)} \tag{5.1.3}$$

5.1.3.4. Melik's method (Melik)

This was introduced in Section 2.2. It is similar to the logarithmic proportional method but in estimating the starting current, I_{stM} the index, B is determined by a least-squares fit on all three test points.

$$I_{stM} = AV_N^B \tag{5.1.4}$$

where A and B are derived as in Section 2.2.4.2

5.1.3.5. IEE of Japan (IEE_J)

This is a modified form of the logarithmic proportional method. The method used to calculate this estimate, I_{stJ} is empirical and based on the relationship between the errors in starting current predicted by the logarithmic method and the value of the exponent, B_L . For this method it is important to know if the rotor slot is closed or semi-closed. The effect of inadvertently assigning the wrong slot type was investigated and is discussed in Section 5.1.7.3.
For Closed Slots :

$$I_{stJ} = I_1\left(\frac{V_N}{V_1}\right)^{B_{JC}} \tag{5.1.5}$$

$$\text{where } B_{JC} = 0.35 + 0.7B_L \tag{5.1.6}$$

For Semi-Closed Slots :

$$I_{stJ} = I_3\left(\frac{V_N}{V_3}\right)^{B_{JS}} \tag{5.1.7}$$

$$\text{Defining } B_L' = \frac{\log(I_2 / I_1)}{\log(V_2 / V_1)} \tag{5.1.8}$$

$$\text{and } B_L'' = \frac{\log(I_3 / I_2)}{\log(V_3 / V_2)} \tag{5.1.9}$$

$$\text{Then when } B_L'' > B_L' \qquad B_{JS} = 1.05B_L'' - 0.35(B_L' - 1) \tag{5.1.10}$$

$$\text{and when } B_L'' \le B_L' \qquad B_{JS} = 0.7B_L'' + 0.35 \tag{5.1.11}$$

5.1.3.6. Lee's method (Lee)

The method described in Lee's paper was based on the application of least-squares regression analysis to graphs of log(B) against $\log(B_L)$. Program SAT_XTL.PAS used constants as shown in the equations below though it is certain that the use of fewer decimal places could be justified. eg. 0.924 instead of 0.92399 as the index in equation (5.1.14).

Lee's method defines

$$I_{stL1} = I_1 \left(\frac{V_N}{V_1} \right)^{B_E} \tag{5.1.12}$$

where B_E is defined as below and B_L' as above.

Closed Rotor Slots :

When $B_L / B_L' > 1.002$ then $B_E = 1.0384 B_L^{0.66179}$ (5.1.13)

otherwise $B_E = 1.0195 B_L^{0.92399}$ (5.1.14)

Semi-Closed Rotor Slots : (corrected criterion, not as printed in paper by Lee)

When $B_L / B_L' \geq 1.015$ then $B_E = 1.0601 B_L^{1.1183}$ (5.1.15)

otherwise $B_E = 1.0727 B_L^{0.47732}$ (5.1.16)

The constants used in all four equations above are those in Lee's paper which are slightly different from those derived by using program PLOTB.PAS which are shown in Tables 5.1.4 and 5.1.5.

For the semi-closed slots, Lee's paper states that the criteria used for sorting the slots into two groups is $B_L' / B_L \geq 1.015$. This is a typographical error and the correct division is as above. When applied to the data for the semi-closed slots, there are only two machines which satisfy the criteria $B_L' / B_L \geq 1.015$. This makes the suggested curve fit unjustifiable and there is obviously an error in the paper. A check was done on other possible ratios. It was found that applying the criterion $B_L / B_L' \geq 1.015$ to the semi-closed slots resulted in the division into two groups as given in Lee's work.

Because of the uncertainty generated by this error, Lee's least-squares fits on the graphs of log(B) against $\log(B_L)$ were repeated using program PLOTB.PAS. Results very similar to Lee's were found as discussed below and shown in Figures 5.1.2 and 5.1.3 for the closed and semi-closed slots respectively.

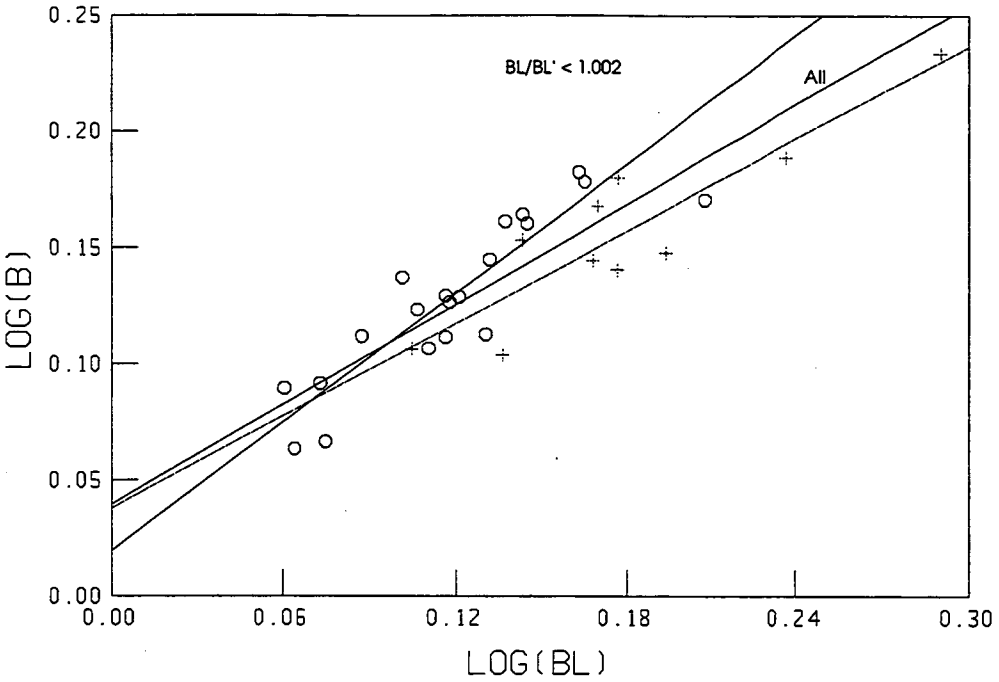

Figure 5.1.2 Graph of log(B) against log(B_L) for closed slots

5.1.4. Some Comments On The Paper By Lee

The work of Lee is the most comprehensive study to date of induction motor starting currents. The data base used was however fairly small and perhaps not fully representative of all machines. For example, all but one of the closed slot machines had rated voltages of 200 V. It is not stated whether machines of more than one manufacturer were used. This is not intended as a severe criticism since as mentioned previously, it is difficult to obtain reliable data of this type from manufacturers. It would be pointless to use data from machines that had not been properly tested to compare the performance of the methods mentioned here as in many cases the differences between the predicted starting currents given by the different methods are small.

Mainly because of the uncertainty caused by the error described in Section 5.1.3.6 it was decided to check the curve fits obtained by Lee and this eventually led to the development of the two new methods which use less data than Lee's method and produce better results than the other methods with comparable data requirements.

5.1.4.1. Check on Lee's fits

The constants shown in Tables 5.1.4 and 5.1.5 were calculated by fitting, to the points (log(B), log(B_L)), the line log(B) = m log(B_L) + c using program PLOTB.PAS. In the case of the closed slots, the constants agreed with Lee's. Three lines were fitted. The first to the ten motors for which $B_L/B_L' > 1.002$, the second to the remaining 21 and the third to all 31 closed-slot motors. The improvement in coefficient of determination, r justifies the separation of the two groups based on the graph of log(B) against log(B_L) shown in Figure 5.1.2.

	Shown	No.	A	m=B	c	r
1 > 1.002	+	10 motors	1.0385	0.6618	0.0377	0.8087
2 <= 1.002	o	21	1.0195	0.9240	0.0193	0.8500
3 all motors		31	1.0404	0.7161	0.0396	0.782

Table 5.1.4 : PLOTBPAS Straight line fits to relation for closed slot motors.

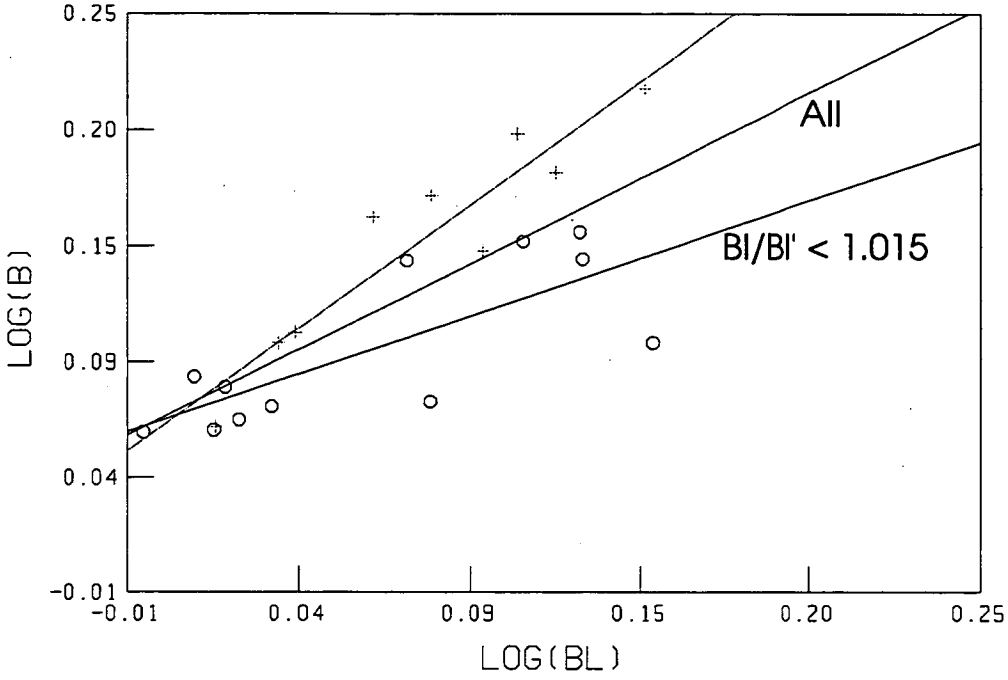

Figure 5.1.3 Graph of log(B) against log(B_L) for semi-closed slots

In the case of the semi-closed slots, the results differed from those of Lee's paper. The log(B) against log(B_L) graphs did not look significantly different when plotted but the numerical values of the indices were not quite the same, which was puzzling. The computed values of B, B_L and B_L' agreed with those given in Lee's paper, at least to the first three decimal places. However for one of the machines the computed value of B_L/B_L' was 1.0148 and this was sorted into the first category in Lee's paper but into the second by SAT_XTL.PAS. This accounted for the slightly different computed fit constants, A and B in the equation $I_{st} = A\ V^B$.

(Note Lee's constants for the semi-closed slot were A = 1.0601 and 1.0727 ; B = 1.1183 and 0.47732). The graphs for the semi-closed slot motors are shown in Figure 5.1.3 .

Line Identification		A	m=B	c	r
B_L/B_L' >= 1.015 +	9 motors	1.0664	1.0622	0.0643	0.878
B_L/B_L' < 1.015 o	12 motors	1.0699	0.4989	0.0675	0.588
all motors	21 motors	1.0707	0.7387	0.0683	0.585

Table 5.1.5 : PLOTB.PAS Straight line fits to relation for semi-closed slot motors.

5.1.5. New Methods For Predicting Starting Current

Three additional methods described below were developed as extensions of existing work.

5.1.5.1. Reversed describing function method (DF1 and DF2)

The describing function method outlined in Section 2.2.4.1. was extended to the prediction of full-voltage starting current. The original describing function method was designed to interpolate between two sets of locked rotor test results; one at reduced voltage and the other at rated voltage.

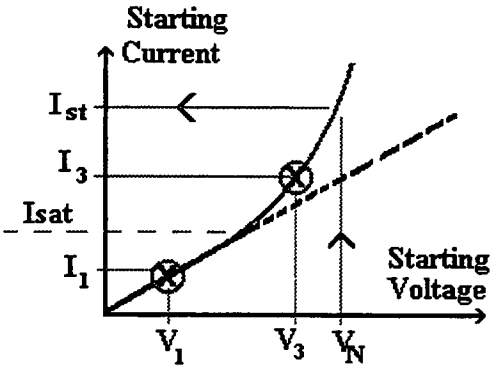

Figure 5.1.4 : Extrapolation for I_{st} Reversed Describing Function Method

In the new reversed method, two data points were used namely (V_1 , I_1) and (V_3 , I_3) ie the voltages which produced rated and twice rated current respectively. The latter point was equated to the saturated state and the latter to the unsaturated ; V_1 = Vred, I_1 = Ired, V_3 = Vst, I_3 = Ist in Section 2.2.4.1). The resulting curve was extrapolated to predict starting current at full voltage, V_N as shown in Figure 5.1.4.

Because locked-rotor test data availability was taken for purposes of this comparison to be restricted to points as in Table 5.1.1, the saturated condition was assumed to exist at I_3 (2.0 pu current). The resistive part of the locked-rotor impedance was neglected since no data for this was available. These assumptions will be shown to be reasonable by the relative accuracy of the method which calculated the starting current, I_{stDF} as :

$$I_{stDF} = \frac{V_N}{(X_{t0} + DF.X_{ts})} \qquad (5.1.18)$$

{See Section 2.2.4.1 for the definition of DF and the reactance components X_{t0} and X_{ts} }

The reversed describing function (DF) method was found to be highly dependent on the value chosen for the current, I_{sat} at which the initial onset of leakage path saturation occurs. Two values of initial saturation current, Isat were used; namely 1.08 and 1.25 times rated current. These are referred to as DF1 and DF2 respectively. The choice of these values is discussed in Section 5.1.9.1. Low values of Isat cause large errors in the procedure since it does not work properly if Isat is small enough to cause sin ξ >1 in equation 2.5. 4. Using a very large Isat value is equivalent to ignoring leakage path saturation.

5.1.5.2. Developments from Lee's method

The more sophisticated methods required additional test data plus knowledge of the rotor slot type. It was decided to investigate the situation where only two sets of locked rotor test data are available. In a similar way, attention was given to the effect of assigning the incorrect slot type or simply not knowing which one to use.

5.1.5.2.1. For two sets of locked rotor test results (ML)

The method subsequently designated was essentially Lee's method but the criteria of equations 5.1.15 and 5.1.17 were not applied. Instead all the closed-slot machines were treated with the same equation based on the fit appropriate to all closed-slot motors as given in Table 5.1.4 ie

For closed-slots the index was given by $B_E = 1.0404 B_L^{0.7161}$ (5.1.19)

Similarly, taking all the semi-closed slot motors produced a least squares fit to the graph of log(B) against log(B_L) and yielded the index for semi-closed slots as in Table 5.1.6 ie $B_E = 1.0707 B_L^{0.7387}$ (5.1.20)

This meant that only two locked rotor tests were needed ie it was unnecessary to know (V_2 and I_2).

5.1.5.2.2. Coping with an unknown rotor slot type (UNS)

For the method designated UNS (unknown slot type) an attempt was first made to derive the constants A and B by fitting a straight line, log(B) = m log(B_L) + c to data points {log(B), log(B_L)}, from all the machines without regard to slot type. This resulted in a reasonable fit. However it was found that a smaller mean error and standard deviation of the error in predicted starting current occurred by using A and B values which were the means of those for the closed and semi-closed slots ie A=1.0555 and B=0.7274 giving $B_E = 1.0555 B_L^{0.7274}$ (5.1.21)

5.1.6. Method Used For Comparison Of Different Estimates of Starting Current

Several short Turbo-Pascal programs were written to apply each of the methods to compute the difference between the predicted, rated-voltage starting current, I_{stp} and the actual rated-voltage starting current, I_{st}. (The subscript, p was taken in turn to represent each of the methods as defined in Section 5.1.3). This difference was used to define an error term, ε given by :

$$\varepsilon = 100 \frac{(I_{stp} - I_{sta})}{I_{sta}} \% \qquad (5.1.17)$$

Relative frequency distribution graphs were produced as Figures 5.1.5 and 5.1.6 which showed the uncertainty arising from the application of each method. Tables 5.1.6 and 5.1.8 show the spread of the errors for the closed and open slots respectively together with computed confidence limits for the means of the respective total populations.

5.1.7. Calculated Errors In Predicted Starting Current

The predicted starting currents and percentage errors were calculated using the program SAT_XTL.PAS using the methods of Section 5.1.3 plus the additional methods outlined below. The results were stored in data files SATn.OUT with values of n from 1 to 6 as explained in Section 5.1.11. Table 5.1.6 was produced using program MNDVB.PAS and the graphs of Figures 5.1.5 and 5.1.6 were drawn by program PROB_DB.PAS.

5.1.7.1. Results for closed slots

From the estimated starting current for each method several statistical measures were computed using program MNDEVB.PAS and these are shown in Table 5.1.6. The

minimum, maximum and range give an indication of the variation between machines. In addition, the mean of the absolute errors (shown as Mean ||), the RMS error and the standard deviation (S.Dev.) are shown. The percentage coefficient of variation, C_V was computed from the ratio of the standard deviation to the mean. This is a measure of the spread of the data and affects the confidence which may be placed in the calculated mean values. The reliability of the computed means was estimated based on the Student's t distribution. Table 5.1.6 shows, for example, that for the Corrected Proportional method the probability that the true mean value of the error for the infinite set of all closed slot motors lies within ±10% of the quoted mean of 7.64 pu, was greater than 75%. This relatively low confidence level reflects the small sample size and the natural spread of the data.

The results showed that, with the available data, Lee's method performed the best having the lowest error and standard deviation. The ML method developed during this work performed second best (even though it ignored the criterion of equation 5.1.13). The UNS method performed about as well as the Logarithmic Proportional Method.

closed	Min.	Max.	Range	Mean ||	RMS	S.Dev.	Cv	R
Cprop	-23.6	5.9	29.5	7.64	9.52	5.69	74.5	75
Lprop	-7.4	13.5	20.9	4.00	5.17	3.27	81.6	70
Lee	-5.1	8.5	**13.6**	**2.63**	3.22	1.86	70.8	75
Melik	-7.2	13.3	20.5	3.93	5.04	3.16	80.5	75
IEE_J	-8.2	7.8	16.0	3.31	4.08	2.39	72.3	75
DF1	-10.7	15.1	25.8	4.58	5.44	2.93	64.0	80
DF2	-5.1	72.2	77.3	9.82	16.93	13.79	140.4	60
ML	-8.9	7.0	15.9	3.28	3.87	2.05	62.6	80
UNS	-6.0	10.9	16.9	4.17	5.27	3.22	77.1	75

Table 5.1.6 : Range of % errors, ε for closed slots [MNDB1.OUT]

The second table (Table 5.1.7) shows the results of comparing the means, again based on the Student's t distribution. Laid out in the form of a matrix, this shows the probability of reducing the mean absolute error by selecting another method. In cases where the other method gives a worse result, the table is left blank. Lee's method therefore is completely blank whereas the table shows that there is a 45% chance that the apparent improvement found in moving from the Logarithmic Proportional method to Melik's method was due to pure chance. These results may be used to guide the choice of method to be used in the prediction of starting current at full voltage when one or more set of low-voltage locked-rotor test results are available. They may be used as an indication of the advisability of seeking additional locked rotor test data or clarifying the rotor slot type. This is discussed further in Section 5.1.8.

	Cprop	Lprop	Lee	Melik	IEE_J	DF1	DF2	ML	UNS
Cprop		99.5	99.5	99.5	99.5	99.0		99.5	99.5
Lprop			95.0	**55.0**	80.0			80.0	
Lee									
Melik			95.0		80.0			80.0	
IEE_J			80.0					55.0	
DF1		75.0	99.5	75.0	95.0			95.0	60.0
DF2	75.0	97.5	99.5	97.5	99.0	97.5		99.0	97.5
ML			80.0						
UNS		55.0	97.5	60.0	80.0			80.0	

Table 5.1.7 : Chance of reducing the % error by selecting another method. closed slots [MNDB1.OUT]

A frequency distribution graph of the errors, ε in the calculated full-voltage starting current was produced using program PROB_DB.PAS and is shown in Figure 5.1.5. Analysis showed that when the slot type was totally unknown, 35% of the closed slot motors yielded errors of between 0 and 3% but a further 23% had errors between 6 and 9%. (This double-hump was not a division into closed and semi-closed slot types.)

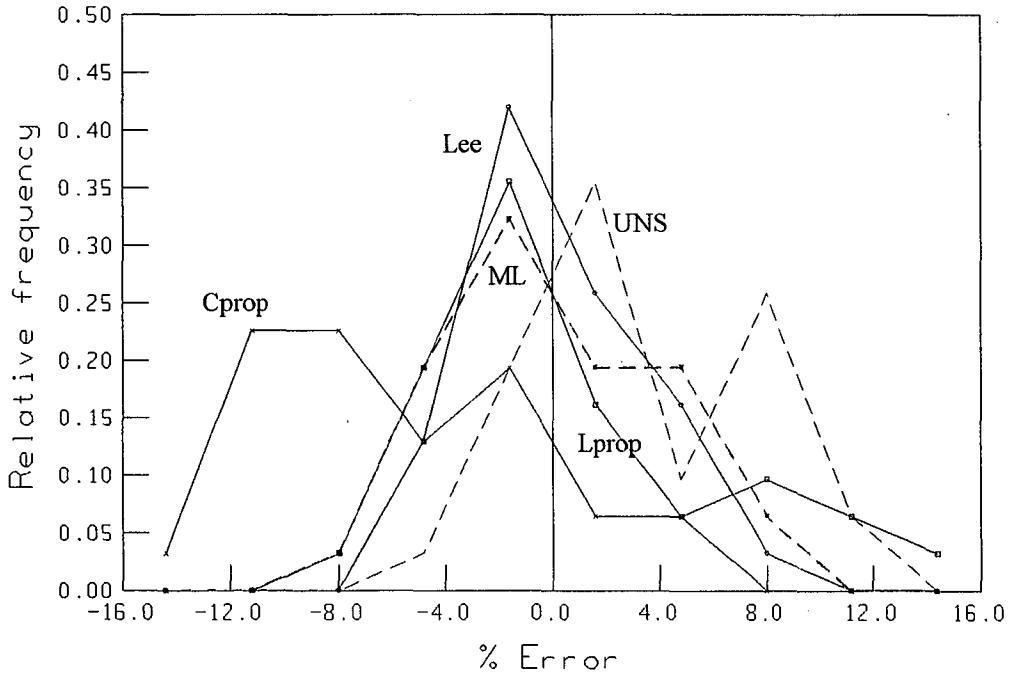

Figure 5.1.5 Frequency distribution of % errors, ε (for Closed Slots)

5.1.7.2. Results for semi-closed slots

For the closed slots the method of analysis was similar to that for the closed slots. The frequency distribution of the errors is shown in the graph of Figure 5.1.6 and Table 5.1.8.

	Min.	Max.	Range	Mean ll	RMS	S.Dev.	Cv	R
Cprop	-14.3	8.6	22.9	6.69	7.61	3.62	54.1	75
L prop	-14.7	9.7	24.4	8.99	9.65	3.52	39.2	80
Lee	-6.5	8.0	14.5	3.06	3.69	2.06	67.4	70
Melik	-15.3	10.2	25.5	9.31	10.04	3.77	40.5	80
IEE_J	-4.9	12.0	16.9	3.18	4.46	3.13	98.5	60
DF1	-16.1	4.8	20.9	9.65	10.34	3.70	38.3	80
DF2	-12.4	13.9	26.3	7.88	8.62	3.49	44.3	80
ML	-8.5	16.5	25.0	4.19	5.75	3.94	94.1	60
UNS	-11.0	12.6	23.6	4.62	5.93	3.73	80.7	70

Table 5.1.8 : Range of % errors, ε for Semi-Closed slots [MNDB2.OUT]

The results showed that the reversed describing function method with early saturation, (DF1 with Isat = 1.08 pu) was not successful with the semi-closed slots; even the corrected proportional method performed better. This is consistent with the fact that semi-closed slots saturate at higher current values than for closed slots. With higher saturation current (Isat = 1.25 pu) the errors were much reduced. This DF2 method performed better than the Log proportional and Melik's methods. Again Lee's method was the best. Analysis showed that there was a 55% chance of improving the error in predicted starting current by using this method in preference to that of the IEE of Japan.

	Cprop	Lprop	Lee	Melik	IEE_J	DF1	DF2	ML	UNS
Cprop			99.5		99.5			97.5	95.0
Lprop	95.0		99.5		99.5		80.0	99.5	99.5
Lee									
Melik	97.5	60.0	99.5		99.5		80.0	99.5	99.5
IEE_J			**55.0**						
DF1	99.0	70.0	99.5	60.0	99.5		90.0	99.5	99.5
DF2	80.0		99.5		99.5			99.5	99.5
ML			80.0		80.0				
UNS			90.0		90.0			60.0	

Table 5.1.9 : Chance of reducing the % error by selecting another method. semi-closed slots [MNDB2.OUT]

As with the closed slots, the ML and UNS methods performed well considering their reduced data requirement.

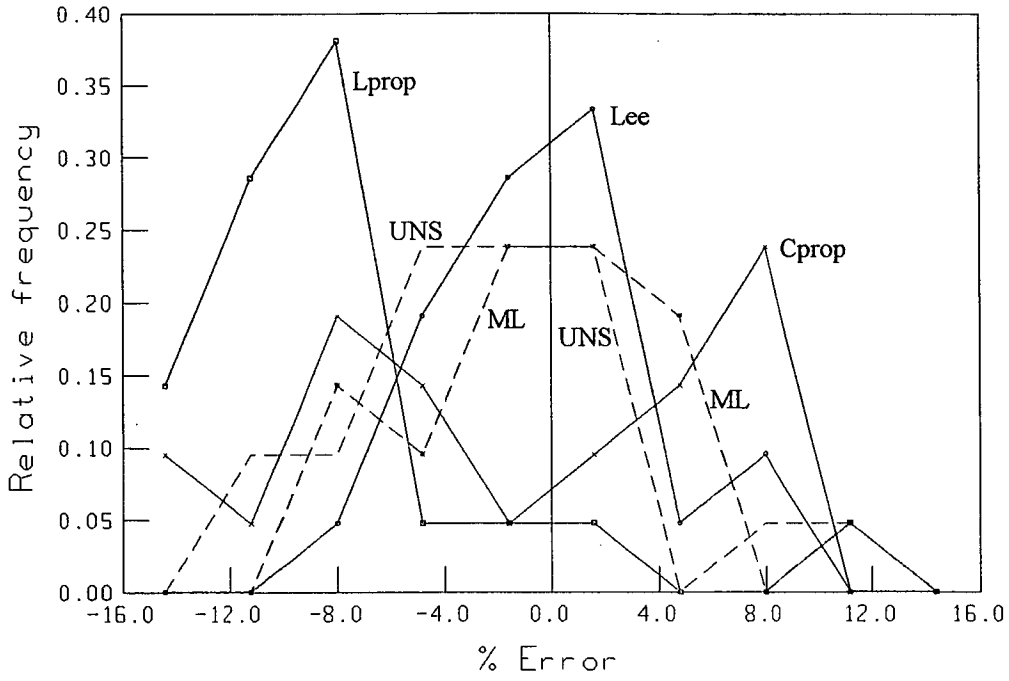

Figure 5.1.6: Frequency distribution of % errors for semi-closed slots

5.1.7.3. Unknown slot type (or error in assigning type)

In order to investigate the effect of not knowing the correct rotor slot type, two copies of the data files were created with the slot types deliberately incorrectly assigned. eg the data for the closed slot motors was processed as if it were from semi-closed slot machines. This did not affect the starting current estimates for the Corrected Proportional, Logarithmic Proportional, Reversed Describing Function or Unknown Slot methods. The results for the Lee, IEE of Japan and Modified Lee methods are given in Tables 5.1.10 to 5.1.13. In each case the first row shows the values with the correct rotor slot assignment. The row immediately below it shows the effect of using the wrong slot type.

	Min.	Max.	Range	Mean ||	RMS	S.Dev.	Cv	R
Lee	-5.1	8.5	13.6	2.63	3.22	1.86	70.8	75
wrong	-12.9	15.7	28.6	**4.20**	5.76	3.94	93.7	70
IEE_J	-8.2	7.8	16.0	3.31	4.08	2.39	72.3	75
wrong	-5.2	14.1	19.3	**5.44**	7.04	4.46	82.0	70
ML	-8.9	7.0	15.9	3.28	3.87	2.05	62.6	80
wrong	-2.7	15.3	18.0	**6.90**	8.05	4.13	59.9	80
UNS	-6.0	10.9	16.9	**4.17**	5.27	3.22	77.1	75

Table 5.1.10 : Distribution of % errors, wrong slot type, closed slots.

It can be seen that the mean absolute percentage errors increase significantly when the wrong slot type is assigned. All the sophisticated methods produce larger errors than the simple UNS fit that ignores slot type and uses data from only two locked-rotor tests. This method performs approximately as well as the Logarithmic Proportional

method for closed slots. Table 5.1.11 shows probability of reducing the error by choosing another method. The difference between the three best methods is only small, being 40-45 % possible that it was due to pure chance.

	Cprop	Lprop	Lee	Melik	IEE_J	DF1	DF2	ML	UNS
Cprop		99.5	99.5	99.5	90.0	99.0		70	99.5
Lprop				**55.0**					
Lee		**55.0**		**60.0**					**55.0**
Melik									
IEE_J		90.0	80.0	90.0		80.0			80.0
DF1		75.0	60.0	75.0					60.0
DF2	75.0	97.5	97.5	97.5	90.0	97.5		80	97.5
ML		99.5	99.0	99.5	90.0	99.0			99.5
UNS		**55.0**		**60.0**					

Table 5.1.11 : Effect of possibility of choosing the wrong slot type on method selection; closed slot. (MNDB5.OUT)

For the semi-closed slots the results were similar. Treating these as closed slots again produced mean absolute errors greater than those which occurred when the UNS method was used. This new method produced the smallest mean absolute error for semi-closed slots when the slot type was incorrectly assigned. The IEE of Japan's method was nearly as good but this method would require one additional locked-rotor test.

	Min.	Max.	Range	Mean ll	RMS	S.Dev	Cv	R
Lee	-6.5	8.0	14.5	3.06	3.69	2.06	67.4	70
wrong	-14.5	11.5	26.0	**7.00**	8.05	3.96	56.5	75
IEE_J	-4.9	12.0	16.9	3.18	4.46	3.13	98.5	60
wrong	-12.6	10.0	22.6	**5.32**	6.52	3.77	70.8	70
ML	-8.5	16.5	25.0	4.19	5.75	3.94	94.1	60
wrong	-13.4	9.1	22.5	**6.20**	7.14	3.55	57.3	75
UNS	-11.0	12.6	23.6	**4.62**	5.93	3.73	80.7	70

Table 5.1.12 : Distribution of % errors, wrong slot type, semi-closed slots.

	Cprop	Lprop	Lee	Melik	IEE_J	DF1	DF2	ML	UNS
Cprop					80.0			60.0	95.0
Lprop	95.0		90.0		99.5		80.0	99.0	99.5
Lee	60.0				90.0			75.0	95.0
Melik	97.5	60.0	95.0		99.5		80.0	99.0	99.5
IEE_J									**70.0**
DF1	99.0	70.0	97.5	60.0	99.5		90.0	99.5	99.5
DF2	80.0		75.0		97.5			90.0	99.5
ML					**75.0**				**90.0**
UNS									

Table 5.1.13 : Effect of choosing the wrong slot type on method choice; semi-closed slot.

5.1.8. Choice Of Method To Limit Errors

In the complete absence of test data the starting current may be guessed using the figures of Tables 5.1.2 and 5.1.3 as a guide. Usually some indication of machine design or at least one locked-rotor test will be available. An estimate could be based on AS 1359, Part 41 (Table 41.2), the IEC 34 equivalent or NEMA MG1 all of which specify allowable locked-rotor kVA to rated kilowatt ratios, [AS1359, 1974], [IEC, 1983] and [NEMA, 1987]

If only one locked rotor test result is available then a simple proportional method must be used. The uncorrected simple proportional method, which neglects leakage path saturation, was found to have the largest absolute value of mean error for both closed and semi-closed rotor slots. These results are not shown since the program was modified to correct the estimate by increasing the calculated current by 20%. With the semi-closed slots, this Corrected Proportional method performed better than the Logarithmic method, Melik's method and the reversed Describing Function. However the correction factor was determined on the basis of the data from files LEE1.DAT and LEE2.DAT and it remains to be seen how accurate the correction would be when applied to other data. Lee used a correction factor of 1.25 which over-compensates producing predicted starting currents which are larger than actual.

If the slot type is unknown then the UNS method is the safest. If the slot type is guessed then there is a 50% chance that it will be wrong. If Lee's method is selected for a large number of machines and the slot type is incorrectly assigned then the worst case situation will arise with the semi-closed slot when the slot is treated as closed. Here the mean absolute error will increase from 3 to 7%. If the safe course is chosen, namely using the UNS method, the mean absolute error will be restricted to 4.6%. However for any individual machine the actual error may occur within the range indicated by Table 5.1.14. As shown in Figure 5.1.7 these distributions overlap considerably.

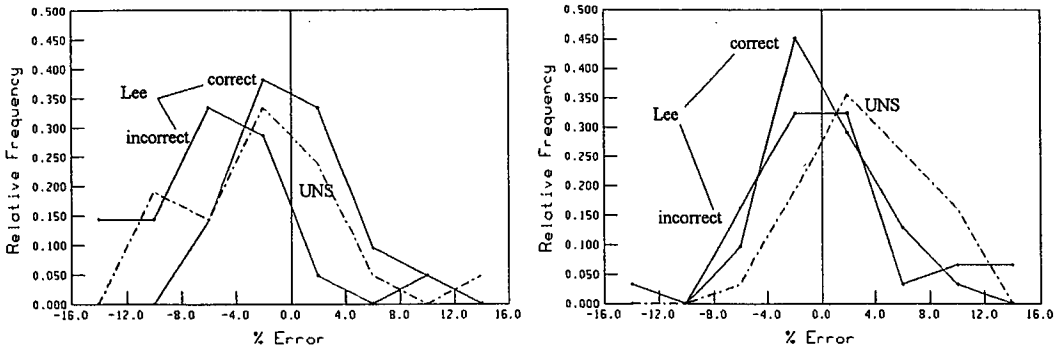

Closed Slot Semi-closed slot

Figure 5.1.7 : Distribution of % errors in estimated starting current; Lee's method with correct and incorrect slot type assigned.

Actual Slot	Method Used	Possible Range of Actual Error	Mean Absolute Error
Closed Slot	Lee (correct slot)	-> 8.5	2.63
	(wrong slot)	-> 15.7	4.2
	UNS	-> 10.9	4.17
Semi-Closed Slot	Lee (correct slot)	-> 8.0	3.06
	(wrong slot)	-> 11.5	7.0
	UNS	-> 12.6	4.62

Table 5.1.14 : Distribution of errors in estimated starting current; Lee's method with correct and incorrect slot type assignment

If only two sets of locked rotor test data are available, namely (I_1,V_1) and (I_3,V_3); then it is possible to use the Log Proportional method, the Describing Function method or the methods designated ML and UNS. Of these, the ML method was by far the best available method given the lack of data. For semi-closed slots the ML method was only out-performed by Lee's method, whilst for the closed slots there was a only a 75% chance of reducing the error by 1% by using the IEE of Japan's method. (The only methods better than the ML method would require one additional set of locked-rotor test data.) The reversed describing function method does not perform as well as the other methods which are available with two sets of locked rotor test data. The accuracy of this reversed describing function method was found to depend greatly on the assumed value of Isat.

If all three sets of data are available and the rotor slot type is known then Lee's method should be used. This achieved mean errors of 2.6% with the closed and 3.1% with the semi-closed slots. These mean absolute errors are extremely low. Again it is stressed that individual motors may produce errors larger than this. The probability of the error exceeding a given value may be estimated from Figures 5.1.5 and 5.1.6 but it is important to recognise that the sample upon which those graphs are based is small and the distributions rather stepped.

The study described above has assigned a series of numerical measures to the advantages gained by moving to a more sophisticated, more data-costly, predictive method. In practice, however, there are factors other than motor reactance to be considered. The most obvious is the assumption that, at the time of starting, the test

voltage is at its rated value. Supply systems are usually permitted to vary within a range of ±6% and this introduces an uncertainty in the voltage prior to starting. The reactance in the supply line may also be uncertain. The supply voltage will drop during starting. A further problem is that the current predicted by this method is from a steady-state locked-rotor test; ie the test measurements are taken after transient currents have died away. In practice, the dc offset in the starting current may be large enough and of sufficient duration, to need to be considered in commissioning protective relay systems. As a consequence of the above, even if results from a locked-rotor test at rated voltage are available, there is no certainty that the value of the nominal steady-state current derived will be adequate for some system design applications; simulation of the transient performance may be required. This situation is discussed further in Chapter 8.

Locked-rotor test results available	Rotor slot type data	Suggested method	Worst case % error	% of motors with absolute error<6%
none	unknown	6.6 pu	47	33
none	known	statistical	closed 23 semi-closed 47	39 24
one	unknown	Cprop	24	44
one	known	Cprop	closed 24 semi-closed 14	45 43
two	unknown	UNS or ML (treat as closed)	12.6 16.5	66 75
two	known	ML	closed 9 semi-closed 16.5	91 72
three	unknown	UNS or ML (treat as closed)	12.6 16.5	66 75
three	known	Lee	closed 8.5 semi-closed 8	97 86

Table 5.1.15 : Suggested method with different levels of available data.

5.1.9. Verification Of Original (Interpolation) Describing Function Method

In numerical simulation of induction motor performance the describing function method as described in Chapter 2 is often used to model leakage path saturation. In this context, the available data is usually the starting current at rated voltage and perhaps one additional locked-rotor test point such as (I_1,V_1) in Table 5.1.1. The method interpolates between the two test points using a clipped sine function as described in Section 2.2.4.1. For currents below the lower data point, the reactance is assumed to be constant. This means that the value of I_1 used should be below the initial saturation current Isat. Since the describing function method determines values of leakage reactance between two known conditions of saturation it is expected to give smaller errors than the reversed extrapolative version which was introduced in Section 5.1.5.1.

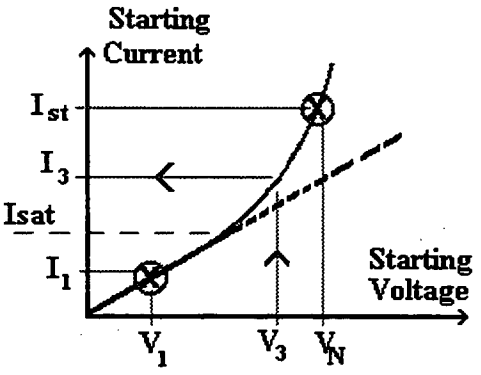

Figure 5.1.9 : Interpolation for I_3 describing function method

The first data point is from a locked-rotor test at reduced voltage, V_1 and the second at rated voltage, V_N. At any given current, the leakage reactance is determined from the sum of saturable and unsaturable parts as defined in Chapter 2.

Once the reactance is known, starting current at any given voltage may be calculated from the total impedance.

(The resistance was ignored for the evaluation of the method since it was not known for the IEE of Japan motors).

Since the describing function method formed the basis of leakage reactance saturation modelling in two of the simulation programs described in Chapter 3, it was considered desirable to check its ability to predict the values of reactance at several values of stator current. The opportunity was taken to use the available data from the IEE of Japan study to do this by assessing the errors generated by using the describing function method to predict the intermediate currents I2 and I3 when given I1 and the starting current at rated voltage, I_{st}. This was done using the program DF_SAT.PAS which also allowed investigation of the extent to which changes in the assumed value of I_{sat} affected the accuracy of the predicted currents. Two I_{sat} values were used namely 1.08 and 1.25 pu current. These are referred to as DF1 and DF2 respectively. Higher values of Isat were not used since the graph of Figure 5.1.12 shows that for values of Isat above 1.5 pu the percentage error increases.

Case	Method	Min.	Max.	Range	MeanII	RMS	S.Dev	Cv	R
I_2	DF1	-5.2	1.2	6.4	1.40	1.78	1.10	78.5	75
	DF2	-8.2	-1.6	6.6	4.07	4.36	1.57	38.6	90
	Cpr	-12.3	16.5	28.9	5.32	6.84	4.30	80.9	75
	ML	-3.0	1.4	4.4	**0.74**	**1.03**	0.72	96.8	70
	UNS	-2.4	2.0	4.5	**0.86**	**1.05**	0.61	70.5	75
I_3	**DF1**	-4.3	4.8	9.2	**1.93**	**2.23**	1.12	58.2	80
	DF2	-8.6	1.6	10.2	2.21	3.00	2.02	91.4	70
	Cpr	-12.3	16.1	28.5	5.03	6.34	3.86	76.6	75
	ML	-5.4	3.1	8.5	**1.52**	**1.95**	1.22	80.6	75
	UNS	-4.4	4.2	8.6	**1.98**	**2.25**	1.07	54.0	80

Table 5.1.15 : Distribution of % errors in predicted currents, I_2 and I_3 with closed slots

5.1.9.1. Results of comparison

The results of the processing by program PROB_DC.PAS are shown in Table 5.1.16. The tables show the mean errors, range and probability, R that the actual mean errors for the complete set of closed slot machines lies within a 5% confidence limit of the quoted mean. For the closed slots, the describing function method did not perform as well as either the ML or UNS method. For this type of slot, with the low level of Isat,

87% of the motors had errors in I_2 between -3 and 1%. This compares with 74% of the machines having errors between -1 and 1% when the ML method was used. However for the semi-closed slots the DF method was better than either the ML or the UNS method. Here 76% of the motors had errors between 1 and 5% with the low Isat DF method whereas for the ML and UNS methods most of the errors were between 3 and 7%.

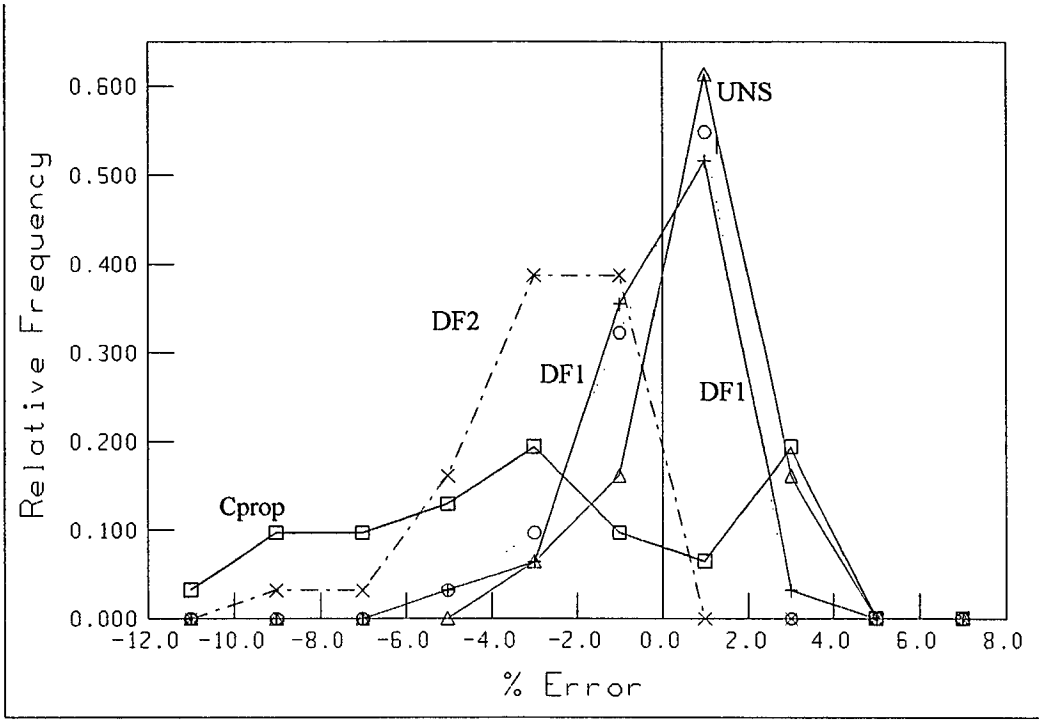

Figure 5.1.9 Relative frequency distribution of % errors in I_2 and I_3 closed slot

Frequency distribution graphs for the errors in calculated I_2 and I_3 using each of the methods are shown in Figures 5.1.9 , 5.1.10 and 5.1.11. The Five cases tested are shown as follows :

Method	Shown in graphs
DF1 (Isat = 1.08 pu)	+
DF2 (Isat = 1.25 pu)	X
Cprop	□
ML	O
UNS	Δ

If only one locked rotor test is available, then the corrected proportional method must be used. The suggested method is as follows : First determine the estimate for the reduced voltage required to obtain 1 pu current on starting based on the assumption that the proportional method gives an estimate for rated-voltage starting current that is 20% too high (as found in Section 5.1). Next use this constructed reduced-voltage data to apply the describing function method using an Isat value of 1.17 (mean of the two values above). This method was adopted because it seemed logical and it will be seen that it worked quite well with the 52 motors tested.

Case	Method	Min.	Max.	Range	Mean	RMS	S.Dev	Cv	R
	DF1	-2.5	5.4	7.9	2.77	3.08	1.33	47.9	80
	DF2	-4.7	2.1	**6.7**	**1.44**	**1.84**	1.15	79.5	70
I_2	Cprop	-12.0	10.1	22.1	6.68	7.72	3.86	57.8	75
	ML	-0.8	7.5	8.3	4.52	4.86	1.79	39.5	80
	UNS	-1.5	6.6	8.1	3.84	4.17	1.62	42.3	80
	DF1	-2.0	8.5	10.5	4.99	5.42	2.12	42.5	80
	DF2	-4.0	5.2	**9.2**	**3.02**	**3.34**	1.42	47.1	80
I_3	Cprop	-10.5	11.5	22.0	6.31	7.10	3.24	51.3	80
	ML	-0.4	9.4	9.8	6.53	6.93	2.32	35.4	80
	UNS	-1.5	8.1	9.6	5.37	5.74	2.02	37.5	80

Table 5.1.17 : Distribution of % errors in predicted currents, I_2 and I_3 with semi-closed slots

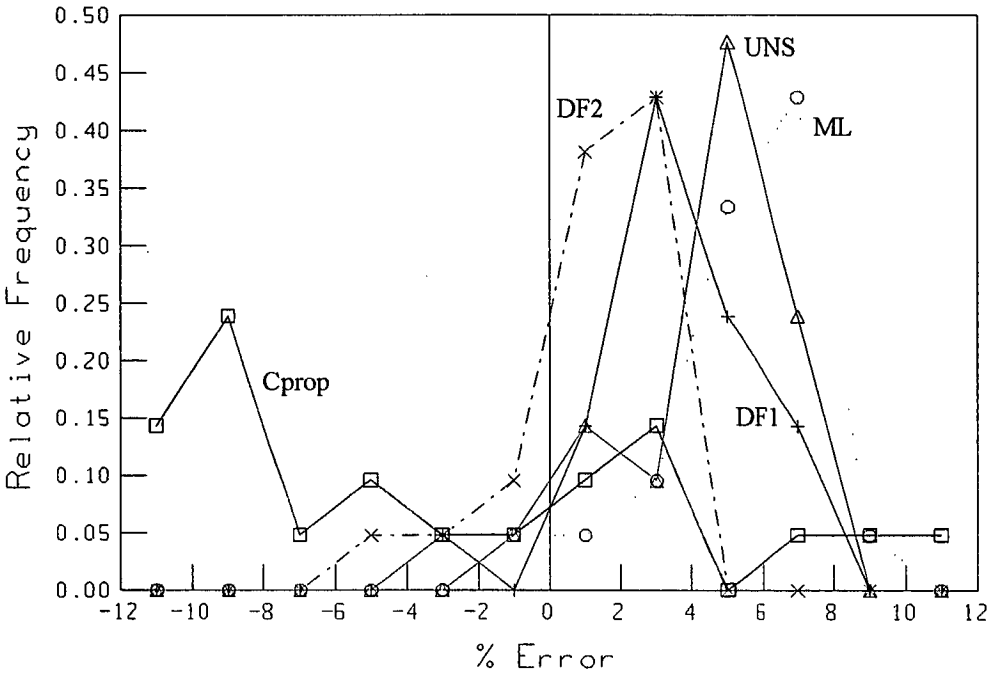

Figure 5.1.10 Relative frequency distribution of % errors in I_2 and I_3 semi-closed slot

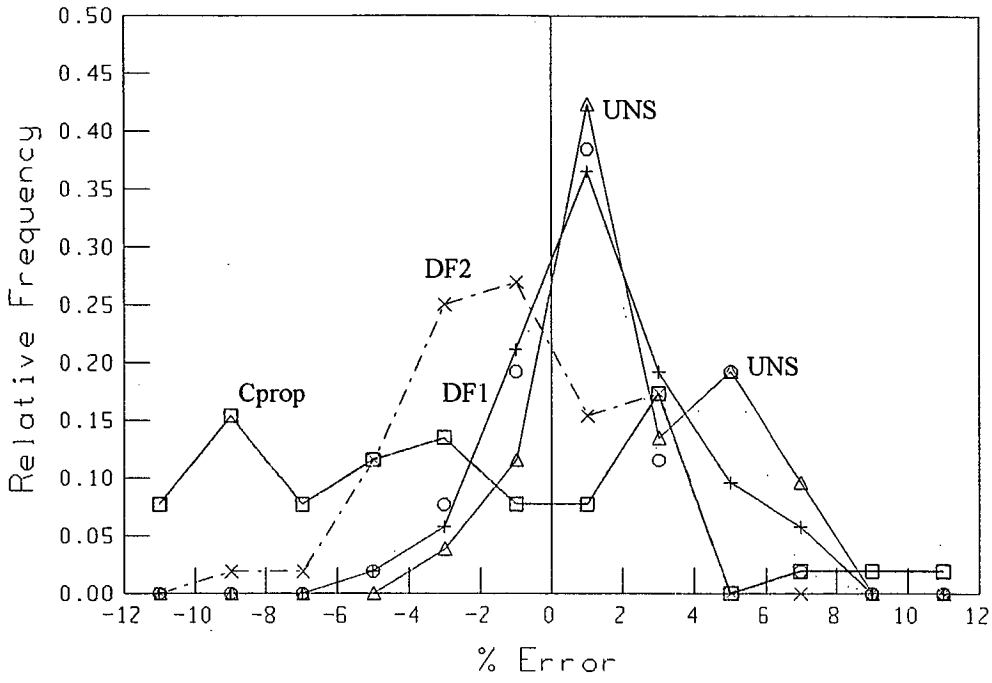

Figure 5.1.11 : Relative frequency distribution of % errors in I_2 and I_3 all slot types

Significant differences occurred in the magnitude of the errors when low (1.08 pu) and high (1.25 pu) values of I_{sat} were used. Figure 5.1.12 shows the effect of different assumed I_{sat} values on the RMS error for both I_2 and I_3 computed over all 52 motors using the DF method. It can be seen that the minimum RMS error occurs when I_{sat} is approximately 1.25 pu. For values of I_{sat} less than about 1.08 pu the DF method is prone to complete computational failure. This occurs because the Isat value is less than the lower test point, I_1 . For $I_{sat} < I_1$ the inverse sine function in equation (2.5) will fail. As Isat increased, the RMS error levelled off at a value which depended on slot type and starting voltage. The pu values of 1.08 was selected because it is at the lower end of the possible range. The second value of 1.25 pu for Isat was chosen because it was approximately in the range where the RMS error is at its minimum. It was not considered worth while to try to determine the actual value of Isat at which the RMS error for all motors occurred since this would depend on the values of current at which the method was tested. Here values of I_2 and I_3 were used equal to those in Table 5.1.1, simply because they were available as data. If suitable motor performance data is available then it may be possible to reduce the error in estimated leakage reactance on a particular motor by iterative selection of an appropriate Isat value as discussed in Section 6.2.

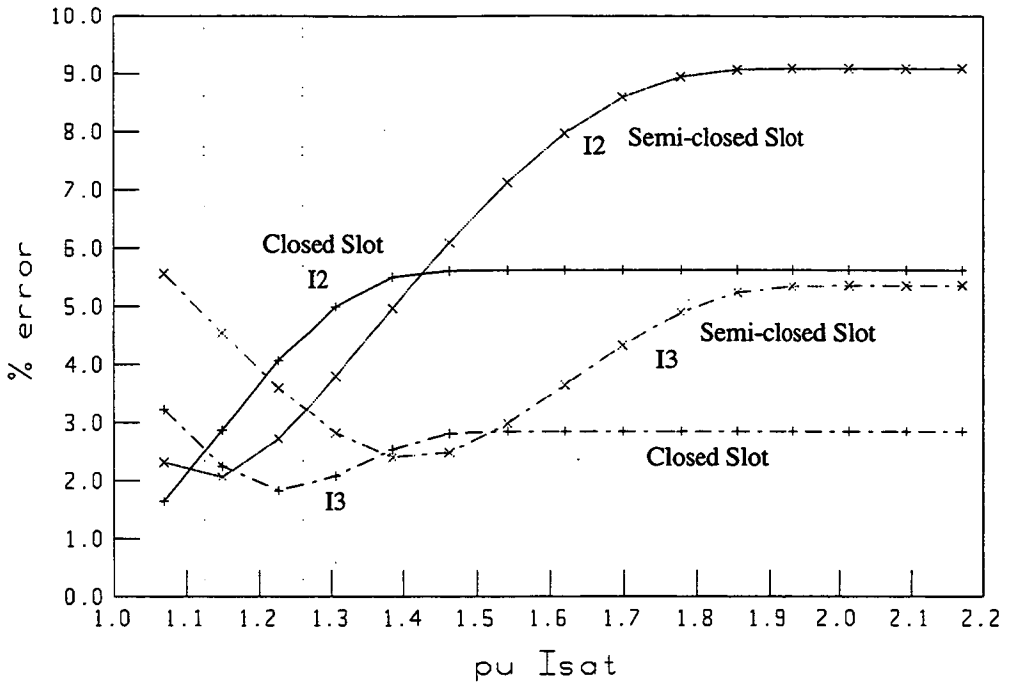

Figure 5.1.12 : Variation in RMS % error with varying levels of Isat

The above results confirm that the DF method may be used with reasonable accuracy even if the resistance values are unavailable. This supports the comment by Agarwal and Alger, [1960] that it is the leakage reactance that dominates in the prediction of starting current and supports the use of the describing function method in the programs of Chapter 3. It is noted that, if the rotor slots are known to be closed then, the ML method gives better results without requiring additional data.

5.1.9.2. Complete locked-rotor saturation curve

The program DFC_SAT.PAS was used to produce the complete locked-rotor saturation curve as shown in Figure 5.1.13 for the 6th motor in the closed slot data file. This machine was chosen because it gave rise to the largest absolute error in estimated starting current. The lowest line represents the totally unsaturated machine, constant reactance.

It can be seen that the error in estimated locked rotor current is small for all methods but significant if saturation is ignored. The two DF methods accurately predict the full-voltage starting current (Which was used as a data item to the process). The ML and UNS methods actually work from the lower current and extrapolate upwards. For this particular motor, the ML method performed rather worse than the UNS at high levels of current although the % errors at lower currents are smaller. Considering the extent of the extrapolation shown in Figure 5.1.13 it is not surprising that some error occurs. What is significant is that as long as one of the methods is used (even the ML method) the results are significantly better that if a linear variation is assumed. This was true for all the 51 motors used and is probably true for most standard industrial motors of rating less than about 100 kW. The only way to be sure is to obtain more than one set of locked-rotor test data.

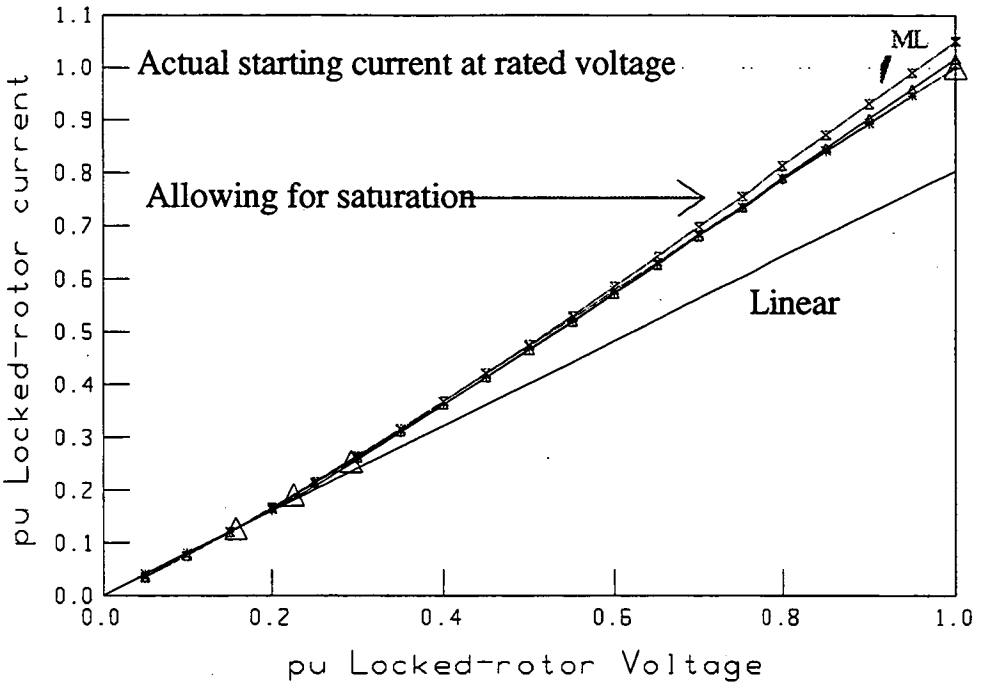

Figure 5.1.13 : Saturation curve for the 6th motor in the closed slot data file.

5.1.10. Guidelines For Selecting A Method For Representing Leakage Path Saturation In Simulation Programs

Tables 5.1.18 and 5.1.19 below may be used to guide selection of a method for the representation of leakage path saturation in cage induction motors when locked rotor test results are available at more than one voltage. If the rotor slot type is known then the ML method should be used for closed slot machines at low values of voltage (<0.5 pu) and the DF with an assumed Isat value of 1.25 pu for higher supply voltages or for semi-closed slot machines. The absolute error is unlikely to be greater than 5%. The most significant feature of the curve of Figure 5.1.13 is that it demonstrates that all the methods perform significantly better than assuming a linear (unsaturated) machine.

As designed, the DF method works best when the reduced voltage LR test is performed at approximately 0.8 pu voltage rather than at 2 pu current. The evaluation in this Section was restricted to the available test data as Table 5.1.1. It is possible to use the other methods outlined in this chapter to calculate simulated reduced voltage test data which may be required by certain simulation programs. For example, the method outlined above may be used to reconstruct the complete locked-rotor saturation curve which is needed for the Saturation Factor Method used by Lipo and Consoli, [1984].

		Closed Slot					Semi-Closed Slot				
		DF1	DF2	Cprop	ML	UNS	DF1	DF2	Cprop	ML	UNS
I_2	DF1				99.5	97.5		99.5			
	DF2	99.5			99.5	99.5					
	Cprop	99.5	90.0		99.5	99.5	99.5	99.5		97.5	99.5
	ML						99.5	99.5			80.0
	UNS				75.0		97.5	99.5			
I_3	DF1				90.0			99.5			
	DF2	75.0			90.0	70.0					
	Cprop	99.5	99.5		99.5	99.5	90.0	99.5			80.0
	ML						97.5	99.5	55		95.0
	UNS	55.0			90.0		70.0	99.5			

Table 5.1.18: Chance of reducing the % error in estimated I_2 or I_3 by selecting another method when the slot type is known

In cases where the slot type is unknown then the ML method cannot be used since it needs the slot type data. Either of the UNS or DF methods may be adopted with acceptance of the fact that the error may be up to 8%. Table 5.1.19 shows the result of applying the DF and UNS methods to all the motors without regard for slot type. For the lower current, I2 the DF method gave a slightly smaller mean error but a broader range. For I3, there was a 90% chance that the error would be reduced by using the DF1 method instead of the DF2 but the actual improvement in going from the DF2 to DF1 and UNS is only slight.

	Method	Min.	Max.	Range	Mean ||	RMS	S.Dev	Cv	R
	DF1	**-5.2**	**5.4**	**10.6**	**1.95**	**2.39**	1.37	70.3	80
I2	DF2	-8.2	2.1	10.3	3.01	3.57	1.92	63.6	80
	Cprop	-12.3	16.5	28.9	5.87	7.21	4.19	71.3	80
	UNS	-2.4	6.6	9.0	2.06	2.77	1.85	89.6	75
	DF1	**-4.3**	**8.5**	**12.9**	**3.16**	**3.85**	2.20	69.4	80
I3	DF2	-8.6	5.2	13.8	2.54	3.14	1.85	72.7	80
	Cprop	-12.3	16.1	28.5	5.55	6.66	3.67	66.2	80
	UNS	-4.4	8.1	12.5	3.35	4.04	2.26	67.3	80

Table 5.1.19 : Distribution of % errors in predicted currents, I_2 and I_3 when the slot type is unknown

All Slot Types Combined		DF1	DF2	Cprop	UNS
	DF1 (Isat = 1.08 pu)				
	DF2 (Isat = 1.25 pu)	99.5			99.0
I2 (≈ 1.5 rated)	Corrected proportional	99.5	99.5		99.5
	Unknown Slot Type	60.0			
I3 (≈ 2.0 rated)	DF1		90.0		
	DF2				
	Cprop	99.5	99.5		99.5
	UNS	60.0	97.5		

Table 5.1.20 : Chance of reducing the % error in estimated I_2 or I_3 by selecting another method when the slot type is unknown

5.1.11. Programs And Files Used In Section 5.1

Table 5.1.21 shows the various programs and data files used in this part of the work and the relationships between them. The table was made to record and keep track of the several small programs and data files which were written during the work reported on in this section of the thesis. All programs and data files are stored in the discs in the pocket at the end of the thesis. In the table, the character n is used as a variable to designate the case studied. The value of n was assigned within a range from 1 to 6 as follows.:

n = 1 for CLOSED SLOTS
n = 2 for SEMI-CLOSED SLOTS with correct separation as BL/BL' ratio.
n = 3 for SEMI-CLOSED SLOTS with Lee's incorrect separation as BL'/BL ratio (see discussion in Section 5.1.3.6)
n = 4 data for all machines combined with out regard for slot type.
n = 5 Closed slots treated as if they were semi-closed (see below).
n = 6 Semi-closed slots treated as if they were closed slots.

The last two cases were done to investigate the effect of incorrectly assuming the slot type. This might be done if the slot-type data were uncertain.

Table 5.1.22 shows a similar list of files for the comparison of method for deriving the intermediate currents, I_2 and I_3 from two locked rotor tests; one at rated voltage and the other at rated current.

I/P Data File	Program Name	Output File	Comment
LEEn.DAT (File1)	SAT_XTL.PAS	ISTn.OUT (File4)	File of errors + Istp. as TP data file; t:=' '
	Determines starting current at rated voltage by 9 different methods using results from up to 3 locked rotor tests.	SATn.OUT (File2)	File of errors + Istp. in WORD table format; w:=','
		AFn.OUT (File5) BFn.OUT (File6)	Files of B, B_L' and B_L' two different criteria based on B_L/B_L' ratio Equations 5.1.13, 5.1.8 and 5.1.9
		Q3. (File3)	program diagnostic file
LEEn.DAT	PROB_DA.PAS	PRAn.OUT	Frequency distribution of quoted Ist, +
LEEn.DAT	MNDVA.PAS	MNDAn.OUT	mean, max, min. Std. Dist. of quoted Ist.
AFn.OUT BFn.OUT	PLOTA.PAS LSQ_UNIT.PAS		Graphs of B/B_L as Lee and Section 5.1.12
AFn.OUT BFn.OUT	PLOTB.PAS LSQ_UNIT.PAS		Graphs of $\log(B)/\log(B_L)$ as Figures 5.1.2 & 5.1.3
ISTn.DAT	PROB_DB.PAS	PRBn.OUT	Frequency distribution of errors in estimated Ist.
ERRTn.OUT	PROB_DD.PAS	PRDn.OUT	Frequency distribution of errors in I_{st} compares correct and wrong slots.
ISTn.OUT	MNDVB.PAS	MNDBn.OUT	mean, max, min. Std. Dist. of errors in Ist. Estimate of Confidence limits

Table 5.1.21 : List of programs and data files used in sections 5.1.3 to 5.1.8

Input Data File	Program Name	Output File	Purpose of Program
LEEn.DAT (File1)	DF_SAT.PAS	DF.OUT (File2) ERRTn.OUT (File3) ERRWn.OUT (File4)	Determines % errors in I_2 & I_3.based on different methods.
LEEn.DAT (File1)	DF_SATB.PAS (Uses UNIT PLOT_SAT.PAS)	DF.OUT (File2) ERBTn.OUT (File3) ERBWn.OUT (File4)	Complete locked-rotor saturation curve for any given motor as Figure 5.1.13
LEEn.DAT (File1)	DFC_SAT.PAS (Uses UNIT PLOT_SAT.PAS)	DFCn.OUT (File2) ERRTn.OUT (File3) ERRWn.OUT (File4)	RMS error in I_2 and I_3 plotted against assumed pu Isat
Isat_er1.OUT Isat_er1.OUT	PLOTC.PAS		Draws graph of variation in errors with Isat as Figure 5.1.12
ERRTn.OUT	PROB_DC.PAS	PRCn.OUT	Frequency distribution of errors in estimated I_2 and I_3.
ERRTn.OUT	MNDVC.PAS	MNDCn.OUT	WORD table format : mean, max, min. Std. Dist. of errors in I_2 and I_3. Estimate of Confidence limits

Table 5.1.22 : List of programs and data files used in Section 5.1.9

5.1.12. Verification Of Error In Lee's Criteria For Semi-Closed Slots

The splitting of the closed slot data into two sets using the comparison of B_L and B_L' is justified by examining the coefficients of determination of the least-squares fits to the separate data sets and to the complete set. For the complete set of closed slot motors this increased from 0.78 to 0.82 and 0.85 respectively for the upper and lower lines of Figure 5.1.14. This marginal increase in the coefficients of determination justifies the splitting into two populations.

A similar examination for the semi-closed slots was used to confirm that the correct criteria for splitting these motors should be as stated in Section 5.1.3.6 and not as in Lee's paper. For Figure 5.1.15 the coefficients of determination are 0.57 for the complete set increasing to 0.58 and 0.88 for the upper and lower lines respectively.

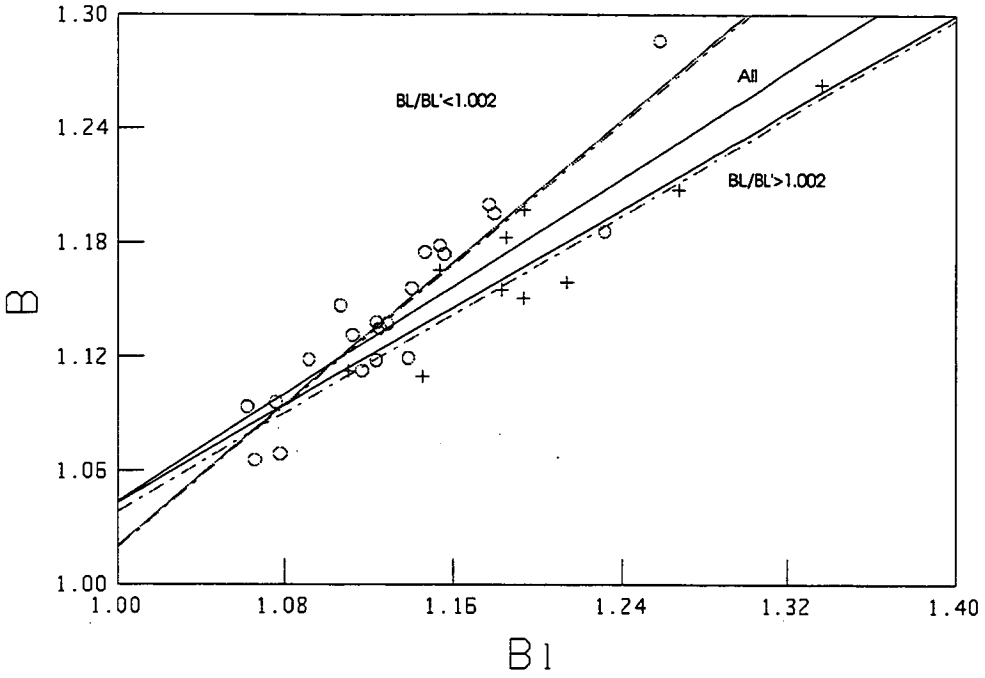

Figure 5.1.14 : Graph of B/Bl for closed slots

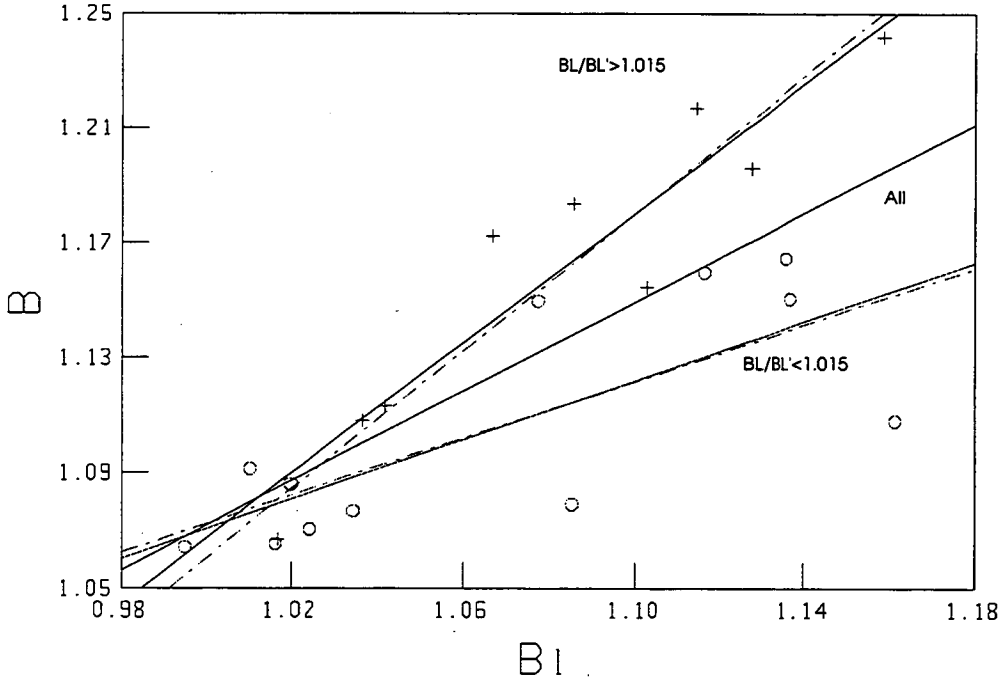

Figure 5.1.15 : Graph of B/Bl for semi-closed slots

5.2. Comparison Of Uniform-Deep-Bar And Double-Cage-Circuit Models For Skin Effect In The Rotor

As described in the introduction to Chapter 5, there were problems with the application of the UDB method to some motors. Some of these problems were due to faulty application of the UDB method because at the time, it was not fully appreciated that the data given in Table 4.4 was in fact only capable of representing the motor under restricted circumstances. However the failure led to the investigation into the relationship between the UDB and DCC models, the realisation that the UDB was a subset of the DCC and to the development of the new Variable Width Bar method developed in Section 5.3.

It was decided to investigate the relationship between the cage and bar models with the aim of trying to develop guidelines for selection of either the UDB or DCC model for skin effect in rotors. The UDB model is fully specified by the set of four rotor parameters at slip =1 and slip =0 ie by $\{S\} = \{R_{st} R_{dc} X_{st} X_{dc}\}$. Alternatively it may be specified by the parameters X_{dc} and R_{dc} at slip=0 plus the depth of the equivalent bar or by the actual bar dimensions together with the stator/rotor transformation ratio. Since this study focused on performance parameters rather than design information, attention was focussed on the method based on the complete set {S}. The working hypothesis was adopted that the UDB model gave a variation in impedance which represented the variation of the whole rotor, ie including the non-slot portions of the rotor such as zig-zag reactance; (Section 2.2.6.2.3).

The DCC model is usually defined in terms of the circuit parameters given by the set $\{C\} = \{R_a R_b X_b X_{ab}\}$ with Xa = 0. It is permissible to set Xa = 0 because the system contains one degree of freedom. Several DCC models exist which can fit a given set {S}. The only way in which the "correct" DCC circuit may be ascertained is by supplying additional impedance value at some slip, s where 0 > s > 1. Any one of the parameters could have been chosen but the decision to set Xa = 0 was made because for many machines it is the smallest parameter.

In practice, the leakage reactance of the upper slot is usually small. The situation shown in Figure 5.2.1 is oversimplified because the currents in the upper and lower portions of the rotor slot are not in phase under high slip conditions and their magnitudes are unequal.

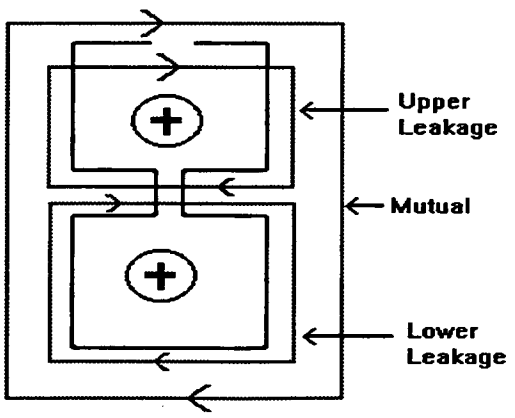

Figure 5.2.1 :
Flux paths in double-cage rotor slot

Nevertheless, it can be imagined that there will be a tendency for there to be less flux in the upper leakage path since this flux must cross two airgaps rather than one. It can also be seen that the mutual flux will be greater than the leakage fluxes due to opposition of the driving MMFs in the narrow region halfway up the slot.

Since a degree of freedom exists in the equations it seems reasonable to set $X_a = 0$. A non-zero value for X_a was used by Chalmers and Mulki, [1970] but the difference in motor performance could equally well be modelled by other effects such as leakage path saturation.

It was clear that starting with the circuit, the set {S} could be calculated and hence the equivalent bar model derived. The reverse derivation of {C} from {S}, which is given in Section 5.2.1 below, allowed calculation of the cage equivalent of a given bar. In order to compare the two models, two Turbo-Pascal programs were written to allow comparisons to be made from the two alternative starting points.

The first program was called BC.PAS. It started from the uniform bar dimensions and computed the DC value of rotor impedance from first principles. Equations (2.12) and (2.13) were then used to calculate the impedance at starting. This gave {S} which was then used to derive the equivalent set {C} as Section 5.2.1.1. The set of circuit parameters, {C} was then used to derive the variation of rotor parameters over the whole slip range. This variation was compared with that predicted by equations (2.12), (2.13) and (2.14) which are based on direct use of the equivalent uniform deep bar model. The results of this process are given in Section 5.2.1.3

The second Turbo-Pascal program, called CB.PAS proceeded in the reverse direction. Starting from the set {C} it derived the set {S} and hence the equivalent bar depths as in Chapter 2. These were used to compute the impedance variation over the slip range. The predicted variation was then compared with that given by using the circuit as a starting point. This work is described in Section 5.2.2.

The results of both programs are summarised in Section 5.2.3 which discusses the options available for modelling skin effect in rotor conductors.

Most of the material in this Section has been presented at the AUPEC Conference in 1993, [Arneaud, 1993].

5.2.1. Double Cage Circuit Equivalent Of Uniform Deep Bar

5.2.1.1. Derivation of {C} from given {S}

At any slip, the total effective rotor circuit impedance referred to the stator is given by equations (2.2.9) - (2.2.11) which refer to the double-cage rotor circuit of Figure 2.2.4 which has $X_a = 0$.

At slip, s close to zero ; $$R_{dc} = \frac{R_a R_b}{R_a + R_b} = R_a - \frac{R_a^2}{R_a + R_b} \qquad (5.2.0)$$

Hence $$R_b = \frac{R_a R_{dc}}{R_a - R_{dc}} \qquad (5.2.1)$$

Let $m = (R_a + R_b)/X_b$ (Called the 'Double-Cage Design Ratio')

Giving $$X_b = \frac{R_a^2}{m(R_a - R_{dc})} \qquad (5.2.2)$$

Also at s close to zero; $$(X_{dc} - X_{ab}) = \frac{R_a^2 X_b}{(R_a + R_b)^2}$$

Using equation (5.2.0) and the definition of m, this can be rewritten as

$$(X_{dc} - X_{ab}) = \frac{R_a^2}{(R_a + R_b)} \frac{X_b}{(R_a + R_b)} = (R_a - R_{dc}) \frac{1}{m}$$

$$\Rightarrow X_{ab} = X_{dc} - (R_a - R_{dc}) / m \tag{5.2.3}$$

At s=1;

$$R_{st} = \left[\frac{R_a R_b (R_a + R_b) + R_a X_b^2}{(R_a + R_b)^2 + X_b^2} \right] = \frac{\frac{R_a R_b}{(R_a + R_b)} + \frac{R_a X_b^2}{(R_a + R_b)^2}}{1 + \frac{X_b^2}{(R_a + R_b)^2}} = \frac{m^2 R_{dc} + R_a}{m^2 + 1}$$

Hence $R_a = (1 + m^2) R_{st} - m^2 R_{dc}$ (5.2.4)

Also at s=1;

$$(X_{st} - X_{ab}) = \frac{R_a^2 X_b}{(R_a + R_b)^2 + X_b^2} = \frac{\left[\frac{R_a^2 X_b}{(R_a + R_b)^2} \right]}{\left[1 + \frac{X_b^2}{(R_a + R_b)^2} \right]} = \frac{(R_a - R_{dc}) / m}{1 + \frac{1}{m^2}} = m \frac{(R_a - R_{dc})}{1 + m^2}$$

Hence $$X_{ab} = X_{st} - \frac{m(R_a - R_{dc})}{1 + m^2} \tag{5.2.5}$$

Combining (5.2.3) & (5.2.5) $$X_{dc} - \frac{(R_a - R_{dc})}{m} = X_{st} - \frac{m(R_a - R_{dc})}{1 + m^2}$$

$$\Rightarrow \frac{X_{dc} - X_{st}}{R_a - R_{dc}} = \frac{1}{m} - \frac{m}{1 + m^2}$$

and $$R_a = R_{dc} + m(1 + m^2)(X_{dc} - X_{st}) \tag{5.2.6}$$

Comparing (5.2.4) & (5.2.6)

$$R_a = R_{dc} + m(1 + m^2)(X_{dc} - X_{st}) = (1 + m^2) R_{st} - m^2 R_{dc}$$

yielding $$(m^2 + 1)[m(X_{dc} - X_{st}) - (R_{st} - R_{dc})] = 0$$

whence $$m = \frac{R_{st} - R_{dc}}{X_{dc} - X_{st}} \tag{5.2.7}$$

So the calculation sequence for DCC parameters from the set of rotor impedances at slips of 1 and 0 (ie from {S}) was incorporated into program BC.PAS as follows based on the equations given by the figures in brackets :

(5.2.7) $m = \dfrac{(R_{st} - R_{dc})}{(X_{dc} - X_{st})} = \dfrac{(R_a + R_b)}{X_b}$

(5.2.4) $R_a = (1 + m^2)R_{st} - m^2 R_{dc}$

(5.2.1) $R_b = \dfrac{R_a R_{dc}}{R_a - R_{dc}}$

(5.2.2) $X_b = \dfrac{R_a^2}{m(R_a - R_{dc})}$

(5.2.3) $X_{ab} = X_{dc} - (R_a - R_{dc})/m$

It is stressed that once {S} is known, then (with $X_a = 0$), {C} is wholly determined (as are the design ratio, m and the two alternative depths of the referred equivalent uniform bar as derived in Chapter 2).

5.2.1.2. Method used to compare derived DCC with original UDB

Starting with UDBs of known dimensions and material, the sets {S} were calculated and hence the corresponding DCCs were derived using equations **(5.2.1) -- (5.2.7).** This process is documented in the graph of Figure 5.2.2 . The program BC.PAS was modified over a period of time to allow four options to be activated. The results obtained by using these extensions of the program will be discussed later in the thesis.

The first of these extensions was activated by setting the Boolean variable READ=TRUE. This allowed comparison between rotor parameter variation given by the UDB model starting from the bar width and depth and the variation given by starting from a specified set {S}. The second was activated by setting READ=TRUE. It allowed data for {S} to be taken from test measurements derived as in Chapter 7. Theoretical values of {S} were used taken from bars which were not truly uniform and the effect of trapezoidal or other non-uniform shapes was investigated. The third mode of operation of the program BC.PAS was developed after the extension of the UDB analysis to produce the Non-Uniform-Bar model (NUB) as shown Section 5.4. This program option was activated by selecting SIMUL=TRUE. In this case, comparisons were made between the rotor parameter variation predicted by the UDB and the NUB methods and also between these methods and practical measurements of rotor resistance and reactance made over the whole slip range.

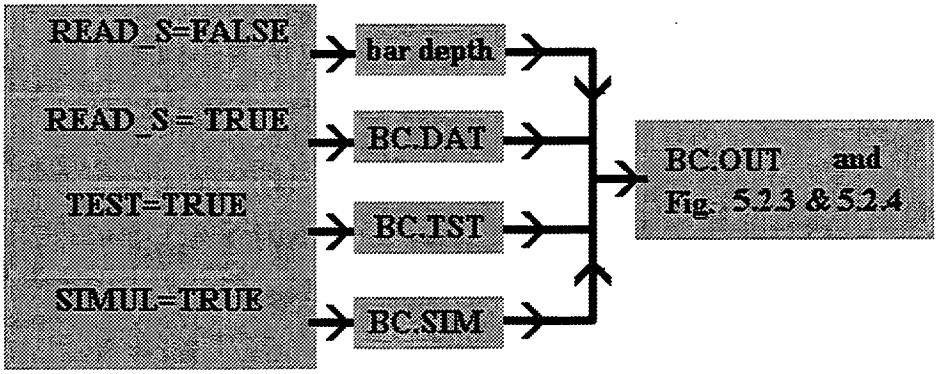

Figure 5.2.2 : DCC Rotor Parameter Variation Derived from UDB Starting Point

5.2.1.3. Results of deriving DCC from UDB starting point

For the uniform bars, bar depths were varied from 0.01m to 0.06m. In all except the very large bar sizes the UDB and DCC models gave indistinguishable results which are shown in Figure 5.2.3 for a bar of depth 40 mm and Figure 5.2.4 for a 60 mm bar.

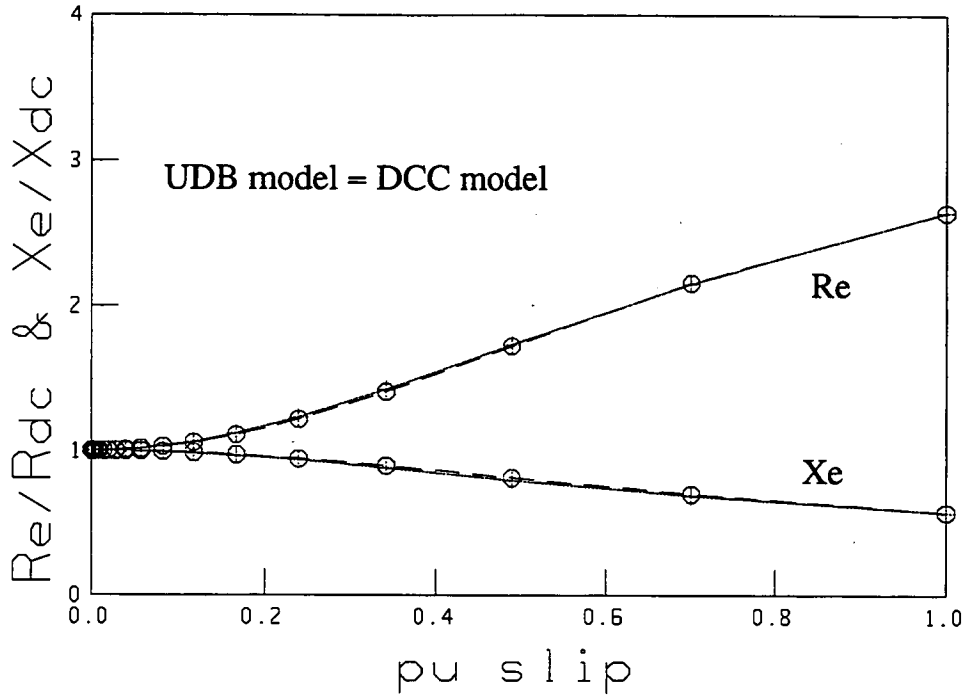

Figure 5.2.3 : DCC model Derived from UDB of 40 mm depth

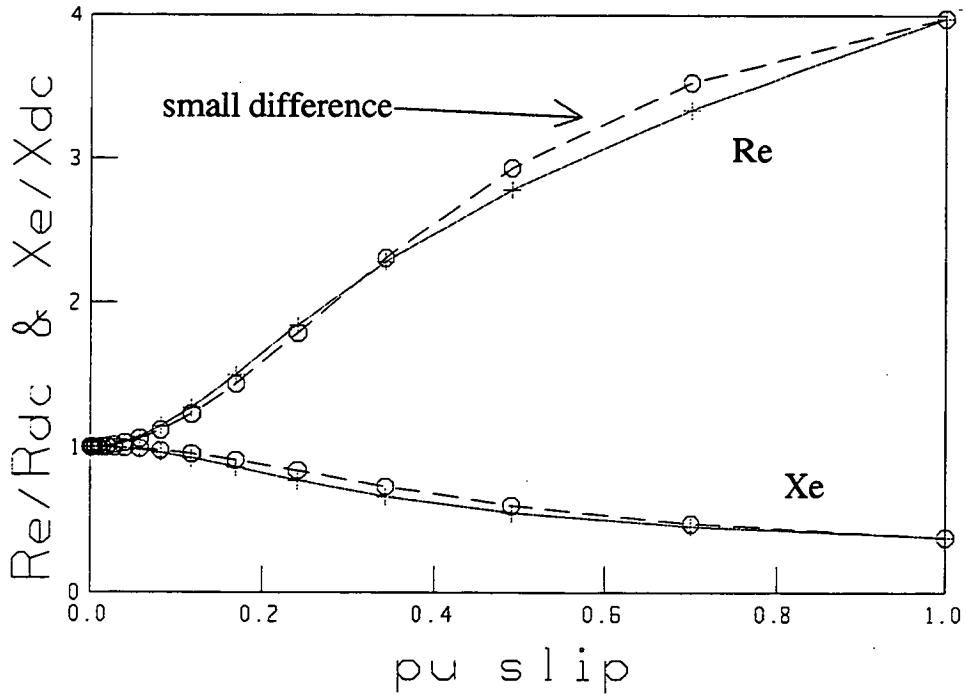

Figure 5.2.4 : DCC model Derived from UDB of 60 mm depth

Even for such a large bar there is little difference between the UDB and DCC models. This verifies that the DCC model can be nearly always considered to include the UDB model, ie it is a superset of it.

5.2.1.4. Comments on the results

It is clear from the results of figures 5.2.3 and 5.2.4 that if a machine has a genuine uniform bar (with an open slot) then it may be represented with equal accuracy by either model provided that the bar is not greater than about 0.05m deep at 50 Hz; ie about five times the skin depth. The DCC model assumes that the current density is uniform over each of the two bar segments which although not strictly the case (Figure 5.3.3) can be seen to be approximately true for bars with depth less than about 50 mm.

5.2.2. Uniform-Deep-Bar Equivalent Of Double-Cage Rotor

An attempt was then made to fit UDB models to some cage rotor models. Data for the DCC model, set {C}, was taken from the 8.2 MW machine given by Rogers and Shirmohammadi, [1987] and for two smaller motors used by Chalmers and Mulki, [1970]. In addition a comparison was made with two machines from the INSPEC program database discussed in Chapter 3. The data for all four of these machines is shown in Table 5.2.1.

	ID	kW	Vline	f	Ra	Rb	Xab	Xa	Xb
1	Rogers and Shirmohammadi	8200	6600	60	0.1180	0.0414	0.2702	0	0.2896
2	Chalmers and Mulki	6248	4000	35.5	0.665	0.0503	0.224	0	0.712
3	Chalmers and Mulki	194	415	50.0	0.396	0.065	0.131	0.009	0.387
4	5600hp boiler feed pump (INSPEC)	4180	4000	60.0	0.0647	0.0071	0.0544	0	0.0502
5	500hp drip-proof (INSPEC)	374	575	60.0	0.0194	0.0985	0.0917	0	0.15726

Table 5.2.1 Data for Cage to Bar Comparison with Program CB.PAS.

5.2.2.1. Method adopted for cage to bar comparison

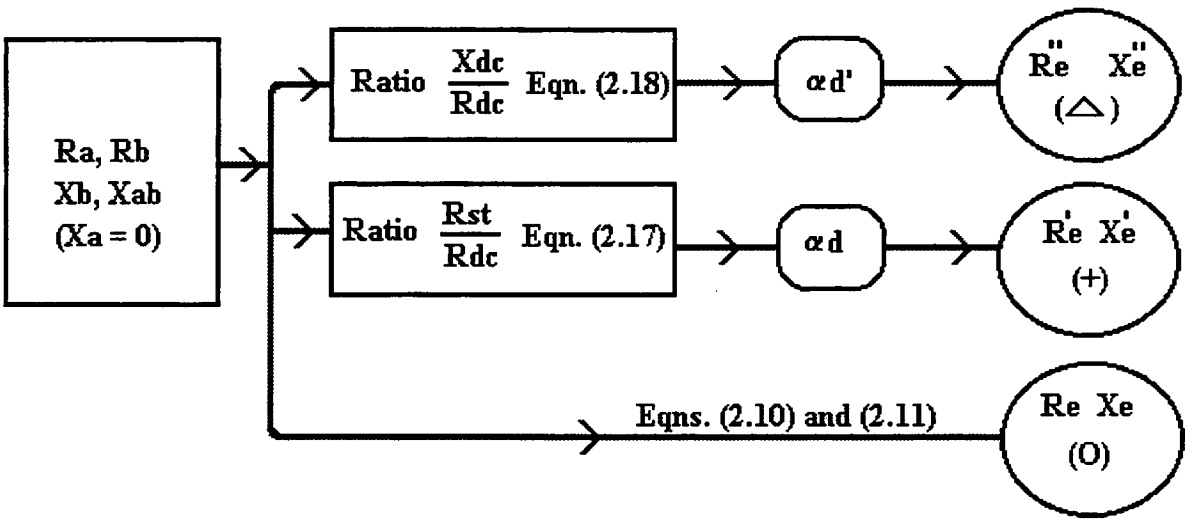

Figure 5.2.5 : Methods used for calculation of rotor parameters at any slip

The set {S} was calculated from the given circuit parameters, {C}. From {S}, the two alternative equivalent uniform bar depths were derived using the methods of Section 2.2.5.2. {The first, UDB' was based on d', (ratio X_{dc}/R_{dc}) and the second

model, UDB was based on d, (ratio R_{st}/R_{dc}). } The selection path for these methods is shown graphically in Figure 5.2.5. The rotor frequencies were calculated at several slip values. Equations 2.12 and 2.14 were used to derive new values of rotor impedance, called {R"e X"e} and {R'e X'e} respectively. These were compared with those obtained using equations (2.10) and (2.11) directly. The results of these comparisons are shown in Figures 5.2.6 to 5.2.10.

5.2.2.2. Results of numerical comparison

The components of {S} derived by using the program CB.PAS are shown in Table 5.2.2 together with the two alternative values, d1 and d2, derived for the depth of the equivalent uniform bar. In the graphs of Figures 5.2.5 to 5.2.9 the rotor resistance and reactance values are normalised about the DC values, Rdc and Xdc and the variation plotted against slip rather than against absolute frequency. This was done to allow comparison between the different machines in Table 5.2.1.

The first value of design ratio, m1 was computed from {S} as $m_1 = \frac{(R_{st} - R_{dc})}{(X_{dc} - X_{st})}$

The second was derived from the circuit directly as $m_2 = \frac{(R_a + R_b)}{X_b}$.

These were expected (and found) to be identical except in the case of the 194 kW motor which had a non-zero value for the upper cage reactance, X_a . This comparison was done as a check on the program. By inspecting the graphs of rotor impedance variation with slip it can be seen that the different methods used did not give the same results over the slip range. This indicates that whereas any reasonably sized uniform bar may be represented by a double cage equivalent circuit with no loss in accuracy the reverse is not true.

The two values for the depth of the equivalent bar were not always identical. If the bar were truly uniform the depths would be the same because from first principles it is unimportant whether depth is derived from the resistance or reactance ratio. The second and fifth machines showed the greatest differences in computed depth. In comparison, for motor number three, the impedance variations predicted were almost identical.

Motor ID	Rst	Xst	Rdc	Xdc	m_1	m_2	d'	d
8.2MW	0.098	0.307	0.031	0.429	0.55	0.55	63.2	43.8
6.25MW	0.3549	0.533	0.0468	0.8402	1.00	1.00	93	136
194kW	0.1927	0.299	0.0558	0.4167	1.16	1.19	**50.5**	**52**
5600hp	0.0255	0.0818	0.0064	0.0952	1.43	1.43	**65**	**55**
500hp	0.0183	0.093	0.0162	0.0960	0.75	0.75	41	15.3

Table 5.2.2 : Results of Numerical Comparison ; UDB' and UDB from DCC

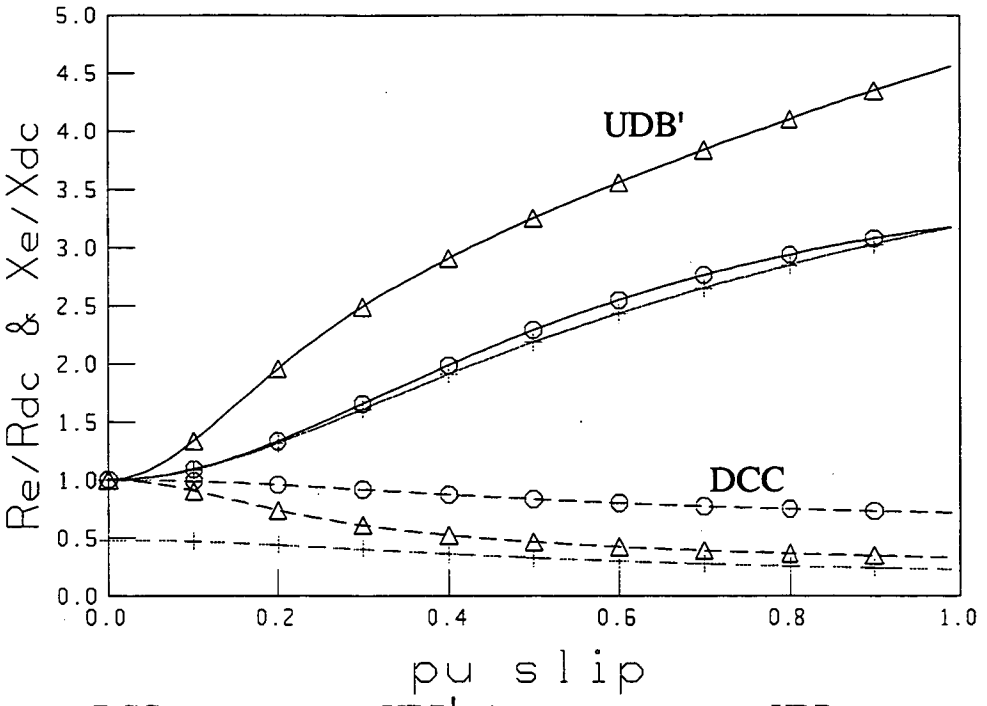

DCC, o UDB' Δ UDB +

Figure 5.2.6 : UDB Derived from DCC, (8.2 MW)

kW	Vline	f	Ra	Rb	Xab	Xa	Xb
8200	6600	60	0.1180	0.0414	0.2702	0	0.2896
Rst	Xst	Rdc	Xdc	m_1	m_2	d'	d
0.098	0.307	0.031	0.429	0.55	0.55	63.2	43.8

Table 5.2.3 : Nameplate data and rotor model parameters for 8.2 MW motor

Actual rotor slot profile data was not available for any of the machines in Table 5.2.1. It is therefore not possible to discus the graphs with complete confidence. However it is likely that the 8.2 MW motor had a uniform bar with a semi-closed slot which would cause the value of X_{dc} to be larger than the true uniform bar value of $2\pi f \frac{\mu_0 dl}{3w}$. (ie the error term of Swann and Salmon, given in equation 2.2.15 is significant). This is thought to be responsible for the negative offset of the UDB model X_e' curve (shown +) and for the poor fit for the UDB' model (shown Δ) in Figure 5.2.6. The UDB' model is constrained to fit at low slip because equation 2.2.14 was used to determine the reactance variation. At larger slip values it departs from the DCC model because it forces the same variation on the reactance component due to the bridge as on the rest of the slot. The resistance variation is widely in error because based on the high reactance at low slip it fits a bar that is too deep.

The resistance variation based on the UDB model was in good agreement with the circuit. This is to be expected if the bar is substantially uniform as it would be in a motor of this size. If the offset is corrected for, the UDB model can be seen to give the same results as the DCC model.

This DCC model of the 8.2 MW machine is shown in Chapter 6 to give a good fit to manufacturer's performance data and in Chapter 8 to contribute to accurate modelling

of run-up under load. This tends to confirm that its representation of the rotor parameter variation is reliable.

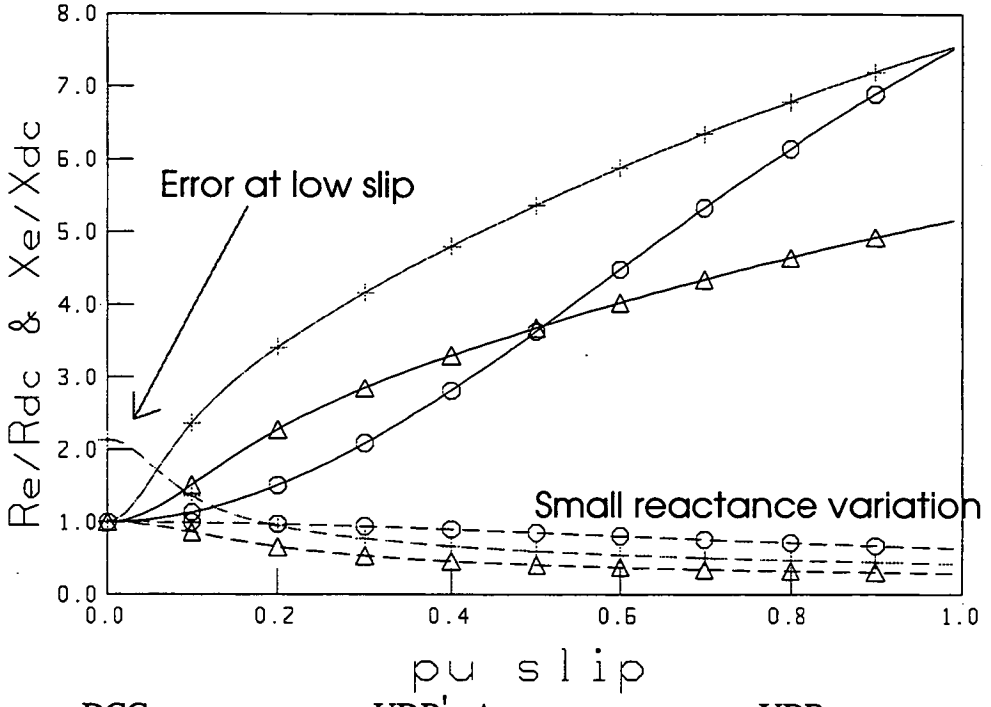

DCC, o UDB' Δ UDB +

Figure 5.2.7 : UDB Derived from DCC, (6.25 MW)

kW	Vline	f	Ra	Rb	Xab	Xa	Xb
6248	4000	35.5	0.665	0.0503	0.224	0	0.712
Rst	Xst	Rdc	Xdc	m_1	m_2	d'	d
0.3549	0.533	0.0468	0.8402	1.00	1.00	93	136

Table 5.2.4 : Nameplate data and rotor model parameters for 6.25 MW motor

For this motor the impedance variation was not well modelled by either UDB-type model. The reactance variation is greater than the DCC model except at low slip in Figure 5.2.7 where the presence of an anomaly is identified. This is not the same as the offset in Figure 5.2.6 but, due to lack of design data, the matter was not pursued further.

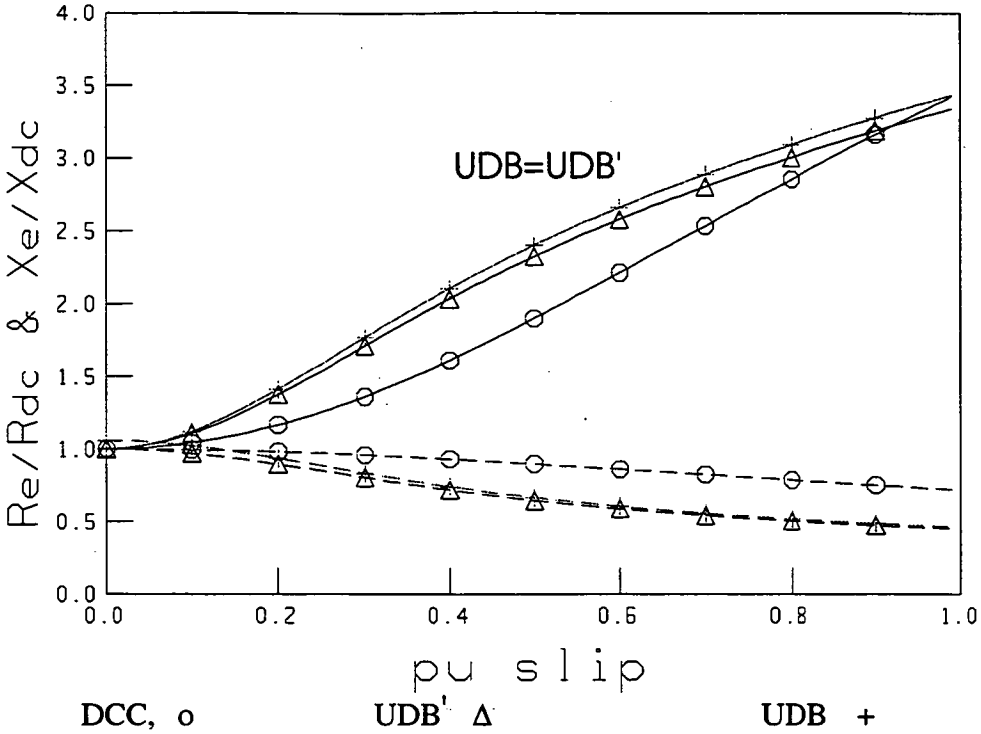

DCC, o UDB' Δ UDB +

Figure 5.2.8 : UDB Derived from DCC, (194 kW)

kW	Vline	f	Ra	Rb	Xab	Xa	Xb
194	415	50.0	0.396	0.065	0.131	0.009	0.387
Rst	Xst	Rdc	Xdc	m_1	m_2	d'	d
0.1927	0.299	0.0558	0.4167	1.16	1.19	**50.5**	**52**

Table 5.2.5 : Nameplate data and rotor model parameters for 194 kW motor

For the 194 kW motor the equivalent bar depths as calculated from the Rst/Rdc and Xdc/Rdc ratios were very close. As shown in Figure 5.2.8, the UDB and UDB' models agreed closely with each other but not with the DCC results except at the slip extremities where the models are constrained by the data used as a starting point. In this case the upper cage reactance, X_a , even though small, was not negligible.

Attempts to improve the fit by trial and error estimates of bar depth were unsuccessful which underlined the fact that the models are not equivalent. Part of the problem is that the two formulae for reactance (2.13) and (2.14) are only equivalent for truly uniform bars.

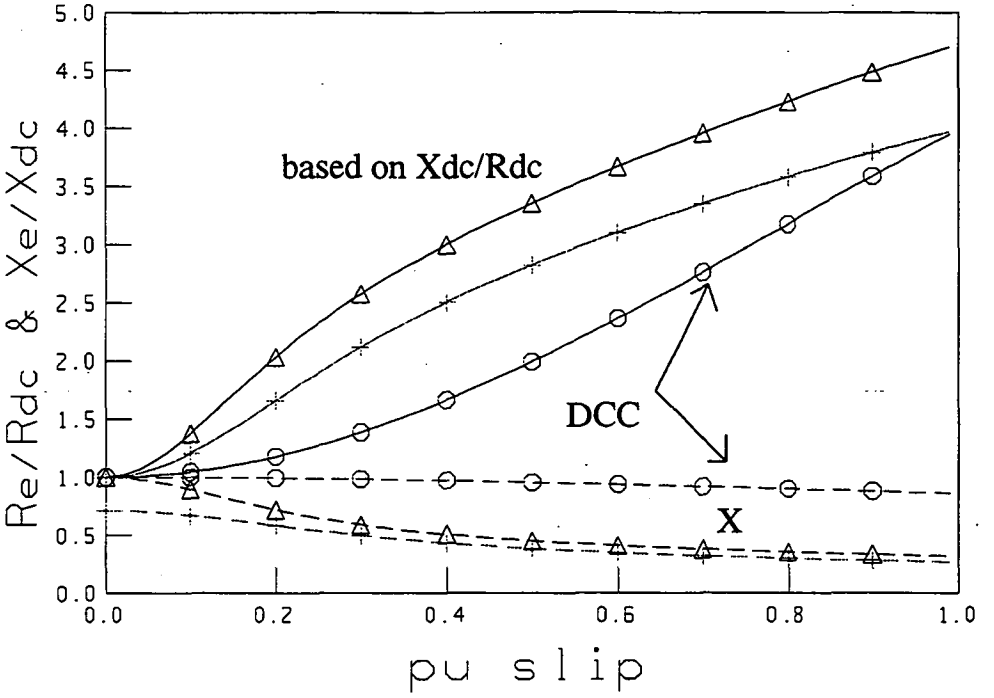

DCC, o UDB' Δ UDB +

Figure 5.2.9 : UDB Derived from DCC, (INSPEC "5600 hp")

kW	Vline	f	Ra	Rb	Xab	Xa	Xb
374	575	60.0	0.0194	0.0985	0.0917	0	0.15726
Rst	Xst	Rdc	Xdc	m'	m	d'	d
0.0255	0.0818	0.0064	0.0952	1.43	1.43	**65**	**55**

Table 5.2.6 : Nameplate data and rotor model parameters for "5600 hp" motor from INSPEC

This was the second largest motor studied and its reactance variation was similar to the 8.2 MW motor. The reactance was not quite so well modelled as the 8.2 MW motor, even if an offset is allowed for, leading to suspicions about the actual bar shape. The resistance variation was not well modelled by either UDB-Type model.

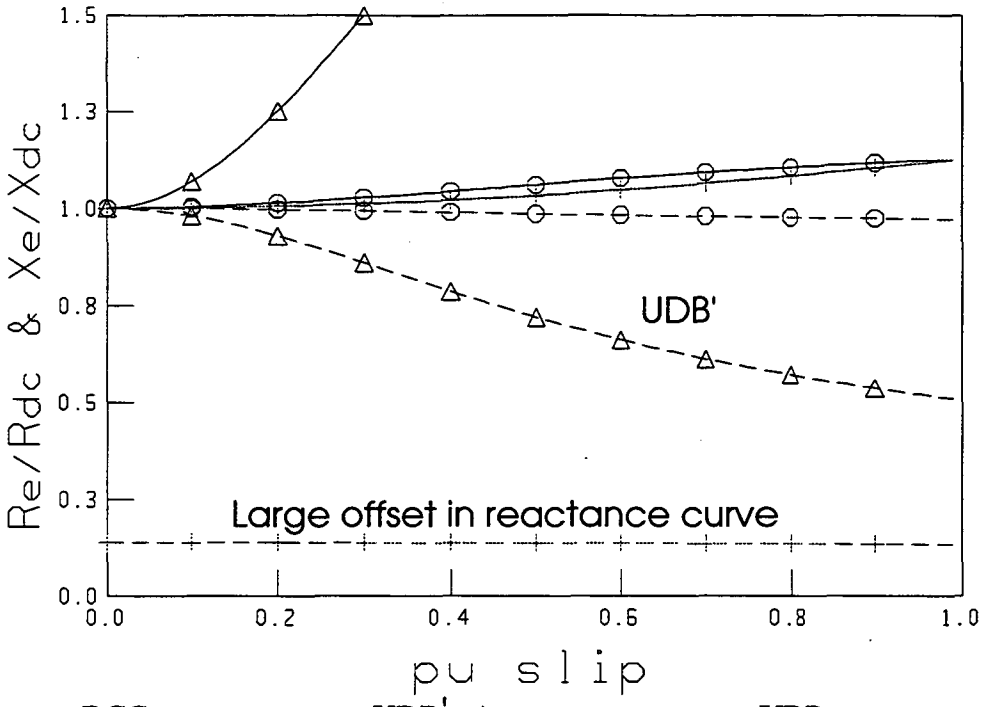

DCC, o UDB' Δ UDB +

Figure 5.2.10 : UDB Derived from DCC, (500 hp, INSPEC)

kW	Vline	f	Ra	Rb	Xab	Xa	Xb
4180	4000	60.0	0.0647	0.0071	0.0544	0	0.0502
Rst	Xst	Rdc	Xdc	m'	m	d'	d
0.0183	0.093	0.0162	0.0960	0.75	0.75	41	15.3

Table 5.2.7 : Nameplate data and rotor model parameters for "500 hp" motor from INSPEC

This was a smaller motor with quite large differences in the values for the two equivalent bar depths, d and d'. Again if the offset for the reactance curve is corrected for, then the UDB method will agree quite well with the DCC results.

The net result of the above work is to show that the UDB method cannot be relied upon to produce results which fit the variation in rotor impedance. The examples shown are typical and it is only with a very few large motors with presumably fairly uniform rotor slots and short slot bridges, that reasonable agreement occurs with the DCC model.

5.2.3. Selection Of A Model For Skin Effect

It has been demonstrated that given the parameters for a DCC model, then the equivalent UDB parameters may be calculated directly and vice versa.

The results show that, the DCC and UDB models are not generally equivalent in practice so that it cannot be assumed that a UDB model exists which will fit the rotor impedance variation over the complete slip range. In some cases, with particular slot geometries, the errors are very large. The effect of the slot bridge is to make equations(2.2.13) and (2.2.14) of limited value.

Unless the rotor bar shape is known to be truly of uniform cross section (ie. without a semi-closed opening) it is likely that the UDB model will give poor results for reactance even with relatively small rotor bars. Even where the bar depth is reasonably uniform, calculating equivalent bar depths as described above did not work very well, mainly due to the neglecting of the slot-bridge region. It is necessary to use performance data to optimise the value used for the depth of the equivalent bar.

If standard manufacturer's performance data are available then the DCC equivalent circuit parameters may be calculated as shown in Chapter 6. The DCC model has been shown to be a super-set of the UDB since any uniform bar of depth less than about 55 mm will be well represented by its equivalent DCC model. There seems little point in using the UDB model if a superior model can be derived from the same data.

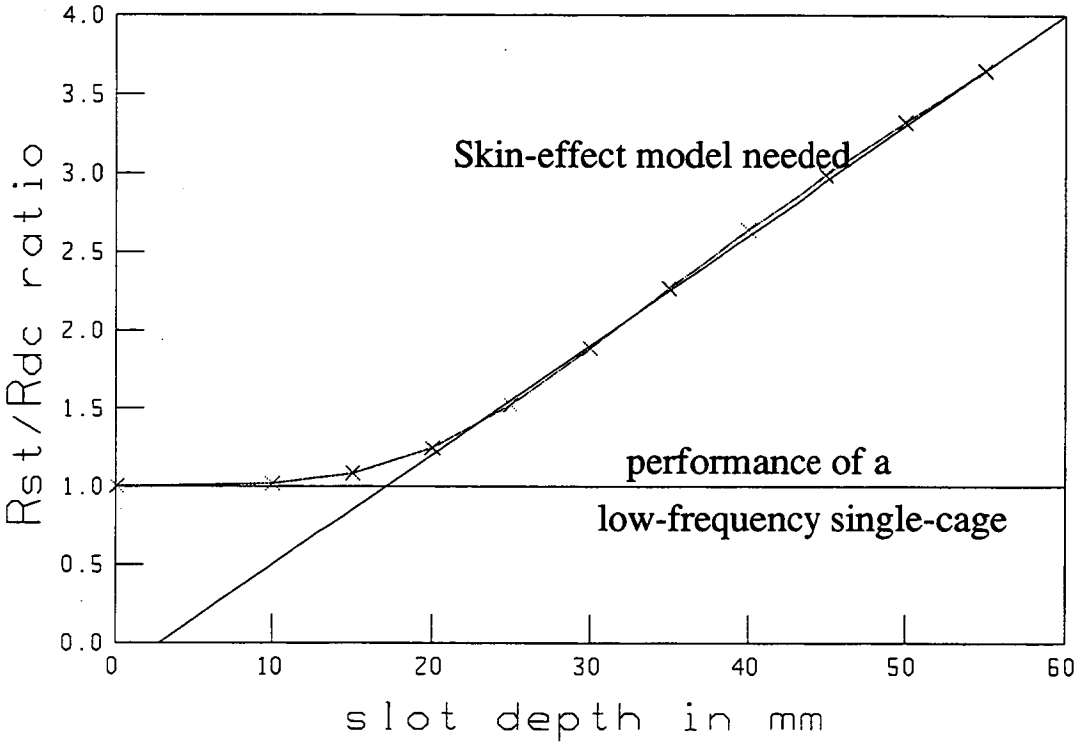

Figure 5.2.11 : Conditions for considering skin-effect as important

d (mm)	0.1	10.0	15.0	20.0	25.0	30.0	35.0	40.0	50.0	60.0
Rst/Rdc	1.00	1.02	1.08	1.25	1.52	1.88	2.27	2.64	3.32	3.98

Table 5.2.8 : Computed Rst/Rdc variation with slot depth for a cold uniform-width aluminium bar at 50 Hz [using equation (2.2.12)].

By examining Figure 5.2.11 it can be seen that for Rst/Rdc values of greater than about 1.25 the variation in rotor resistance with frequency becomes significant. For values above this the DCC model is recommended, with some reservations about the assumption that X_a =0, and with the recognition that, for closed and semi-closed slots, it requires special care in the modelling of leakage reactance variation due to saturation as discussed in Section 5.1.

5.3. VARIABLE-WIDTH-DEEP BAR (VWB) METHOD

The results of Section 5.2 showed that the UDB was not always a good model for rotor impedance variation with frequency due to skin effect. It was decided to investigate the underlying assumptions of Alger's analysis and to attempt to improve on the model. It was realised that the rotor impedance could be calculated from the slot geometry if the flux pattern at all parts of the magnetic circuit was known. This would require a sophisticated finite element program which allowed for saturation of stator and rotor iron (especially slot teeth). In the assumed absence of design data this was not considered a useful path to follow. It was decided to retain the assumption that flux travelled straight across the slot and to investigate the effect of taking into account the variation in slot width in the determination of current density.

Alger's general analytical method was repeated with the bar width, w taken as a function of radial position measured from the bottom of the slot. (This meant that w was included in the integration process.) The derived current density at various radial depths and frequencies was then used to calculate rotor circuit impedance at various values of rotor frequency.

An important part of the work done in this chapter is the documentation of the systematic checking of the analytical method and the program by reduction to simpler cases.

5.3.1. Derivation Of General Equation For Current Density

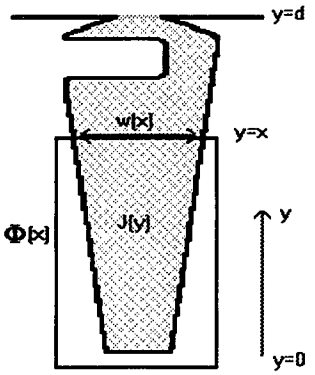

Figure 5.3.1 :
Variable-Width Slot

Consider a point, P located distance, x from the bottom of the rotor slot. Let the RMS leakage flux above point P linking the rotor bar (but not the stator) be Φ.

The RMS induced voltage is $E_{rms} = -j2\pi f\Phi$ and with impressed voltage, V the current density at point P is given by

$$J = \left(V - E_{rms}\right)/\rho \qquad (5.3.1)$$

$$\text{With } E_{rms} = -j2\pi f\int_{x}^{d} B(y)dy$$

$$\Rightarrow \frac{dE_{rms}}{dx} = -j2\pi fB$$

where $$B = \mu_0 H = \frac{\mu_0}{w(y)}\int_0^y w(x)J(x)dx$$

Differentiating (5.3.1) with respect to x gives $$\frac{dJ}{dx} = -\frac{1}{\rho}\frac{dE_{rms}}{dx} = \frac{j2\pi fB}{\rho}$$

(since V is independent of x)

$$\Rightarrow \frac{dJ}{dx} = \left[\frac{j2\pi f\mu_0}{\rho}\right]\frac{1}{w(x)}\int_o^x w(y)J(y)dy$$

$$\Rightarrow \frac{d^2J}{dx^2} = \left[\frac{j2\pi f\mu_0}{\rho}\right]\left[\frac{1}{w(x)}J(x)w(x) + \left(\int_o^x w(y)J(y)dy\right)\left(\frac{d}{dx}\frac{1}{w(x)}\right)\right]$$

$$\Rightarrow \frac{d^2J}{dx^2} = j2\alpha^2\left[J + \left(\frac{d}{dx}\frac{1}{w(x)}\right)\frac{w(x)}{j2\alpha^2}\frac{dJ}{dx}\right] \qquad \text{with } \alpha^2 = \frac{\pi f\mu_0}{\rho}$$

$$= j2\alpha^2 J + \left(\frac{d}{dx}\frac{1}{w(x)}\right)\left(w(x)\frac{dJ}{dx}\right)$$

$$\Rightarrow \frac{d^2J}{dx^2} = j2\alpha^2 J - \frac{1}{w}\frac{dw}{dx}\frac{dJ}{dx} \qquad (5.3.2)$$

An analytical solution to this does not exist except in series form. Since the calculation of the series terms would have been done by computer program it was decided to use a modification of the Runge-Kutta Turbo-Pascal procedure, originally produced and used for the performance simulation program described in Section 3.4, to solve for current density numerically using the two-point boundary conditions :

At the bottom of slot, x=0, $\frac{dJ}{dx} = 0$ and at the top of slot, x=d; $\frac{dJ}{dx} = \frac{j2\alpha^2 I}{w_{top}}$

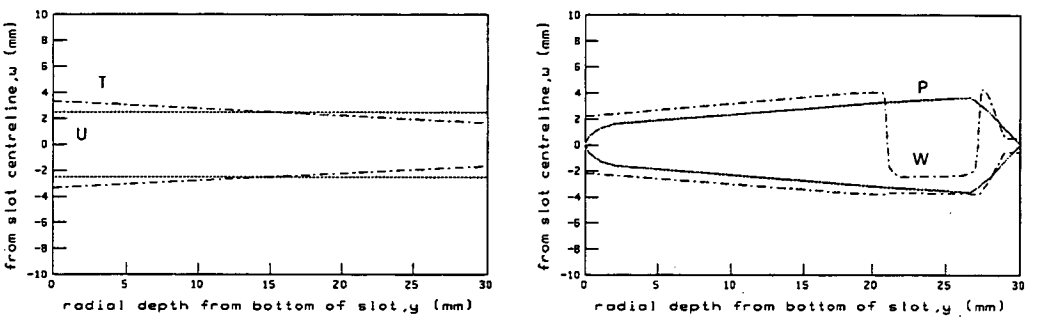

solid = U; dashed = T solid = P; dashed = W

Figure 5.3.2 : Slot shapes studied in this section; U, T, P and W

Several slot shapes were investigated as shown in Table 5.3.1. The slot width variations for each type of slot are shown in Figure 5.3.2. In each case the mean width of the slot was 5 mm and the radial depth 30 mm. This ensured that at low frequencies the resistances were equal. Graphs are also shown for similarly shaped slots with mean width of 3 mm and depth of 15 mm. In each case the RMS current in the slot was chosen to be such that it gave a mean current density of 5 MA/m^2. Since magnetic saturation is ignored in the calculation of flux density, the results are not affected by this choice. However, it was felt that by using realistic values some feel could be obtained as to the order of the computed leakage flux densities.

Since the results for the uniform slot were known, the calculation method was applied to the uniform slot as part of the systematic checking of programming. The trapezoidal slot was included to allowed the results to be compared with the UDB model by reducing the taper gradually to almost zero. For the P and W type slots the slot shape was read in as a set of discrete points and the intermediate values found by linear interpolation. Twenty unevenly spaced data points were used. This was

considered adequate since in practice the slot width would vary somewhat due to imperfections in building up the laminations. The data for the trapezoidal slot was also read in order to check this method of data entry. As a visual check, the slot data was retrieved from the files and plotted to obtain the graphs of Figure 5.3.2.

Slot ID	Description/Data Source
U	Uniform slot width
T	Trapezoidal slot
P	Pope 7.5 kW, 415V 50 Hz, 4 pole, single cage
W	WEG slot (copied from catalogue cover), [WEG, 1986]

Table 5.3.1 : slot shapes used in Section 5.3

The source file for program JB_RK4.PAS is included in the disk pocket together with data files for the slots studied. Data files are of the form SLOT_* where * is U, T, P or W.

For a trapezoidal section with upper and lower widths w_1 and w_2, the slot width, w at distance, x from the bottom of the slot is given by

$$w = w_2 - (w_2 - w_1)\frac{x}{d} \qquad (5.3.3)$$

Equation (5.3.2) then reduces to the form of (5.3.4) with the current density, J given by the solution of :

$$\frac{d^2J}{dx^2} = j2\alpha^2 J + \frac{(w_2 - w_1)}{\left[dw_2 - (w_2 - w_1)x\right]}\frac{dJ}{dx} \qquad (5.3.4)$$

This is a useful further check on the non-uniform bar analysis since the second term in equation (5.3.4) disappears for a uniform slot width, yielding Alger's equation for current density variation.

5.3.2. Results Of Numerical Simulation Of J And B

Because equation 5.3.2 is a second-order differential equation in the complex variable, J it must be solved numerically using four first-order real equations. For the RK4 simulation the state variables used were the real and imaginary parts of current density, J and the real and imaginary parts of the differentials.

From the real and imaginary parts of $\frac{dJ}{dx}$, the magnetic flux density at any point distant, x from the bottom of the slot may be calculated from

$$B = -j\left(\frac{\rho}{2\pi f}\right)\frac{dJ}{dx} \qquad (5.3.5)$$

with the flux density at the top of the slot being given by $B_{top} = \frac{\mu_0 I}{w_{top}}$

where w_{top} is the slot width at the airgap. This can be seen to be so by applying Ampere's circuital law to the flux path shown in Figure 5.3.1 with the assumption that the permeability of the steel is very large compared with that of the slot contents.

The results of Figure 5.3.3 to 5.3.6 were compared with the direct use of Alger's formulae and were found to be identical. This helped to increase confidence in the computational process as implemented by the program.

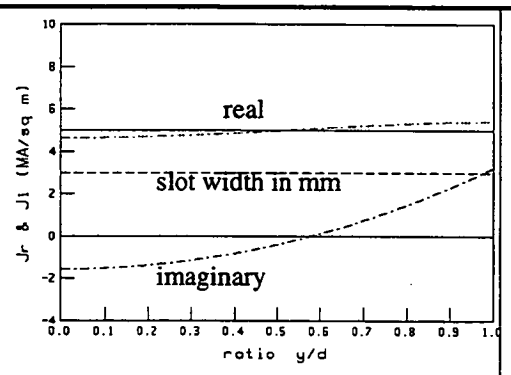

Figure 5.3.3 :
Current density variation

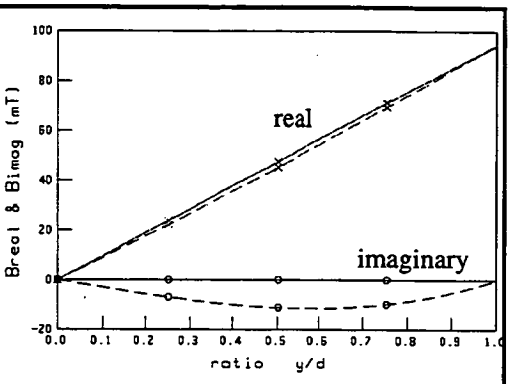

Figure 5.3.4 :
Flux density variation

Uniform slot, 15 x 3 mm; I_{RMS} = 225A ;
solid = 0.1 Hz, dashed = 50 Hz.

It is noted that the main difference between the behaviour of the 15 mm and 30 mm deep uniform width bars was one of magnitude rather than of form.

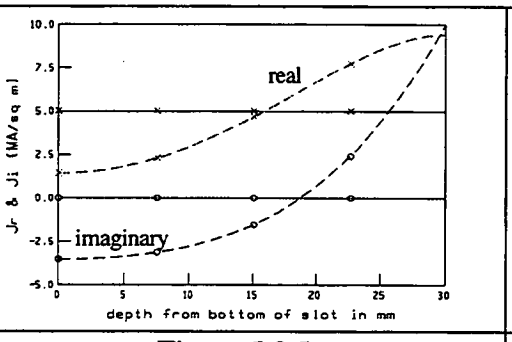

Figure 5.3.5 :
Current density variation

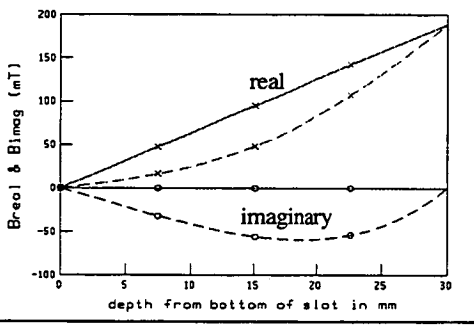

Figure 5.3.6 :
Flux density variation

Uniform slot, 30 x 5 mm; I_{RMS} = 750A ;
solid = 0.1 Hz, dashed = 50 Hz.

The graphs of Figures 5.3.7 to 5.3.10 illustrate the effect of variable slot width on the variation of current and magnetic flux densities with frequency. The effect on flux density at the top of the slot (y/d = 1) is clearly seen. Comparing the P-type slot with the W-type it is noted that the former shows less variation in distribution as the frequency changes from near zero to 50 Hz. In all cases, including the U-type slot, the imaginary component of current density is more affected by distance y.

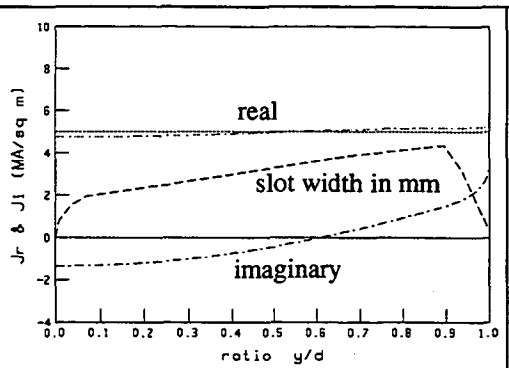

Figure 5.3.7 :
Current density variation

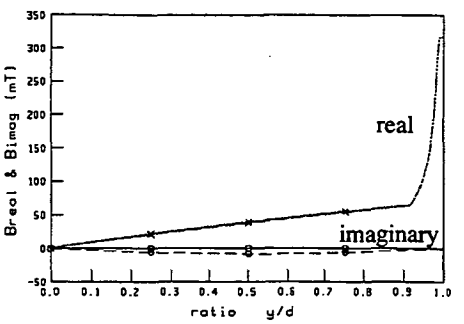

Figure 5.3.8 :
Flux density variation

P-type slot, 15 x 3 mm ; I_{RMS} = 225A;
solid = 0.1 Hz, dashed = 50 Hz.

The W-Type slot was included in the set of chosen slots because of its extreme irregularity in width which was expected to show dramatic changes in current density distribution compared with the slowly changing width of the P-Type slot. This is shown to be the case. The effect on the magnetic flux density is apparent in Figure 5.3.10. The effect of the notch in the slot was to increase the magnitude of the imaginary component of flux density at higher frequencies without significantly altering the real component.

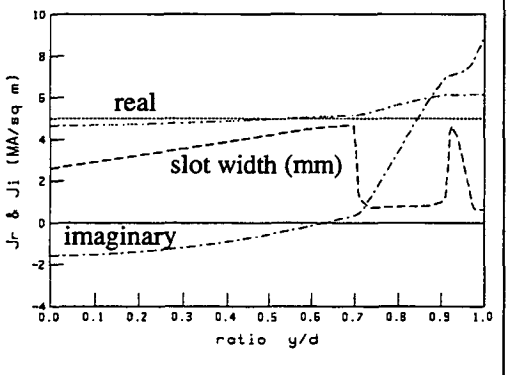

Figure 5.3.9 :
Current density variation

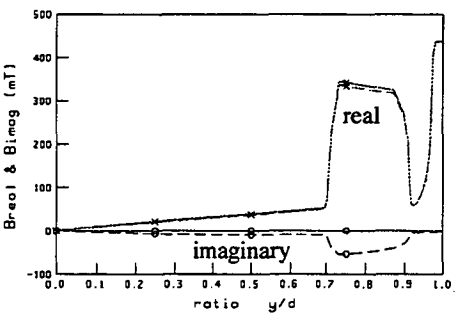

Figure 5.3.10 :
Flux density variation

W-type slot, 15 x 3 mm ; I_{RMS} = 225A;
solid = 0.1 Hz, dashed = 50 Hz.

The phase relationship of the current and flux can be seen to change as the frequency increases. From (5.3.1) it can be seen that the applied voltage, V per metre of axial length is given by

$$V = \int_{x=0}^{x=d} (-j2\pi fB + \rho J)dx \qquad (5.3.6)$$

The flux and current densities vary with time and distance from the bottom of the slot as well as with frequency. This is shown in the polar plots of Figures 5.3.11 to 5.3.15. The RMS voltage, E_{rms} induced in the bar is given by $E_{rms} = -j2\pi f\Phi$ where the RMS leakage flux, Φ is calculated over the whole bar depth.

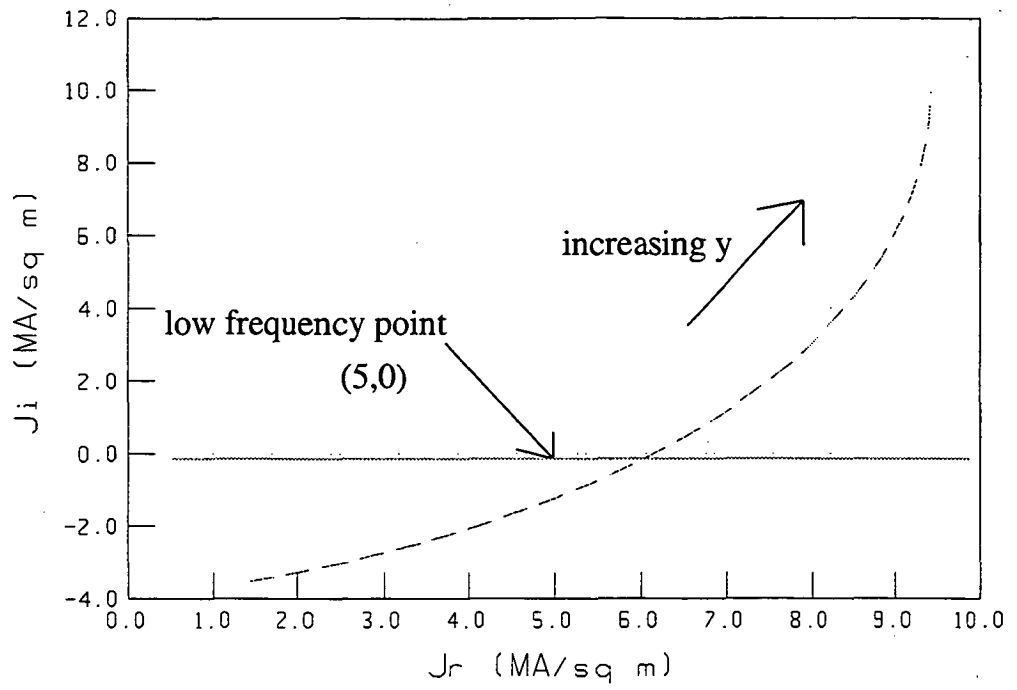

Figure 5.3.11 : Current density variation
U-type slot, 30 x 5 mm ; I_{RMS} = 750A at 50 Hz.

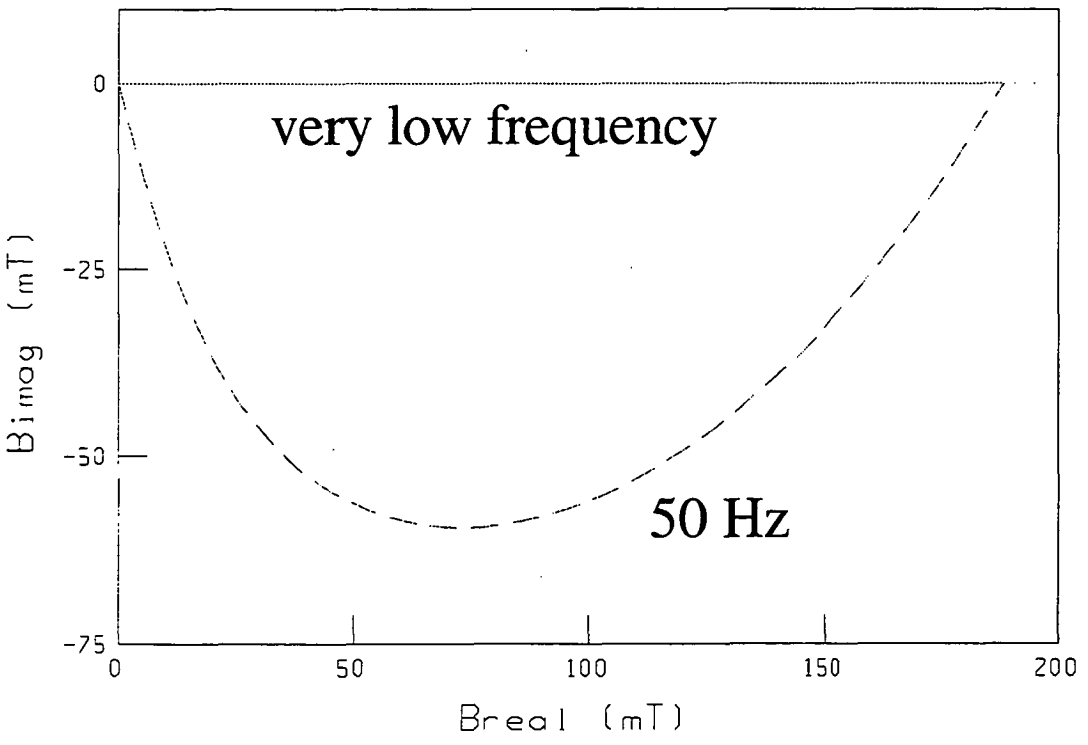

Figure 5.3.12 : Flux density variation
U-type slot, 30 x 5 mm ; I_{RMS} = 750A at 50 Hz.

Figures 5.3.13 and 5.3.14 show plots of several phasors representing J and B at different depths in the W-Type slot at a constant frequency of 50 Hz.

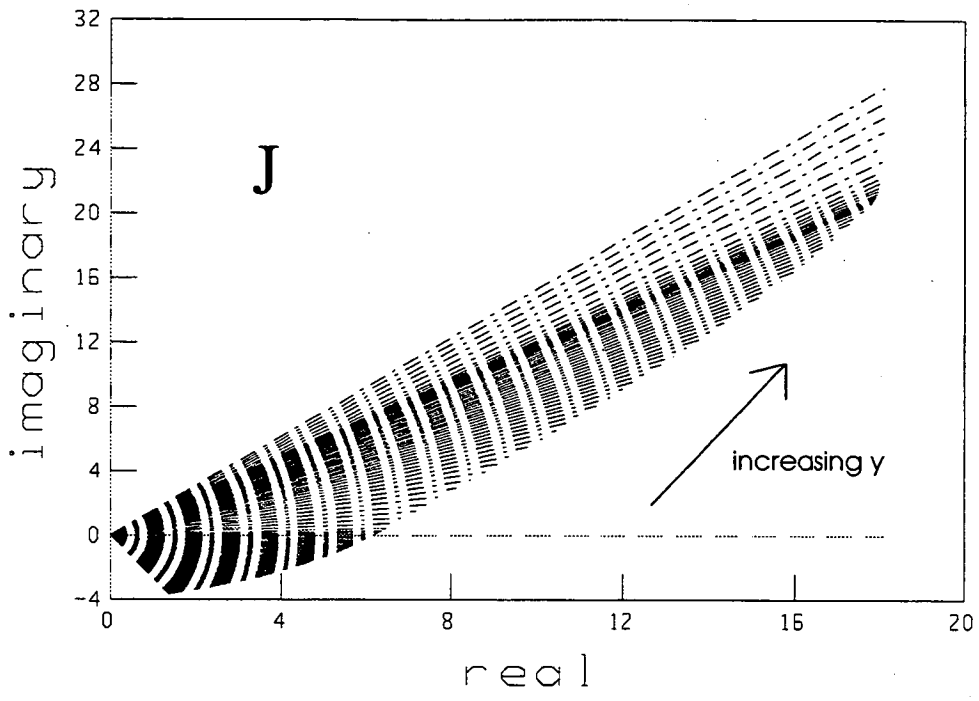

Figure 5.3.13 : Phasor diagrams of J for 30 mm deep, W type slot at 50 Hz.
Variable distance, y from bottom of slot
J in MA/m^2

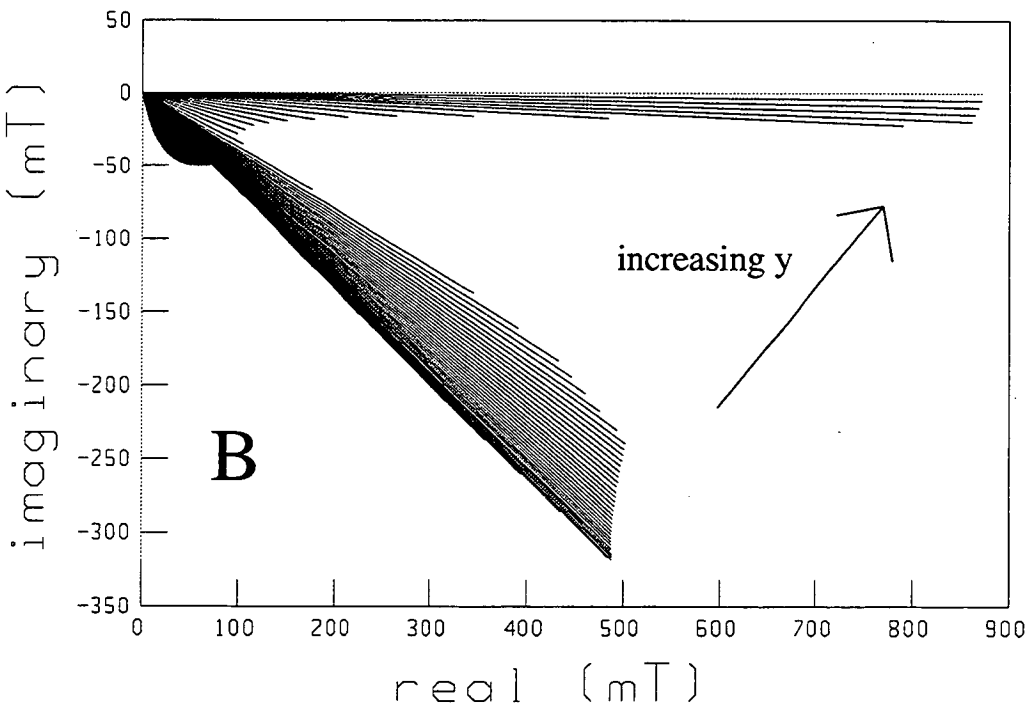

Figure 5.3.14 : Polar plot of magnetic flux density variation for W-type slot 30 x 5 mm ; I_{RMS} = 750A; 50 Hz, variable distance, y from bottom of slot.

Figure 5.3.15 shows a series of phasor diagrams of B for a 30 mm deep W-type slot at a constant distance from the bottom of the slot of 26 mm at frequencies from close to zero to 50 Hz. It shows how the phase of the magnetic flux density increasingly lags the current density. This graph relates directly to equation (5.3.5).

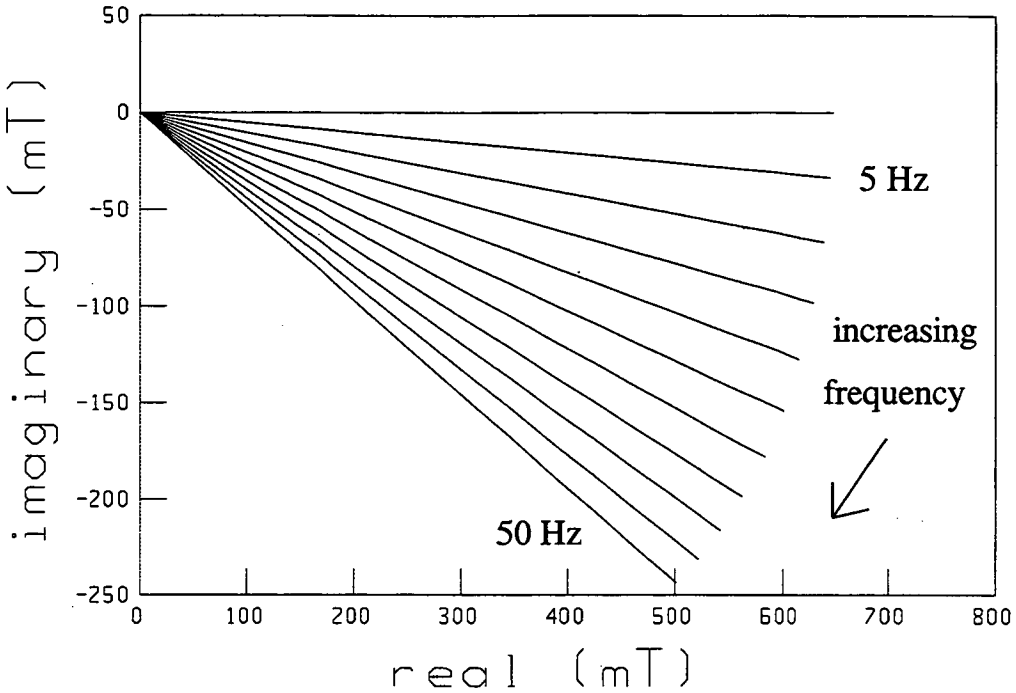

Figure 5.3.15 : Phasor diagrams of B for 30 mm deep W-type slot at a constant distance of 26 mm from the bottom of the slot at frequencies 0 - 50 Hz

5.3.3. Impedance From VWB Model

Once the current density, J was known then the leakage inductance was calculated from the slot dimensions as described in Section 2.6.1. (It was assumed that the relative permeability of the steel was infinitely large).

Values of J obtained were used to calculate the total slot component of rotor leakage reactance for several non-uniform bar types as $X_e = 2\pi f L_e$ where $L_e = \frac{N\phi}{I}$ and the partial turns and flux were numerically integrated throughout the slot depth.

In a similar way, the effective AC resistance, R_{ac} was determined by considering

$$I^2 R_{ac} = \rho \int_{x=0}^{x=d} w(x) J^2(x) dx \qquad (5.3.7)$$

The exclusion of the non-slot components of rotor leakage reactance was justified qualitatively in Chapter 2. The approach adopted in this Chapter was to compare the UDB, DCC and VWB models with each other over the slip range from 1 to zero and to leave the comparison with experimental results to Chapter 7.

5.3.3.1. Checks on the computer program

The computational path for the calculation of rotor impedance as a function of frequency using the non-uniform bar method was rather complex. The chances of an error occurring during the writing of the program code were considered high. During the computation several checks were made to develop confidence in the results.

Firstly, the total slot area was summed during the integration process and compared with the expected area. Secondly the current density was integrated over the whole slot and compared with the RMS current used as a starting point. In addition, the relative dimensions of the slot shapes were varied so that, for example the trapezoidal slot, T became almost uniform with the results then being compared with those obtained using the procedures for a uniform slot. This developed confidence in the program's ability to perform the correct analysis method whatever slot type was specified.

A further check was performed by letting the current density distribution in the uniform slot vary as a linear approximation. This was not intended to be an accurate representation of the actual current density distribution. By creating a data file with the same format as those produced by the JB_RK4.PAS program but with current density varying as $J(x) = a + bx$ it was possible to compare the derived impedance values with those derived from the analysis below.
Consider a line of flux as shown in Figure 5.3.16,

$$\Phi(x) = \frac{\mu_0 l}{w} I(x)dx \tag{5.3.8}$$

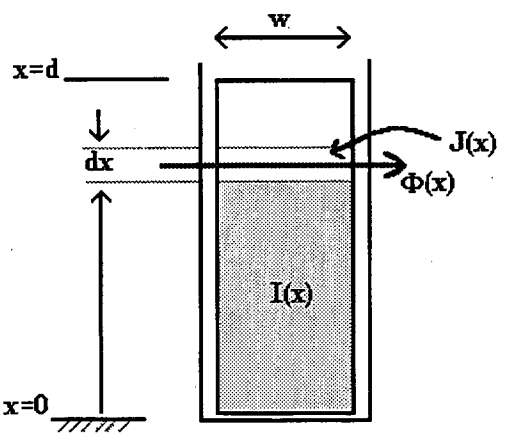

The current linked by this flux line is

$$I(x) = w \int_{y=0}^{y=x} J(y)dy$$

$$I(x) = w \int_{y=0}^{y=x} (a + by)dy$$

$$= w\left[ay + by^2/2\right]_{y=0}^{y=x}$$

$$= w\left[ax + bx^2/2\right]$$

Figure 5.3.16 Analytical determination of leakage inductance.

This flux links N turns, where $N = \frac{x}{d}$

The total current is $I = wd\left[a + bd/2\right]$

The inductance of the rotor bar is given by the integration of the total flux linkages over the whole slot depth.

$$L = \frac{1}{wd\left[a + bd/2\right]} \int_{x=0}^{x=d} \frac{x}{d} \frac{\mu_0 l}{w} w\left[ax + bx^2/2\right]dx$$

$$L = \frac{\mu_0 l}{wd^2[a+bd/2]} \int_{x=0}^{x=d} [ax^2 + bx^3/2]dx \qquad = \frac{\mu_0 ld[a/3+bd/8]}{w[a+bd/2]} \tag{5.3.9}$$

In a similar way the expression for the ac resistance was derived as

$$R_{ac} = \frac{\rho}{wd} \frac{\left(a^2 + \frac{1}{3}b^2d^2 + abd\right)}{(a+bd/2)^2} \tag{5.3.10}$$

If the constant b=0 then equation (5.3.9) reduces to the familiar expression for the inductance of a bar as the frequency tends to zero (uniform current density)

$$L_{dc} = \frac{\mu_0 ld}{3w} \tag{5.3.11}$$

The dc resistance is given by $$R_{dc} = \frac{\rho}{wd} \tag{5.3.12}$$

combining these two expressions it can be seen that $$\frac{X_{dc}}{R_{dc}} = \frac{2\alpha^2 d^2}{3} \tag{5.3.13}$$

where $\alpha^2 = \frac{\pi f \mu_0}{\rho}$

This verifies the equivalence of the equations (2.2.13) and (2.2.14) due to Alger and Kostenko and Piotrovsky from an electromagnetic as opposed to a purely mathematical manner as shown in Section 2.6.

In order to check the program ZE1.PAS, the values of constants a and b were assigned to be : $a = 4.0 \times 10^6$ and $b = 250 \times 10^6$. These gave a current density variation which roughly approximated that of the uniform bar at a frequency of about 35 Hz. ie ranging linearly from 4 MA/m^2 at the bottom of the slot to 11.5 MA/m^2 at the top of the slot. By substitution in (5.3.7) the expected inductance was calculated to be 2.209 μH per metre of slot length. Using program ZE1.PAS with the linearly generated values for current density read from a data file with the same format as those produced by the RK4 solution of equation (5.3.2) gave an inductance of 2.25 μH. In a similar way the resistance per metre of length was calculated to be 0.323 mΩ using equation (5.3.10) and 0.326 mΩ using the program. Considering that the slot was only subdivided into 50 segments and the computation was performed in single precision, this was considered reasonable. For the more complex slot shapes the error in calculated inductance might be slightly larger but it was not very large. The summations of area and total current were all within less than 1% of the expected values. In practice, the errors due to simplifying underlying assumptions would be more significant that the computational errors; eg assuming that the flux goes straight across the slot. This procedure tended to give confidence that gross programming errors were absent from the program.

5.3.4. Impedance From DCC Equivalent Of VWB Models

The above VWB model was applied to U, T, P and W-type slots (as defined in Figure 5.3.2). For each slot current density was calculated for a range of frequencies from

close to zero to 60 Hz for points from the bottom up to the top of the slot. These current density distributions are stored as files *.# where * stands for the slot type (U, T, P, W, S and R) and # was A to M for frequencies 0 - 60 Hz. eg the file W.G contained data for the WEG type slot at 30 Hz. Program ZE1.PAS was used to determine the rotor impedance variation yielding **{S}** as defined in Section 5.2.

Once the impedance variation was calculated using the VWB model it was realised that the results could be compared with both the DCC and UDB models by fitting these to the impedance values at low and high slip.

The program BC.PAS was used with the READ_S option set TRUE to allow direct reading of the set **{S}** from data file BC.DAT. This allowed fitting of a UDB model with the same **{S}**. Following the method of Section 5.2, the DCC model parameters, **{C}** were calculated using equations **(5.2.1)** - **(5.2.7)**. These DCC model parameter values were used in equations **(2.10)** & **(2.11)** to graph the impedance over the full slip range.

Figures (5.3.3 to 5.3.8) show the results in Ohm per metre with a slot depth of 0.03m. The graphs show the variation in rotor impedance as modelled by the VWB model and by the DCC and UDB models with the same {S}. To allow comparison, all slots were made of equal area so that the DC resistances would be equal at 0.3 Ohm which represents cast aluminium at 20^0C (resistivity of 4.5×10^{-8}).

The results are shown graphically in Figures 5.3.17 to 5.3.20 with the circuit parameters for the DCC circuit and the UDB depths given in Table 5.3.1.

	Rst	Xst	Xdc	d' (mm)	d	m	Ra	Rb	Xb	Xab
U	0.571	0.597	0.790	30.00	30.27	1.41	1.108	0.411	1.079	0.216
T	0.674	0.864	1.119	35.71	34.70	1.47	1.481	0.376	1.264	0.315
W	0.451	0.678	0.762	29.48	24.73	1.79	0.934	0.442	0.770	0.407
P	1.103	1.635	2.142	49.41	55.40	1.58	3.117	0.332	2.177	0.364
S	0.767	0.507	1.126	35.82	38.81	0.75	1.032	0.423	1.929	0.155
R	0.573	1.235	1.393	39.85	30.36	1.73	1.388	0.383	1.025	0.763

Table 5.3.1 : Equivalent DCC parameters from VWB-based impedance variation uniform bar 30 x 5 mm, aluminium at 20 ^{0}C.

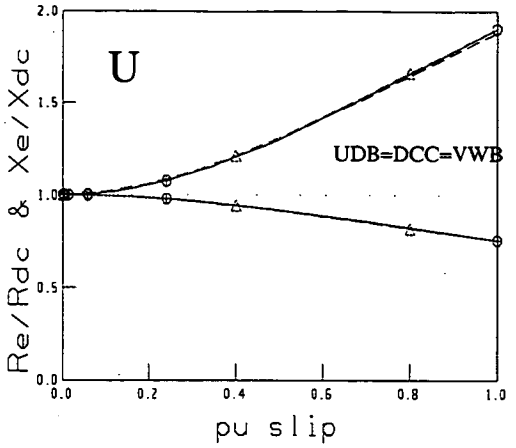

Figure 5.3.17 : U-type slot.

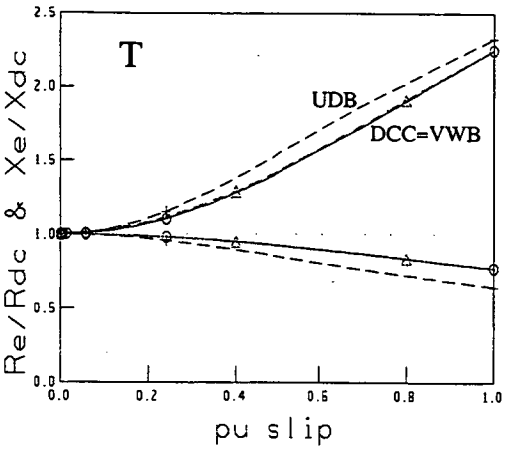

Figure 5.3.18 : T-Type slot

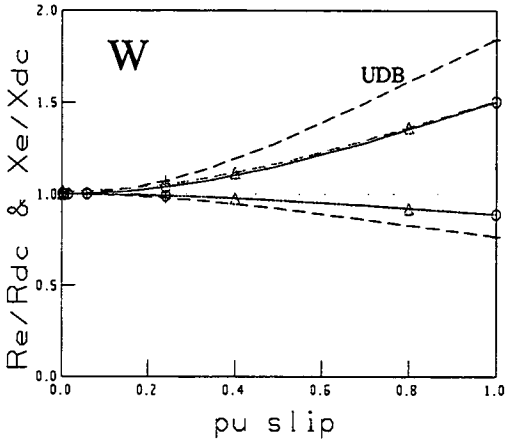

Figure 5.3.19 : W-type slot.

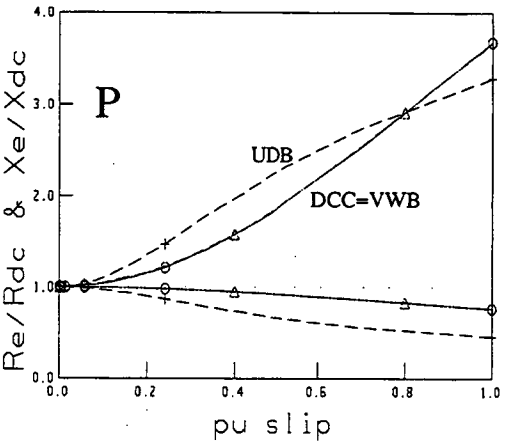

Figure 5.3.20 : P-Type slot

Comparison of VWB with DCC and UDB Models; 30 mm deep slot.

5.3.5. Comments On VWB models

It was found that, with the same **{S}**, the UDB, DCC and VWB models agreed completely for the uniform slot. This was expected and served to confirm that the programs were working correctly. For slot depths above about 0.015m, with the W and P-type slots, the UDB model differed considerably from the DCC and the VWB models. The DCC model agreed well with the VWB starting point for all cases tried. This is significant because it shows that the double cage circuit is capable of representing quite complex slot shapes. Because the non-slot reactance terms were neglected in the VWB model, (Section 2.2.6.2.3) it was uncertain at this stage if the DCC would be able to adequately represent the total rotor circuit referred impedance.

In Chapter 7 measured values of rotor impedance variation with slip are compared with those predicted by the VWB model and found to be in close agreement. The VWB model suffers from the need to obtain slot dimensions and the fact that it is based on an RK4 solution of equation (5.3.2). In practice, the DCC model is preferred for use within numerical simulation programs which allow for variation of rotor impedance with slip. However the results of this section and Section 5.2 can be used to confirm that this choice is valid. They also strongly support the rejection of the use of the UDB model especially if there is no allowance for the slot bridge as given in equation (2.2.1.5).

5.4. Simulation Of The Effect Of Temperature On Rotor Impedance

Once the VWB method was developed as discussed in Section 5.3, it was decided to apply it to bars with different resistivity to simulate an increase in temperature. The general effect of temperature on rotor impedance has been discussed in Chapter 2. The results of the simulation work presented here confirm the reported variation in measured rotor reactance with temperature mentioned in Chapter 2. The work also allowed an estimate to be made of the relative significance of the variations due to frequency and temperature. This is significant because some authors indicate that the observed effect of temperature on rotor reactance is due to either the temperature affecting the stator/rotor effective turns ratio or to the dependence of the equivalent reactance on the values of the two rotor loop resistances, [Andria, Dell'Aquila, Salvatore and Savino, 1987], [Klaes, 1993]. It is clear from the preceding analysis that some variation in rotor reactance will occur due to the redistribution of the current density pattern which occurs at higher values of resistivity. The work in this Section confirms that the temperature affects the reactance by changing the resistivity of the material and hence the nature of the current displacement effects which occur at higher frequencies.

The simulation work also allows the relative significance of the changes in rotor resistance due rise in temperature and skin effect to be assessed for various rotor bar depths.

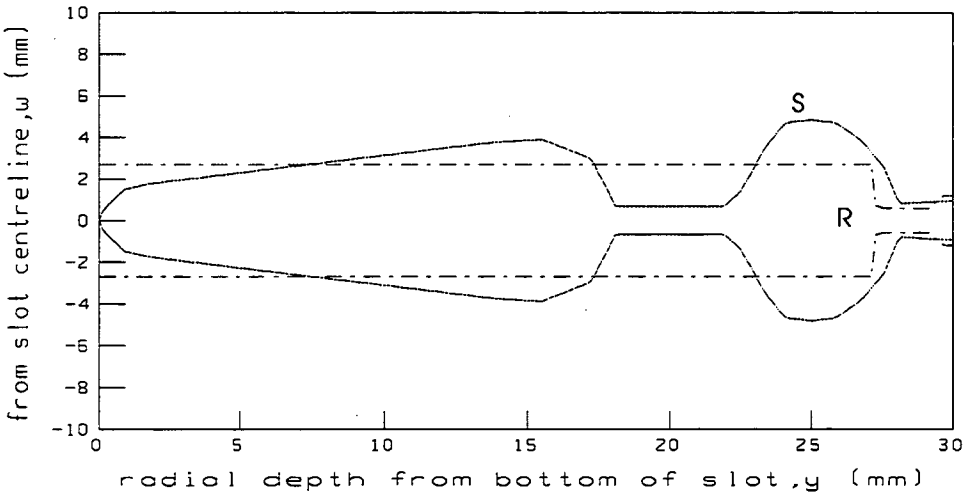

Figure 5.4.1 : Slot shapes S(solid) and R (dashed)

5.4.1. Method Used For Investigating The Effect Of Temperature

For the work reported in this section, bars of cross-section U, W and P as in Table 5.3.1 and Figure 5.3.2 were used. In addition, slot shapes from two additional motors were used. These shapes were called S and R and are shown in Figure 5.4.1. All bars had radial lengths of 30 mm and mean widths of 5 mm. This ensured that at the same temperature and at low frequency the resistances were the same. Two extremes are presented in the graphs of Figures 5.4.2 to 5.4.6. The first used a resistivity of 4.5 x 10^{-8} to represent cast aluminium at 20 ^{0}C. The second used a resistivity of 6.34 x 10^{-8} which represents a temperature increase to a mean operating temperature of 120 ^{0}C, [IEEE, 1988].

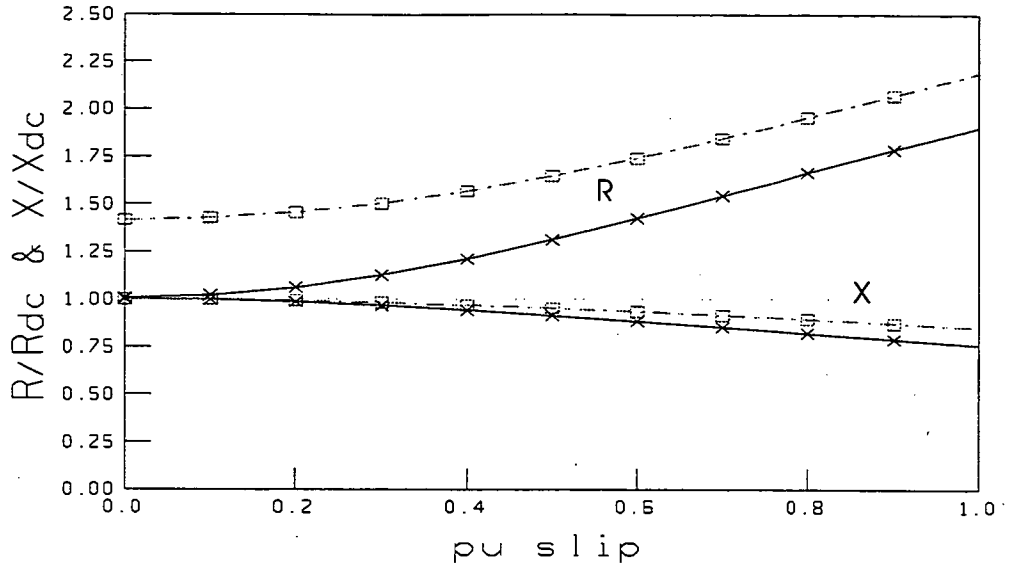

Figure 5.4.2 : Effect of temperature variation in the U-type slot
(solid = cold; dashed = hot)

5.4.2. Results Of The Simulation

The results of the simulation were not unexpected but the technique highlighted some differences between different rotor bar designs. In all cases the effect of temperature on rotor reactance was much smaller than that of frequency. The graphs of Figures 5.4.2 to 5.4.6 show the variation for the U, W, P, R and S slot types. The resistances and reactances are shown relative to a cold bar at low frequency.

The results show that the separation of the hot and cold curves for relative resistance is non-uniform. Figure 5.4.4 for the P-type bar shows curves which actually meet at 1 pu slip. This means that the motor starting performance will be relatively unaffected by temperature. The variation in resistance for the U and R-type bars is approximately the same. In the case of the S-Type bar, the two curves approach one another most closely in the mid-slip range (approximately at slip=0.5 per-unit). These simulation results relate to the slot portion of the rotor bar. The rotor end-region will probably be both at a slightly lower temperature and less affected by skin effect.

	cold, 20 ^{0}C		hot, 120 ^{0}C		
Bar	50 Hz		50 Hz		
Type	Rcold	Xcold	Rhot	Xhot	Rhot/Rcold
U	1.90	0.76	2.19	0.80	1.15
W	1.51	0.89	1.83	0.93	1.21
P	3.66	0.76	3.64	0.86	0.99
R	1.90	0.89	2.14	0.93	1.12
S	2.57	0.45	3.05	0.52	1.19

Table 5.4.1 : Rotor impedance for each slot type; hot and cold relative to a cold bar at low frequency (30 mm deep bar).

These results are summarised by Table 5.4.1 in which the resistance or reactance, relative to the cold, low-frequency value is shown for each slot type. The result for the P-type bar with Rhot<Rcold can be ascribed to numerical errors in the long

Runge-Kuta computational procedure. (The expected result would be greater than 1.0). A accumulated numerical error of 1 significant figure would account for it.

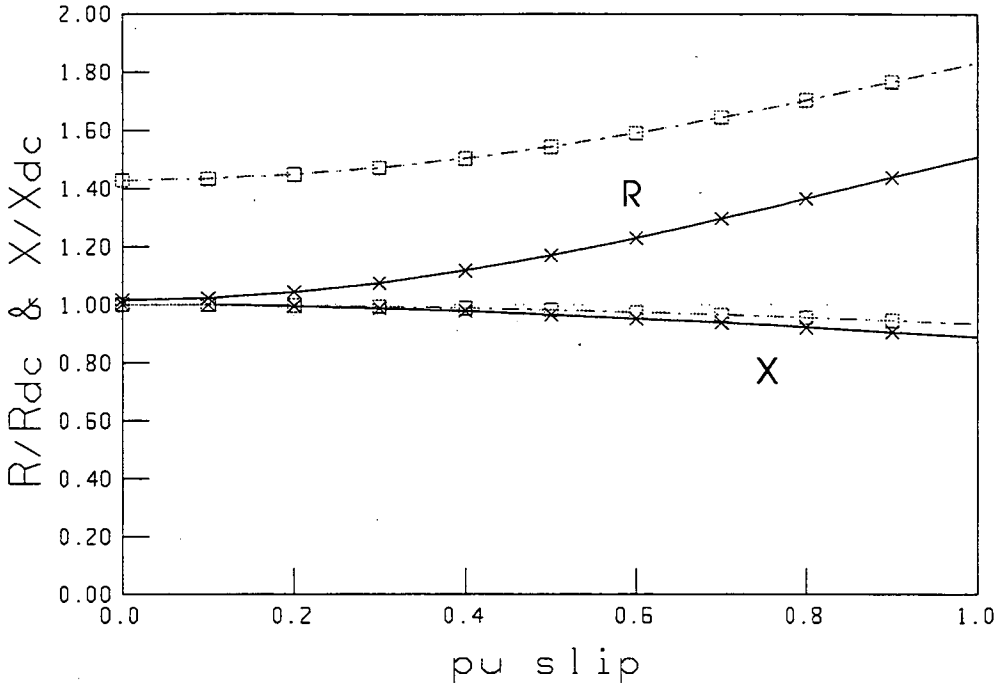

Figure 5.4.3 : Effect of temperature variation in the W-type slot
(solid = cold; dashed = hot)

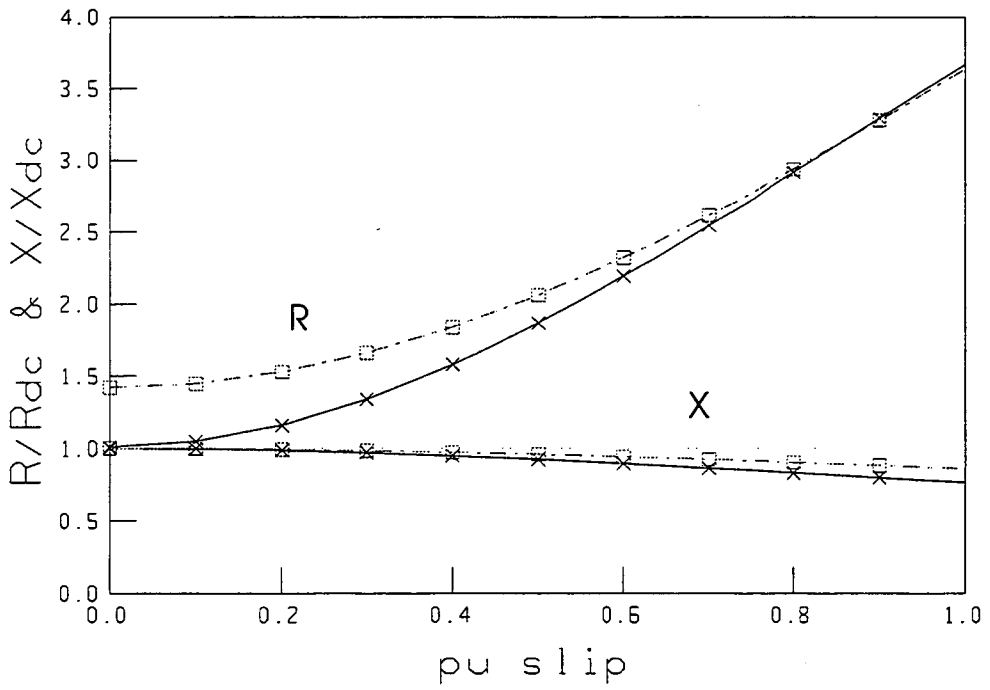

Figure 5.4.4 : Effect of temperature variation in the P-type slot
(solid = cold; dashed = hot)

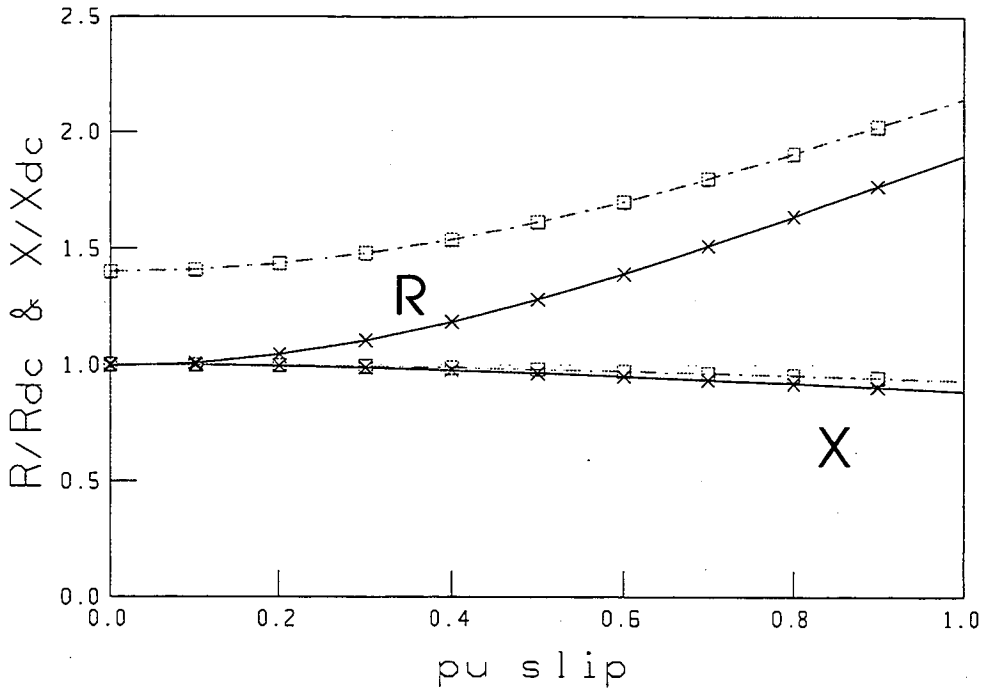

Figure 5.4.5 : Effect of temperature variation in the R-type slot
(solid = cold; dashed = hot)

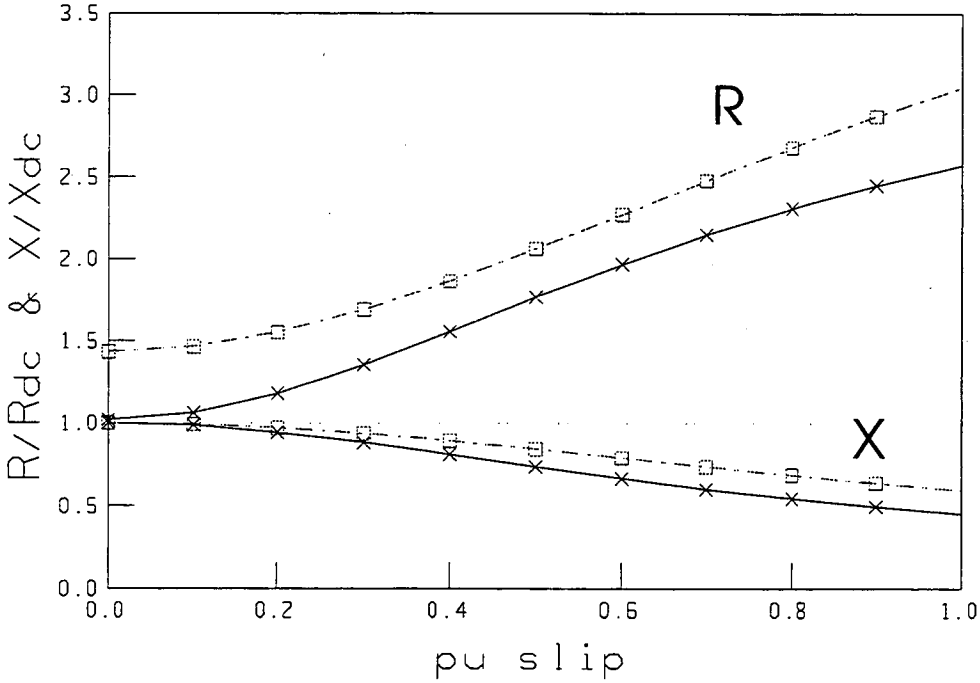

Figure 5.4.6 : Effect of temperature variation in the S-type slot
(solid = cold; dashed = hot)

5.4.3. Comment On The Results

Table 5.4.1 shows that, at 50 Hz, there is a small increase in rotor reactance with increasing temperature which confirms the experimental results reported by Grantham, [1987] and mentioned in Chapter 2. The quantitative aspects of this reactance variation will not be discussed further because in practice it is smaller than the uncertainty in reactance variation due to other causes.

For this magnitude of temperature change, the ratio of hot and cold resistances at low frequency is about 1.4 for aluminium bars. This ratio reduces with rise in frequency. Intuitively this can be seen to occur because the effect of increased resistivity is less pronounced as the current crowds into the upper portion of the bar.

More formally, the ratio of low frequency resistance is given (for aluminium bars of uniform width, w and length, l) as

$$\frac{R_{DChot}}{R_{DCcold}} = \left[\frac{l\rho_{hot}}{wd}\right] / \left[\frac{l\rho_{cold}}{wd}\right] = \frac{\rho_{hot}}{\rho_{cold}} = \frac{T_{hot}+225}{T_{cold}+225} \qquad (5.4.1)$$

At higher frequencies, f_1 and f_2 the ratio of hot to cold resistances is given from equation (2.2.12) as

$$\frac{R_{fhot}}{R_{fcold}} = \frac{\dfrac{\alpha_h d[\sinh(2\alpha_h d)+\sin(2\alpha_h d)]}{\cosh(2\alpha_h d)-\cos(2\alpha_h d)} R_{DChot}}{\dfrac{\alpha_c d[\sinh(2\alpha_c d)+\sin(2\alpha_c d)]}{\cosh(2\alpha_c d)-\cos(2\alpha_c d)} R_{DCcold}} \qquad (5.4.2)$$

$$\text{where } \alpha_h = \sqrt{\frac{\mu_0 \pi f_1}{\rho_{hot}}} \text{ and } \alpha_c = \sqrt{\frac{\mu_0 \pi f_2}{\rho_{cold}}}$$

Equation (5.4.2) may be simplified to give

$$\frac{R_{fhot}}{R_{fcold}} = \sqrt{\frac{T_{hot}+225}{T_{cold}+225}} \frac{[\sinh(2\alpha_h d)+\sin(2\alpha_h d)][\cosh(2\alpha_c d)-\cos(2\alpha_c d)]}{[\sinh(2\alpha_c d)+\sin(2\alpha_c d)][\cosh(2\alpha_h d)-\cos(2\alpha_h d)]} \qquad (5.4.3)$$

The first term in (5.4.3) is always >1 since $T_{hot} > T_{cold}$. The second part of (5.4.3) will depend on both frequency and temperature in a non-linear manner. This makes it difficult to establish a break even point where the rise in reactance due to temperature is equal to the reduction in going from 0 to 50 Hz.

Table 5.4.2 shows the simulated effect of temperature and frequency changes on uniform bars of varying depth. R1 and R0 are the resistances at 50 Hz and DC respectively. The last column shows the ratio of two ratios and is a measure of the change in resistance due to frequency in relation to that due to temperature. It is shown that the crossover point where the increase in resistance in going from 0 to 50 Hz with a cold bar equals the change in going from hot to cold at DC is at bar depths of about 25 mm. This reduces slightly (20 mm) for 60 Hz operation.

bar depth (mm)	R1/R0 cold	R1/R0 hot	R1hot R0cold	R1/R0cold R0hot/R0cold
15	1.0835	1.0429	1.4685	0.7694
25	1.5218	1.2948	1.8233	**1.0807**
35	2.2695	1.8440	2.5967	1.6117
45	2.9901	2.4899	3.5062	2.1234
55	3.6496	3.0809	4.3384	2.5917

Table 5.4.2 : Relative effect of skin effect at 50 Hz and temperature rise of 100 °C on rotor resistance for a uniform bar of width 1/6 of its depth.

The simulation showed that for bars of size less than 20 mm, even moderate increases in temperature resulted in a greater increase in rotor resistance than occurred due to the frequency change from 0 to 50 Hz.

Figure 5.4.7 shows the ratio of $R0_{hot}$ to $R0_{cold}$ for a 20 mm deep uniform-width aluminium bar. The horizontal line at about 1.25 is the ratio of $R1_{cold}$ to $R0_{cold}$, (ie the change due to skin effect). It can be seen that at a temperature of about 80 °C the change in dc resistance, R0 due to temperature is equal to the change experienced in the rotor when the pu slip changes from 0 to 1. For the starting value of rotor resistance, R1 the equality occurs at a slightly higher temperature of 110 °C.

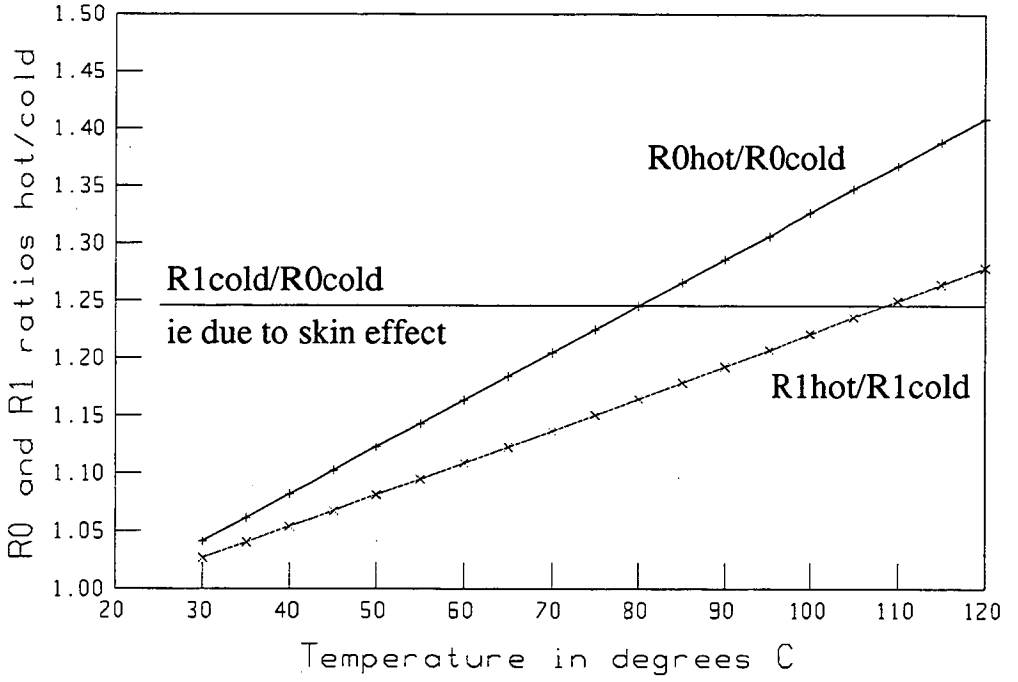

Figure 5.4.7 : Relative effects of temperature and skin effect for a 20 mm deep aluminium bar of uniform width.

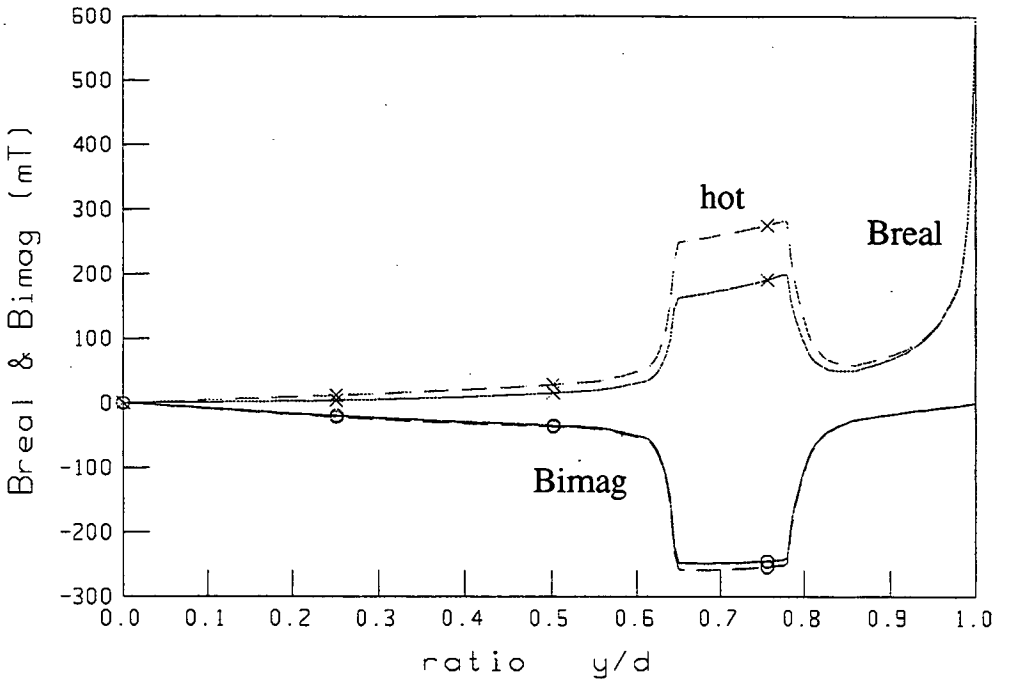

Figure 5.4.8 : Effect of temperature on magnetic flux density, B in a 30 mm deep, S type, aluminium bar.
solid = cold dashed = hot

Figure 5.4.8 shows that the temperature has little effect on the distribution of magnetic flux density (permeability of the steel is taken as infinite). The current density distribution is affected as shown by Figure 5.4.9. Consideration of this graph leads to a qualitative explanation for the increase in resistance and reactance with temperature. At higher temperature, the current density is reduced at the top of the slot and increased at the bottom. Since increased temperature tends to make J more evenly distributed over the slot length it will be closer to a low frequency situation. This means that the reactance will be higher since there will be more flux linked per ampere with less current crowding into the top of the slot.

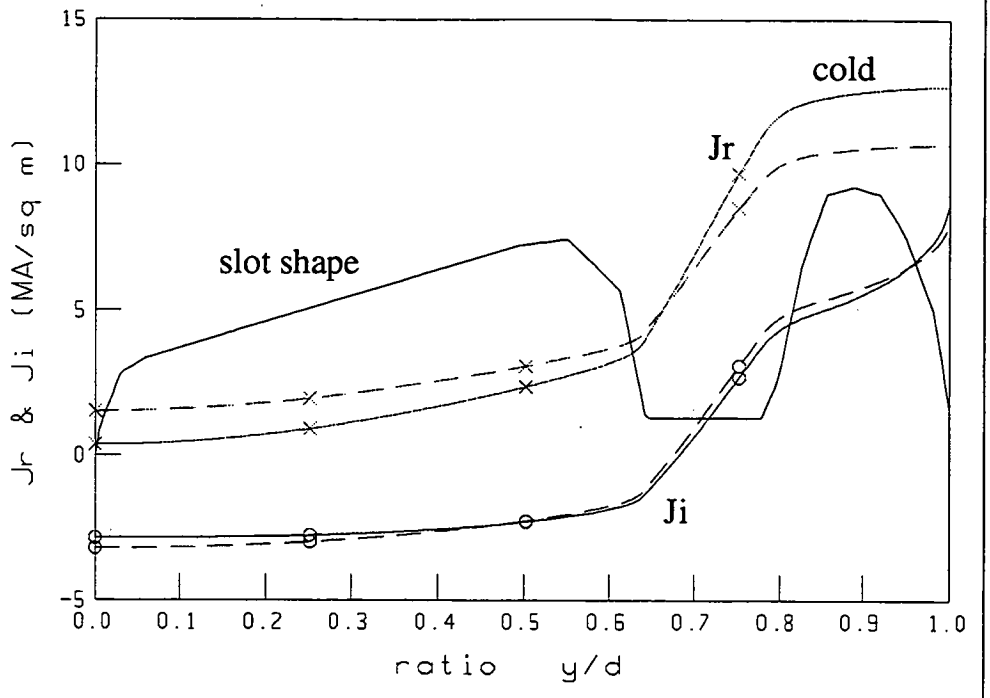

Figure 5.4.9 : Effect of temperature on current density, J in a 30 mm deep, S type, aluminium bar.
solid = cold dashed = hot

5.4.4. Conclusions Regarding The Effect Of Temperature

It has been shown that the variation in bar reactance due to temperature arises, at least partly, from the change in resistivity affecting the penetration depth. This contradicts the assertion by previous authors that the variation is due to other effects [Andria, Dell'Aquila, Salvatore and Savino, 1987], [Klaes, 1993].

The resistance variation is such that, when the full (Class B) operating temperature range is considered, it is more significant than skin effect for bars below 25 mm in depth. This will change slightly for 60 Hz and full Class F operation but precision is perhaps optimistic here given the uncertainty which nearly always exists about the actual machine temperature.

In Chapter 8, the effect of temperature on the various simulation yields, and in particular the time taken for the motor to run-up to speed, will be shown to be very dependent on the assumed operating temperature.

5.5. Magnetising Reactance And Core Loss

It was shown in chapter 4 that the parameters considered in this section do not have much effect on the simulated performance of the induction motor under starting conditions. Nevertheless, it was considered useful to include this brief section in the thesis in the interests of completeness.

5.5.1. The No-Load Test

It is common practice to determine the values of the magnetising reactance and core loss resistor in the equivalent circuit from a no-load test, [IEEE, 1988]. The assumption is often made that , since the slip is small, the rotor current is zero and all loss is either friction and windage or core loss. In practice there will be just sufficient rotor current to produce enough torque to overcome the friction and windage. This current will produce loss in the rotor circuits.

We can estimate the rotor loss if we can measure the slip accurately. If the slip value is derived from speed measurements then the error may be high since (Ns-Nr) tends to zero as the speed becomes close to synchronous, This error in computed slip may arise from errors in measuring Nr or from mains frequency drift. eg. if the true rotor speed is 1498 rev/min and the actual supply frequency is 50.1 Hz then, if the supply frequency is taken as 50 Hz, the % error in the slip is 60%. This problem can be avoided by using stroboscopic methods but it is difficult to see these being incorporated into a PC-based data acquisition system. An additional point to note is that the usual stroboscopic method measures the apparent rotation of the shaft at slip speed when illuminated by a light flashing in synchronism with the supply frequency. This requires a fairly long period of time for each measurement. During this time the speed of the machine is taken as constant, ie the dynamic response of the stroboscopic method is poor.

Typically, no-load losses are 25% of full load losses with the friction and windage losses (at rated slip)approximately equal to the full load core loss, [Pereira, 1991].

In this section of the thesis it is shown by simulation that if the circuit impedance is computed at the NL slip value and this impedance used to compute core loss, then the estimated core loss resistor is reduced by about 5 to 15% and the magnetising component by nearly 30%.

5.5.1.1. Method for simulating core loss

The double-cage form of the exact equivalent circuit was used to simulate the effect of performing the no-load test measurements at two values of slip. The first was at a true slip=0, where the circuit input impedance was given by $(R_1 + rc) + j\,(X_1 + xm)$. That is, the rotor part of Figure 5.5.1 could be omitted from the calculation of input impedance without introducing any error.

The second was at a slip such that the output power was equal to the specified friction and windage loss. ie $W_{fw} = I_2^2 \frac{R_e(1-s)}{s}$ where R_e is the effective rotor

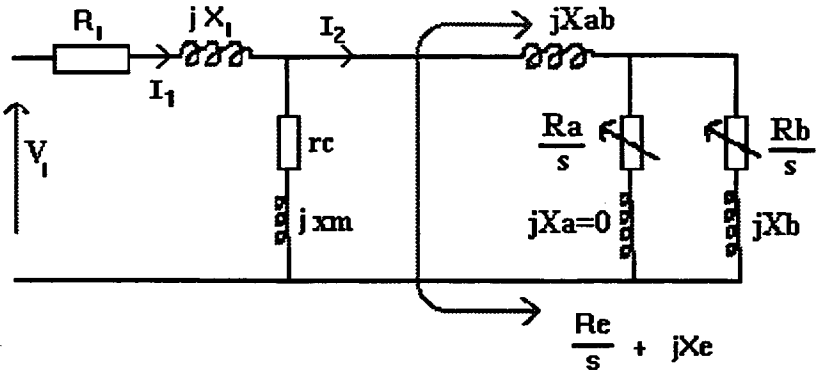

Figure 5.5.1 : double-cage circuit with series form of magnetising branch

circuit resistance at the slip value. [R_e is practically constant over the small slip range]. The slip was varied iteratively until the correct power output occurred. The input impedance of the circuit was calculated from the double-cage circuit parameters to be $(R_1 + R_{0s}) + j\,(X_1 + X_{0s})$ where R_{0s} and X_{0s} are the derived approximations for the series form of the magnetising branch components.

By comparing R_{0s} and X_{0s} with rc and xm, the errors in assuming that the magnetising branch parameters could be determined form the input impedance measured at the no-load speed were calculated.

5.5.1.2. Results of simulated core loss

	pu slip	R0s	% error	Power	X0s	% error
8.2 MW	0.000126	2.94	-5.7	0.0193	0.1676	-10.9
11000hp	0.000360	2.82	-15.7	0.0572	0.4695	-29.4
ecp	0.0004189	2.88	-8.6	0.0301	0.2519	-16.4
50hp dp	0.0006745	2.47	-12.3	0.0500	0.3111	-23.0

Table 5.5.1 : Simulated errors in assuming zero slip during NL test.

Data for four motors was taken from the INSPEC database mentioned in Chapter 3. It can be seen that the % errors are quite large. These errors may be avoided by driving the induction motor under test by a synchronous motor or by allowing for the rotor losses at the no-load slip. Alternatively, measurements of input impedance can be made as the motor passes through synchronous speed as it runs up from rest while unloaded, [Grantham, 1987].

5.5.2. Rotor Core Loss

Under normal operation, the rotor core loss will be small since the rotor frequency is low. During starting the rotor core loss is not negligible but the increase in total core loss is often compensated for by the reduced frictional and windage losses at lower speed. In order to determine core loss accurately under all conditions either extensive testing or detailed design information must be available, [Zhu and Ramsden, 1993]. Stray load losses will also become apparent and these highlight the difficulty in representing a motor by a circuit. All of these uncertainties make exact prediction of the net shaft torque impossible without methods which rely on design data and are therefore excluded from the scope of this work.

5.5.3. Magnetising Reactance Variation With Supply Voltage And Frequency

When the motor is supplied from a system which experiences large deviations in supply voltage and frequency the magnetic flux density in the main flux paths will vary considerably. This may not affect the value of X_m . If, for example, the paths are initially unsaturated and the supply voltage falls by 15% then the magnetising flux will be reduced but this will have no effect on the reactance which is already in the linear region. It is impossible to tell if a particular level of voltage reduction will affect the value of X_m that should be used in the equivalent circuit without having access to a no-load saturation curve.

It was shown in Chapter 4 that X_m affects the dynamic performance during starting only slightly. A 30% increase in the inductance, L_m due to coming out of saturation is less significant than the direct effects of a 5% decrease in voltage or frequency. Similarly, the effect of changes in rotor parameters are more than three times the effect of changes in L_m . If the no-load saturation curves are available then they may be included but it is probably not worth spending the time to perform special tests because other factors will probably have a more significant impact on the veracity of the simulated performance.

It is noted that these comments are not appropriate to the modelling of small scale disturbances in the power supply or other types of stability investigations. He and Lipo, [1984] have shown that for these types of studies the main flux saturation must be modelled. The recommended method for this is that of Osama et al, [1993].

6. DETERMINATION OF CIRCUIT PARAMETERS FROM MANUFACTURER'S PERFORMANCE DATA

When the simulation program developed in Chapter 3 was first used on the motors of Table 4.4, some of the manufacturer's quoted circuit parameters were found to be inconsistent with the quoted performance data. At first, the simulation program was doubted but subsequent checking confirmed that the discrepancy was due to something else. This problem was reported by Waters and Willoughby, [1983] and has been supported by private correspondence with two separate groups of consulting engineers working with induction motor simulation studies.

The problem arises because the parameters are sometimes based on assumptions which are inappropriate for modelling the motor performance over the full dynamic range of operation. When skin effect in the rotor and leakage path saturation are ignored this results in a single-cage rotor model which is valid over a limited range of slip and current. Values quoted by the manufacturer may give predicted performance data which fits the nominal performance data in the region close to rated slip and current but not elsewhere. The first check on any derived circuit model is the re-calculation of any known steady-state performance data. Leakage reactances determined from locked rotor tests represent the saturated high frequency condition and cannot be expected to give accurate results at full-load (small slip, low current, less than Isat).

Two alternative methods were investigated for the derivation of circuit models from performance data and these are discussed and compared in Section 6.1. The inclusion of recursive optimisation methods to ensure better fitting of complete curves of torque and current against speed is addressed in Section 6.2. The use of performance data rather than quoted circuit parameters as a starting point has the significant advantage that each data item may be associated with an allowed tolerance to AS1359 (or IEC34 equivalent). The effect of these tolerances is discussed in Section 6.3.

It was decided not to include discussion on the calculation of performance parameters (such as efficiency) since they are input data items to the process. From the point of view of the applications engineer (the point of view of the thesis) the performance parameters supplied by the manufacturer are the starting point for assigning numerical values for the circuit model. The point of this chapter was to investigate the uncertainty generated in predicted output by the tolerances in this input data. The determination of performance parameters from test data is a manufacturer's problem and outside the scope of the thesis, (though understandably of concern to motor manufacturers).

6.1. Methods Based On Steady-State Operating Points

The parameter values for the simplest form of the equivalent circuit which is shown in Figure 6.1.1 below, may be derived by a non-recursive algorithm due to Pereira, [1991] or by the more sophisticated methods of Waters and Willoughby, [1983] or Rogers and Shirmohammadi, [1987] ; {referred to as (R&S) subsequently}. Of the last two, only the latter is discussed in detail since, in practice, either of these could be used as a starting point with iterative adjustment to the circuit parameter values to minimise a specified error function in performance parameters.

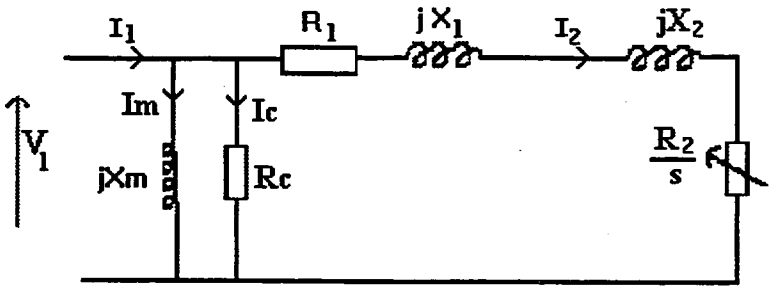

Figure 6.1.1 : The approximate equivalent circuit

6.1.1. Pereira's Algorithm

Since the method is well documented by Pereira, the focus here is on the data required and the embedded assumptions of the algorithm. The data items required are shown in Table 6.1.1 which indicates with the symbol *, those items which are also required for the (R&S) method described in the next Section. The method is available as a Turbo Pascal unit called PEREIRA.PAS.

del_star	*	machine type DELTA or STAR
p1	*	rated power output
V_{ll}	*	rated line voltage
f1	*	rated frequency
s1	*	Per unit slip for rated power output
The folowing data for three load conditions : at 1, * , 0.75 and 0.5 pu load :		
n	eg n1, n2 and n3	efficiency at stated load
pf	eg pf1, pf2 & pf3	power factor at stated load
rat	: rat1 rat2 & rat3	pu loads at which n & pf are quoted

Table 6.1.1 : Data required for Pereira's algorithm

It was assumed by Pereira that :

- The constant losses, P_{FWC} are related to the core loss, P_{core} and friction plus windage loss, Wfw by two approximations; namely that :
  (1) core loss is between 1.35 and 1.5% of the total output
  (2) core loss is about 50% of constant losses, P_{FWC}
  In programming Pereira's method, P_{core} was therefore taken as
  $$P_{core} = (0.0071 * p1 + 0.25 * P_{FWC}) \quad (6.1.1)$$

- The difference between the stator current, I_1 and the referred rotor current I_2 is ignored in the determination of the total loss and hence the constant loss. This implies a circuit with large Xm and Rc.

- I_m and $I_2 \sin(\phi_2)$ are assumed constant over the range of the three data points at which n1 and pf1 are quoted ie from 50% load to rated load.This is reasonable if the machine speed is approximately constant in that range.

	R&S 8MW		Pereira 932kW	
	Quoted	Simulation	Quoted	Simulation
Current (pu)	1.000	1.000	1.000	1.010
Power Factor	0.91	0.906	0.80	0.802
Net pu Torque	1.000	1.006	1.00	1.044
Efficiency	0.985	0.98511	0.940	0.953

Table 6.1.2 : Results of Pereira's Algorithm

Pereira's algorithm is based on the low-slip version of the approximate equivalent circuit of Figure 6.1.1 and does not allow for leakage path saturation nor for eddy current effects. Because it does not use quoted starting current data it cannot allow for the fact that the leakage reactance at high slip may be lower than in the normal operating range. Its main advantage is that it uses readily available data. It was derived to determine the circuit parameters to be used in induction generator studies and works well in a restricted range of operation. This can be seen from Table 6.1.2 where it compares well with the saturable double-cage model in the region of normal slip.

The algorithm may be used as a starting point for the iterative process described in Section 6.2. On its own, without the subsequent optimisation, Pereira's algorithm is not very accurate outside the normal range of operating slip; ie when the input data is recalculated the discrepancies are large. This follows from the fact that the input data used is all at low slip. Two examples of this are given in Figures 6.1.2 and 6.1.3 which show that the calculated starting torque and current is low. In the case of the 8 MW motor of Figure 6.1.3 the actual values are known to be as indicated.

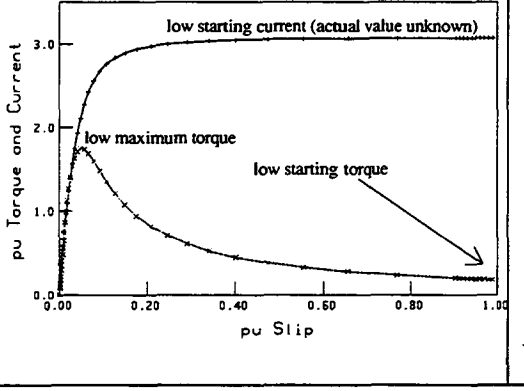

Figure 6.1.2 : Pereira's 932kW motor

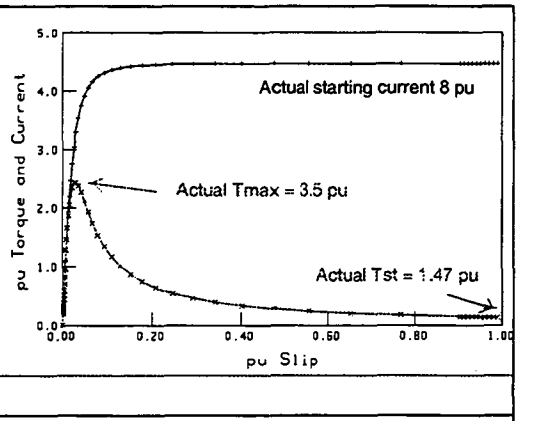

Figure 6.1.3 : R&S 8.2MW motor

Simulated results based on exact equivalent circuit and parameters as Pereira's algorithm showing failure to match quoted current and torque at high pu slip.

6.1.2. Rogers And Shirmohammadi's Method

This method requires two items of design data : Isat and m. It was shown in Section 5.1 that the value of Isat may be initially assigned to 1.25 pu. The value of m, which determines the extent of skin effect in the rotor, is difficult to assign a priori. Initial values between 0.5 and 2 are suggested by Rogers and Shirmohammadi. Values within this range were found to work well for large motors but the existence of these two data items of uncertain value is the main reason for advocating the recursive

optimisation outlined in Section 6.2. If torque/speed curves are available from the manufacturer then these can be used to guide the choice of m, [Alger 1951].

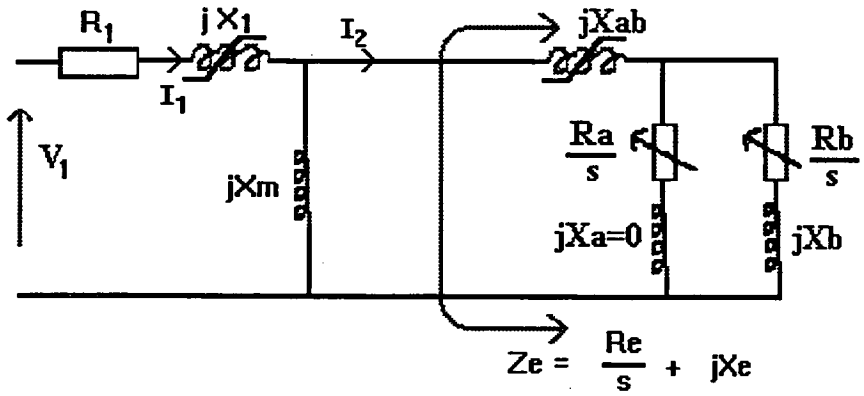

Figure 6.1.4 Double-Cage Circuit with Leakage Path Saturation

The method is based on the double-cage rotor circuit with stator and rotor leakage path saturation as shown in Figure 6.1.4.

By making the assumption that the leakage reactance of the upper rotor cage is zero, the method derives values for all the other circuit parameters. The lower cage reactance is assumed to be unaffected by saturation and the effect of saturation on the total rotor reactance is allowed for by varying Xab. The core losses are included with the mechanical losses using the efficiency modification described below. This method is acceptable in defining a model to be used for the simulation of motor performance because in such cases it is only the final effective reactance which is important.

6.1.2.1. Efficiency modification

By considering the power flow and losses through the motor at rated load the diagram of Figure 6.1.5 may be drawn. The modified efficiency, η' is larger than the quoted efficiency at rated load by a factor of (1 + FWC) where FWC is the per-unit constant loss. This may be shown as follows :

$$\eta' = \frac{Pout'}{Pin} = \frac{Pout + P_{FWC}}{Pin}$$

$$= \eta\left(1 + \frac{P_{FWC}}{Pin}\right)$$

$$= \eta(1 + FWC) \qquad (6.1.2)$$

This approach allows the "constant losses" to be subtracted from the gross output. The increase in rotor core loss at high slip is usually ignored as is the variation of friction and windage loss with shaft speed. More sophisticated treatment of the "constant losses" is possible if the variation with speed is known. In chapter 4 it was shown that the value of core loss did not affect any of the simulation yields significantly. In Chapter 8 it will be shown that the treatment of these losses as constant yields simulation results which are close to the measured values.

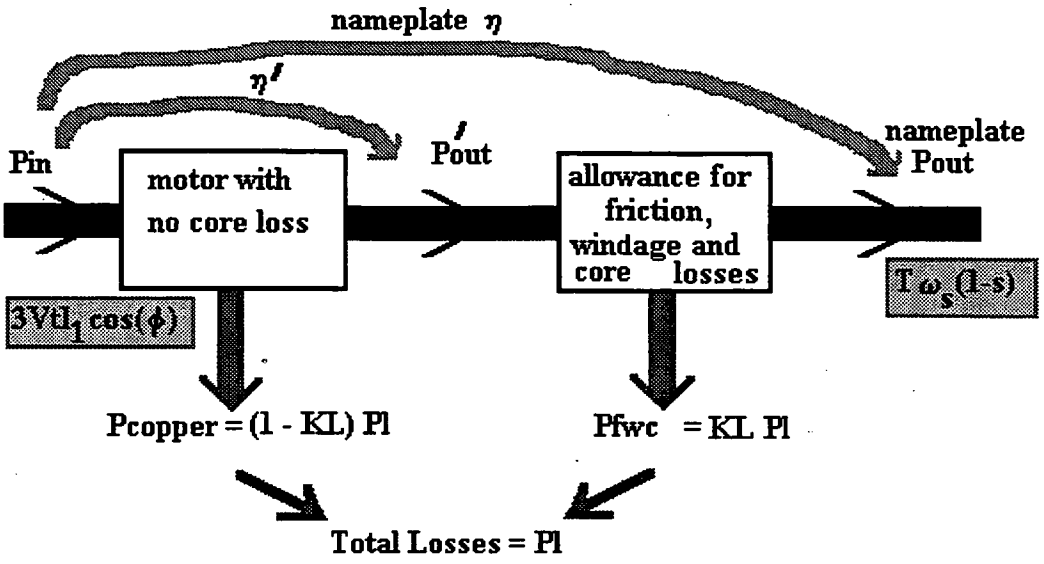

Figure 6.1.5 : Inclusion of friction, windage and core losses by using modified efficiency

6.1.2.2. Values at rated slip (R_1 , Xm and R_{dc})

The circuit shown in Figure 6.1.4 can be reduced to that of Figure 6.1.6 by replacing the rotor part of the circuit with the equivalent impedance, $R_e + j X_e$ to give the circuit of Figure 6.1.6.

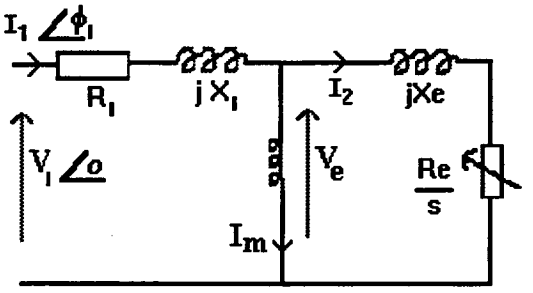

Figure 6.1.6 : Assumed circuit at rated load (ie at rated slip)

Assume that at rated slip, I_2 is wholly real. Hence $I_1 \cos(\phi_1) = I_2$

$$\frac{3I_2^2 R_{dc}(1-s_1)\omega_s}{s_1\omega_s} = 3V_1 I_1 \cos(\phi_1)\eta'$$

substituting for I_2

$$\frac{3I_1^2 \cos^2(\phi_1) R_e (1-s_1)\omega_s}{s_1\omega_s} = 3V_1 I_1 \cos(\phi_1)\eta$$

which gives the rotor resistance at low slip $R_{dc} = \dfrac{s_1 V_1 \eta'}{I_1 \cos(\phi_1)[1-s_1]}$ (6.1.3)

Note that here the effective rotor resistances at low (R_{dc}) and high (R_{st}) slip are not equal and a double-cage model is being used even though the circuit of Figure 6.1.6 appears at first glance to be a single-cage one.

I_1 has real and imaginary parts through R_{dc} and X_m

$$\text{so } \tan\phi_1 = \frac{(V_e / X_m)}{(s_1 V_e / R_{dc})} = \frac{R_{dc}}{s_1 X_m}$$

where V_e is the voltage across the magnetising branch.

Hence $$X_m = R_{dc} / (s_1 \tan \phi_1) \quad (6.1.4)$$

By considering the copper losses, $P_{in}(1-\eta') = I_1^2 R_1 + I_2^2 R_{dc}$

$$V_1 I_1 \cos\phi_1 (1-\eta') = I_1^2 R_1 + \frac{I_1^2 \cos^2(\phi_1) s_1 V_1 \eta'}{I_1 \cos(\phi_1)[1-s_1]}$$

$$R_1 = \frac{V_1 \cos\phi_1}{I_1}\left[1-\eta'-\eta'\frac{s_1}{(1-s_1)}\right] = \frac{V_1 \cos\phi_1}{I_1}\left[1-\frac{\eta'}{(1-s_1)}\right] \quad (6.1.5)$$

6.1.2.3. Rotor resistance at starting (R_{st})

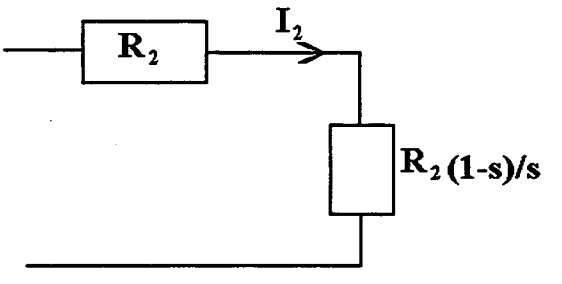

Figure 6.1.7 : Rotor circuit

Generally, $T_e = \frac{3I_2^2 R_2}{s\omega_s}$

Let starting value of R_2 be R_{st}

then torque, $T_{st} = \frac{3I_{st}^2 R_{st}}{\omega_s}$ (6.1.6)

At rated slip, s_1, $$T_{rated} = \frac{3(I_1^2 \cos^2\phi) R_{dc}}{s_1 \omega_s} \quad (6.1.7)$$

therefore

$$R_{st} = \frac{T_{start}}{T_{rated}} \frac{(I_1 \cos\phi)^2}{I_{st}^2} \frac{R_{dc}}{s_1} = \frac{[\text{pu starting torque}]\cos^2\phi}{[\text{pu starting current}]^2} \frac{R_{dc}}{s_1} = \frac{T_{st} R_{dc} \cos^2\phi}{s_1 I_{st}^2} \quad (6.1.8)$$

Note that for values between s=0 and s=1, R_2 is approximately given by $R_2 = R_r + (R_{st} - R_r)s$ but a more accurate representation is possible if the proper double cage circuit is used (with the correct design ratio, m).

6.1.3. The R&S Method As A Turbo-Pascal Program

The program PARAM.PAS was used to implement the method of parameter derivation for an 11000 hp heat transport pump taken from R&S's paper, (Subsequently referred to as the 8.2 MW motor). Initially it was done exactly as outlined in the reference but later modifications were made because the algorithm failed for some smaller motors. First of all, the stator resistance as determined by equation (6.1.5) was constrained to be between the limits $0.5R_{dc} < R_1 < 1.5R_{dc}$ by adjusting the estimate for FWC. A warning is given that the specified FWC leads to an inappropriate value of R_1. Secondly, for each given value of slip it proved necessary to iteratively calculate consistent corresponding values of current, leakage reactance and rotor resistance. Convergence occurred within 10 iterations.

The above modifications avoided the problem of negative impedances which occurred with some motors (particularly those less than 20 kW). A circuit with negative reactances is mathematically possible and may give a good fit to performance data but is not considered acceptable. For example, without the modifications, with the data from the 7.5 kW Toshiba motor from the UNSW, the method failed to converge with positive values for all the circuit parameters. In addition, motor data is usually over specified. For example, the set $\{V_1\ I_1\ pf_1\ rat_1\ n_1\}$ contains one redundant element. For some of the smaller WEG motors the manufacturer's parameters are inconsistent. That is, using the torque and speed to calculate power output gives a value different from the nominal rating and different again from the value derived from the electrical power input and quoted efficiency. This is not important in practice but it makes it difficult to make comparisons between methods if there are inconsistencies of the order of 10% in the input data. (However, it underlines the extent to which unreliable input data can limit the accuracy of the simulated performance no matter how sophisticated the simulation model is). This inconsistency was overcome by adjusting the quoted data to produce a set that was more self-consistent.

The derived circuit model was used to recalculate the quoted performance data and determine the RMS error of all the calculated items. The results are shown in Table 6.1.3 where they may be compared with the parameters quoted in the source reference. Some small differences exist and these may be due to slightly different optimisation methods. Optimisation is discussed in Section 6.2.

6.1.4. Results Of Parameter Determination

The method was applied to the performance data of the 8.2 MW motor. Several selections of m and Isat were used, two of which are given as Case1 and Case2 in the Tables below. Also shown are the computed circuit parameters from the reference which were used to re-calculate the performance data. The three cases shown do not differ significantly. In each case the RMS error is small. All impedances are in pu on a base impedance of 4.737 Ohm.

The graph of Figure 6.1.8 shows calculated torque and current using the model of Figure 6.1.4 with both the R&S circuit data and that of Case2 of Table 6.1.3.

The values of Isat and FWC used in determining these were not given in the reference. FWC was set = 0.003046 pu or 25 kW or 20% of the total losses. This value was used in preference to the 25% suggested in the reference because it gave a lower RMS error.

		R&S data	Case1	Case2
m		**0.55**	0.5	0.55
Isat (pu)			3.0	2.55
Stator Resis.	R1	**0.00462**	0.00458	0.00527
Magnetising	Xm	**3.133**	3.367	3.33
Unsat. Stator	Xs0	**0.0601**	0.06001	0.04078
Sat. Stator	Xss	**0.00473**	0.00257	0.00202
Outer Cage	Ra	**0.0249**	0.02417	0.02488
Inner Cage	Rb	**0.00874**	0.00953	0.00941
Inner Cage	Xb	**0.06113**	0.06740	0.06235
Unsat. Rotor	Xr0	**0.0523**	0.05308	0.07154
Sat. Rotor	Xrs	**0.00473**	0.00257	0.00393
Resistance dc	Rdc	0.00683	0.00683	0.00683
Reactance, dc	Xdc	0.10697	0.08931	0.10638
Starting Res.	Rst	0.02069	0.02070	0.02069
Start React.	Xst			
rotor/total		0.44	0.44	0.6
FWC Loss	kW	25	25	25
loss factor		0.003046	0.003807	0.003046

Table 6.1.3 : Circuit parameters for the 8.2 MW motor.
(Values in **bold** are from reference, others from program PARAM.PAS)

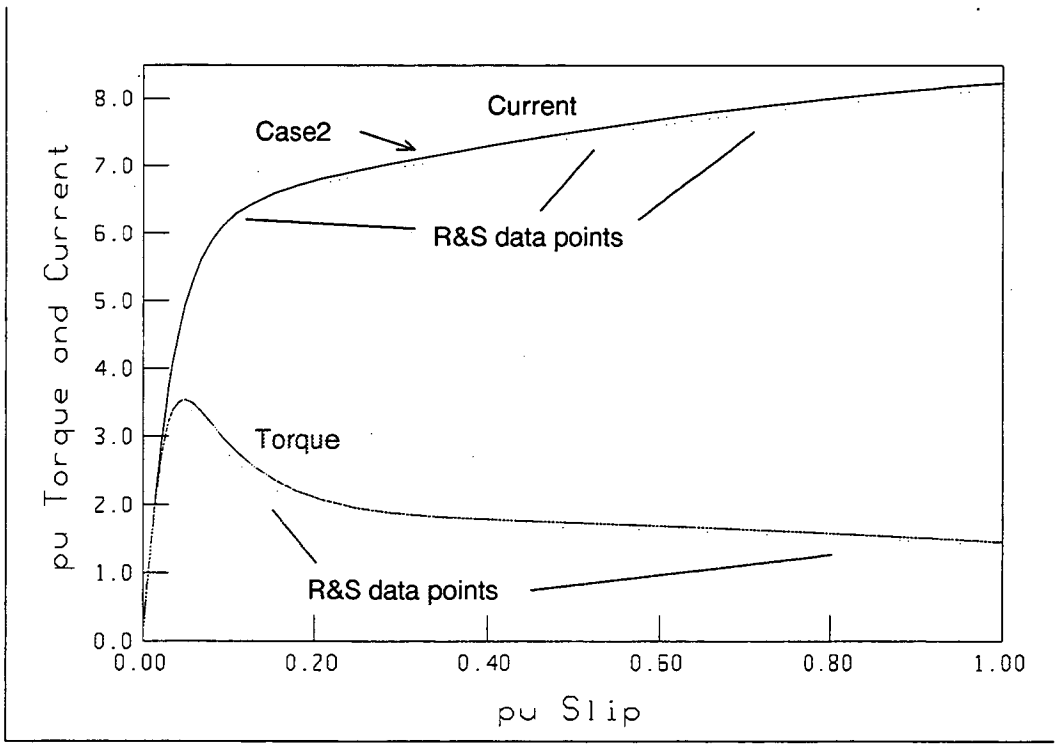

Figure 6.1.8 : Torque and current against slip for R&S 8.2 MW motor

The unknown value of Isat proved more of a problem. It was thought that, in theory, it could be determined by calculating backwards from the given values of the circuit parameters as follows :

$$\text{First}\quad X_{tl} = \sqrt{\left(\frac{V_{start}}{I_{start}}\right)^2 - (R_{st} + R_1)^2} \qquad (6.1.7)$$

Where the voltage and current may be either at full or reduced voltage.

$$\text{Then DF} = \tfrac{2}{\pi}\left[\xi + \tfrac{1}{2}\sin(2\xi)\right] \quad \text{where } \xi = \sin^{-1}\left(\frac{\text{Isat}}{I_{start}}\right) \qquad (6.1.8)$$

$$\text{And DF must also satisfy DF} = (X_{tl} - X_{so} - X_{ro})/(X_{ss} + X_{rs}) \qquad (6.1.9)$$

Solving these for the above data it was concluded that the Isat value must be greater than 8 pu ie the machine is unsaturated at all working currents. This extraordinary conclusion (given that the reference makes much of the need to include saturation in the simulation model) arises from the fact that the use of equation 6.1.9 to deduce Isat requires more significant figures than are available. The method works well if sufficient precision is available in the values quoted for X_{tl} , X_{so} and X_{ro} . This was verified with data for other motors.

In practice, Isat values can be determined iteratively to obtain the best fit to manufacturer's quoted performance data. This is what was done eventually since there is only one specified value of Isat which gives the correct starting current in each case with full and reduced starting voltages. Discussion of the simulated electromagnetic torque and current during starting with and without leakage path saturation (as Figure 8 of the reference) relates to the dynamic performance and will be left to Chapter 8.

6.1.5. Conclusion Of Section 6.1

	nom.	R&S circuit	Case1	Case2
Rated Load		slip = 0.0062 pu		
current	1.0	1.021	0.966	0.973
power factor	0.906	0.899	0.905	0.904
Torque	1.0	0.994	0.947	0.959
efficiency	0.985	0.96587	0.96724	0.97279
pull-out slip		0.0451	0.0468	0.0477
Tmax	3.5	3.450	3.468	3.538
Starting				
current	8.0	8.141	8.216	8.229
power factor		0.194	0.197	0.202
Torque	1.47	1.406	1.446	1.449
RMS % error		**1.903**	**2.20**	**1.881**

Table 6.1.4 : Re-calculated performance data from circuit data as Table 6.1.3

The results of this part of the work showed that, for large motors, it is possible to calculate equivalent circuits which give errors in individual performance data items of less than 5% and RMS errors of the order of 2% over the full operating range as a

motor. If the database is restricted to that necessary for the Pereira algorithm, then the single cage circuit model derived will be reliable only at low slip and current.

It was found necessary to perform iterative adjustments to some of the algorithm input data in order to obtain the least error in computed performance. The method was applied to many more motors. The results for some of these are given in Table 8.1.2 in Chapter 8.

6.2. Optimising The Matching Of The Performance Curves.

A review is presented of methods used to improve upon the initially derived values for the equivalent circuit parameters. This usually requires the re-calculation of the quoted performance data based upon an assumed equivalent circuit model. It is found that none of the existing methods are entirely satisfactory for general use though several of them may be used in restricted circumstances. As mentioned in Section 3.1, the author has discussed the findings presented here with the author of the INSPEC software and an improved version of this has been produced , renamed INSPECT to avoid confusion with the IEE's INSPEC. This revised version has not been evaluated at the time of writing.

6.2.1. Review Of Several Methods Used

Methods other than those discussed in Section 6.1, exist for the determination of motor parameters from performance data. Chalmers and Mulki, [1970] used a design synthesis method to derive a set of motor parameters which matched specified performance data. Adjustments to the design parameters (such as m) were done interactively based on design experience. Waters and Willoughby, [1983] introduced the use of formulae taken from Alger, [1951] to formalise the process of estimating the initial double cage circuit parameters. Unfortunately, although the authors mention the variation of impedances with leakage path saturation, this important effect is ignored in the parameter calculation.

Ansuj et al, [1989] used analysis of the sensitivity of predicted output to small changes in circuit parameter estimates to improve those estimates. They concluded that performance characteristics could be calculated to within 1% of the quoted values (0.2% or better is claimed in another part of the paper). It is doubted that the method as outlined would be able to predict performance to anything like this accuracy for a wide range of motors at operating points other than those used as data in the optimisation process. This result is discussed later in the conclusion to Section 6.3. The authors neglected leakage path saturation and used a linear fit for the variation of rotor impedance with slip. It must be concluded that the modelling of leakage reactance variation has been included inadvertently within the simple skin-effect model. As mentioned in Section 5.1.1 this will not cause any error when the given data points are recalculated but may introduce error if reduced voltage starting is simulated. The skin effect model may have been a fortuitously good fit, or perhaps the motor quoted was carefully selected.

With some motors, it has been found that the quoted performance data is inconsistent and probably contains rounding or allowed tolerances. The effect of the additional uncertainty introduced by data tolerances in discussed in Section 6.3.

Johnson and Willis , [1991] used an approach based on semi-arbitrary assignation of circuit parameters followed by the application of Newton's method, [Lastman and

Sinha, 1988]. Per-unit parameter values were quoted which were said to be a good starting point for most motors. Unfortunately, the method was based on a double cage equivalent circuit without leakage path saturation. Two models were derived, one which gave a good fit to the current/slip curve but a poor fit to the torque/slip data. The other model fitted the torque curve but not the current. It is felt that the main reason that two models were needed (instead of one) is the failure to include leakage path saturation which is present in most small to medium sized modern motors. The recognition, by the authors, that motor data is available in several forms is a major step in making a parameter determination method generally useful since all manufacturers publish data in their own format. For example, reduced voltage starting data is difficult to obtain and design data (such as m in Section 6.1) almost impossible to find.

Klaes, [1993] considered the determination of parameters from the point of view of indirect field oriented control. As such, the variation of rotor parameters with slip was ignored although both main and leakage flux saturation was modelled. A total of at least 10 locked-rotor test points were required with a variable frequency, sinusoidal supply. The first 5 test points were done at low frequency and were used to determine the magnetising inductance variation with stator flux. The second set of 5 points were performed at high frequency and were used to determine the leakage reactance variation with stator current. Strictly the last set of results will give the leakage reactance values appropriate to slip=1. However the values are used as starting points for an optimisation process and so it probably does not matter.

6.2.2. General Comments On Previous Work

Since the optimisation method requires some performance data it seems much more convenient to use a deterministic method as a starting point and to apply the optimisation routine to these parameter values. As pointed out by Ansuj et al, it is often possible to get within 10% of quoted performance data without optimisation.

Johnson and Willis' work is an example of parameter determination method based on pure optimisation without pre-calculated parameters as a starting point.
One of the interesting points raised in this work is the failure of Newton's method, to converge with some sets of data. As a result of this, the method used had an interface for user interaction from the keyboard. This feature allowed the specification of additional constraints on the motor performance. It could therefore be used to gradually develop a motor model that fitted all the constraints. The point was made that specifying too many constraints at the outset will probably lead to failure to converge. The problem with such a method is that it relies on expert knowledge by the user to make the necessary adjustments to the program parameters to aid convergence. The author's experience with using the first version of the INSPEC program with undergraduate students has emphasised the need for a method which can be applied uniformly to all types of motors without the user having to know , for example, that a certain type of motor will probably be best modelled with a design ratio, m close to 1.5.

An attempt was made to develop e-mail communication with these authors and to seek their comment on work previously done. Unfortunately, this was unsuccessful probably because many of the authors are practising engineers with little time to follow up old work. Section 6.2.3 has been included to illustrate some the problems that arise in practice and how they were overcome. It is fairly easy to demonstrate that a method works for one particular set of data. The author's experience has shown

that algorithms need to be evaluated against a wide data-base of motors before general conclusions may be drawn.

6.2.3. The Hybrid Method Suggested

Once the initial parameters have been obtained it is then possible to recalculate the quoted performance data. Because the motor is not a circuit but rather a complex electro-magnetic-mechanical space, the equivalent circuit contains assumptions which are not wholly true. There are therefore errors in the computed performance.

The first task of optimisation is to decide the region of interest. As has been seen with Pereira's algorithm, if the range of operation is restricted, then a simple circuit will give good results. For more wide ranging studies, or where departure from rated slip and current is significant it is important that data outside of the normal operating range is included in the circuit optimisation process. For example, if sudden load application from an unloaded state is of interest then it seems a good idea to include the pull-out torque point in the model constraints.

Several formal optimisation methods are available. A quasi-Newton method was tried briefly with the program PARAM.PAS redefined as a Turbo-Pascal unit. It was found that the method was not reliable and often converged to mathematically correct but practically unreal solutions. This indicated that more work would have to be done on the development of suitable constraints within the optimisation routine. Since it was only necessary to use the method on about 25 motors and it was possible to achieve rapid convergence by interactive adjustment of parameter estimates from the keyboard, it was decided not to pursue this. The results for the 8.2 MW motor shown in Tables 6.1.3 and 6.1.4 took less than 15 minutes elapsed time; whereas program development and verification would have taken much longer than this. As the program was run for each subsequent machine the time taken to obtain a small enough RMS error function was reduced due to increased understanding of the processes.

6.2.4. Some Sample Cases

A file RS.DAT was created containing performance data for 25 motors ranging in rating from 2.2 kW to 8.2 MW in various voltages and pole numbers. Parameters were determined using both the program PARAM.PAS and the commercial program INSPEC described in Chapter 3.

In all cases it was possible to fit equivalent circuit parameters which gave errors of less than 10% of the computed performance data item. Some cases were considerably better than this. In cases where the % errors are greater than 5% the main limitation to reducing the error still further is thought to be the self-inconsistency of the manufacturer's quoted performance data. Two cases are discussed here to illustrate the operation of the method. Latter in Chapter 8, Table 8.1.4 gives derived parameters for a further 4 motors.

6.2.4.1. 2.2 kW motor with single-cage rotor

This motor was selected because it was planned that it be used as the subject of practical tests the results of which are presented in Chapter 7. Results for simulated starting of this motor under different load conditions and with slightly different circuit parameter values are given in Chapter 8.

Table 6.2.1 and the graphs of Figure 6.2.1 show calculated circuit and performance data for the above motor. The graphs of torque and current against slip were produced using the INSPEC program which unfortunately does not allow data to be imported into other applications. Points were therefore read off the graph and inserted into the data file used by the Turbo-Pascal plotting program to allow comparison with the PARAM.PAS output discussed below. Two INSPEC-based models were used. In each case the upper graph (O) relates to the double cage circuit whilst the lower one (+) is based on the single cage model. The INSPEC program failed to converge for the double cage circuit with Isat = 3 pu and the design ratio m < 0.835. The double cage circuit modelled the curves of torque and current against slip better than the single cage model. However the single cage model gave a better fit to the predicted efficiency and power factor.

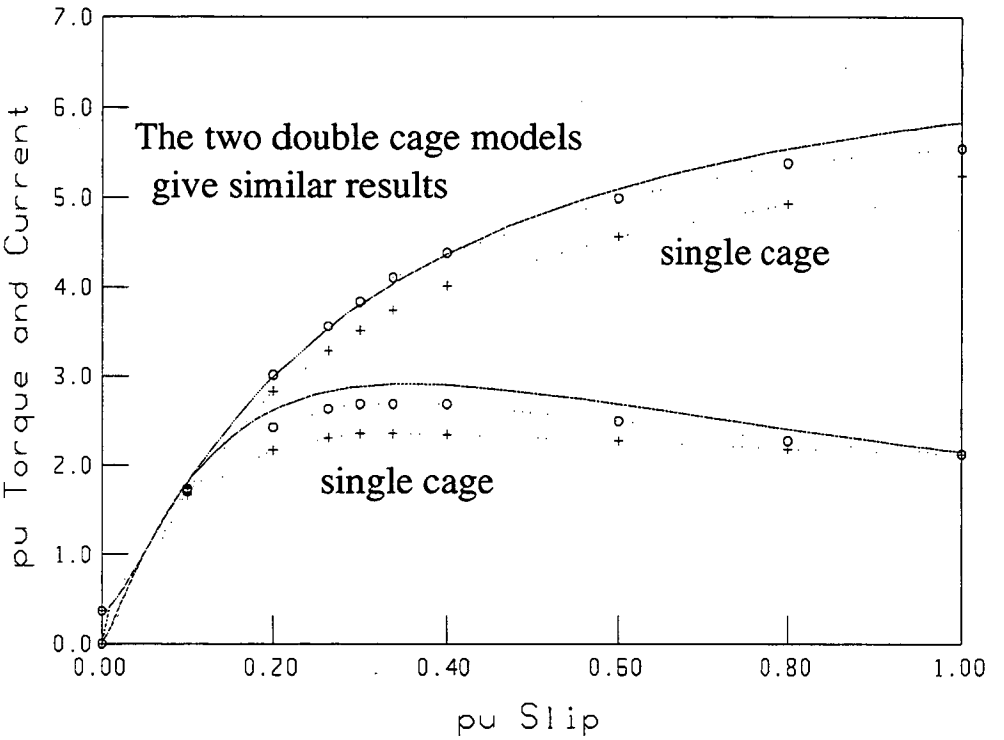

Figure 6.2.1 : Steady-state current (upper pair of curves) and torque (lower) against slip curves for Pope 2.2 kW motor (INSPEC dotted, PARAM.PAS solid)

The PARAM.PAS program fitted a high impedance lower cage so that the machine is approximately a single cage rotor. From some points of view this is a more satisfying result, since with a motor of this size, a single-cage model is the intuitive choice. This model calculated efficiency at 0.5 and 0.75 pu load with errors of less than 3%. The error in the power factor at 0.5 pu load was 11%. The INSPEC program did not calculate performance at specific partial loads and it is impossible to read the graphs to the required accuracy so no comparison is possible for these points.

In Chapter 8 a comparison is given of the simulated dynamic performance using the parameters determined using the program PARAM.PAS and INSPEC, as shown in Table 6.2.1, with the model based on measured machine impedances as determined in Chapter 7. It will be shown that the model derived from parameters obtained from

using the PARAM.PAS program fitted the simulated performance based on the test parameters better than the equivalent INSPEC model.

Pope Electric Motors for 2.2 kW, 415V 50 Hz 4.6A star, base impedance 52.1Ω			Calculated Values (pu)		
			PARAM	INSPEC	
			dbl cage	dbl cage	single cage
pu rated slip	s1	0.04666	0.0467	0.0460	0.0467
Rated efficiency	n1	0.82	0.8048	0.8246	0.8199
power factor	pf1	0.86	0.865	0.886	0.860
pu starting torque	Tst	2.1	2.14	1.52	1.49
pu starting current	Ist	5.6	5.8	5.1	5.58
pu max. torque	Tm	3.2	2.91	2.68	2.20
design ratio	m		0.65	2.0	NA
pu initial saturation,	Isat		1.05	0.001	1.0
Magnetising	Xm		2.592	2.456	2.769
Stator Resis.	R1	STATOR	0.0635	0.065	0.065
Unsat. Stator	Xs0		0.04837	0.0660	0.0630
Sat. Stator	Xss		0.02386	0.0660	0.0630
Outer Cage	Ra		0.05464	0.1082	NA
Inner Cage	Rb		0.62524	0.08099	0.045
Inner Cage	Xb	ROTOR	1.04597	0.0946	NA
Unsat. Rotor	Xr0		0.07055	0.0413	0.0627
Sat. Rotor	Xrs		0.03579	0.0413	0.0627
dc Resistance.	Rdc		0.05025	0.0463	0.0450
Starting Res.	Rst	ROTOR	0.05334	0.0587	NA
dc Reactance	Xdc		0.11310	0.0735	0.1254
Starting React.	Xst		0.1083	0.0674	NA
Const. Loss (kW)	FWC		0.169	0.174	0.170
Reactance split X_2/X_{tl} , at s=1, I=Ist			0.6	0.5	0.5

Table 6.2.1 : Circuit and performance data for Pope, 2.2 kW motor

6.2.4.2. 7.5 kW motor with double-cage rotor

This motor was the subject of extensive studies reported on by Grantham and others at the University of New South Wales, Australia, [Brown and Grantham, 1975] and [Grantham, 1985 and 1987]. Since measurements of the variation in rotor parameters for this motor had been published it was decided to subject it to the INSPEC program for comparison purposes. The quoted performance data was obtained from the UNSW including the complete steady-state current and torque curves against slip. Some of this information is given in Table 6.2.2.

For this motor the INSPEC and PARAM.PAS programs were again compared with the quoted performance data. In this case the agreement was much better than for the 2.2 kW motor. The INSPEC program failed to converge for Isat=3 and m<0.66 which meant that care had to be taken to avoid the system hanging. This pattern seemed to be consistent in that the INSPEC program would sometimes fail to converge or just

hang and lock up the PC requiring a re-boot of the system. It was not as tolerant of non-optimum starting values for the design constants, m and Isat as the PARAM.PAS program written by the author. When driven with approximately the correct parameters as a starting point it tended to avoid these problems and usually arrived, by recalculation, at a closer fit to the input data items than the PARAM.PAS program.

7.5 kW	4 pole	rated slip, s1	0.038 pu	
415 V	50 Hz	rated current, I1	13.6 A	
		PARAM.PAS	INSPEC	
	Quoted (pu)	m=0.65, Isat=3.3	m=0.7, Isat=2.0	m=1.8, Isat=1.0
pf1	0.877	0.88	0.874	0.876
n1	0.874	0.860	0.877	0.878
Tst	2.64	2.69	2.64	2.66
Ist	6.14	6.4	6.13	6.16
Tm	2.66	2.71	2.83	2.66

Table 6.2.2 : Performance data for Toshiba 7.5 kW motor from the UNSW.

When the derived parameters were compared with the published UNSW work, a discrepancy was discovered in the value of the 'zero frequency' referred rotor leakage reactance component. In the 1985 paper, Xdc is given as 9 Ohm but in 1987 the value is closer to 7 Ohm, (both being read from graphs). Since the currents at which the measurements were made were not quoted in the papers it is possible that the leakage path saturation conditions were different. Figure 7.6, in Chapter 7, shows that this cannot be entirely ruled out even for a No-Load test. It is more likely that the discrepancy is due to the fact that, as the slip approaches zero, the resistive component of the rotor equivalent circuit swamps the effect of the leakage reactance component; this leads to a situation where almost any value of leakage reactance will satisfy the measurement conditions.

A second problem arises from considering the resistance values Rdc = 2.2 Ω and Rst = 5.1 Ω. If we assume that the current in the rotor at rated slip is $I_1 \cos(\phi)$, then the rated torque is given by equation (6.1.7) to be 51.5 Nm which compares well with the quoted figure of 49.7 Nm at 1443 rev/min. At starting, the rotor current is much larger than the magnetising branch current so, to a first approximation, the rotor current equals the starting current. Using the 5.1Ω figure measured for R_{st} in equation (6.1.6) gives a starting torque of 680 Nm. This does not agree well with the value given by manufacturer of 2.64 times the rated torque or 131.2 Nm. (It is possible that the 5.1Ω relates to a delta connected motor but even conversion to an equivalent star still gives 4.4 pu starting torque which is too great).

The torque curve in Figure 11 of the 1985 paper does not agree well with the measured curve and the measured curve does not fit the manufacturer's curve for that motor. For example, the minimum torque during run-up occurs at about 300 rev/min for Toshiba's curve and at about 600 rev/min on the UNSW measured curve. The simulated curve has no significant minimum. These are shown in Figure 6.2.2 below. The simulated curves were based on a double cage fit to the measured set **{S}** as described in Section 5.2.

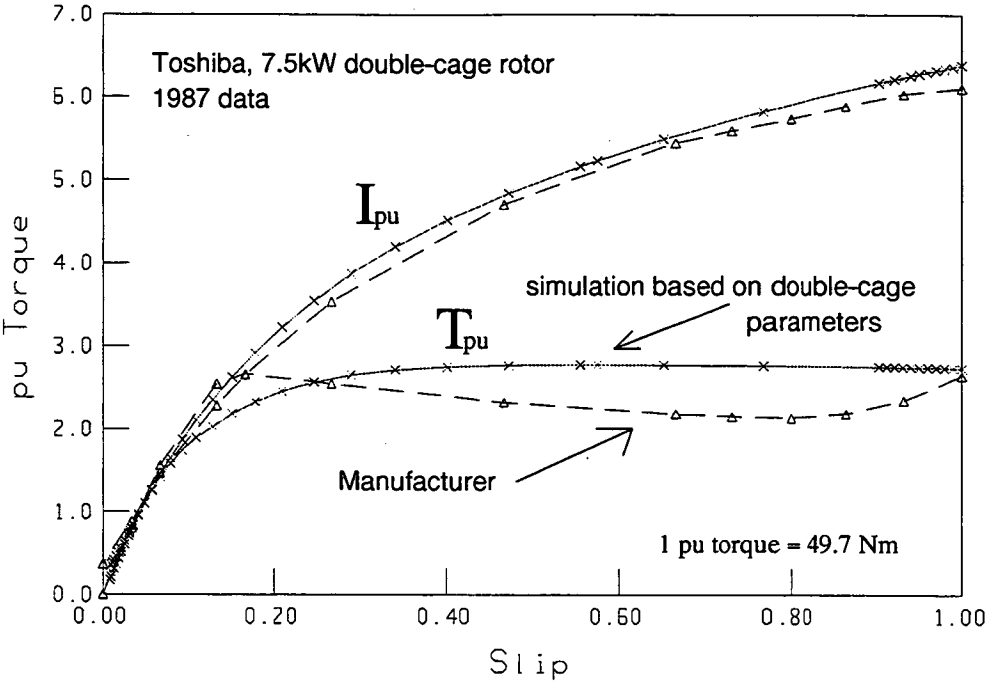

Figure 6.2.2 : Discrepancies with the Toshiba 7.5 kW motor and UNSW results

These discrepancies have been mentioned to the UNSW group and an attempt is being made to repeat the measurements with the new DSP-based equipment mentioned in Chapter 7 but the results are not available at the time of writing. It was originally intended to try to compare the UNSW results with simulated impedance variation as derived using the VWB method as described in Section 5.3. Unfortunately the above uncertainty and the fact that it has proved impossible to obtain rotor slot dimensions from the manufacturer have precluded this.

6.2.5. Conclusion Of Section 6.2

In general, simulation models will give better results if the performance to be predicted may be represented as an interpolation in the current, torque, speed space rather than as extrapolation into unknown conditions. The statistical methods of Chapter 5 may be used to predict saturation conditions from reduced voltage tests and thus can be used as a guide to assigning values of Isat. It is more difficult to use the locked-rotor impedance to predict the rotor circuit impedance at rated slip. If simulation in the mid-slip range is required then assessment of significance of skin effect in the rotor is essential. Even small motors such as the 2.2 kW motor studied here, were better fitted with a double-cage model even though the derived cage had a high-impedance inner cage so that it was close to being a single cage.

One issue not considered by any of the previous authors is the fact that manufacturer's performance data has allowable tolerances which are quite large. This means that even if an optimisation method is used to minimise a specified error function the performance being matched may not be that of the actual motor. ie the precision of the method may have improved but the accuracy is still doubtful due to the large uncertainties in the quoted performance parameters due to allowable tolerances. This issue is discussed in Section 6.3.

6.3. The Effect Of Manufacturer's Performance Tolerances On The Derived Parameters

The predictions of any computational model will only be as good as the data which is used. While steps may be taken to improve the differential equation model by including the parameter variation effects discussed in Chapter 5, the uncertainty in data values may place limits on the extent to which this process is productive. The main objective of the work described in this section was to assess the relative significance of data uncertainty. The work has been reported at the IPEC95 conference in Singapore, [Arneaud, 1995]

6.3.1. Data For Models

For this study, the method used for deriving the circuit parameters was that of Rogers and Shirmohammadi, [1987] in the form of a commercially available program, INSPEC, [Rogers, 1993] which required five items of performance data and three of design data as shown in Table 6.3.1. The machine chosen for the study was taken from the data-base supplied with the INSPEC package and described as "a 500HP drip-proof motor ". It would have been better for the process to be applied to a wide range of motors and the mean coefficients of response plotted as in Chapter 4. However the INSPEC program did not allow the input of several sets of data from a data file in sequence nor did it produce an output file of the derived parameters for use by the companion INSTART program. This meant that if INSTART were used not only would the program have to be run 32 times but each time the individual simulation yields would have to be read from the PC screen. The cursor could not be used to read off the program yields and they could not be written to a file for access by other applications in this version of INSPEC and so the uncertainties in the determined values of the program yields would be large.

The method adopted was to use the INSPEC program to obtain the optimised circuit parameters for each set of toleranced performance parameters and then to use these as input data to the simulation program IM_SIM.PAS described in Chapter 3. This was tedious because it was easy to make an error and so each input data item had to be checked by repeating the reading to confirm that the result was the same. The amount of work involved in (manually) producing results for one motor tended to discourage the treatment of additional cases. It is likely that about 15 to 20 motors would have to be treated in this manner for the mean yields, (as defined in Section 6.3.3) to be statistically significant. This would be very tedious without automation. At present, none of the available automatic numerical methods converges reliably on a circuit model with positive impedance values; the programs require some interaction with the user. Since the optimisation methods worked reasonably when used over a restricted tolerance range, it was realised that the problem was the wide tolerance range allowed by AS1359. However these tolerances have been set by international committees and it was felt that unilaterally modifying them to arbitrary new values would be unrealistic. It was decided that the results for the 500 hp motor were sufficiently convincing (of the effect of performance parameter tolerances) to avoid the need to repeat the process for several motors.

6.3.2. AS1359 Tolerances

The permitted manufacturer's tolerances based on AS 1359.69 Table 69.1 are similar to the IEC34 and NEMA-MG1 standards. For example, for the motor used in this study and taken from the INSPEC data-base, the nominal values and values with permitted tolerances were as Table 6.3.1.

6.3.2.1. Need to restrict the tolerance range

When an attempt was made to calculate the circuit parameters for permutations of the above tolerances, it was found that in order to retain a practical double-cage circuit (ie. positive impedances) it was necessary to restrict the tolerance range to less than that permitted by AS1359. For example, with the other parameters held constant and Ist varied from 2.9 kA to about 3.3 kA the resulting values for the double-cage parameters were as shown in Figure 6.3.1. The graph shows an extreme sensitivity at 3.235 pu starting current (an absurd degree of accuracy). The computational model attempted to approximate a single-cage rotor by assigning large values to R_b and X_b. The machine studied was of such a size that current displacement effects were large enough to be considered. A practical motor would not have this combination of performance parameters since Ist and Tst are not truly independent variables. In practice, the performance is rather more constrained than permitted by AS1359.

The mathematically corresponding values of effective rotor circuit input impedance were insensitive to Ist variation. Figure 6.3.2 which shows the two complex input impedances to the rotor circuit, referred to the stator, at zero and unity slip, called (R_{e0} , X_{e0}) and (R_{e1} , X_{e1}) plotted against Ist).

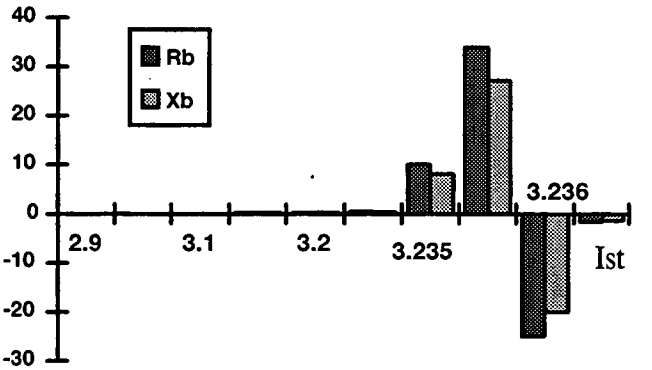

Figure 6.3.1 : Double Cage R_b, , X_b / Quoted Ist

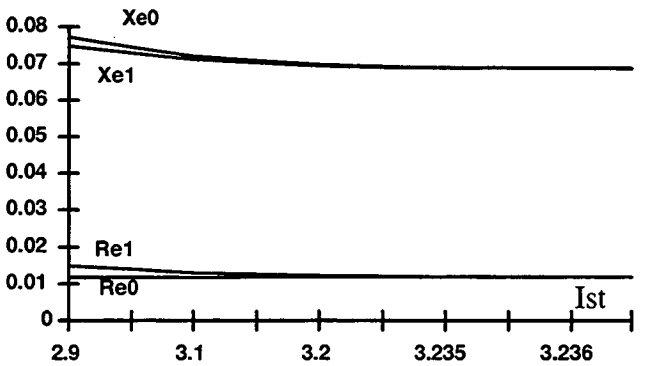

Figure 6.3.2 Effective Rotor Impedance/ Ist

This behaviour is explained by considering the ratio of the rotor resistances at the slip extremities which is given in Section 6.1 as

$$\frac{R_{e1}}{R_{e0}} = \frac{T_{st}}{s_1}\frac{pf_1^2}{I_{st}^2} \qquad (6.3.1)$$

Hence combinations of parameters which yield a ratio less than 1 are invalid for practical rotors. (Since $R_{e0} < R_{e1}$) As a consequence of this initial attempt, it was decided to restrict parameter tolerances in the subsequent fractional factorial studies to those in Table 6.3.1.

The objective of the first part of the study was to determine the effect, of tolerances in manufacturer's performance data, on equivalent circuit parameters as calculated by INSPEC. As well as $\{R_a , R_b , X_b , X_{ab}\}$ Four additional yields of the process were determined, namely (R_{e1} and X_{e1}) and (R_{e0} and X_{e0}).

The second part of the study aimed to measure the effect of the same data uncertainty on the results of simulated direct-on-line starting from an infinite-bus (constant voltage and frequency) mains supply. The numerical simulation was performed using an RK4 method. The program used for the evaluation of the yields was the final version of the program IM_SIM.PAS described in Chapter 3. This included full dq representation including stator transients, leakage path saturation and deep-bar effect in the rotor. It was used in preference to the INSTART program because the commercial program gave graphical output only and the program yields were not available directly.

Manuf. Perf. Parameter	Nom. Value	Tol. Allowed	Incl. Tol.	Used	% tol
pu efficiency, η_1	0.9471	- 0.1 of (1 -η)	0.9418	3.0	-0.56
pu slip, s_1	0.0097	± 0.2 pu of stated	0.01164	0.0113	16.5
power factor, pf_1	0.900	- (1-cos ϕ)/6 (0.02 <tol<0.07)	0.880	0.88	-2.2
starting current, I_{st}	2901	+ 0.2 pu of stated	3481	2948	1.67
pu starting torque, T_{st}	0.705 (low!)	-0.15 pu of stated	0.6	0.66	-6.4
Inertia Constant, H	0.5	± 0.1 pu of stated	0.45 to 0.55	0.55	10
Design Ratio,m	Not defined in standard		0.5<m<1.0		-50
Initial Saturation, Isat	As Chapter 5		3<Isat<10		-70

Table 6.3.1. Tolerances permitted and used in factorial study on 500 hp motor from the INSPEC database

The low value of the nominal starting torque of 0.7 pu quoted in the INSPEC data file is not necessarily an error . This was checked to be within the guidelines for low starting torque motors as given in the standards referred to above.

This motor was used in the simulation studies of Chapter 8.

6.3.3. Definition Of Yields From The Simulation Process

Several yields of the numerical simulation were defined in order to characterise the graphical output by discrete data points. These are an extension of the yield definitions given in Chapter 4. Several additional program yields have been defined and these are shown in bold text.

Transient period	
TPM	pu peak positive transient torque.
t1	time for TPM
TPN	pu peak negative transient torque.
t2	time for TPN
TST	pu starting torque as mean of TPM and TPN.
CP1	pu peak transient line current
t4	time for CP1
IT1	number of positive-going zero crossings on the transient torque/speed curve.
t7	time at which the last torque zero-crossing occurred.

Quasi-Steady-State (s<0.5 pu)	
t9	time for speed to rise to 0.5 pu.
TPS	pu peak torque after electrical transients have died away.
SP3	pu speed at which TPS occurred
t3	time for TPS
CP2	pu RMS line current when speed is at 0.5 pu.
t5	time for the pu speed to settle between 0.95 and 1.05 pu
t6	time for current to fall below 1 pu
Sm	pu maximum speed
t8	time at which Sm occurred.

Table 6.3.2 : Definition of yields from the simulation process

6.3.4. Results Of Simulations

For each of the yields a coefficient of performance (COP) was evaluated using equation (4.1.1). This related a change in yield attributable to each of the eight variable factors in a similar way to the work done in Chapter 4. Due to lack of space only the main effects are shown in Sections 6.3.9 and 6.3.10. Second order interactions were smaller.

During the first part of the study the influence of performance parameter tolerances on the derived equivalent circuit parameters was examined. Table 6.3.4 shows that the "hidden layer" quantities {Ra Rb Xb Xab} were more susceptible to the application of tolerances than the actual effective rotor input impedances. It is this net rotor impedance that was used to determine rotor current and electromagnetic torque. This emphasises the point that several double cage circuits exist which have very different parameter values but which will give approximately the same simulated motor performance.

During the simulation the yields were determined by a search routine within the RK4 procedure. A visual check on the torque, current and time graphs against speed was made to ensure that the simulations were well behaved. In three cases, the treatments produced low values of inner cage resistance, R_b and this resulted in low starting torque and failure to start within a reasonable period of time. These treatments were with tolerances applied to the factors given in Table 6.3.3 below with the other factors retaining their nominal values.

Case No.	Tolerances applied to these factors					
35	Isat	s1	m	Tst	pf1	H
36	Isat	s1	η1	Tst	pf1	Ist
37	s1	η1	Ist			

Table 6.3.3 : Three impractical cases

This behaviour underlined the fact that even with the reduced range of tolerances it is possible to arrive at an impractical machine which, while complying with the performance specification at the starting and rated load conditions, performs badly in the mid-slip region. The minimum torque in the torque speed curve is not used as a data item and, from a computational point of view, is therefore free to adopt unacceptably low values.

6.3.5. Relative Effect Of Data Uncertainty And Model Sophistication

The design parameter, Isat was used to model leakage path saturation using a describing function method as discussed in Chapters 2 and 5. Setting Isat high led to saturation being ignored.

The double-cage design ratio, $$m = \frac{(R_{e1} - R_{e0})}{(X_{e0} - X_{e1})} = \frac{(R_a + R_b)}{X_b} \quad (6.3.3)$$

defined the type of rotor bar used. For simple numerical models where current displacement and leakage path saturation are ignored, the effects of m and Isat are ignored. By examining the computed COPs for each yield it was possible to determine the change in each yield attributable to the inclusion of these effects.

In a similar way, the manufacturer's performance parameters, {s1,η1,Tst,pf1,Ist} could be related to each of the yields of the simulation process ie. it was possible to compute the change in each yield attributable to each of these parameters.

Although the study was restricted to a single motor it is believed that the conclusions are generally valid for machines of large size. For some very large machines the electrical transients may persist into the pull-out torque region leading to significant differences between steady-state and dynamic pull-out torques, [Krause, 1987].

6.3.6. Transient Period

Within the transient period, some of the yields of interest are the magnitudes of the positive and negative transient torques and the number of torque oscillations during the run-up. These yields were heavily dependent on the values of Isat and m used and it may be concluded that if these items are of interest then the computational model should certainly include saturation and current displacement effects.

Excluding the three cases given in Table 6.3.3, the average number of negative-going torque oscillations was 21 with a maximum of 29, a minimum of 12 and standard deviation of 4.6. Nominal data gave 17 oscillations. In consideration of shaft/coupling fatigue life due to frequent starting it can be seen that a safety factor of approximately 2 could be applied between the nominal and maximum.

The magnitude of the first current peak, CP1 was seen to be dependent on Isat, m and s1 in that order. This could be important for the determination of forces on busbars or cable runs. The timing of the first current peak, not surprisingly, depended mainly on supply frequency and hence showed low COPs for all factors.

6.3.7. After the Electrical Transients Have Decayed

The time, t9 taken to reach speed of 0.5 pu was dependent on Isat, s1, Tst, pf1, Ist, η1, H and m in that order. It is clear that in order to predict this yield to any accuracy it is necessary both to obtain reasonably accurate performance data and to use a saturable-double-cage model. Similar conclusions were made regarding the other run-up times shown in Table 6.3.2.

After the speed reached 0.5 pu, attention was focussed on the peak steady-state torque (transient pull-out) and the quasi-steady-state RMS current. Table 6.3.5 shows that TPS was affected mainly by Isat with small contributions from s1, η1 and H. The time, t3 at which TPS occurred was influenced mainly by Isat, s1, Tst and pf1.

6.3.8. Conclusions Regarding Effect Of Tolerances

The study demonstrated the usefulness of the factorial method in the assessment of the influence of possible variation in performance parameters on the simulated output of the dynamic performance of induction machines. Although the study was restricted to direct-on-line starting it could easily be extended to other conditions. It was found that the predicted performance was sometimes affected as much by the data uncertainties as by the inclusion of model complexities. In other cases, particularly during the electrical transient period, the modelling of leakage path saturation and/or rotor current displacement was seen to be more significant.

The results of this study indicate that a serious effort must be made in the gathering of data to be used for input to sophisticated models for the simulation of induction motor dynamic performance. If the circuit parameters are determined from performance data that has uncertainties of the order permitted by AS1359, then it is probably unwise to believe that the sophisticated model will generate accurate results. In such a case, the hoped for increase in confidence in the results gained by including, for example, leakage path saturation will be lost by potential errors due to circuit parameter uncertainty.

The consideration of uncertainty in manufacturer's performance data due to allowed tolerances calls into question the usefulness of claiming optimised fits to this data with errors of less than 1% (eg as Ansuj et al, [1989]). Such precise optimisation only seems worthwhile if the exercise is based on performance data derived from tests on the particular motor of interest. This may be done as part of a variable speed drive commissioning routine or as on-line adjustment of a numerical simulation used as part of a control scheme. It is not worthwhile for design studies prior to manufacture even if these are based on type-test data.

The work done in this chapter shows that differences caused by small approximations in setting up the numerical model (such as setting $X_a = 0$ in Chapter 5) are insignificant in comparison the variation arising from (AS1359) tolerances in input data of up to 20%.

Greater certainty in the performance parameters can only be obtained from test results on the actual motor, load and power supply. These are preferable to type tests. The question must however be asked: "If so much test and design data is available, then is the simulation really necessary?"

It is also apparent that the range of tolerances permitted by the Australian and equivalent IEC standards is too large. Varying individual parameters to the permitted tolerance limits results in a motor with slightly different circuit parameter values. Such circuits are usually still practically machine designs. However some combinations of tolerances are only consistent with impractical machine designs; eg with negative resistances. In other words, it is not possible to build a practical motor which will give the performance indicated in Table 6.3.3. The standards are written as though the individual motor performance parameters are independent whereas they are not.

The North American NEMA standard is, in some ways, worse since it specifies one sided tolerances, eg minimum starting torque. This is acceptable from some points of view but where these performance parameters are used as the starting point of a modelling process it leads to very large uncertainties in the derived circuit parameters.

6.3.9. Percentage COPs For Circuit Parameters.

% tolerance		-50%	-70%	16.5%	-0.56%	-6.4%	-2.2%	1.67%
YIELDS NOM. VALUE		FACTORS						
		m	Isat	sl	ηl	Tst	pfl	Ist
0.0273	Rs	-1.01	0.98	-2.12	**18.52**	0.98	-2.36	1.01
0.0738	Xs	0.16	**28.20**	0.15	-1.19	0.17	0.45	-1.57
3.0305	Xm	-0.90	**10.73**	0.10	-1.37	-0.11	-14.46	-0.39
0.0199	Ra	**53.14**	7.51	**-10.52**	-4.24	-9.58	0.22	**-11.15**
0.0688	Xab	-5.43	**25.57**	1.92	-1.04	1.14	0.10	-0.44
0.0196	Rb	**-50.53**	**-12.71**	**48.06**	-8.80	**17.04**	8.35	2.36
0.0395	Xb	**-57.13**	-2.63	**16.73**	-5.66	4.02	3.56	-3.26
0.0099	Re0	3.45	-5.45	6.80	-3.60	-3.23	-1.33	-3.16
0.0782	Xe0	-3.27	**23.67**	-0.30	-0.45	-0.59	-0.06	-1.03
0.0149	Re1	-1.03	-1.10	0.78	-0.72	-5.80	-1.49	-2.72
0.0732	Xe1	**32.55**	**19.44**	**-12.50**	-1.03	-8.17	0.27	-7.62

Table 6.3.4 : Circuit Coefficients of Performance based on "500HP drip proof" motor.

6.3.10. Percentage COPs_For Dynamic Performance.

% tolerance		-50%	-70%	16.5%	-0.56%	-6.4%	-2.2%	1.67%	10%
VALUE	YIELD	m	Isat	s1	η1	Tst	pf1	Ist	H
3.124	TPM	**-16.9**	**-27.7**	8.15	**-10.9**	0.96	1.09	-1.32	4.70
0.028	t1	**13.46**	**43.58**	5.53	-2.33	-1.98	-5.66	-2.00	**-13.2**
-1.81	TPN	**-12.3**	**-15.8**	6.14	**-17.2**	-0.85	0.52	-1.68	3.27
0.037	t2	**10.10**	**27.05**	1.56	**-10.1**	-4.45	4.23	-4.49	**-10.3**
0.660	TST	**-23.2**	**-44.0**	**10.90**	-2.20	3.44	1.88	-0.83	6.65
9.546	CP1	8.05	**-13.5**	-4.20	-1.68	-1.88	-0.39	0.53	-0.86
0.016	t4	-0.57	-0.69	0.72	0.08	0.61	-0.15	0.34	0.15
17.00	IT1	-5342	-5274	-5294	5364	-5317	5372	5364	5329
0.29	t7	6.88	**69.48**	**50.91**	**19.38**	**27.71**	**25.75**	**18.68**	**-17.1**
2.71	TPS	0.00	-23.2	-5.65	-4.35	-2.45	-2.11	-2.14	4.11
0.896	SP3	5.45	1.39	-7.16	-1.07	-2.31	-2.09	-1.51	1.00
0.920	t3	**15.81**	**96.53**	**47.35**	**21.27**	**34.52**	**34.84**	**17.45**	**-10.9**
6.396	CP2	6.85	**-17.7**	-3.82	0.69	-1.95	-0.87	0.85	-0.85
0.674	t9	7.88	**113.5**	**78.07**	**28.75**	**50.59**	**50.85**	**25.56**	**-19.1**
0.94	t5	**13.48**	**93.13**	**47.38**	**20.52**	**34.04**	**34.21**	**17.01**	**-10.1**
0.99	t6	**16.16**	**89.47**	**41.90**	**19.60**	**31.81**	**32.18**	**15.95**	**-9.45**
1.014	Sm	2.49	-1.22	-5.47	-1.54	-1.92	-1.88	-1.52	1.37
0.999	t8	**12.50**	**88.93**	**44.18**	**19.31**	**31.59**	**31.66**	**16.01**	-8.89

Table 6.3.5 : Dynamic Simulation Coefficients of Performance based on "500 hp drip proof" motor.

7. OBTAINING THE CIRCUIT PARAMETERS FROM TEST RESULTS

7.1. Introduction To Test Method

The use of three standard tests : Stator DC resistance, No-Load (NL) and Locked-Rotor (LR) is well established and defined in the IEEE "Standard Test Procedure for Polyphase Induction Motors and Generators", [IEEE, 1988]. In this chapter the use of a PC-based system to perform both the data acquisition and analysis is described. Similar PC-based approaches have been adopted by Klaes, [1993] and Grantham and others in the group at the University of New South Wales, [1987]. Gosbell and Dalton, [1991] used a error minimisation method to derive the parameters from a series of complex input impedance measurements taken at low slip. The work of these authors is discussed in Section 7.2 and the reasons for the development of the new method are developed in Section 7.3. Sections 7.4 and 7.5 detail new methods for the derivation of input impedance of the complete motor and the referred rotor impedance from captured waveforms. Results for two experimental machines are given in Section 7.6 with comments on the experimental procedures and results given in the final Section 7.7.

Since the exact equivalent circuit of Figure 2.1.1 has six parameters it is impossible to determine these from the stator dc resistance, NL and LR tests. The resulting degree of freedom means that there exists an infinity of equivalent circuits which will satisfactorily reproduce the given test results. Each of these circuits will produce a slightly different result when used to predict performance at conditions other than the standard no-load and locked-rotor conditions. Which circuit should be used? There is no way of knowing which circuit is best without additional information. If the core loss is incorporated into the friction and windage loss as suggested in Chapter 2 then in theory, there are as many constraints as there are unknowns and the circuit becomes uniquely defined.

The locked rotor test produces a value for the total leakage reactance without splitting it into stator and rotor components as required by Figure 2.1.1. Two approaches are possible to effect the split. The IEEE Standard Test Procedure suggests using the design classification to split the total leakage reactance into its stator and rotor parts. See also [NEMA, 1987]. The alternative to this is to use additional test data. However, because the motor performance as observed at the terminals is insensitive to the allocation of leakage reactance, it is difficult to use test data as a basis for splitting the reactance. It was shown in Chapter 4 that if the single cage model is to be used, then the reactance allocation is unimportant. However, if the double cage rotor circuit of Figure 2.2.4 is used then it becomes important to identify the proportion of the total reactance which is variable with slip. In fact, under these circumstances, it is better to think of the circuit reactances as representing slip-invariant and slip-dependent components of leakage reactance rather than as stator and rotor leakage reactances. The components of the rotor reactance which do not vary with slip (eg part of the end leakage) may be included in the traditional "stator reactance" part of the simulation model.

The method adopted in this work was to use the NEMA design data as a starting point and assume that the total leakage reactance was equal to the locked rotor reactance. The leakage components were then modified until the circuit fitted both the

no-load and locked rotor test results with the design reactance split. It is recognised that this is not entirely consistent with the last two sentences of the previous paragraph but it will be shown to give results which compare favourably with both the manufacturer's performance data and simulated rotor impedance variation based on the variable width bar. The method was incorporated into the program GETR2X2.PAS which derived the rotor parameter values from measurements of motor input impedance at no-load, locked-rotor and various intermediate speeds. This process is discussed in Section 7.5.

Test results for two laboratory motors are given. The first is a standard 2.2 kW industrial motor which was used in Chapter 6 and the other a 4 kW motor with a double cage rotor.

7.2. Methods Of Measuring Circuit Input Impedance

The work by Klaes was focussed on the dependence of the parameters on saturation and was considered appropriate for VSD applications where the slip would be kept small under normal operating conditions. He used a single-phase, variable frequency supply to perform up to 16 locked-rotor tests. Initial estimates of the circuit parameters were based on nameplate data and used as a starting point for an optimisation process. The parameters were adjusted using the locked rotor test data. No attempt was made to model skin effect in the rotor or stator though variation with temperature is mentioned. The method seems inappropriate for large machines where skin effect is significant but could well be directly applicable to motors of rating less than about 30 kW with relatively uniform rotor bar shapes.

Gosbell and Dalton's work assumed that the parameters derived from impedance measurements over a range of slip values from no-load to 10% of rated load were appropriate for the full range of operation with VSDs. Since a constant frequency mains supply was used for the tests, the derived stator parameter values are those appropriate to 50 Hz operation. It has been shown, in Chapter 4, that stator resistance does not significantly affect dynamic performance. The stator reactance variation would be important but due to the normally stranded conductors in the stator, the skin effect here would be negligible. For large motors, where skin effect in the rotor would be present, the rotor frequency is always low due to the drive being constrained to operate in the low-slip region. Since the load range is limited to less than 10% of rated, this method will therefore give the low-frequency, unsaturated values of the circuit parameters and must be combined with locked-rotor tests to give the complete double-cage circuit for non-VSD modelling.

The work done, both in the past and currently, by Grantham and others at the University of New South Wales is based on the rapid measurement of parameters as the motor accelerates from rest. In their early work, the fast electrical transients were ignored. It was suggested by the author in 1989 that this would lead to errors in the derived parameters in cases where the transients had not died away rapidly. Initial reverse rotation is now used to eliminate the effect of starting transients. The measurements are made by a PC-based data acquisition system. More recently, a DSP chip has been used to perform the computation in real time, [Tabatabaei-Yazdi and Grantham, 1995].

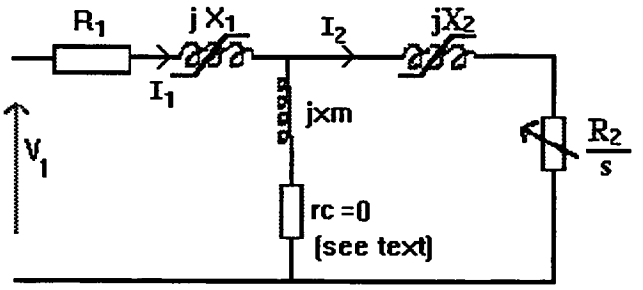

Figure 7.1 : Motor equivalent circuit.

7.3. Method Used For This Work.

The method adopted in this work is similar to the UNSW work but with two variations. First, it was unnecessary to perform the computation in real time and so a DSP chip was not needed. The data was stored in files in the PC and processed later by a separate program. The second modification was made to take into account imperfections in the supply system and this is discussed below.

It was recognised that three factors influence the values of motor input impedance, (R_S +j X_S), namely frequency, leakage path saturation and winding temperature. It has been found that great care needs to be taken to avoid confounding the effects of the three different factors which affect the rotor impedance variation. If test results (or performance data) are taken with a given combination of factors then it may not be assumed that the results are applicable to other combinations. In some cases an inaccurate model may work if a pair of factors always occurs in the same combination, eg. high frequency and current at starting for both the locked rotor test and the required simulation. The fact that the rotor leakage alone is slip-dependent means that the calculated total leakage reactance at any slip is slightly dependent on the assumed reactance split.

For the LR tests the stator was energised for enough time for the electrical transients to decay plus approximately 1.2 cycles of mains frequency. This was done by a trial method. That is, a preliminary recording was made of the transient currents after energising the motor with the rotor locked. By examining the transient response it was possible to be sure determine the approximate time necessary. An additional 1.2 cycles was added to be sure that a complete cycle (from zero crossing to the next) would be captured.

For the 2.2 kW motor, the NL test was performed at true synchronous speed by driving the motor with a synchronous motor. For the 4 kW motor this was impossible because there was no synchronous motor available and the controls on the dc drive motor were rather coarse. There was also a tendency for the dc motor's field rheostat to warm up rather quickly giving speed drift with time.

The measurement of phase differences was critical to the derivation of motor input impedance. In order to achieve accurate phase measurement it was necessary to extract exactly one cycle of each of the voltage and current waveforms. A low pass filter at the input to the data acquisition card ensured that transient spikes did not distort the waveforms to the point where this process was impaired. Discrete, (rather than fast) Fourier analysis was used to calculate the fundamental component of each

waveform. The operation of this procedure was checked using simulated input waveforms and found to be correct to less than half a percent error.

The UNSW work assumed balanced, sinusoidal waveforms. The program GETRX.PAS operates on the positive-phase-sequence (PPS) component of the fundamental waveform. This was found to be necessary due to variation in the laboratory supply. Without it, it proved impossible to obtain repeatable results unless all readings were taken in the early hours of the morning and on weekends. The main problem was variation in phase rather than in voltage magnitudes. The motor impedances determined from the processed voltage and current waveforms were therefore the PPS values. Small negative phase sequence (NPS) voltages and currents were also present due to supply imbalance but these could not be used to derive the NPS impedances because their magnitudes were small in relation to the associated uncertainties.

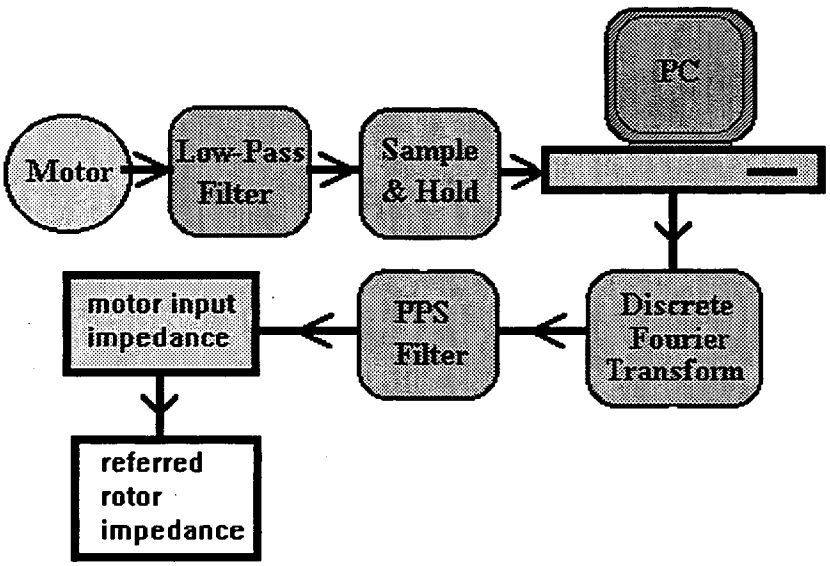

Figure 7.2 : Data acquisition and processing system

7.3.1. Data Acquisition Hardware

The commercial data acquisition package STAT30 was used to acquire data from each channel using a Boston Technology, PC-30D data acquisition card with a throughput of 200 kHz. The STAT30 program was used to sample the three, phase voltage and current waveforms. Two additional channels were used, one for a signal proportional to rotor speed and the other being the square-wave output from a toothed wheel optical pickup on the shaft. With eight channels, this allowed a sample rate of 25 kHz per channel and the next lowest option of 20 kHz was used.

An anti-aliasing, (anti-spike) filter was used on each channel. A simultaneous sample-and-hold circuit was controlled from the PC30-D card to ensure simultaneous sampling of all signals. The system is shown in Figure 7.2 .The data used to demonstrate the method was sampled from the 2.2 kW, 415V, 4-pole 50 Hz, Pope TEFC cage induction motor designated M83 (University of Tasmania, Hobart, Electrical Power Engineering Laboratory).

7.4. Derivation of Motor Input Impedance.

The data files were stored on disc. A text file (FILIST.DAT) was created to contain a list of the names of the files in which the raw test data from the PC30-D card was stored. For example, the files were called RA.DAT, RB.DAT etc. with the '.DAT' part of the name being added automatically.

Program GETRX.PAS was written and used to process data from the files listed in FILIST.DAT to yield the positive phase sequence impedance of the fundamental. The fundamental frequency was determined as the mean value of the derived frequencies of the six input waveforms as determined by the time between zero crossings. For each waveform a small error will occur which depends on the closeness of the sampling point to the zero crossing. It was confirmed by simulation that the fundamental frequency as derived above was an accurate replication of the true frequency unless the waveforms were grossly distorted. The program has a built in check to warn if the derived frequency departs from the range (48-52 Hz). The program GETRX.PAS used the Turbo Pascal units; CONV, FOUR, PH_CHK and PPS which contain procedures the functions of which are described below.

7.4.1. CONVM;To Replace Comma Separator

The STAT-30 software used a comma as the default separator. Whilst this may be altered before using the program, it proved easy to forget to over-ride the default. Rather than have two kinds of data files, it was easier to incorporate a Turbo Pascal program unit within the main program to replace commas in the data file with spaces. The newly created data file (without the commas) has the letter 'S' prefixed to its original name.

The first 15 lines of data file RA.DAT were as follows :

"Sample Taken at : ","20:13:59 Thur 10 Nov 1993"	
"Channel 1 : Volts"	Red phase voltage
"Channel 2 : Volts"	Yellow phase voltage
"Channel 3 : Volts"	Blue phase voltage
"Channel 4 : Volts"	Red phase current
"Channel 5 : Volts"	Yellow phase current
"Channel 6 : Volts"	Blue phase current
"Channel 7 : Volts"	Speed output
"Channel 8 : Volts"	toothed wheel output (0 - 5V)

```
Channel:",    1,    2,    3,    4,    5,    6,    7,    8
.00000,-0.131836,0.297852,-0.239258,-1.733398,0.988770,0.651855,0.915527, 4.997559
.00005,-0.136719,0.295410,-0.239258,-1.740723,1.015625,0.629883,0.915527, 4.997559
.00010,-0.126953,0.300293,-0.241699,-1.728516,1.027832,0.603027,0.917969, 4.997559
.00015,-0.122070,0.297852,-0.246582,-1.716309,1.025391,0.595703,0.915527, 4.997559
```

Table 7.1 : Raw data from STAT30 software.

The output file was SRA.DAT , the first 5 lines of which are shown below :

```
unit conv.pas dated 10th Nov. 1993
   500      8          {No. of points & No. of Channels}
0.00000 -0.131836 0.297852 -0.239258 -1.733398 0.988770 0.651855 0.915527 4.9977
0.00005 -0.136719 0.295410 -0.239258 -1.740723 1.015625 0.629883 0.915527 4.9977
0.00010 -0.126953 0.300293 -0.241699 -1.728516 1.027832 0.603027 0.917969 4.9977
```

Table 7.2 : Comma removed from STAT30 data file.

7.4.2. FOURM; To Extract Fourier Fundamental

The discrete Fourier transform was used in preference to the FFT as this preserved the phase information and speed of calculation was not essential. In theory it would be necessary to sample at a multiple of the mains frequency in order to preserve phase information. Since the mains frequency is prone to drift (in the extreme between 47.5 and 52.5 Hz) a phase-locked loop would be needed to achieve this. Data was sampled for just over 1.5 cycles of the mains waveform and a subset of one cycle of this was extracted. The single cycle was identified by computing an error sum, ε given by :

$\varepsilon = \sum_{ch=1}^{ch=6}(R_{ch} - R_1)$, where R_{ch} and R_1 were the readings from the ch-th and 1st channels. Beginning at 18.5 ms after the start of sampling, this error term was computed for all the voltage and current waveforms. As the complete cycle was reached, ε tended towards zero. When ε began to increase it was concluded that the single cycle was completed. The periodic time of the mains was taken as the time from the first sample to that sample which occurred after 18.5 ms and which had minimum error, ε . It was intuitively felt that, even with asynchronous sampling, the phase error would be small since the sampling rate was so fast (20 kHz) compared with the required (Nyquist) rate of 100 Hz. This was checked by numerical simulation. (Program CHK_SMPL.PAS) in which balanced, three-phase waveforms were generated at frequencies ranging from 47.5 to 52.5 Hz. With high sampling rates the errors in the magnitudes of the fundamentals of each individual phase quantity were less than 0.5% and the phase errors in individual phases were less than 0.5 degree. In addition, because the errors for voltage and current were in the same direction, the errors in average per-phase impedance (magnitude and direction) were undetectable to 5 significant figures.

For example, for a simulation with a sampling frequency of 20 kHz and mains frequency of 47.5 Hz, and balanced three-phase voltages and currents with phase angle between currents and voltages of 83.1 degrees the results were as shown in Table 7.3.

Simulated mains frequency 47.50 Hz; mean phase angle taken as 83.1 degrees.

	A	B	Magnitude	phase	Phase Relative	to
Vr	1.3929	0.2462	1.0002	10.023	0	Vr
Vy	-0.9087	1.0888	1.0028	129.847	119.82	Vr
Vb	-0.4842	-1.3350	1.0041	250.062	240.04	Vr
Ir	0.4106	-1.3596	1.0043	-73.196	-83.22	Vr
Iy	0.9668	1.0371	1.0025	47.009	-82.84	Vy
Ib	-1.3774	0.3226	1.0003	166.819	-83.24	Vb

Table 7.3 : Simulated extraction of exactly one cycle for preservation of phase information in Fourier transform.

Similar results were obtained using frequencies in the range from 47.5 to 52.5 Hz.

Program FOUR.PAS 11th November 1993

A	B	Magnitude	phase
0.2837	-0.1113	0.3048	-21.426
-0.0476	0.3108	0.3145	98.704
-0.2555	-0.2015	0.3254	218.253
0.2591	-1.6758	1.6957	-81.210
1.3665	1.0160	1.7028	36.632
-1.6294	0.6631	1.7592	157.856
0.9165	0.0000	0.9165	0.000
-0.0585	-0.4436	0.4474	262.489

Table 7.4 : Fourier components of voltage and current waveforms

The processed data file containing the Fourier fundamentals of the voltage and current waveforms was then used as input data file for unit FOUR.TPU. The output from this unit was stored in a new file with the name FS**.dat. Only the fundamental was derived.

7.4.2.1. PHASE_CHK: **to check phase separation**

This was used to ensure that the results of the process FOUR yielded three phase voltages and currents that were sensible. It was originally included as a debugging check but was left in as its output is dumped in a temporary file RX.Q which may be viewed if needed. For the 2.2 kW motor some of the variation in phase angle for the currents was due to the machine having slightly unbalanced phases in the stator winding, a point confirmed by the manufacturer as normal for that design.

First the phase angles for each quantity were derived from the input waveforms.

```
Phase angles measured (Data from file ra.DAT)
 -21.43              98.70              218.25  Voltages
 -81.21              36.63              157.86  Currents
```

Then the displacement of adjacent phasors was calculated. A warning is given if the phase angle departs from the correct phase angle of 120 degrees by more than 5 degrees. Phase imbalances of this order have been reported elsewhere, [Gosbell and Dalton, 1987].

	voltages	currents	pf angle
Red-Yellow	120.32	120.93	59.78 Red
Yellow-Blue	120.13	117.84	62.07 Yellow
Blue-Red	119.55	121.22	60.40 Blue

Table 7.5 : Check on displacement of phasors.

7.4.3. PPSM: **To Extract PPS Components**

The positive phase sequence components were extracted for each waveform by applying the symmetrical components transform : $V_1 = \frac{1}{3}\left[V_a + hV_b + h^2V_c\right]$ where $h = 1\angle 120°$.

Up to this point, all computation was done in terms of the voltages inputs to the PC30_D card (ie in the -5 to +5 V range). Scaling to actual machine winding voltages

and currents was performed using data from previously done calibration tests on the data acquisition system. The file CALIBRAT.DAT was used for holding calibration data with the format : Channel number followed by line fit constants y = m x + c and coefficient of determination from least squares procedure. This is shown in Table 7.6. The calibration process is documented in Section A7.1.

```
file calibrat.dat for use by unit PPS.pas.
1   0.01186 0.00690 0.99410     m       c     coefficient of determination
2   0.01175 0.00532 0.99598
3   0.01212 0.00218 0.99840
4   0.87187 -0.01791 1.00671    m       c     coefficient of determination
5   0.85035 0.00449 0.99819
6   0.83827 0.03005 0.98798
7   0.00205 -0.01271 1.00585
8   1.0     0.0     1.0   {square wave}
```

Table 7.6 : Calibration data (prior to test on 2.2 kW motor).

This allowed the actual phase quantities to be derived as :

```
Mean pf angle    60.751
Mean Voltage  26.033  Mean Current    2.008
```

A check was made to ensure that the voltages did not depart significantly from the mean voltage. (The large number of decimal places is not intended to indicate accuracy but are a result of output formatting from the computational process).

voltage	pu error	current	pu error
25.11804	-0.035153	1.96544	-0.021420
26.31319	0.010756	1.99719	-0.005613
26.66832	0.024397	2.06276	0.027034

Table 7.7 : Magnitudes of phase voltages and currents.

The "error" terms quoted above are in relation to the mean voltage or current. Ideally all voltages would equal the mean value. They are not an estimate of the error in the measured voltage (which is unknown, though the uncertainty can be estimated). The relative magnitudes of the actual voltages supplied to the motor varied from time to time throughout the day as the building loading varied on different phases. This was the main reason that a decision was made to separate out the PPS components of the fundamental quantities and to base the parameter determination on the ratio of these quantities rather than on the RMS voltages and currents of the complete waveforms.

Once the PPS components of the fundamental voltage and current was known, then the mean per-phase motor input impedance in ohm was determined for those particular values of machine temperature, speed, voltage and current. The final output from this process was stored in a file RX.DAT as shown in Table 7.8 for four different sets of measurements. This file was edited to add the number of data points in the file and a file identifier. It was then renamed R2X2.IN and used as input for the subsequent program GETR2X2.PAS.

```
Based on file Fsra.DAT  Speed V ph I th R X Z al
  453.3 26.03304  -21.492 2.00823  -82.245
   6.3335  11.3107  12.9632   60.8
Based on file Fsrb.DAT  Speed V ph I th R X Z al
  727.2 27.04682   52.660 2.00167   -4.947
   7.2388  11.4096  13.5121   57.6
Based on file Fsrc.DAT  Speed V ph I th R X Z al
 1075.6 30.96126  -48.028 2.00030  262.398
  10.0372  11.7827  15.4783  -310.4
Based on file Fsrd.DAT  Speed V ph I th R X Z al
 1328.3 46.71788  242.097  1.96746  206.944
  19.4145  13.6717  23.7453   35.2
```

Table 7.8 : Final output from program GETRX.PAS

Although the processing of the data may appear complex, the actual data acquisition took less than 50 ms. For the tests on the 2.2 kW motor, the data processing was done on another PC whilst waiting for the induction machine to settle down before taking the next reading. For the 4 kW motor, the analysis was done on the same PC at the end of the complete test.

7.5. Method Of Derivation Of Rotor Circuit Parameters From Impedance Measurements

This section presents a new method for determining the rotor resistance and reactance values for a cage induction machine at a particular value of slip from measurement of input impedance when driven at different speeds. The method may be compared with that of Brown and Grantham, [1975]. In that work the solution of equation (7.2), expressed in terms of two real non-linear equations, was found using the Newton-Raphson method, [Lastman and Sinha, 1988]. This is unnecessary since the equations may be solved directly as follows :

From Figure 7.1, the input impedance per phase, $R_S + j\,X_S$ is given by :

$$R_s + jX_s = R_1 + jX_1 + \frac{(r_c + jx_m)\left(\frac{R_2}{s} + jX_2\right)}{\left(r_c + \frac{R_2}{s}\right) + j(x_m + X_2)} \qquad (7.1)$$

$$\Rightarrow \left[(R_s - R_1) + j(X_s - X_1)\right]\left[\left(r_c + \frac{R_2}{s}\right) + j(x_m + X_2)\right] = (r_c + jx_m)\left(\frac{R_2}{s} + jX_2\right)$$

This can be re-arranged to

$$\left[(R_s - R_1)\left(r_c + \frac{R_2}{s}\right) - (X_s - X_1)(x_m + X_2)\right] + j\left[\left(r_c + \frac{R_2}{s}\right)(X_s - X_1) + (x_m + X_2)(R_s - R_1)\right]$$

$$= \left[\frac{r_c R_2}{s} - x_m X_2\right] + j\left[r_c X_2 + \frac{x_m R_2}{s}\right] \qquad (7.2)$$

Equating real parts of equation (7.2) gives

$$(R_s - R_1)r_c + (R_s - R_1)\frac{R_2}{s} - (X_s - X_1)x_m - (X_s - X_1)X_2 = \frac{r_c R_2}{s} - x_m X_2$$

or

$$-(r_c + R_1 - R_s)\frac{R_2}{s} + (x_m - X_s + X_1)X_2 - \left[(X_s - X_1)x_m - (R_s - R_1)r_c\right] = 0$$

Let

$$A = (r_c + R_1 - R_s), \tag{7.3}$$

$$B = (x_m - X_s + X_1) \tag{7.4}$$

$$C = (X_s - X_1)x_m - (R_s - R_1)r_c \tag{7.5}$$

$$D = x_m(R_s - R_1) + r_c(X_s - X_1) \tag{7.6}$$

Then we can write

$$-A\frac{R_2}{s} + BX_2 - C = 0 \tag{7.7}$$

Equating imaginary parts of equation (7.2) gives :

$$X_2(R_s - R_1) + r_c(X_s - X_1) + \frac{R_2}{s}(X_s - X_1) + x_m(R_s - R_1) = r_c X_2 + \frac{x_m R_2}{s}$$

or

$$-(x_m + X_1 - X_s)\frac{R_2}{s} - (r_c + R_1 - R_s)X_2 + \left[r_c(X_s - X_1) + x_m(R_s - R_1)\right] = 0$$

This can be written as

$$-B\frac{R_2}{s} - AX_2 + D = 0 \tag{7.8}$$

Combining equations (7.7) and (7.8) gives

$$X_2 = \frac{BC + AD}{(A^2 + B^2)} \tag{7.9}$$

and

$$\frac{R_2}{s} = \frac{BX_2 - C}{A} \tag{7.10}$$

The terms $(R_{S1} + jX_{S1})$ and $(R_{S0} + jX_{S0})$ are introduced and used for the values of $(R_S + j\,X_S)$ at s=1 and s=0 respectively. The algorithm used in program GETR2X2.PAS was as follows :

1. A given measured V_S and I_S yielded the corresponding R_S and X_S by using program GETRX.PAS.
2. The I_S value was used to determine the values of R_{S1} and X_{S1} appropriate to that level of leakage path saturation.
3. The value of V_S was used to set the R_{S0} and X_{S0} values to be used in the calculation of the series form of magnetising branch quantities, x_m and r_c.
4. estimate the total leakage reactance as equal to X_{S1} and split it into X_2 and X_1 components using the /NEMA MG1 guidelines.
5. then compute {A,B,C,D} as above.
6. then compute rotor leakage reactance based on {A B C D} as equation **(7.9)**.

7. finally compare this value with the assumed reactance stator/rotor split and adjust the leakage estimate at step 4 until the error is less than some specified epsilon. (eps =1e-06 was used in the program GETR2X2.PAS which is easily small enough).

7.5.1. Note On Common Approximation

If at slip = 1, $R_{st} << R_c$ AND $X_{st} << X_m$,

where R_c and X_m are the parallel form of the magnetising branch quantities, r_c and x_m given by $R_c = \frac{(r_c^2 + x_m^2)}{r_c}$ $\quad X_m = \frac{(r_c^2 + x_m^2)}{x_m}$

then equation **(7.1)** reduces to $R_{s1} + jX_{s1} = R_1 + jX_1 + R_{st} + jX_{st}$
giving $R_{st} = R_{s1} - R_1$ and $X_{st} = X_{s1} - X_1$

which is the commonly used assumption for locked-rotor test analysis.

The above assumption is not necessarily valid for certain types of motor. For example, with dual voltage motors or those designed for a wide range of mains supply voltage the magnetising branch components may make a significant contribution to the locked-rotor impedance. This situation is likely to become worse as moves towards standardisation of voltages lead to motors originally designed for 380 or 415 V operation being run on 400 V supplies.

For motors manufactured to the AS1359 (and IEC34) standards, a requirement exiss to operate satisfactorily over a range of voltage and frequency. For Zone A, a variation of ±0.2 pu in frequency and ±0.2 pu in voltage is allowable with the motor expected to achieve rated torque without exceeding an additional temperature rise of 10 degrees. For Zone B, the tolerances are larger but the temperature rise permitted is also larger and the performance allowed to differ from the nameplate value. It is likely that motors operated at the high flux extremity of the Zone A region will draw considerably more magnetising current than with rated supply. This means that to assume that the magnetising current is negligible close to rated slip, ie neglecting X_{st} in equation **(7.1)**, could lead to error and this error is uncertain because the degree of magnetic saturation designed into the motor is unknown unless a series of no-load tests are done at different voltages.

This has implications for the method used in testing induction motors. If accuracy of the order of 10% is all that is needed then it is not particularly important whether the NL test is done at exactly synchronous speed. The above assumption simplifies the analysis. If however, the test results are going to be used in a sophisticated algorithm which allows for main flux or leakage path saturation and similar effects and if high accuracy is sought, then it seems sensible to use a recursive method; to include the leakage reactance voltage drop in the analysis of the NL test results and the magnetising current in locked rotor analysis.

The algorithm introduced here does not assume that the magnetising branch is absent during the locked-rotor test nor that the leakage may be ignored during the no-load test. It searches for a set of values for the equivalent circuit parameters which minimises the error in assumed rotor/stator leakage reactance split whilst fitting the

measured input impedance at both locked-rotor and no-load. The method for determining the magnetising reactance is similar to that of de Mello and Walsh, [1961] with the difference that the stator leakage reactance is adjusted iteratively.

At low values of slip, the input impedance is close to $(r_c + R_1) + j(x_m + X_1)$; (See Figure 7.1). The method is not therefore able to determine the rotor impedance at very low values of slip since the input impedance is then dominated by the magnetising branch. (B and A in equations 7.3 and 7.4 are given as the differences of two large, almost equal quantities). In addition, since the rotor and synchronous speeds are similar, it is not accurate to compute slip as the per-unit difference between them. To avoid this problem the rotor impedance was determined in the range $1 \geq s \geq 0.20$ pu rather than at lower slip values. Determination of the zero-slip values of the rotor impedance was done by extrapolating the curve back to zero. Since the variation in R_S and X_S in the region of low slip is extremely small (as confirmed by simulation) this was not considered a risky process.

The analysis above was performed including the r_c term to allow comparison with the UNSW work mentioned above. In order to be consistent with the circuit model of Figure 2.2.4, the parameter determination method of Chapter 6 and the steady-state performance simulation program IM2.PAS in Chapter 8, it was necessary to set the value of r_c in Figure 7.1 to zero. As discussed in Chapter 2, this requires modification of the friction and windage losses to include an additional component equal to the core loss at rated load. While this approach may cause horror to motor designers, from a simulation point of view it is quite permissible to model the motor performance by any appropriate model. It is, however, essential that the same model be used in the derivation of the parameters as is used in the performance simulation.

7.6. Results Of Experimental Work

Two sets of experimental data were obtained. In the first set of tests, a standard industrial 2.2 kW 4 pole, 415V cage motor was used with nominal performance data as shown in Table 6.2.1. This motor was not really suitable for the purpose of demonstrating the variation of rotor parameters with frequency because it was a standard industrial motor with a single cage rotor. However, no better motor was available at the time and it was considered useful to apply the new method of analysis of test data to the available motor and simultaneously try to locate another motor which would display more significant deep-bar effects. Eventually such a motor was located at the Hobart Technical College and permission was given to perform tests on it. The second set of results were then obtained from this motor which was a 4 kW Siemens, 2Ga14 Universal Experimental Machine Set with a double cage rotor.

In both cases, currents and voltages were measured in the steady state using the fast data acquisition system described previously. All readings were completed rapidly as only slightly more than one cycle of the waveforms was sampled at a time. The positive-phase-sequence components of the Fourier fundamentals were then extracted and the per-phase input impedances were calculated for both cases. The stator resistance was measured separately.

7.6.1. The 2.2 kW Single-Cage Motor

The synchronous speed measurements were performed with a phase voltage range of 0.1 to 1.05 pu and the locked rotor test over a range of currents from 0.1 to 3.5 pu. The machine under test displayed considerable variation in leakage reactance with

current. This was totally unexpected and the results were doubted and rechecked several times both using the PC-based equipment and with conventional instruments. It was later found that it had semi-closed rotor slots.

7.6.1.1. The "no-load" test

The induction machine was driven by a synchronous motor to ensure zero slip conditions. The motor speed tended to vary slightly during the synchronous speed test. Instantaneous measured speeds at the instant of sampling the voltages and currents varied from 1494 to 1499 rev/min. This tended to affect the value of measured input resistance. This was not considered important because the general trend was clear and a precise value of input resistance at synchronous speed was not needed. However, it does underline the difficulty of taking precise measurements of "No-Load" conditions. Perhaps a bit more damping and inertia would have helped to reduce the observed tendency of the motor's speed to oscillate. The 4-pole synchronous machine used to drive the induction motor was originally built as a generator and did not have any damper bars. The supply frequency at the time of the test was just below 50 Hz. The speed was measured to an error of less than 0.2 % using a toothed-wheel and microprocessor-based counter circuit built by the author's colleague, Mr. Glen Mayhew (Project Officer).

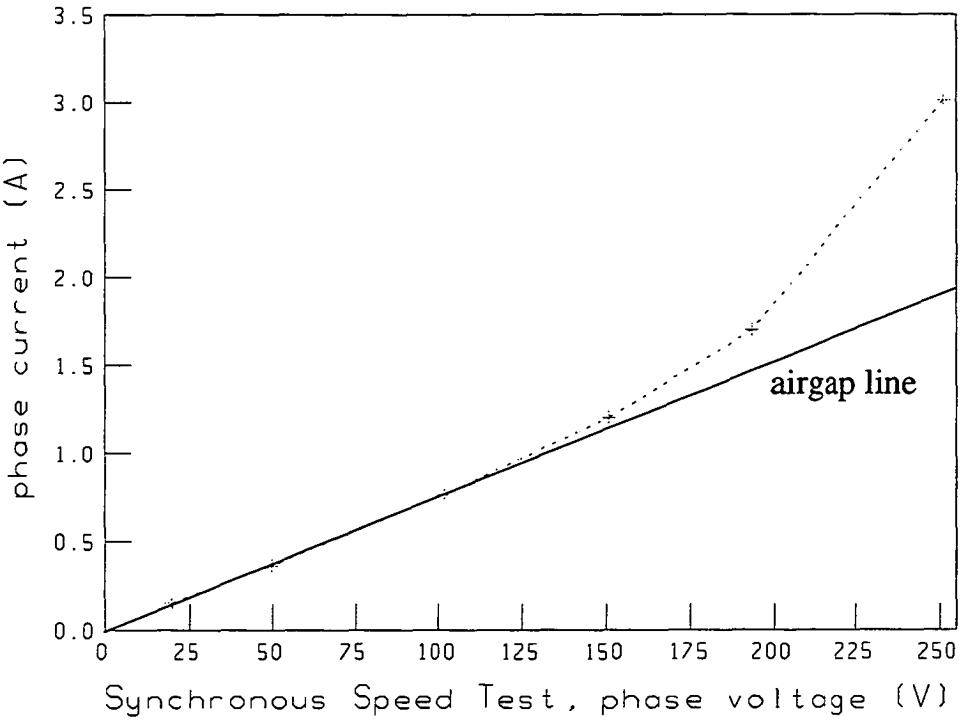

Figure 7.3 : Results of synchronous speed test on 2.2 kW motor

The saturation of main flux paths seems to start to occur at a terminal voltage of about 115 V per phase or 0.48 pu. This is rather low.

The reactance variation with supply voltage when driven at synchronous speed is shown in Figure 7.4. The apparent dip in the curve at very low voltage/current is not considered reliable because at this low level of current the relative errors were high. In practice these very low voltages were not used in the subsequent derivation of the rotor impedance variation and so any error is unimportant.

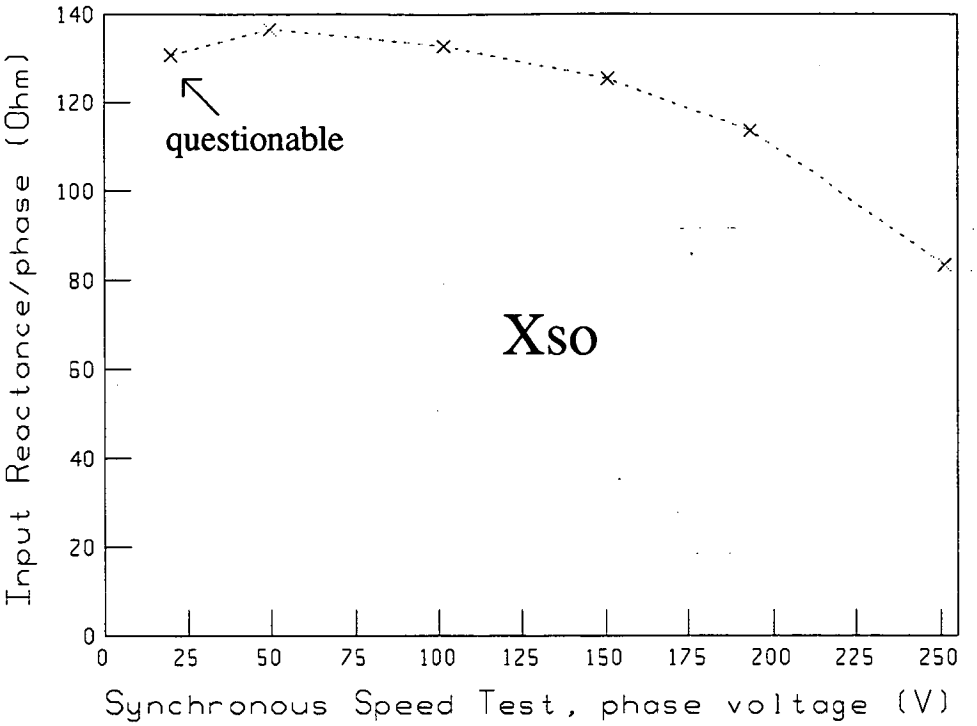

Figure 7.4 : Input reactance per phase for 2.2 kW motor when driven at synchronous speed.

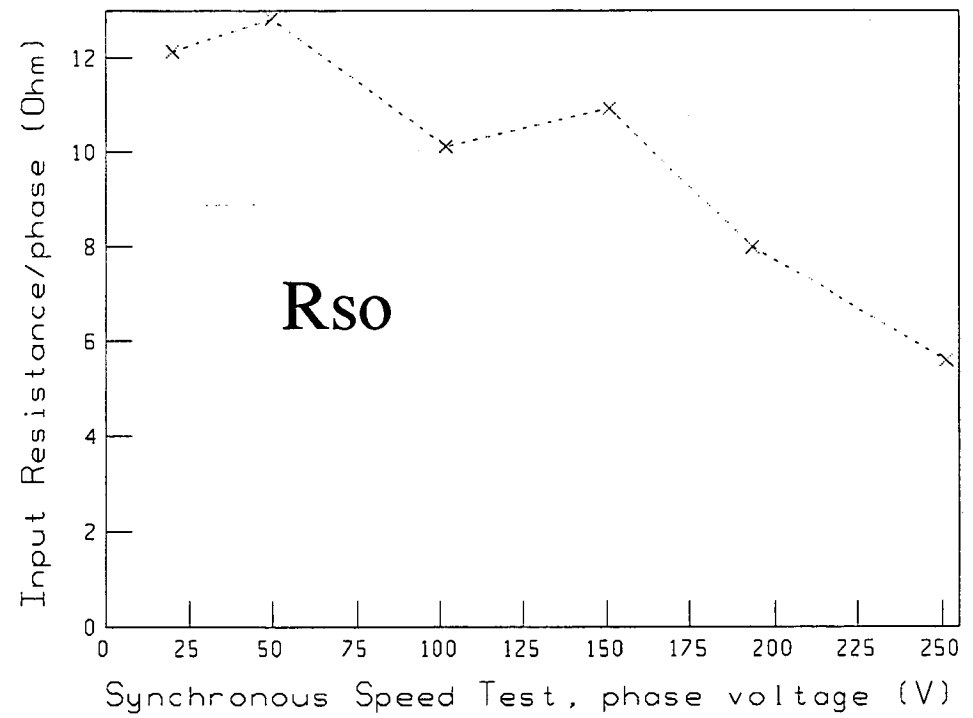

Figure 7.5 : Input resistance per phase for 2.2 kW motor when driven at synchronous speed.

7.6.1.2. The locked-rotor test

The variation in input impedance under locked-rotor conditions is shown in Figure 7.6. The graph contains points derived from measurements taken on two successive days but these two sets cannot be separately identified on the graph, which indicates a degree of repeatability.

The most interesting part of this graph is the dramatic increase in the leakage reactance at very low current. At first this was doubted but re-checking proved that the result was not random. Similar results were noticed in a graph given for a 4 hp motor by Lipo and Consoli, [1984].

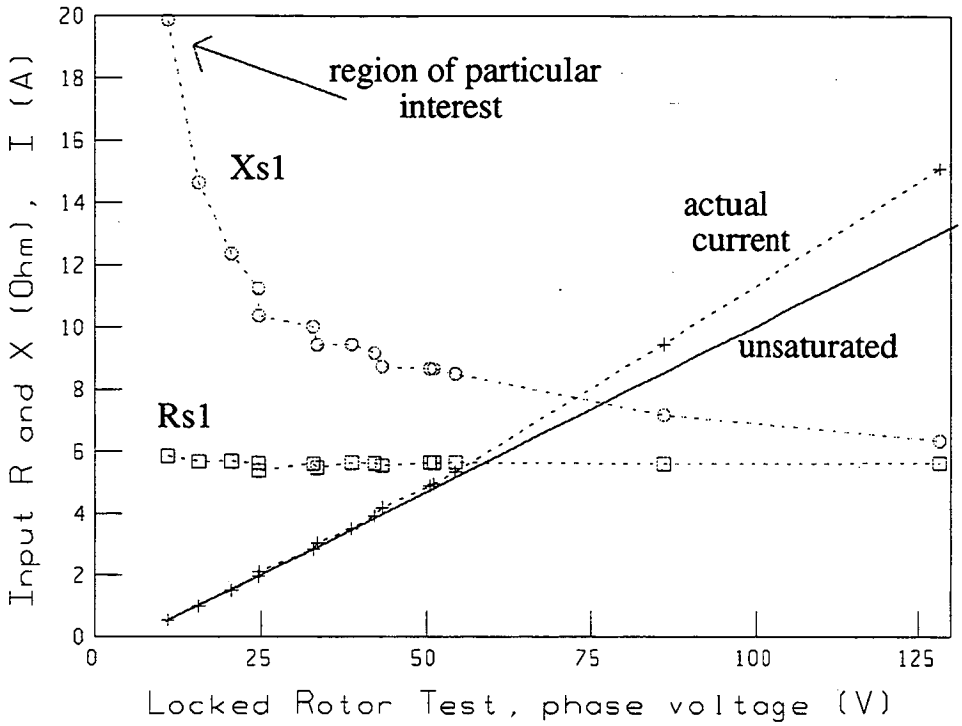

Figure 7.6 : Locked rotor test results for 2.2 kW motor

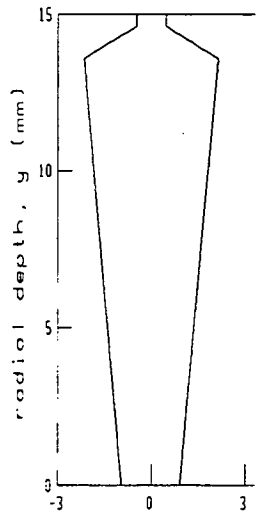

Figure 7.7 : Rotor slot shape

Figure 7.7 shows the shape of the rotor slot for the 2.2 kW Pope motor. This was slightly different from the P-Type slot used in Chapter 5 which was taken from a larger 7.5 kW motor.

The sharp rise in leakage reactance is thought to be due to the presence of a slot bridge which saturates at extremely low currents. When the current falls below a critical value of about 2 A, this region comes out of saturation allowing more leakage flux to pass per ampere. This behaviour is probably a deliberate design feature because it has the advantage that under light load conditions the input reactance per phase of the motor increases leading to reduced current from the mains.

The manufacturer's quoted figure for starting current was given as 5.6 pu or 25.8A. The locked-rotor current at rated voltage measured from the envelope of the waveform of an actual direct-on-line start was 29.7A which is higher than expected but within the 20% tolerance range allowed by AS1359. A comparison of the predicted starting currents at rated voltage based on several of the methods discussed in Chapter 5 is given in Table 7.9.

Quote	Test	Prop	Cprop	Lprop	UNS	DF1	DF2	ML	Lee
25.8	28	23.2	27.8	33.7	33.4	31.5	35.3	34.5	31.1

Table 7.9 : Predicted starting current for 2.2 kW motor using various methods

The data points used in the graph for Figure 7.6 do not include a point close to 1.5 pu current. Lee's method is highly sensitive to using test currents other than the specified values of 1.0, 1.5 and 2.0 pu. If the closest available values from the test data are used, then the predicted starting current is 39.9 A which is too high. The predicted values for the ML and Lee's method shown in Table 7.9 were based on a separate measurement at a current of 1.5 pu. Interestingly the corrected proportional method gave the smallest difference between predicted and test current. This emphasises that the more sophisticated methods might be better on average but not as good in any particular case.

7.6.1.3. Measurements at various speeds

The test machine was then driven by a dc motor at speeds in the range 0.26 to 0.8 pu and the PPS circuit impedance (R + jX) was derived from the filtered waveforms of current and voltage as described previously. The results are given in Table 7.10. From this, the referred rotor circuit impedance was determined using values of locked rotor and synchronous speed impedance corresponding to the actual current and voltage at that test point.

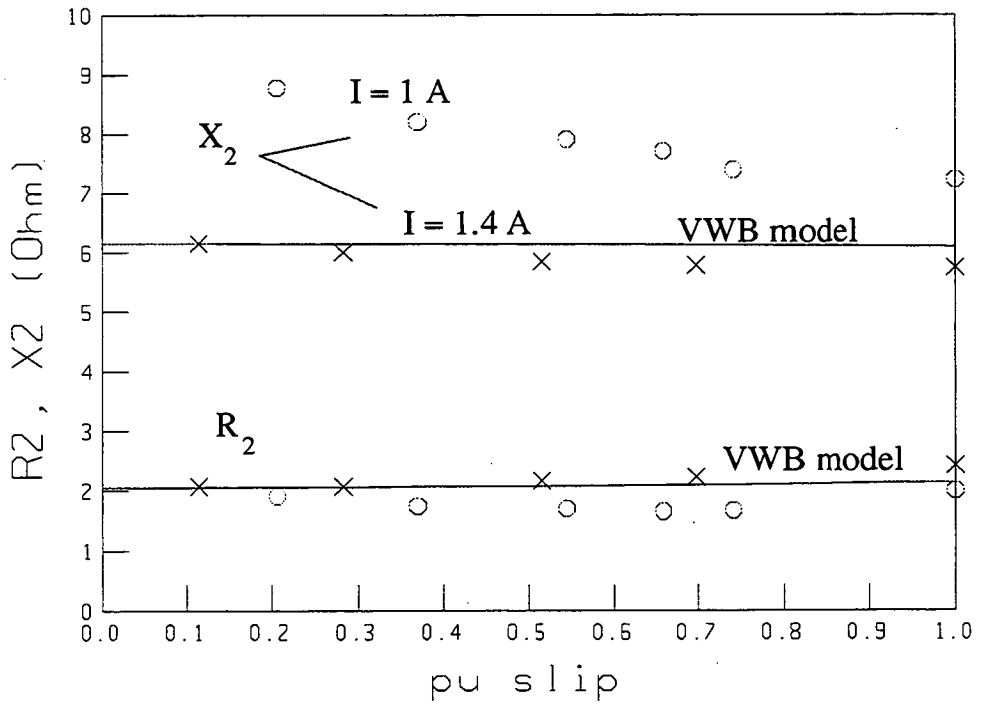

Figure 7.8 : Derived rotor impedance variation for 2.2 kW motor (X) for stator current of 1.4 A and (O) for current of 1 A.

Test results were obtained for two slightly different levels of stator current. The effect of the different leakage path saturation conditions on the measured values of input impedance was pronounced. This resulted in two distinct graphs for rotor impedance. (The data points were taken on the same day, with the same equipment set-up, with a maximum of 15 minutes between the sets of results). The temperature of the motor (as inferred from stator resistance readings) did not change during the test.

The effect on referred rotor resistance was not as great but nevertheless still observably different; ie the scatter in the data points for each line is much less than the difference between the lines. This confirms the variation of referred resistance with leakage path saturation discussed in Chapter 2. Points (X) were for stator current of approximately 1.4 A and those marked with a (O) are for current of 1.0 A. Both of these currents were expected to give unsaturated values of leakage reactance; ie to be the same. However, as shown in the graph for the locked-rotor test, the leakage reactance varied quite substantially even at these low currents. With hindsight it might have been better to use slightly higher currents to avoid the region of rapidly changing leakage path saturation. The decision to use low currents was based on the faulty assumption that leakage path saturation would not occur at currents less than rated. This assumption has been shown to be invalid and this has implications for the measurement methods used in standard locked-rotor tests and the prediction of performance under light load conditions. For example, the method of Gosbell and Dalton would fail if it were used on this motor or on the motor used by Lipo and Consoli since it ignores the possibility of saturation occurring at low currents.

The variation due to skin effect was found to be much less than that due to leakage path saturation. Figure 7.8 shows a 17 % increase in resistance and a 7 % reduction in reactance over the operating slip range when the current was 1.4 A.

Figure 7.8 shows two solid lines which represent the variation based on the VWB model developed in Chapter 5 using slot dimensions taken from a drawing kindly supplied by the manufacturers, (Simpson Pope of Adelaide, SA).The simulated results fit the test data for the readings take at a current of 1.4 A better than those for 1.0 A. It is believed that this is due to the neglect in the development of the VWB method of the variation in magnetic permeability occurring in the slot bridge at low currents. Unfortunately both the 1A and 1.4A values are in the region of the X_{s1}/ V saturation curve where the rate of change is high.

Speed	V	ph	I	th	R	X
rev/min	Volt	degrees	Ampere	degrees	Ohm	Ohm
453.3	18.41	-21.49	1.420	-82.245	6.334	11.31
727.2	19.128	52.66	1.416	-4.947	7.239	11.41
1075.6	21.896	-48.03	1.415	262.40	10.04	11.78
1328.3	33.039	242.10	1.391	206.94	19.41	13.67
388.8	15.44	-26.64	1.115	26.517	5.44	12.728
512.2	15.49	86.41	1.092	19.92	5.66	13.015
682.7	15.454	116.44	1.059	51.541	6.19	13.211
945.1	16.715	227.03	1.077	166.26	7.58	13.540
1190.9	19.41	-33.83	1.054	-85.348	11.45	14.412

Based on files Fsra.DAT to Fsrd.DAT and Fss387 to Fss1192

Table 7.10 : Variable speed test data for 2.2 kW motor.

7.6.1.4. Comparison of measured and simulated impedance variations

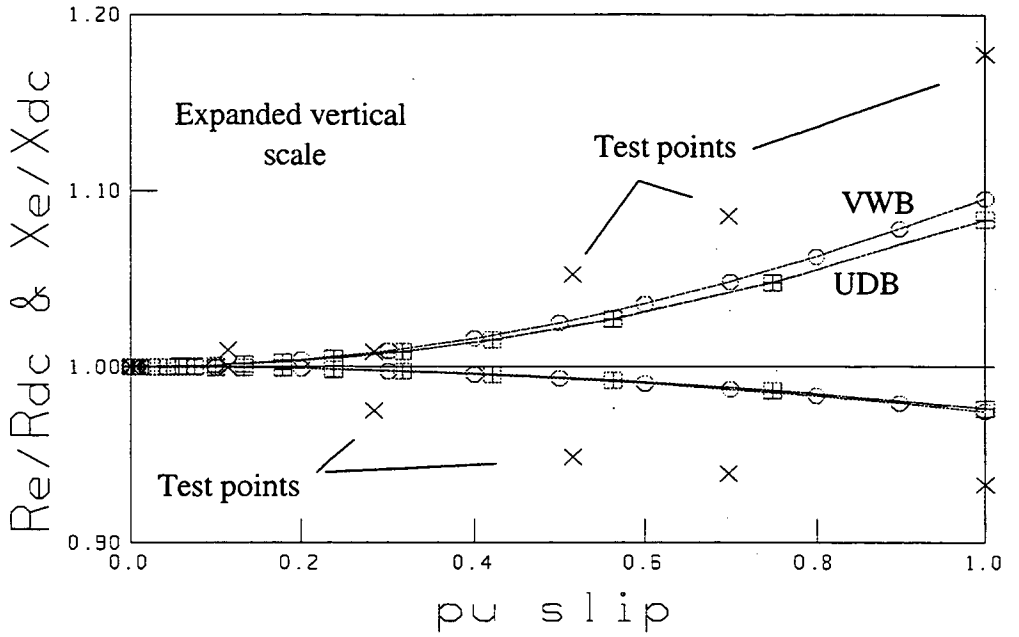

Figure 7.9 : Comparison of UDB, VWB and test results for 2.2 kW motor

Figure 7.9 shows the results of using a UDB model, with bar depth of 15 mm, to derive the impedance variation. The vertical scale has been expanded for clarity and by plotting the normalised impedance rather than the value in Ohms the differences between the simulation and test results has been emphasised. This gave almost identical results to the VWB model (shown as 'O'). Test points are shown as 'X' . To a large extent, the variation in rotor parameters due to slip is swamped by the variation due to magnetic saturation.

UDB, DCC and VWB models were also derived directly from the test data and this gave DCC circuit parameters as in Table 7.11 which fitted the test data better than those derived via the known bar dimensions. Interestingly, the UDB model was slightly deeper than the actual bar depth of 15 mm (approximately 20 mm). It may well be that for this motor the measured leakage reactance is significantly affected by components other than the main slot reactance. eg end-ring leakage. If this is so, then none of the methods based on the calculation of reactance from slot geometry will work particularly well.

Rdc	Xdc	Rst	Xst	m	X1	R1
2.05	6.15	2.43	5.73	0.90	5.73	3.41

Ra	Rb	Xb	Xab	Xa	xm	rc
2.74	8.13	12.0	5.39	0	124	0.0

Table 7.11 : Parameters (in Ohm) for the Pope 2.2 kW motor
Derived from test results

The value of 0.90 determined for the double-cage design ratio, m does not compare well with the best fit values of 0.65 and 2.0 obtained from the PARAM.PAS and INSPEC programs in Chapter 6. This is not particularly important since the motor is very close to being accurately modelled by a single cage and the value of m is given by the ratio of two differences between, nearly equal numbers.

The circuit parameters of Table 7.11 can be compared with those derived from the performance data using the methods of Chapter 6. In Chapter 8, the simulated performance of the 2.2 kW motor using the different sets of circuit parameters, is compared with the nameplate performance.

The results obtained for the 2.2 kW motor were inconclusive which was not surprising because for this small motor there was not expected to be much skin effect. However the usefulness of the experimental method was demonstrated and enough experience was obtained to develop confidence that if a motor with a larger variation due to skin effect could be found then the results might be used to confirm the results derived from simulation using the UDB and VWB methods.

7.6.2. Siemens 2Ga14 Universal Experimental Machine Set

This set had several alternative rotors available. The rating of the Universal Experimental Machine Set with the double cage rotor fitted was given as shown in Table 7.12. The rotor slot cross-section was as given in Section 5.3 and identified there as the S-Type rotor slot.

415 V line	7.8 A	Star connected
50 Hz	1440 rev/min	0.84 pf
4 kW	Rotor Type : R2	efficiency 0.85 pu

Table 7.12 : Siemens 4 kW motor with double cage rotor, designated R2.

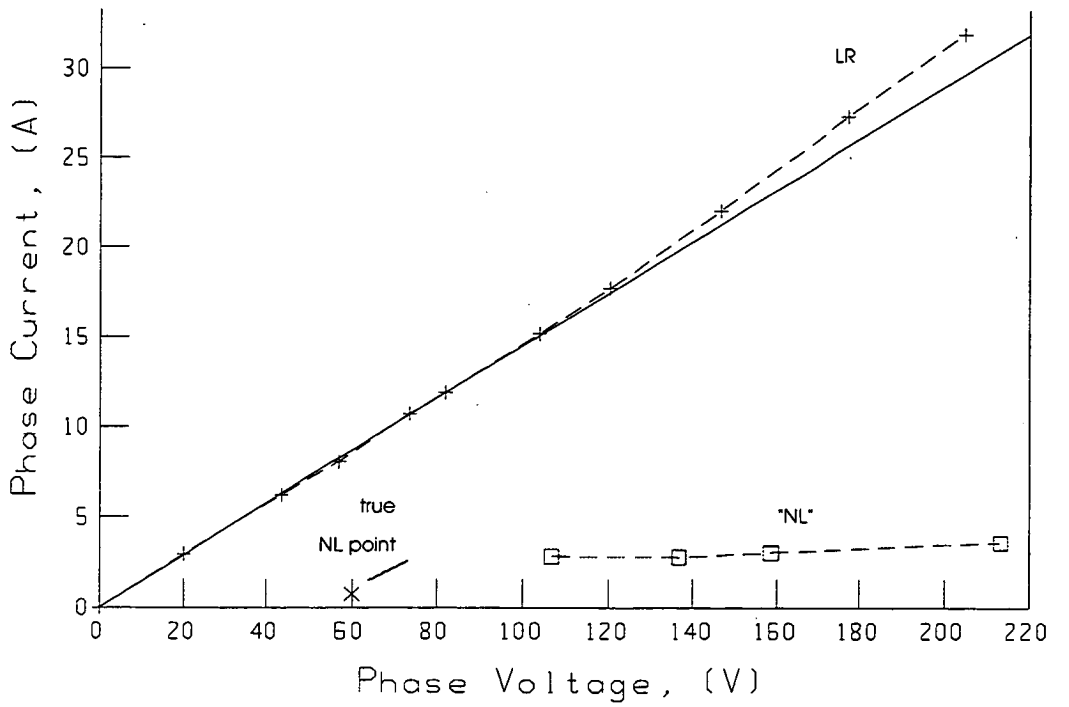

Figure 7.10 : No-load and locked rotor test results on Siemens motor

The results for this machine did not display much leakage path saturation and in this way they form a sharp contrast to those from the 2.2 kW motor. Unfortunately the

laboratory supply was restricted to just under 220 V per-phase on open circuit and so the curve could not be extended right up to the nominal 415 V (line) rating.

7.6.2.1. Locked-rotor test

The locked rotor test did not show significant leakage path saturation at the current levels used. Table 7.13 shows the predicted starting current at rated line voltage of 415V as well as the reduced test voltage of 355V (line).

Voltage	Test	Cprop	Lprop	UNS	DF1	DF2	ML	Lee
205V	31.9	34.7	31.0	32.7	31.4	31.4	33.4	32.9
240V	-	40.7	36.6	38.9	36.4	37.2	39.9	39.1

Table 7.13 : Predicted starting current for 4 kW motor using various methods

7.6.2.2. No-load test

The NL test was performed in the more conventional manner by running the induction motor "unloaded". Unfortunately it proved impossible to remove the coupling between the motor and an eddy-current brake. (It was particularly stiff, I was nursing a back injury and the technical staff member at the Hobart Technical College had disappeared). The "NL" test procedure was followed with the brake attached. This restricted the range of voltage that could be usefully applied during the test because it was found that the motor slowed down considerably when the voltage was reduced below about 0.5 pu. Four data points were take which are shown in Figure 7.10.

In an attempt to overcome this, the induction motor was driven by a dc motor to a speed in the region of synchronous and the impedance was measured as before. This did not work at all well and the measured impedances showed a large scatter.
The following day I returned with a stroboscope. It proved impossible to adjust the speed of the dc motor to exactly synchronous speed because the field control rhestat was rather coarse. The induction motor was accelerated above synchronous speed using the dc motor with a voltage of 60 V (phase) applied to the induction machine. The dc motor was then de-energised allowing the induction machine to coast down towards synchronous speed. When the speed was truly synchronous, the impedance data was sampled. This gave the values of X_{s0} and R_{s0} shown in Table 7.14.

Perhaps the simplest way to measure the "no-load" test results is following the improved method now used by the UNSW group, ie to take fast measurements while the motor accelerates up to speed. The danger here is that if the transients persist then the readings will be inaccurate. For small motors (<200 kW) it is likely that the electrical transients will have died away by the time the low-slip region is reached especially if sufficient inertial load is connected to the motor.

7.6.2.3. Measurements at various speeds

The results in Table 7.14 show data in the file R2X2.IN generated by program GETRX.PAS from variable speed test data.
A reactance split of 0.66 was assumed because this fitted the test data best (fewest iterations).

Rs1	Xs1	Rs0	Xs0	R1
3.30	6.27	8.1	80.5	1.40

File ID	Speed	V	ph	I	th	R	X
Fstth7.htc	181	43.28	24.22	6.00	-36.38	3.55	6.30
Fstth6.htc	330	43.67	77.05	5.90	16.87	3.68	6.42
Fstth5.htc	473	43.92	-46.93	5.78	252.95	3.78	6.58
Fstw6.htc	585.9	69.50	95.35	9.07	36.79	4.00	6.54
Fsts7.htc	615.2	55.07	126.37	7.19	68.15	4.04	6.52
Fstth4.htc	709	43.702	116.94	5.70	58.96	4.07	6.51
Fsts5.htc	761.7	54.54	128.36	6.91	71.20	4.28	6.63
Fstw2.htc	781.3	58.23	45.61	7.37	-11.69	4.27	6.65
Fsts6.htc	945.3	55.12	205.59	6.55	151.78	4.96	6.78
Fstw3.htc	1101.6	64.04	56.58	6.70	6.64	6.15	7.32
Fstw1.htc	1171.9	52.06	79.68	5.14	31.51	6.75	7.54

Table 7.14 : Derived input impedance to 4 kW motor at different speeds

When the results shown in Table 7.14 were processed by program GETR2X2.PAS and Table 7.15 resulted.

From program getr2x2 version dated 7/12/93 with k = 0.66

SLIP	V	I	PHI	R2	X2	RS	XS
1.0000	57.117	8.06	-60.87	2.11	4.25	3.4500	6.1900
0.8793	43.279	5.99	-60.60	2.10	4.26	3.5459	6.2927
0.7800	43.669	5.90	-60.18	1.98	4.40	3.6800	6.4242
0.6847	43.916	5.78	299.88	1.83	4.57	3.7824	6.5832
0.6094	69.495	9.07	-58.57	1.77	4.50	3.9950	6.5357
0.5899	55.068	7.19	-58.22	1.74	4.47	4.0350	6.5126
0.5273	43.702	5.70	-57.99	1.57	4.46	4.0681	6.5065
0.4922	54.537	6.91	-57.16	1.59	4.58	4.2778	6.6288
0.4791	58.232	7.37	-57.30	1.54	4.60	4.2700	6.6499
0.3698	55.019	6.55	-53.81	1.48	4.68	4.9622	6.7827
0.2656	64.041	6.70	-49.94	1.44	5.13	6.1516	7.3158
0.2187	52.057	5.14	-48.18	1.34	5.29	6.7488	7.5420

Table 7.15 : Derived rotor impedance variation for 4 kW motor.

7.6.2.4 Comparison of measured and simulated impedance variations

Figure 7.11 shows :

Data points marked 'X' for the derived variation in rotor impedance with slip

A pair of solid lines which show the variation predicted by the VWB model for a 21 mm deep, S-Type slot (O solid line)

The variation predicted by a 21 mm deep uniform bar, (+ dashed line).

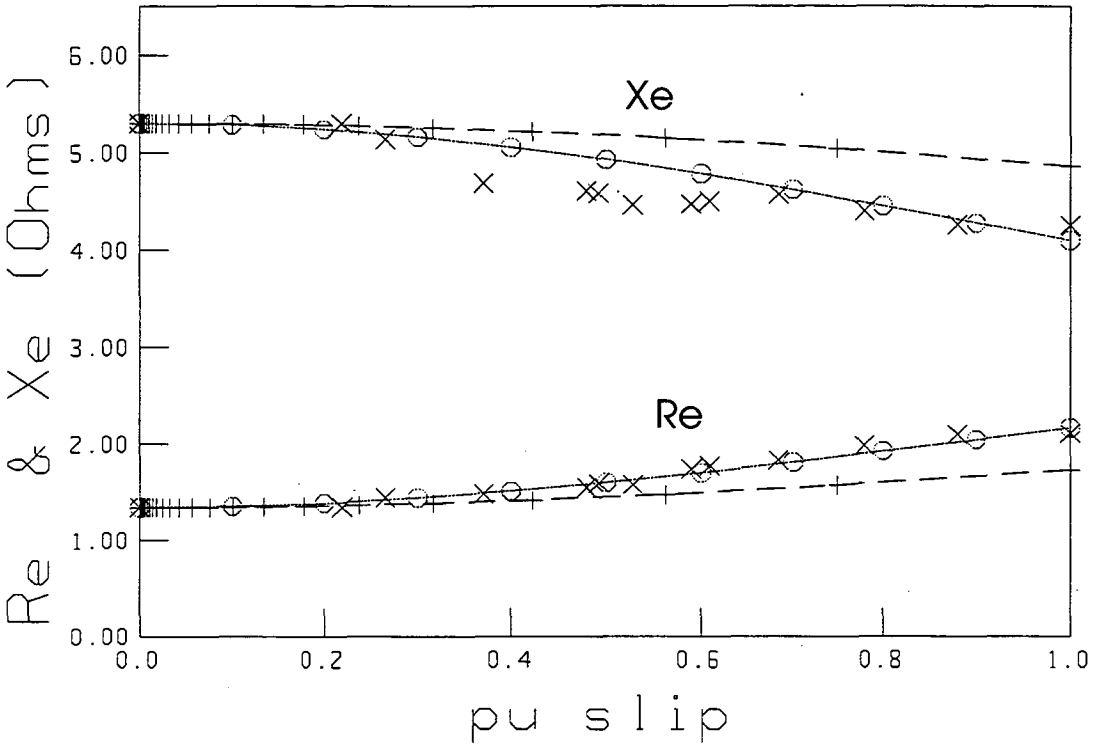

Figure 7.11 : VWB model and test results on Siemens double-cage motor.
Experimental : X VWB model : O solid line UDB : + dashed line

The Siemens 4 kW motor gave results which confirmed the validity of the VWB method for determining the variation of rotor impedance with slip as outlined in Chapter 5. Interestingly enough, the resistance variation was modelled better than the reactance. In the mid-slip region, there was some deviation from the predicted reactance variation . As mentioned above when discussing the 2.2 kW motor, the slot portion of the reactance is not the only component of the total reactance. All the models based on slot geometry (including the VWB model) assume that the only significant reactance which varies with frequency is that due to primary leakage flux as shown in Figure 2.2.6. In practice there will be some variation due to the other leakage flux components changing with slip. It is also likely that some component of endring reactance is also affected by skin effect.

It would have been better to compare the measured and predicted variation for a wider range of motors including some of large rating but unfortunately rotor slot dimensions and test data were not available from the manufacturers for any larger motors.

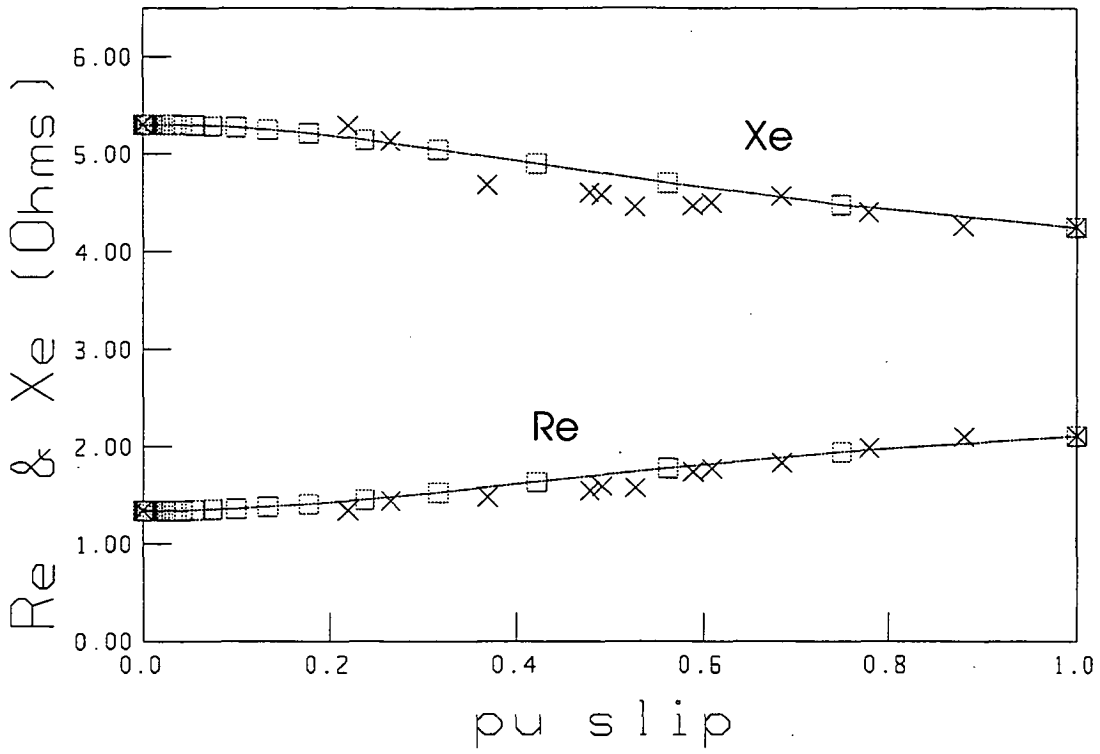

Figure 7.12 : DCC model derived from test data compared with test results for Siemens 4 kW motor. Experimental : X DCC : □

Figure 7.12 shows the results of comparing the rotor impedance variation derived from test results with the predictions of the DCC model derived from the test data. The double cage circuit parameters were derived from the measured impedance values at the slip extremities as described in Section 5.2, the leakage reactance of the upper cage was taken as zero.

Rdc	Xdc	Rst	Xst	m	X1	R1
1.64	5.29	2.11	4.25	0.45	2.19	1.4
Ra	Rb	Xb	Xab	Xa	x_m	r_c
2.21	6.39	19.03	4.04	0.0	78.3	0.0

Table 7.16 : Parameters (in Ohm) for the Siemens 4 kW motor Derived from test results

7.7. Comments On The Experimental Work

Most of the evaluation of computational models performed during the work which is the subject of this thesis was based on simulated machine performance. It was considered essential to supplement this with measured performance.
This experimental work has allowed the confirmation of the usefulness of the new method used in Chapter 5 for the derivation of rotor bar impedance for variable width rotor slots. It has also indicated that attention must be paid to detail if repeatable results are to be obtained for the no-load and locked rotor tests. The existence of variation of locked rotor impedance at low current was unsuspected by the author until experienced during the measurements reported here. The usefulness of PC-based measurement equipment has been demonstrated with the adoption of a recursive method for analysing the locked-rotor and synchronous-speed tests.

In Chapter 8, simulated starting performance using the motor parameters determined in this chapter is compared with that based on the parameters derived in Chapter 6.

7.8. Calibration Of Data Acquisition System

Calibration of the measuring system involved the capture and storage of known current and voltage waveforms using the same technique as outlined for the measurements on the motors. Currents were determined from the voltages measured across a standard shunt. {Cambridge Instruments, L344505, 0.05 Ohm}. For the 2.2 kW motor, each phase was supplied from a three-phase, variable transformer supply. For the 4 kW motor a single phase supply was used with all the channels carrying the same current. This was quicker and produced much the same results. Voltages were measured with a Hewlett Packard 3466A digital multimeter which gave a readout of four significant figures.

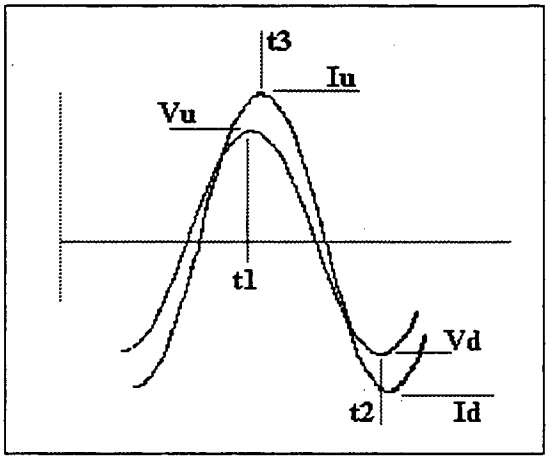

Figure 7.13 : Example of reading waveforms from the PC screen.

Using the STAT-30 package together with the PC30-D data acquisition card just over one cycle of each of the waveforms of voltage and current for the phase to be calibrated were sampled. The cursor was used to read off the values of the positive and negative peak voltages and currents from the screen as shown in Figure 7.13. Times t1, t2 and t3 were also read. These were entered into a second PC running the program CAL.PAS. The program requested the RMS values of current and voltage as read by the standard used for calibration and produced a record of the data as file CALR.DAT.

Red Phase voltage, cal 17/12/93 5 data points in this record.

Actual Voltage	PC File Output	Channel No.
37.99	0.458468988	1
68.38	0.821945903	1
78.21	0.939626047	1
117.25	1.402857056	1
186.50	2.213344203	1

Table 7.15 : Calibration data for the red phase, channel 1.

Table 7.15 shows a set of readings of actual voltage as measured by the Hewlett Packard voltmeter and the PC quantity output to a file. A least-squares routine was used to determine the relationship between the PC screen variable and the

measurement standard. The graphs of Figure 7.14. show an example of the measured test points and sets of interpolated points based on test data.

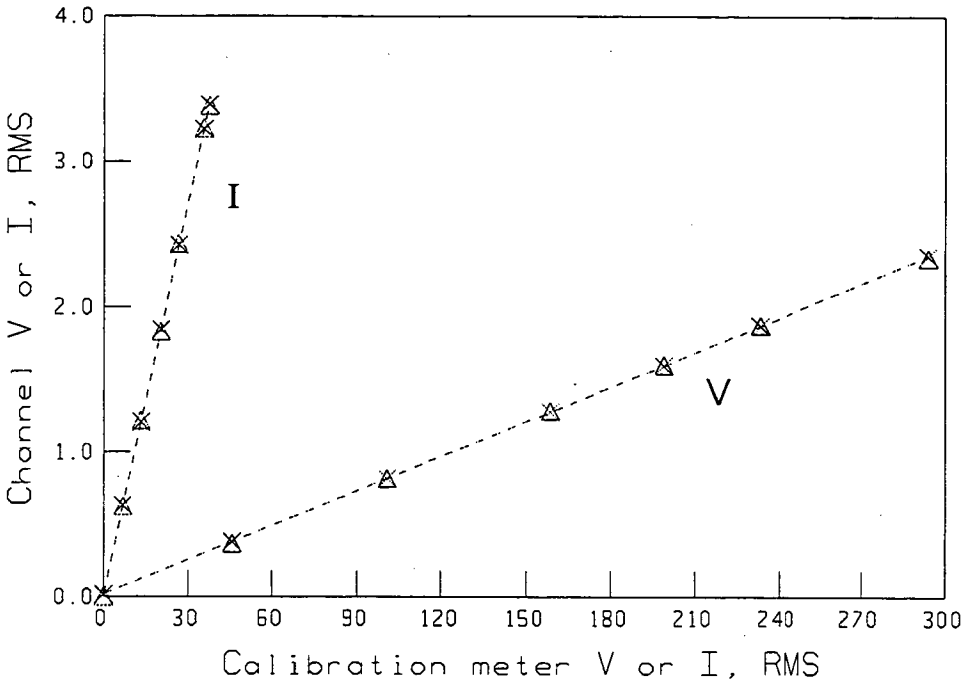

Figure 7.14 : Sample graph of calibration process

Table 7.16 shows the least squares straight line constants fitted to the data from all six channels. The speed channel was calibrated against a laboratory device which had been previously shown to be accurate by comparison with other standards, [Ho et al , 1994].

From Program CAL.PAS dated 17th Dec 1993

Channel	m	c	
vr_cal.DAT	0.01186	0.00690	0.99410
vy_cal.DAT	0.01175	0.00532	0.99598
vb_cal.DAT	0.01212	0.00218	0.99840
CR_cal.DAT	0.87187	-0.01791	1.00671
CY_cal.DAT	0.85035	0.00449	0.99819
CB_cal.DAT	0.83827	0.03005	0.98798

Table 7.16 : Calibration constants for all three phases and shaft speed

8. SIMULATION OF MOTOR PERFORMANCE

The main purpose of this chapter is to illustrate the experience gained in simulation work using the programs INSTART, IM_SIM.PAS and IM2.PAS. The first is a commercial program described in Chapter 3 whilst the other two were written by the author. This experience and discussions with practising consulting engineers, is the basis for the development of the algorithm described in Chapter 9. Several cases are discussed in this chapter with the identification of the circumstances in which various approximate models will probably be unreliable being left to Chapter 9 where guidelines are presented in the form of an expert system algorithm.

In Section 8.1, the motors used in the simulation work are introduced and all the data items are specified. Section 8.2 compares the results of three motor models :

- The complete differential equation model in terms of flux linkages with all transients included as described in Section 3.2; (Differential equation model, in the form of program IM_SIM.PAS).
- The alternative form of the DE model in terms of rotor quantities rather than flux linkages (produced by modifying the program IM_SIM.PAS).
- The double-cage equivalent circuit model which neglects transients, as in Section 2.4; (Circuit model in the form of program IM2.PAS).

Section 8.3 investigates the sensitivity of program output to variations in the detailed models used for :

- the torque/speed curve of the load
- the voltage drop at the terminals during starting
- the temperature of the windings
- leakage path saturation

This was done using the factorial method described in Chapter 3 with the four factors above plus the total load and motor inertia being varied at two levels to give 32, (2^5) treatments.

8.1. Some Problems Regarding Definition Of Data For The Motors Studied.

The nominal performance data for the motors studied in this Chapter, together with the circuit parameters derived using the INSPEC program, is given in Table 8.1.4 These motors are :

- The 8.2 MW motor from the paper by Rogers and Shirmohammadi (See also Section 6.1.4).
- A 660 kW Fume tower fan motor for which data was supplied by Comalco Aluminium, Bell Bay.
- The 500 hp (373 kW) motor from the INSPEC database. This was a slightly different version of the motor than the one used in Chapter 6.
- The 50 hp (37 kW) motor from the INSPEC database.
- The Siemens 4 kW motor with double-cage rotor used in Chapter 7 to verify the VWB method of establishing rotor reactance variation.
- The 2.2 kW single-cage rotor laboratory machine test with results as in Chapter 7.

The above motors are subsequently referred to by their ratings in kW.

In some cases, data items were unspecified or inconsistent with known motor performance. This section of the thesis is devoted to discussing some choices which were made in determining suitable data for some of the above motors. It is stressed

that the aim here was to obtain realistic values for unknown data items that were consistent with known performance rather than to determine precise actual values. This is all that is needed in order to make sensible judgements about the validity of the various methods studied.

8.1.1. The 8.2 MW Heat Pump Motor

The circuit parameters, some graphs of simulated and test performance are given in the paper by Rogers and Shirmohammadi (Figures 6 and 7 of their paper). Ideally, both the DE and DCC methods would have been compared with the test results. In practice, it was impossible to do this honestly since the paper did not give the value of several key data items :

- The value of initial saturation current, Isat is not quoted in the paper and cannot be derived from the reactance data with any accuracy (see Section 6.2),
- The impedance in the line between the motor terminal and an infinite-bus is unspecified,
- The inertia constant of the motor and load is unknown,
- The nature of the torque/speed curve for the load is unspecified.

The procedure adopted to compare the DE and circuit models was to use the test results to derive values for the unknown quantities based on matching the known performance with the DE simulation. These values were then used as input data to the circuit model. The results of the circuit model were then compared with the test/DE results.

During the test a severe voltage depression to about 5 kV was experienced which was sustained for the whole run-up period. The initial starting current was approximately 5 kA. These values were noticed to be very close to the values quoted in the paper for the reduced voltage locked rotor test; ie 0.758 pu voltage and 6.03 pu current. Ignoring the resistive parts and using equation (3.3.1) the impedance between the motor terminals and a hypothetical infinite bus could be inferred to be approximately 0.04 pu with a motor impedance of 0.126 pu (See Figure 8.1.1).

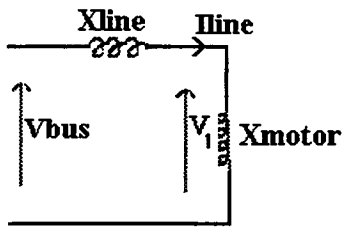

Figure 8.1.1 : Approximation of starting condition

An approximate value for Isat could be derived from the separate saturable and unsaturable components. As mentioned in Section 6.1.4, this is associated with a large uncertainty due to possible rounding errors in the quoted data. The value of Isat and Xline were adjusted iteratively until the correct starting current and voltage drop were achieved simultaneously.

The inertia constant of the motor was not given. A value of 0.5 s was used initially but this gave a much faster run-up than the test results. Then it was noticed that a value of

3.5 s was mentioned in the support documentation for the INSPEC/INSTART program package for an 11000 hp motor with similar (but not identical) circuit parameter values. Using this value the run-up time was closer to the test results but depended somewhat on the nature of the load curve.

Two clues were available to help in modelling the load : Firstly, load torque is given in the INSPEC/INSTART documents as a polynominal function of pu motor speed, N as equation (8.1) and secondly, the final motor load is close to 1 pu. The problem remained of determining values for the constants; kt_1 , kt_2 and kt_3 .

$$T_{load} = T_{base}\left[kt_1 + kt_2(1-N)^{kt4} + kt_3N^2\right] \qquad (8.1)$$

By taking kt4=1 and fitting reasonable values to the three other constants, such that the initial load was not too excessive and the final load was close to 1 pu, a run-up time close to the test results was obtained. Variation of the estimates for the load constants is discussed in Section 8.2.

8.1.2. The 660 kW Fume tower Fan Motor

In addition to the performance data given in Table 8.1.4, a locked rotor test point at a reduced voltage was also given which enabled modelling of leakage path saturation using the describing function method as in Section 5.1. The interesting feature of this motor was the availability of fan load/torque curves at different operating conditions and some starting data recorded by the protection equipment. The fan manufacturer's load data curves were fitted with a function of the form
$T_{load} = T_{base}\left[kt_2(1-N)^{12} + kt_3N^2\right]$ with parameter values as follows :

Condition	kt2	kt3
20 °C, (damper closed)	0.0943	0.185
90 °C, (damper open)	0.0943	0.943

Table 8.1.1 : Fan load curves for 660 kW fume tower motor

A double-cage motor model was fitted to the performance data using the INSPEC program. The fan inertia was unknown but an estimate of its value was made from the external dimensions of the duct work. This was used together with the known starting voltage, current and run-up time to establish a realistic set of data for the motor.

8.1.3. The 373 kW (500 hp) INSPEC Motor

This motor had quoted starting torque of 0.55 pu which seemed too small. The quoted torque was compared with the minimum of 0.8 pu allowed by Table 41.3 of AS 1359.41. However, if the motor is of Design E type, then the starting torque would be permitted to be as low as 0.75 times this or 0.60 pu and a further tolerance of -0.15 pu is allowed by AS1359 Part 69. This means that the quoted figure of 0.55 pu is within the range of possibility; (the minimum actual allowed starting torque for a motor of this rating being 0.45 pu). It was recognised that under certain load conditions this low starting torque could lead to failure to run up to steady-state speed; eg if the supply voltage was low and the load torque particularly high or if the design ratio of the double cage rotor was such that the minimum torque during run-up was less than the starting torque.

In designing the range of factors to be applied in the systematic study described in Section 8.3, care was taken to avoid simulations which required simultaneous variation of tolerances on line reactance, saturation and load curve which would lead to unduly long starting times with this motor due to reduced net accelerating torque.

8.1.4. The 4 kW Siemens Double-Cage Motor

The double-cage circuit parameters derived from test results for this motor are shown in Table 8.1.2 as well as the INSPEC parameters used in Section 8.3 and a set derived using the program PARAM.PAS produced by the author. One of the larger differences is in the value of the stator resistance, R1. As described in Chapter 2, this arises from the different treatments of core loss. What is really significant is the predicted performance using the three models. This is shown in Figure 8.1.2 for the three cases. With the exception of the region of fast electrical transients, the predicted performance is much the same for all three methods. The error in the early transient behaviour caused by using the INSPEC method is due to the approximation used for the separation of saturable and unsaturable parts of leakage reactance. As described in Chapter 6, this leads to modifications of the double cage parameters and the selection of a lower value of Isat, in order to fit the quoted steady-state performance.

	Test Results	Section 8.2 INSPEC	PARAM.PAS
X1	2.19	2.92	1.57
R1	1.4	0.35	2.34
Xm	78.3	43.9	72.9
Ra	2.21	5.43	2.10
Xab	4.04	1.50	3.49
Rb	6.39	2.35	7.27
Xb	19.03	7.48	20.83
Rdc	1.64	1.64	1.63
Xdc	5.29	5.14	4.54
Rst	2.11	3.46	2.02
Xst	4.25	3.39	3.67
m	0.45	1.04	0.45

Table 8.1.2 : Comparison of derived double-cage circuit parameters in Ohm for 4 kW motor : Test results, INSPEC and PARAM.PAS

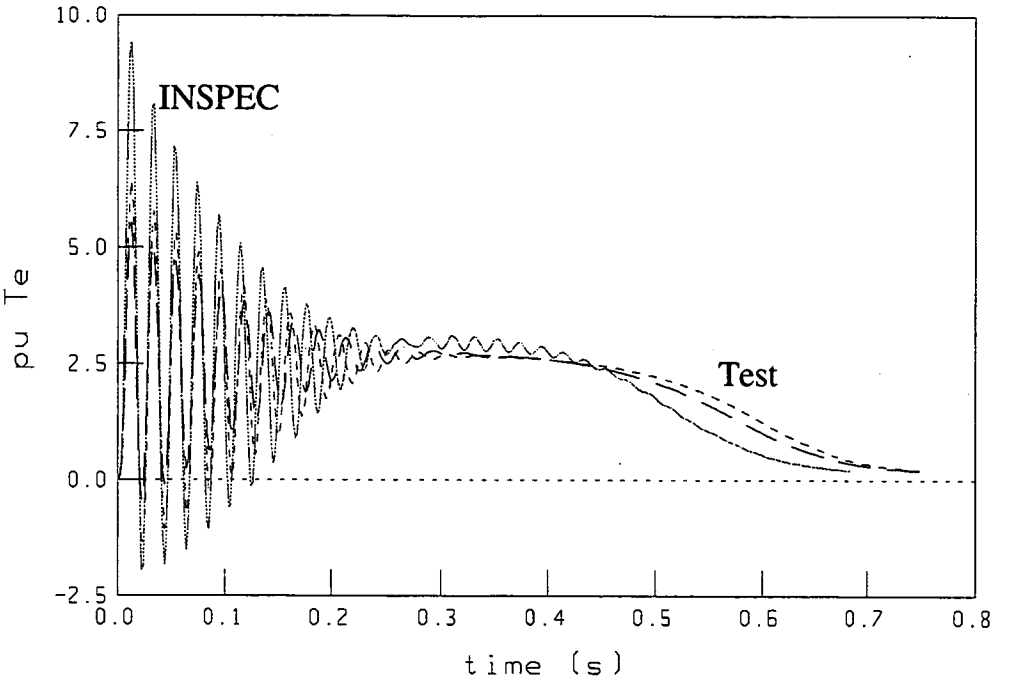

Figure 8.1.2 : Simulated performance of the 4 kW motor with the double-cage circuit parameters from Table 8.1.2

INSPEC = solid PARAM.PAS = — — — Test = - - -

8.1.5. The 2.2 kW Simpson Pope Single-Cage Motor

The circuit parameters derived from test results for this motor are shown in Table 8.1.3 as well as the INSPEC parameters used in Section 8.3. Figures 8.1.3 and 8.1.4 show the simulated performance of the 2.2 kW motor with the three sets of circuit parameters. Although there is little to choose between the models the PARAM.PAS program produced a model which fitted the run-up time more closely. This is not considered a truly significant result because the variation in manufacturer's quoted performance parameters from the actual steady-state performance would lead to a greater derived difference in model predictions.

	Test Results	Section 8.2 INSPEC	PARAM.PAS
X1	5.73	6.87	3.76
R1	3.41	3.39	3.30
Xm	124	128	135
Ra	2.74	5.64	2.85
Xab	5.39	4.30	5.54
Rb	8.13	4.22	32.58
Xb	12.0	4.93	54.50
Rdc	2.05	2.41	2.62
Xdc	6.15	5.91	5.89
Rst	2.43	3.06	2.78
Xst	5.73	5.59	5.64
m	0.90	2.00	0.65

Table 8.1.3 : Comparison of Test, INSPEC and PARAM.PAS parameters for 2.2 kW motor

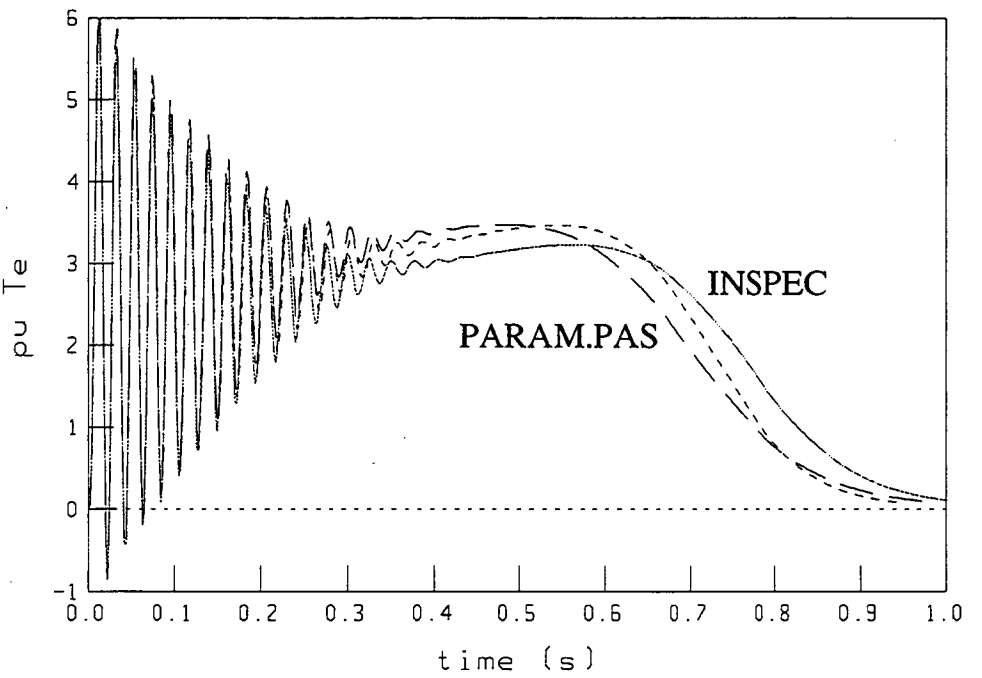

Figure 8.1.3 : Simulated performance of 2.2 kW motor with the double-cage circuit parameters from Table 8.1.3

INSPEC = solid PARAM.PAS = — — — Test = - - -

This page shows a comparison of simulated performance based on parameters determined from test results, INSPEC and PARAM.PAS for the 2.2 kW motor.

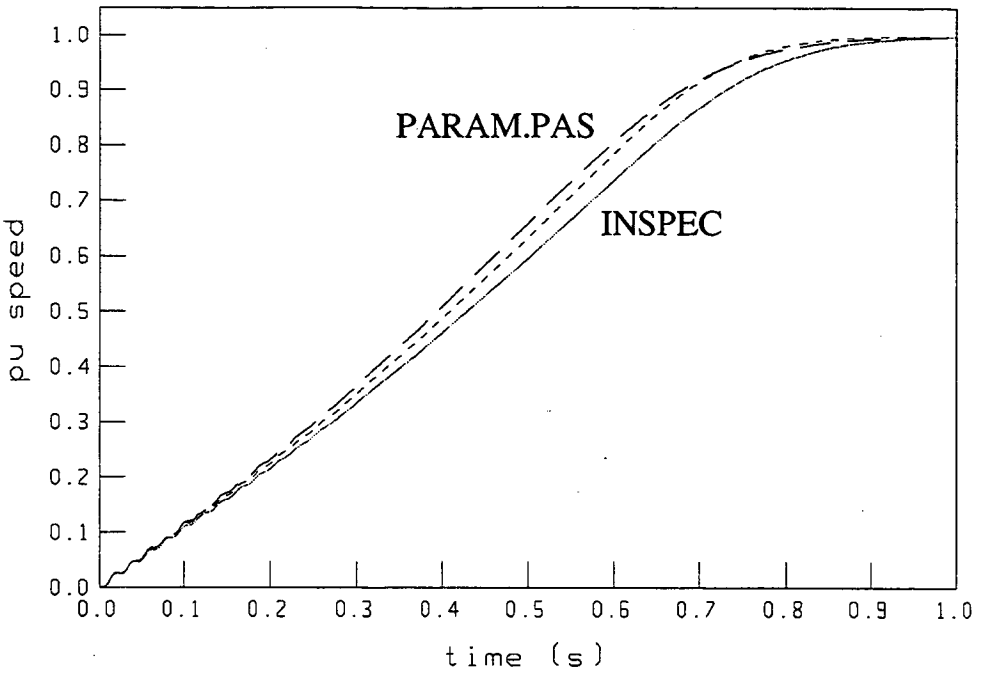

Figure 8.1.4 : Simulated run-up time with the parameters from Table 8.1.3
INSPEC = solid PARAM.PAS = — — — Test = - - -

8.1.6. Data For All The Motors Studied In Chapter 8

data item		Motor rating as identifier					
		8.2 MW	660 kW	373 kW	37 kW	4 kW	2.2 kW
P1	kW	8210	660	373	37.3	4.0	2.2
Vll	V	6600	3300	575	575	415	415
Il	A	804.4	141	440.0	48.0	7.8	4.6
f	Hz	60.0	50.0	60.0	60.0	50.0	50.0
Poles		4	6	4	2	4	4
slip	pu	0.00622	0.009	0.0097	0.0138	0.040	.04666
speed	rev/min	1789	991	1782.5	2958.6	1440	1430
efficiency, pu		0.985	0.958	0.947	0.868	0.84	0.82
pf		0.906	0.850	0.900	0.90	0.850	0.860
Ist	A	6432	839	2583	293	42	22
Ist	pu	8.0	5.95	5.87	6.1	5.38	5.16
Tst	pu	1.47	0.995	0.55	1.20	2.0	1.52
Tmax		3.5	2.6	2.7	2.4	2.4	2.7
Wfw	kW	31.1	8.617	5.23	1.42	0.176	0.174
Isat	A	3497.4	282	1056	144	9.36	0.005
Isat	pu	4.35	2.0	2.4	3.0	1.2	0.001
m		0.55	2.0	5.0	0.25	1.04	2.0
X1	Ω	0.3071	1.5715	0.0766	0.5366	2.92	6.87
R1	Ω	0.02188	0.2378	0.0205	0.5466	0.35	3.39
Xm	Ω	14.841	36.34	2.607	18.59	43.9	128
Ra	Ω	0.1180	1.181	0.1066	1.766	5.43	5.64
Xab	Ω	0.2701	0.9675	0.0500	0.0525	1.50	4.30
Rb	Ω	0.0414	0.1392	0.00785	0.0981	2.35	4.22
Xb	Ω	0.2896	0.6608	0.0229	0.4664	7.48	4.93
Zbase	Ω	4.73	13.51	0.754	6.91	30.7	52.1
Xline	pu	0.055	0.026	0.045	0.045	0.01	0.00
H	s	3.50	4.35	0.50	0.50	0.50	0.80
J	kgm^2	1834	656	12.58	0.498	0.247	0.22
kt1		0.1	0.0	0.1	0.1	0.1	0.01
kt2		0.10	0.0943	0.25	0.25	0.05	0.1
kt3		0.85	0.185	0.8	0.8	0.05	0.01
kt4		1.0	12	1.0	1.0	1.0	1.0

Table 8.1.4 : Performance, circuit and system data for simulated motors

8.2. Comparison With Some Other Models

This section compares the results of simulations based on the numerical solution of the system differential equations with simpler models. The use of space phasors is discussed briefly with examples.

8.2.1. The Quasi-Steady-State (Equivalent Circuit) Model

The equivalent circuit model with allowance for double cage effects in the rotor and leakage path saturation was compared with the differential equation model based on equations in terms of flux linkages. Data for six motors was read from the same data file, A1.DAT and programs IM2.PAS, (Circuit) and IM_SIM.PAS, (DE) were used to implement the models. Data for the machines was as shown in Table 8.1.2.

The simulation yields, as defined in Chapter 6, which were related to the steady-state performance were compared. These yields were :

TST,	starting torque
TPS,	peak torque after decay of electrical transients
SP3,	speed at which TPS occurs
CP2,	current when speed is 0.5 pu
t9,	time at which speed reaches 0.5 pu
t5,	time for speed to settle between 0.95 and 1.05 pu
t3,	time to reach SP3 (TPS)
t6	time for the current to fall below 1.0 pu

Other yields, which related to the transient performance could not be predicted by the circuit model. These were : TPM, t1, TPN, t2, CP1, IT1 and t7.

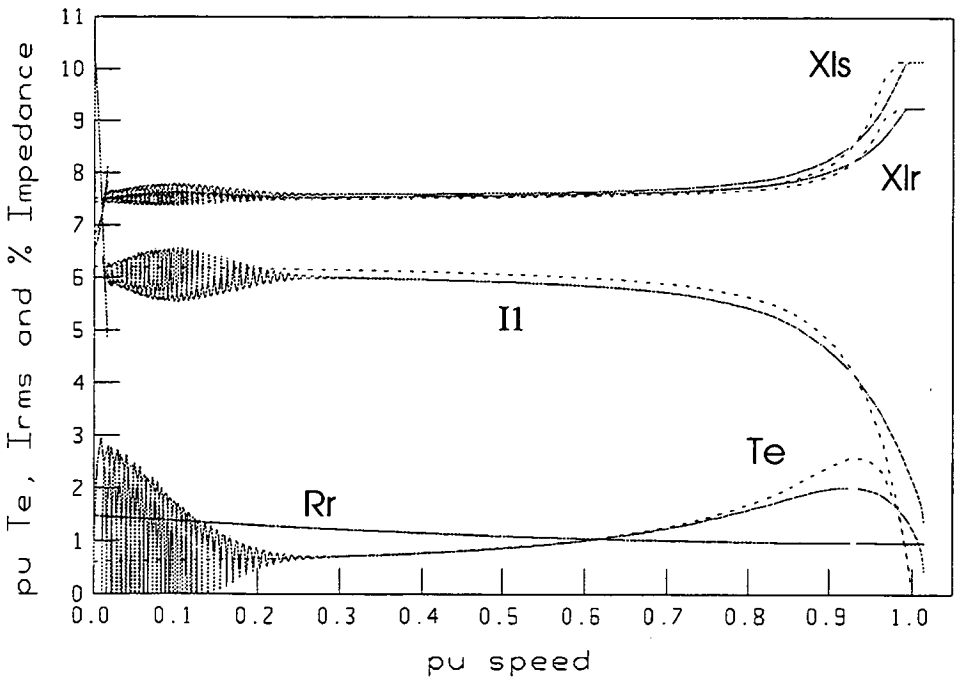

Figure 8.2.1 : Equivalent circuit and DE models compared, 373 kW motor
Circuit = ---- DE= solid

8.2.1.1. Results of the comparison

Figure 8.2.1 shows the variation with motor speed of per-unit torque, stator current and impedances referred to the stator for the 373 kW motor. The leakage reactance dependence on current is shown with the rapid increase at high speed when the current drops. There is some transient overspeeding with this motor, ie the speed increases above synchronous and the current and torque are quite high as the motor goes through synchronous speed. This was noted long ago by Ager, [1941]. This discrepancy between the steady-state and transient torque/speed curves is worst for the 373 kW motor probably due to the fact that it had a long rotor time constant, [Krause, 1987]. A long time-constant is consistent with this motor's very low starting torque which implies low rotor resistance. This leads to persistance of the rotor transients. For the other motors the difference between the torque values was less pronounced than with the 373 kW motor.

For each yield the % error, ε was calculated as, :

$$\varepsilon = 100(\text{YIELD}_{DE} - \text{YIELD}_{Circuit}) / \text{YIELD}_{DE} \qquad 8.2.1$$

motor	model	TST	TPS	SP3	CP2
8200 kW	DE	1.04	2.22	0.96	5.77
	Circuit	0.89	2.47	0.96	5.88
	% Error	**-14.8**	**11.2**	0.1	1.8
660 kW	DE	0.84	2.15	0.94	5.03
	Circuit	0.80	2.36	0.95	5.21
	% Error	-4.5	**9.6**	0.4	3.5
373 kW	DE	0.59	2.02	0.92	5.93
	Circuit	0.61	2.60	0.93	6.08
	% Error	4.4	**28.6**	1.4	2.6
37 kW	DE	1.24	2.23	0.90	5.47
	Circuit	1.14	2.45	0.92	5.45
	% Error	**-7.7**	**9.7**	1.2	-0.3
4 kW	DE	2.11	2.43	0.733	4.35
	Circuit	1.94	2.49	0.743	4.48
	% Error	**-8.2**	2.47	1.36	2.99
2.2 kW	DE	2.66	3.22	0.68	4.96
	Circuit	2.51	3.25	0.68	5.11
	% Error	**-5.4**	1.0	0.5	2.9

Table 8.2.1 : Comparison of simulation yields, DE & circuit

8.2.1.2. Comments on the accuracy of the circuit model

Tables 8.2.1 and 8.2.2 show that the error in most of the comparable yields is less than 5% in most cases. The principal exception to this is in the maximum torque, TPS which is over-estimated by the circuit model when it is used to model dynamic run-up. The discrepancy disappears if the DE model is allowed to reach its final steady state when the transient flux linkages have decayed.

The yield TST was calculated as the mean of the positive and negative torque peaks and as such is not a true representation of the mean starting torque. This is the main reason for the large computed errors in that yield. The graphs of Figure 8.2.2 show that the starting torques are predicted accurately by the circuit model when allowance is made for skin effect and leakage path saturation.

motor	model	t9	t5	t3	t6
8200 kW	DE	5.67	10.99	11.07	11.37
	Circuit	5.33	10.62	10.69	11.13
	% Error	**-6.0**	-3.4	-3.4	-2.1
660 kW	DE	7.23	11.89	11.86	12.22
	Circuit	7.08	11.66	11.65	11.92
	% Error	-2.1	-1.9	-1.7	-2.5
373 kW	DE	1.15	1.62	1.60	1.69
	Circuit	1.07	1.52	1.51	1.54
	% Error	**-6.6**	**-6.1**	**-5.7**	**-8.9**
37 kW	DE	0.81	1.33	1.28	1.40
	Circuit	0.78	1.27	1.25	1.33
	% Error	-3.8	-4.3	-2.7	**-5.0**
4 kW	DE	0.372	0.656	0.520	0.703
	Circuit	0.365	0.665	0.515	0.680
	% Error	-1.88	-1.60	-0.92	-3.24
2.2 kW	DE	0.43	0.80	0.56	0.82
	Circuit	0.43	0.79	0.55	0.80
	% Error	-0.3	-0.6	-2.1	-2.2

Table 8.2.2 : Comparison of simulation yields, DE & circuit run-up times

The above differences in run-up time will be seen to be small in comparison with the differences which might arise due to small permitted changes in supply voltage or to uncertainties in the load torque model or to the operating temperature of the motor. These factors are discussed in Section 8.3

Figure 8.2.2 shows current and torque curves against speed and time during the simulated direct-on-line starting of the five motors used for comparison purposes. These graphs were reproduced in the small size so that they would all fit on the same page to allow easy comparison between the different motors. The upper graph is the pu RMS current and the lower one the pu electrical torque.

For many applications, eg for commissioning protection circuits, the small differences in run-up time and current are unimportant. It is stressed that these results were obtained with a system model which included the voltage dip in the finite bus supply and the effects of motor parameter variation due to skin effect and leakage path saturation. What strikes the reader most clearly is that the differences between the circuit model and the DE model are slight.

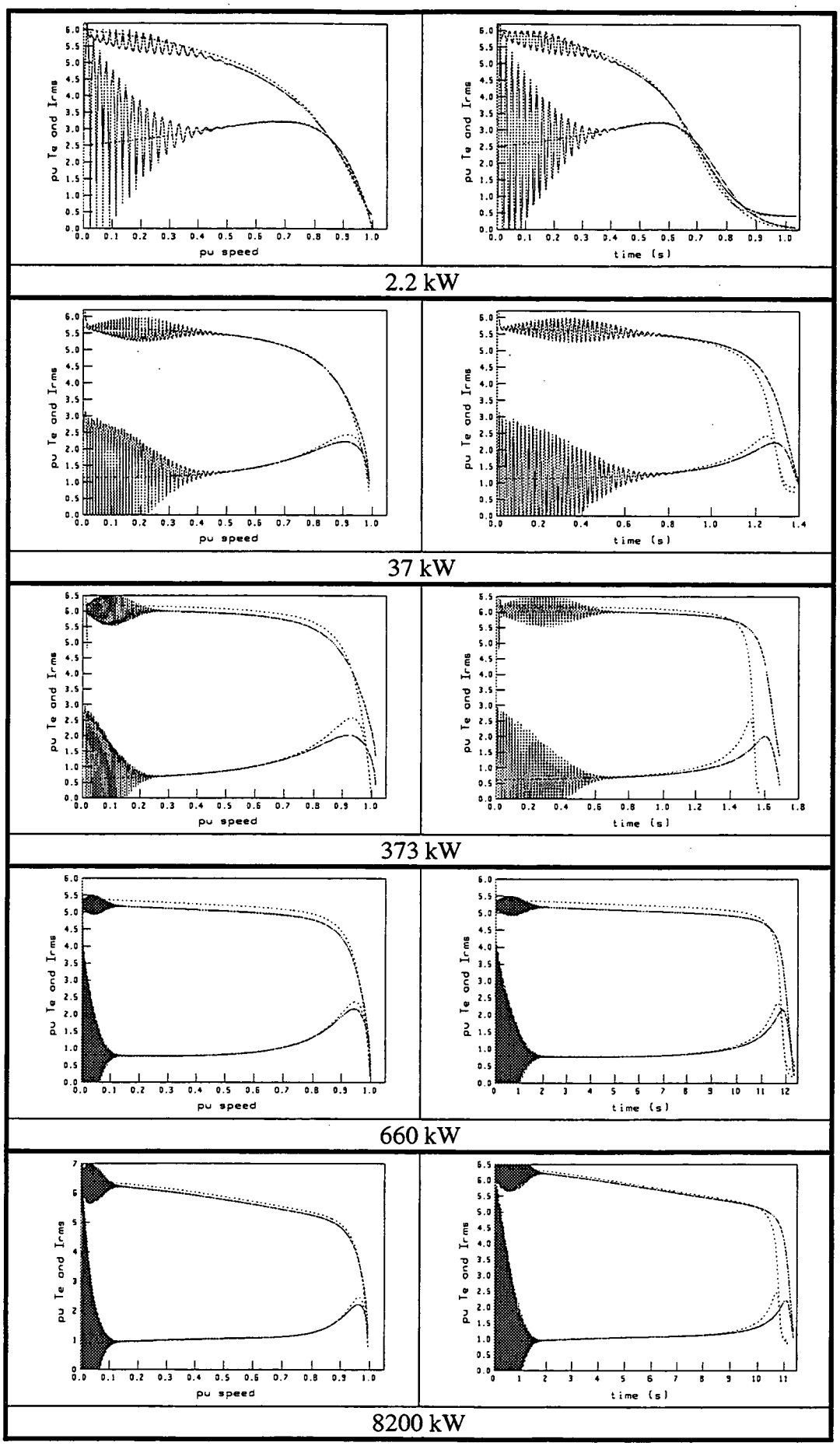

Figure 8.2.2 : DE and Circuit models compared; Circuit is dotted

Figure 8.2.3 shows test data for a direct-on-line start at rated voltage for the 4 kW motor. The simulation was performed assuming sufficient reactance between the motor terminals and the infinite bus to cause a voltage drop of 3% and with the machine parameters at their nominal values as Table 8.1.2. In practice, uncertainties in the supply transformer transient reactance, the load curve and the actual motor temperature would be sufficient to delay starting by about 0.1s or 12%. This inaccuracy would almost never be of any significance. The apparent error in predicted run-up time of 0.1s incurred by using the circuit model is swamped by uncertainties in motor, load or system data.

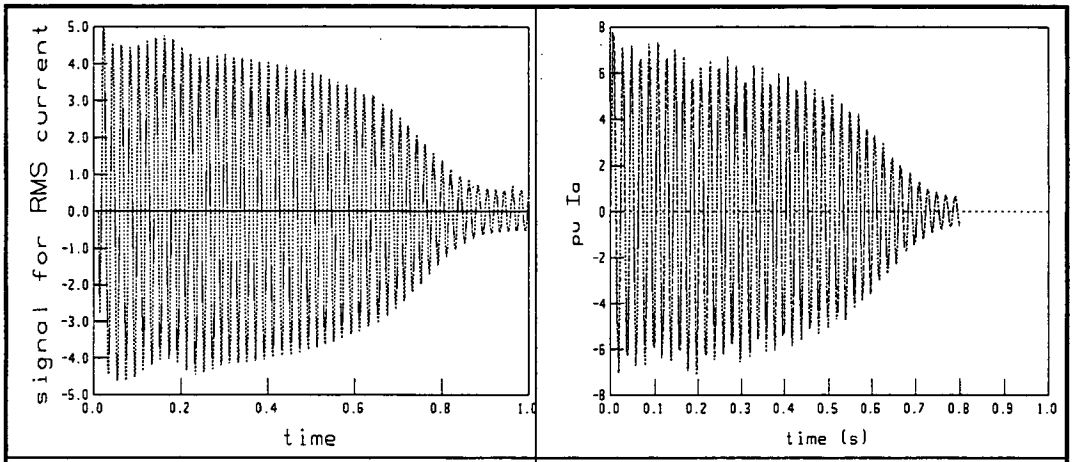

Figure 8.2.3 : Test and simulation results for 4 kW motor.

The main situations in which the differential equation model would appear to be preferred are where there is a need to accurately predict

- the maximum (pull-out) torque
- transient torques or currents.

A study by [Holley et al, 1990] has shown that the use of differential equation models is recommended for bus switching studies with low inertia loads. This type of model would also be needed for studies of torsional oscillation of long shaft systems or the consideration of dc transient offsets in the starting current.

8.2.2. Use Of Analytical Solutions For Transient Torque And Current

The prediction of the transient torque and current by analytical methods was discussed in Chapter 2. These (Laplace transform based) methods can be used to determine the transient dc offset which arises due to delay in switching after the voltage zero. These effects can be seen in Figure 8.2.3 where the test results were taken at a random switching angle whereas the simulation assumes that the motor is switched onto the bus when the voltage in the plotted phase is at a positive-going zero-crossing. This is shown more clearly in the two simulations of Figure 8.2.4 which were based on the 8200 kW motor.

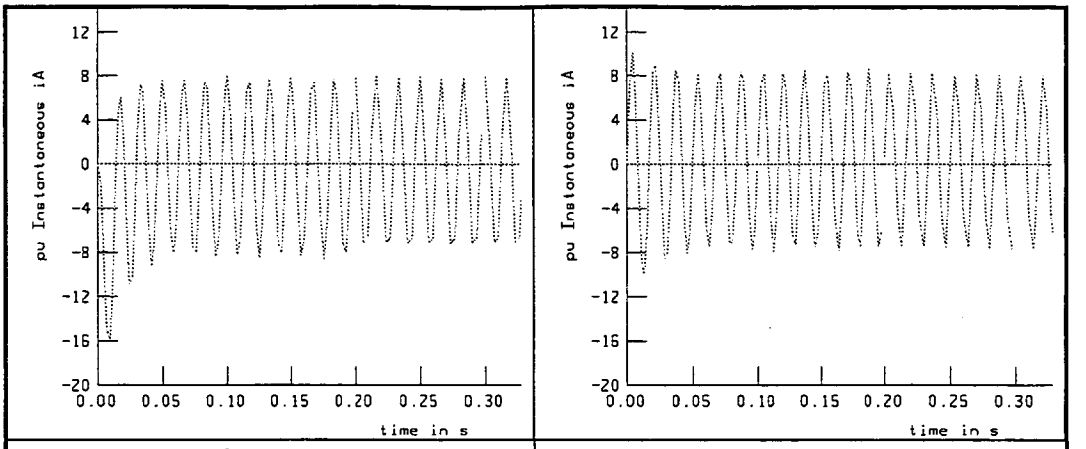

Switching after the voltage zero | Switching at a voltage zero

Figure 8.2.4 : Transient dc offset caused by switching angle delay

In Table 8.2.3, the results of the constant-speed methods of Slater and Wood, [1967] and Smith and Sriharan, [1966] are presented and may be compared with those for the differential equation model for all six motors. Some graphical results are given in Figure 8.2.5 below for the 8200 kW, 660 kW and 37 kW motors. In all these cases, the simulation began as the voltage applied to the phase shown was at a positive-going zero crossing, (zero angle of delay).

motor kW	Peak Torque, pu			Peak Current, pu	
	DE	S&W	S&S	DE	S&S
8200	3.5	5.1	4.9	10.2	8.9
660	3.4	4.1	3.8	8.2	7.3
373	2.6	2.9	2.7	9.4	8.5
37	3.0	2.9	1.5	6.4	6.8
4	5.0	4.7	0.6	5.9	5.3
2.2	6.2	6.2	1.1	6.5	6.2

Table 8.2.3 : Comparison of methods of Slater & Wood (S&W) and Smith & Sriharan (S&S) for prediction of peak torque and current with the numerical (DE) model.

For the larger motors the method of Smith & Sriharan gave good results for torque as shown in Figure 8.2.5. The waveforms for the currents were of similar magnitude for all the motors in the first few cycles after switching on.

For the 8200 kW motor, the modelling of leakage path saturation resulted in a significant under-prediction of the initial current transient and this was reflected in the torque curve. The difference between the current values were due to the way in which the simulations treated the function used for including leakage path saturation. In the case of this machine, the magnetic leakage flux paths are only slightly saturated but a slight increase in current leads to a reduction in reactance and further current decrease by positive feedback. This emphasises any small differences in predicted currents. Even for this case, however, the error is small. For the other motors, the saturation state is away from the knee of the curve and the response is less sensitive.
For the other two large machines the torque curves were identical as shown for the 660 kW motor.

The most serious discrepancies occurred in the torque simulation for the small motors (37 kW and less) where the method failed completely as shown in Figure 8.2.6. This

was at first thought to be due to the rapid speed change with these motors. The inertia was increased in the simulations so that the speed changed little in the period of interest but the result was not different. This implied that the error arises from other factors. The relative values of the motor parameters are the likely source, perhaps the motor time constants affect the issue. This was not pursued because the analytical methods were not considered of great importance due to the likelihood of errors arising in the programming of the equations compared with the relative ease of programming the standard differential equations or using a commercial motor starting simulation package.

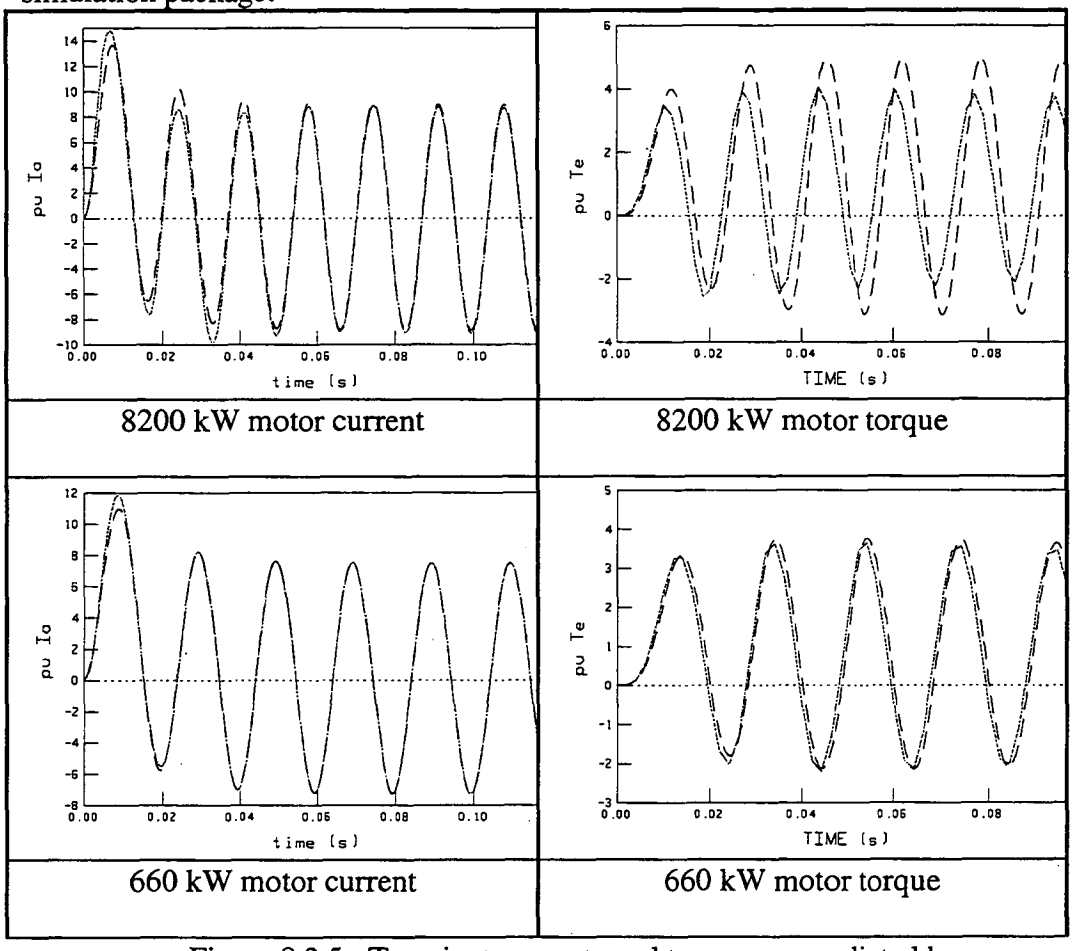

Figure 8.2.5 : Transient currents and torques as predicted by analytical (S&S) shown (---) and numerical shown (solid line) methods.

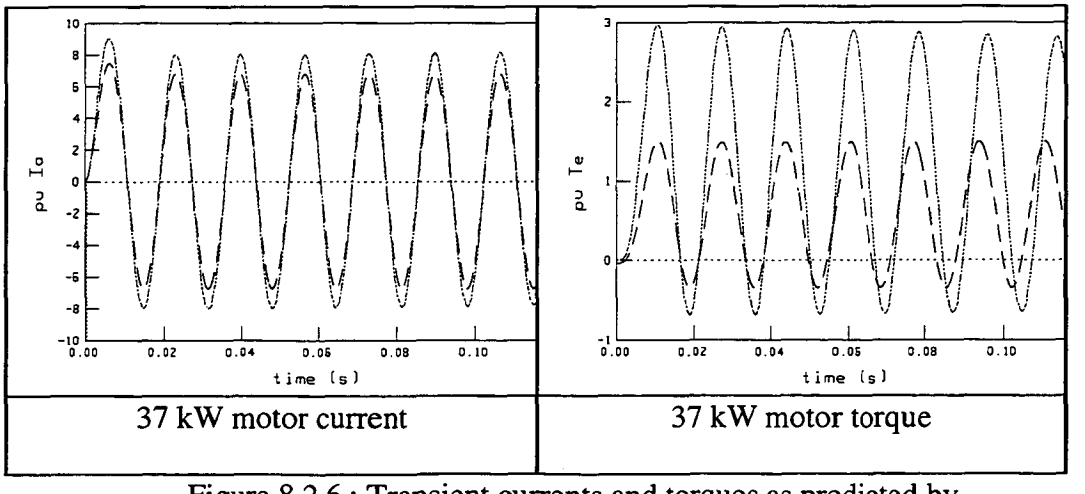

Figure 8.2.6 : Transient currents and torques as predicted by analytical (S&S) shown (---) and numerical shown (solid line) methods.

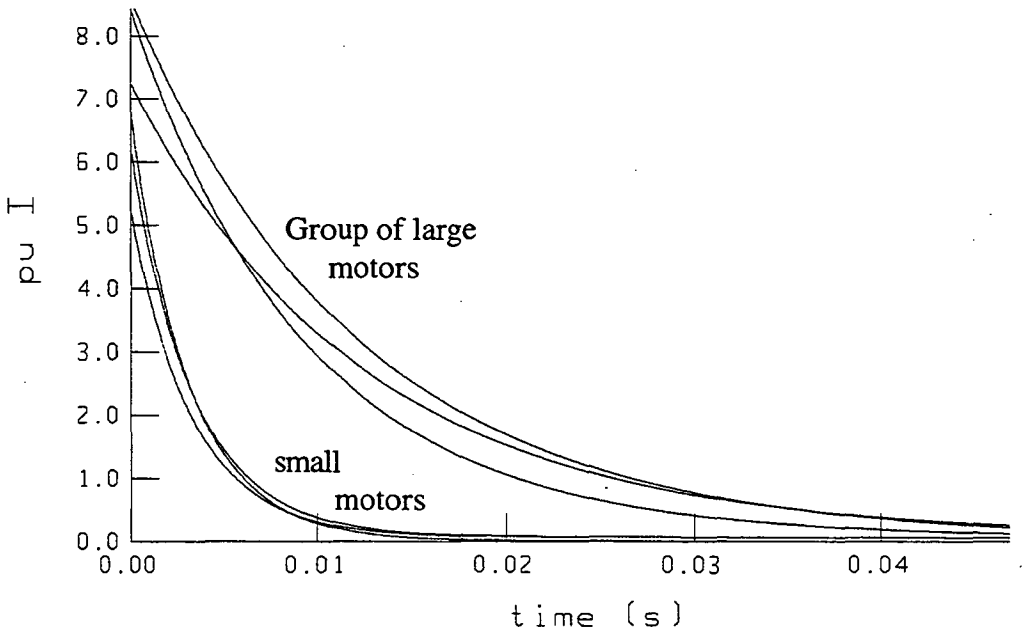

Figure 8.2.7 : Transient component of starting current for motors of Table 8.1.4 (switching delay of 60 degrees)

The analytical method of Smith and Sriharan was used to isolate the transient components of the starting current in phase 'a' of the motors of Table 8.1.4 with the switch on of the supply voltage delayed by an angle between zero and 90 degrees from the positive-going zero crossing of the voltage in the 'a' phase. The general equation for the starting current was of the form :

$$i_{st} = Q_0\left[Q_4\left(\sin Q_1 - Q_2 e^{-t/T_2} - \sin Q_3 e^{-t/T_3}\right)\right] \qquad 8.2.2$$

Where Q_0, Q_1, Q_2, Q_3, and Q_4, are functions of the switching delay, the supply frequency and the motor parameters; (See Smith and Sriharan, [1966]). The appropriate effective values of the motor's self and mutual inductances and resistances at slip=1 and saturated leakage path conditions conditions must be used. Equation 8.2.2 shows that the magnitudes of the initial dc offset due to switching delay will be of the same order as the ac component if $Q_1 \cong Q_3$. Figure 8.2.7 shows that the time constants of the decay varied considerably with motor size, which was expected.

It is recommended that equation 8.2.2 be used to give an estimate of the decay time of the transient offset so that the protection settings may be adjusted appropriately. Failure to do this may lead to failure to start the motor due to premature tripping of overcurrent protection. Many programs for the simulation of starting current ignore the effect of switching at points other than a zero crossing, prsumably because the net effect on run-up times is negligible. Program IM4.PAS incorporates the expanded form of equation 8.2.2 together with the full starting simulation based on a quasi-steady state equivalent circuit model.

8.2.3. Space-Phasor Plots As An Extension Of The Program IM-SIM.PAS

Space phasors have been used to describe motor behaviour because they provide a physical interpretation of the machine's behaviour, [Naunin, 1979] and [Diana and Harley, 1987]. This is useful mainly as a guide to understanding the machine dynamics in particular reference frames. For example, Naunin uses them effectively to

demonstrate that the slipping (encirclement of the origin) of the rotor flux vector in the synchronous reference frame causes the cross product of stator and rotor flux vectors to become negative at times hence producing negative torque.

The space phasor plots are not usually used in commercial motor simulation studies but are included here partly because I found them aesthetically appealing and also because they demonstrate the capability of the simulation program developed by the author to extract and make available to other program packages any of the program variables.

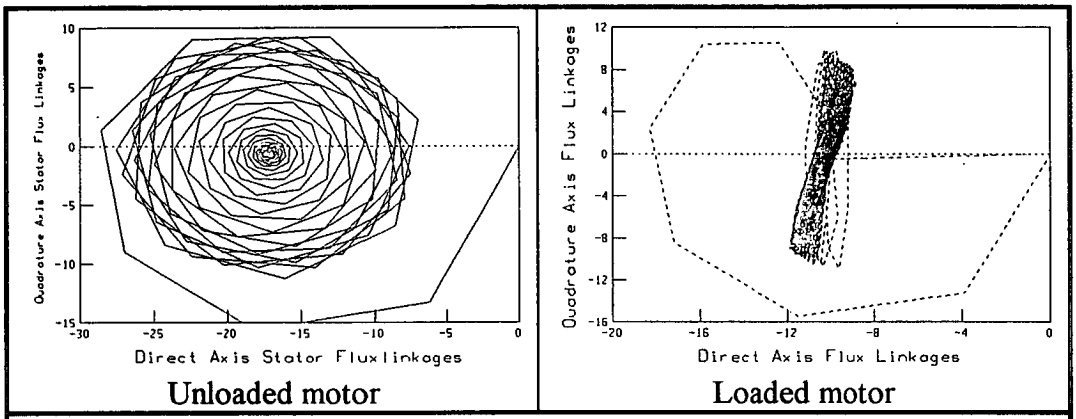

Unloaded motor | Loaded motor

Figure 8.2.7 : Stator flux space phasor for loaded and unloaded 8200 kW motor

The effect of loading the motor is essentially to provide damping so that the phasor settles quickly close to its final position. This position can be seen to be slightly different due to the increase in load and also fixed in space in the synchronous reference frame chosen.

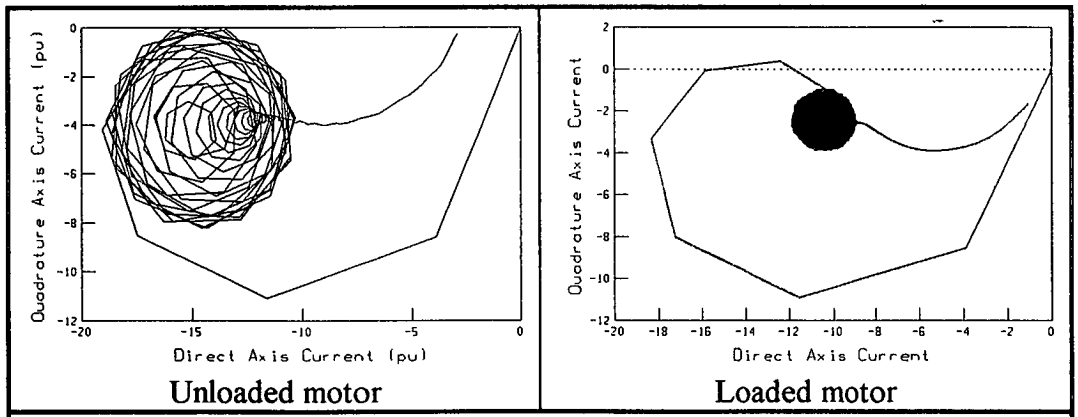

Unloaded motor | Loaded motor

Figure 8.2.8 : Stator current space phasor for loaded and unloaded 8200 kW motor

8.2.4. Errors Introduced By Ignoring Changing Inductances

In Chapter 3 the neglecting of the changes in inductance with time in equation (3.2.1) was discussed. It was decided to investigate the magnitude of the error caused by this assumption by evaluating the size of the missing voltage terms.

If the inductances are assumed variable so that there are voltages induced in the windings due to parametric variation then the terms in pL should be considered. These terms are eliminated (but included in the analysis) by expressing the equations in terms of stator and rotor flux linkages. If they are simply neglected then the error terms are :

$i_{ds}\ pL_s$ $i_{dr}\ pL_r$ $i_{qs}\ pL_s$ $i_{dr}\ pL_r$ $i_{ds}\ pL_m$ $i_{qs}\ pL_m$

The differentials of the inductances were computed within the RK4 procedure as the change in inductance since the previous integration step divided by the step length.

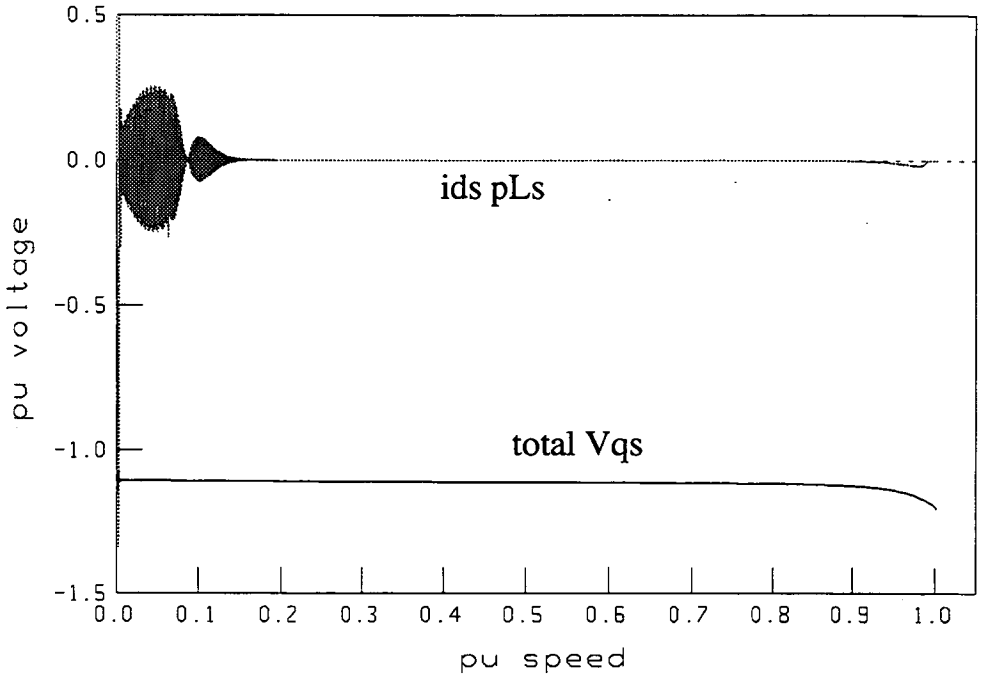

Figure 8.2.9 : $i_{ds}\ pL_s$ and V_{qs} against speed for the 660 kW motor

Of the above terms, the first two were found to be most significant and the last two were zero (due to the assumption of constant magnetising inductance). Figures 8.2.9 and 8.2.10, which are for the two motors in the data file with the largest error terms, show that these terms are small and of consequence only during the fast electrical transient period. There is a certain amount of aliasing in Figure 8.2.6 which arises from the fact that the array size in Turbo Pascal did not allow the full run-up period to be covered with the very small step size used. This meant that the interval between saved points was greater than the step length. The essential conclusions are unaffected.

The negative value of the V_{qs} variable arises from transformation chosen which yields $v_{qs} = -\sqrt{\frac{3}{2}}V\sin(\omega t - \theta_e)$ as given in Section 3.2. ($V_{qr} = 0$, cage rotor)

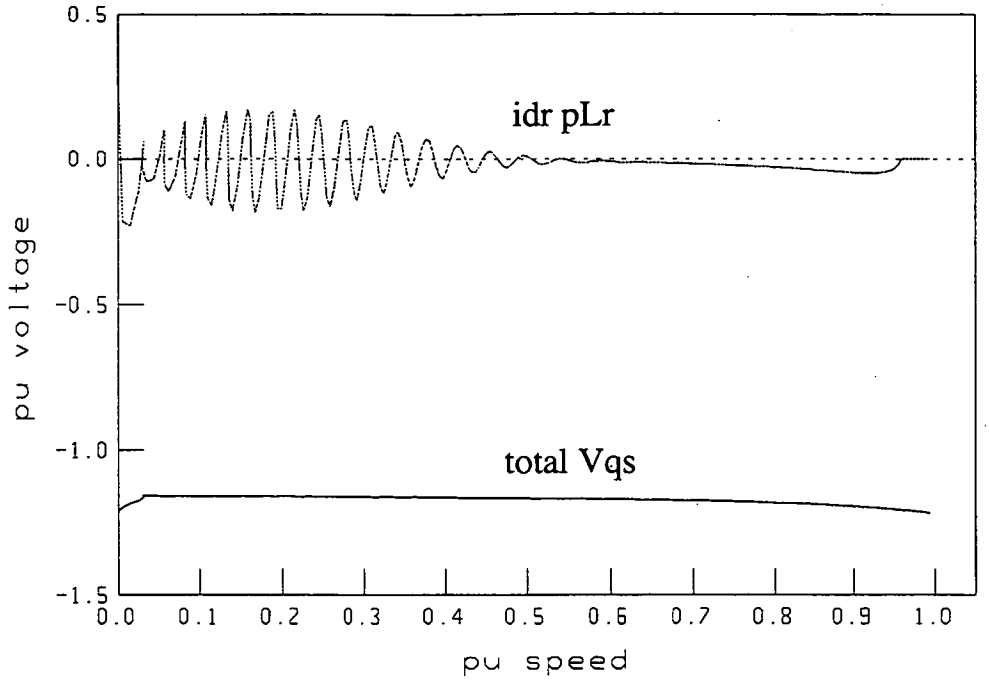

Figure 8.2.10 : i_{dr} pL_r and V_{qs} against speed for the 4 kW motor

8.3. The Effect Of Some Variations On Simulated Performance

This section gives a brief discussion on the effects of small variations in the detailed models used for :

- the torque/speed curve of the load
- the voltage drop at the terminals during starting
- leakage path saturation
- the temperature of the windings.

These results are typical of many such results obtained using both the differential equation and circuit models with data for the six motors from the file A1.DAT.

The results of a formal study of the relative effects of these variations are then presented in the form of calculated Coefficients of Performance which relate the outcomes of the simulation (the yields) to the variations in the above factors as explained in Chapter 4. The load inertia was included as an additional factor making five in all with 32 possible treatments.

8.3.1. The Load Model

The load model was seen to be critical to some simulation yields, especially run-up time. Even small changes in load characteristic affected the run-up time markedly. For the 8.2 MW motor the load torque/speed curve was varied as shown in Table 8.3.1 and Figure 8.3.1 with constants kt1 to kt4 defined as in equation 8.1.

Load Curve	kt1	kt2	kt3	kt4
Nominal Load (N)	0.1	0.1	0.85	1
Early increase (a)	0.18	0.15	0.77	1
Reduce Early (b)	0.05	0.05	0.90	1

Table 8.3.1 : Slight variation in load torque/speed curves for 8.2 MW motor.

As expected, the starting torque and peak transients, TPM, TPN and CP1 were unaffected by the variation in load model. Similarly, the pull-out torque, the slip at which it occurred and the pu current at speed of 0.5 pu all remained at their previous values. The values which did change are shown in Table 8.3.2. The load model is shown to affect the run-up times only. This is because these are affected by the net accelerating torque, (motor, minus load). It is clear that for the setting of timing circuits in protection and control systems, fairly accurate knowledge of the load torque variation with speed is required.

Yield	IT1	t7	t3	t9	t5	t6	t8
Nominal Load (N)	67	1.092	11.07	5.67	11.00	11.37	11.37
Early increase (a)	74	1.226	12.58	6.69	12.50	12.88	12.88
Reduce Early (b)	59	0.993	10.19	5.09	10.11	10.49	10.49

Table 8.3.2 : Numerical yields of simulated d-o-l start from finite system, 8.2 MW motor with different loads as Figure 8.3.1

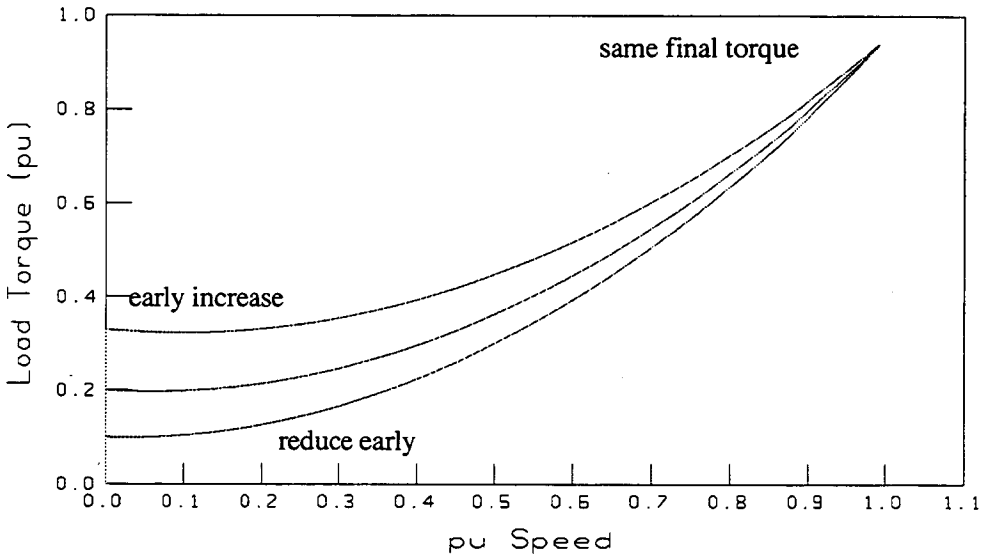

Figure 8.3.1 : Slight variation in load torque/speed curves for 8.2 MW motor as Table 8.3.2

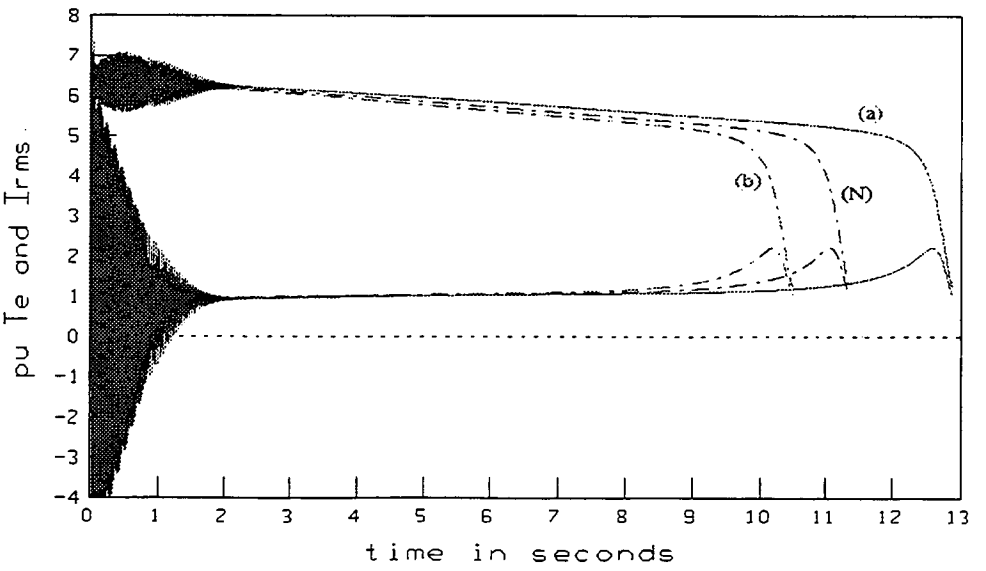

Figure 8.3.2 : Response of 8.2 MW motor with load curves as Table 8.3.1

8.3.2. The Finiteness Of The Supply

The measured variation in motor terminal voltage, for the 8.2 MW motor showed that the system voltage depression persisted until the motor was almost at its final speed when the current dropped sharply. This implies that the AVR action did not affect the voltage at the motor terminals. This might occur if there is significant impedance between the motor and the AVR sensing point. In some offshore applications, the AVR sensing point may be very close to the motor busbars and the voltage droop may not persist for the whole run-up period. The effect of the AVR would need to be allowed for in the simulation, (including exciter saturation, field current limits or field winding time constants). In such cases, a rapid recovery of system voltage will occur. The effect of this would be to reduce the run-up time.

There is a complex inter-dependency between the magnitude of the terminal voltage during starting, the line impedance, the motor current and leakage reactance. For the 8.2 MW motor the voltage dip was large (at nearly 25%) but even the more usual depression of 10% would have a significant effect on the current drawn, the torque produced and hence the run-up time. Figure 8.3.3 shows a graph of terminal voltage and torque against time for the nominal data except that both the nominal and a reduced line reactance were simulated. In some motors it was found that additional line reactance had the effect of reducing the starting current to the point where (otherwise significant) leakage path saturation effects became less pronounced. For the 8.2 MW motor the saturation effects were less marked.

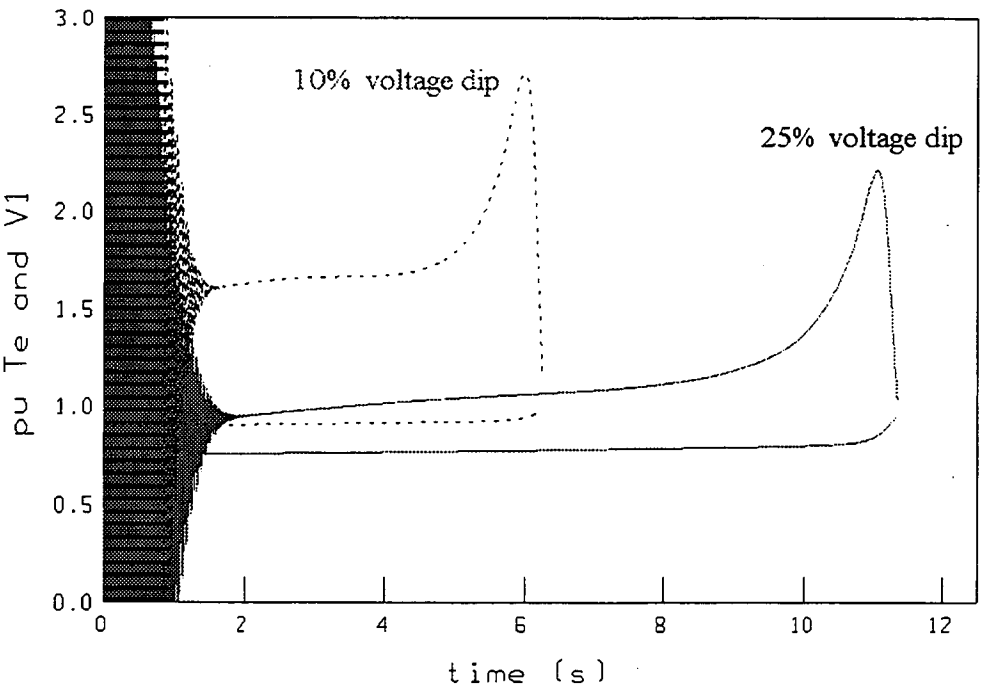

Figure 8.3.3 : Effect on terminal voltage and torque of reducing line reactance from 0.04 to 0.014 pu with 8.2 MW motor : (25% and 10% voltage dip).

In comparison with the voltage variation, the simulated droop in system frequency is small. Simulation with the ratio of generation-system inertia to motor+load inertia varying from 2.5 to 20 showed that the form of the droop in frequency is reasonably well represented by an approximate model described in Chapter 3. With generator

inertia of about 3 times motor inertia, the frequency oscillates significantly before returning to zero due to the lack of damping in this model. In practice the relative size of the equivalent generator representing the power system would usually be larger than 2.5 times the motor size. If not, then the system model would need to be extremely detailed.

8.3.3. Leakage Reactance Variation

During the run-up the motor parameters were varied as shown in the left hand set of graphs in Figure 8.3.4. The effect of the drop in current on the saturated component of the leakage reactances can be clearly seen. For the 8.2 MW motor this was relatively small but the 660 kW motor shows a dramatic increase.

Simple calculation using the approximation given in equation (3.3.1) shows that if a constant (unsaturated) motor impedance of 0.145 pu were used to predict the starting current, then it would decrease from 6.03 pu to 5.41 pu. Even though the predicted terminal voltage would increase to 0.758 pu, the torque would decrease and the run-up time would increase.

If, on the other hand, a constant saturated leakage reactance value were used during the run-up simulation then the initial starting current (and torque) would be the same but predicted torque would be higher at low slip values and the predicted run-up time would be reduced.

A third possibillity is that of fitting a completely new set of motor parameters to the performance data with the constraint that the Isat value is very large so that saturation does not occur. This new model may not fit the specified performance data as well as the model which includes saturation. In particular, the maximum torque is often less than the specified value even if the value of the design parameter, m is adjusted to minimise the error. With the smaller motors (4kW and 2.2 kW) it proved impossible to adjust the design ratio, m in the model sufficiently to match the quoted manufacturer's performance without including leakage path saturation. (Very low values of m led to failure of the program due to the required rotor resistances being too low to sustain the quoted torques.)

In the light of the above, it is important that there be no misunderstanding about the exact meaning of "including saturation" in the modelling of motor starting because the first two interpretations will affect the predicted run-up time in the opposite sense. It is better to describe the first interpretation as "using constant unsaturated leakage reactance values", the second as "using constant saturated leakage reactance values" and the third as "using an unsaturable motor model". As mentioned by Rogers and Shirmohammadi, this is the most logical way to neglect saturation since the other two introduce large errors either in the starting or rated load performance. Figure 8.3.4 below shows that the effect on the torque and current graphs against speed is small for all the motors simulated.

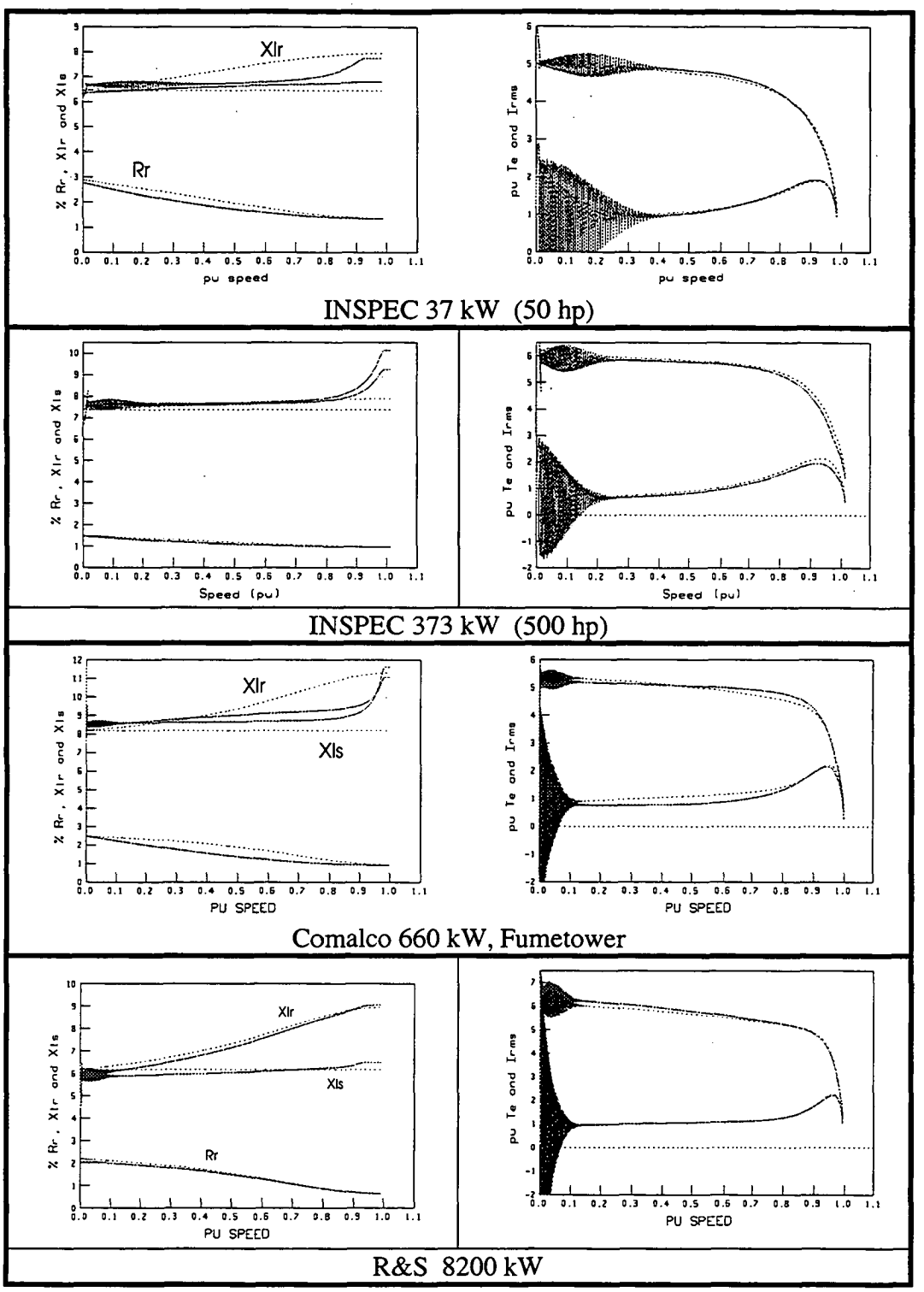

Figure 8.3.4 : Effect of saturation on impedance, torque and current curves against speed : dotted = unsaturable model

Figure 8.3.5 shows how the unsaturable model incorporates the effects of leakage path saturation by treating the reactance change as if it were due to skin effect. This is imposed by the need to have a similar value of total leakage impedance at both starting and rated load as with the saturable model. For the 660 kW motor this causes a significant discrepancy in the predicted torque in the mid-slip region and affects the run-up time. In the case of the 8200 kW motor the saturation effects are small so the rise in reactance is less noticeable. This explains why it proved impossible, with the

small motors, to fit a double cage rotor which incorporated the effects of leakage reactance saturation. In practice the cause of the rise in reactance is immaterial as long as the form of the rise is reproduced when required. This would happen if the current/speed curve were unchanged but the model would perform badly under other conditions, eg reduced voltage starting.

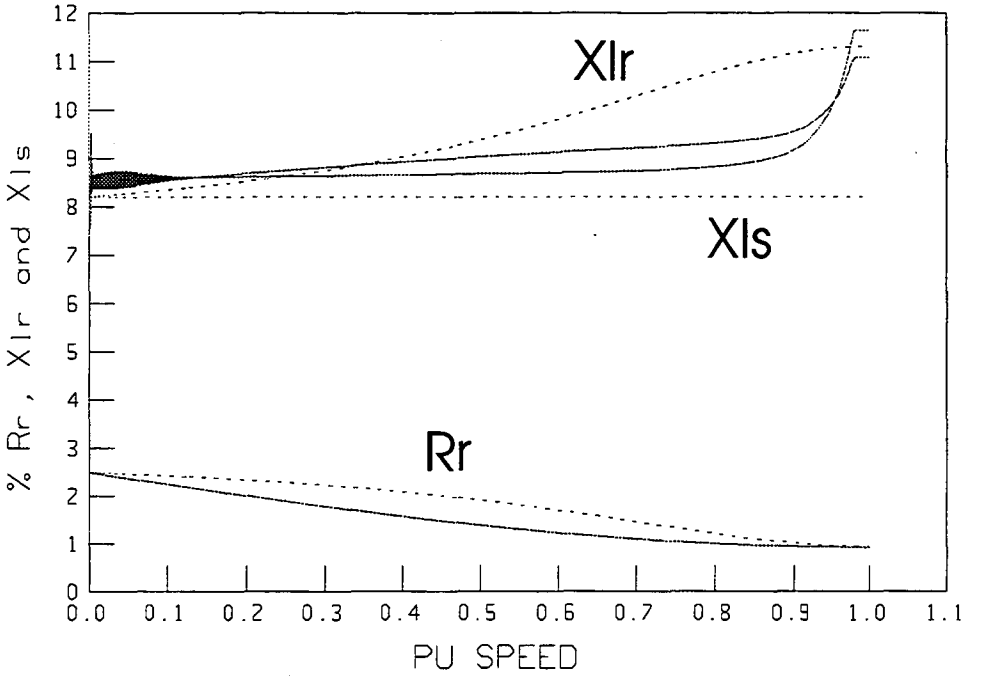

Figure 8.3.5 : Effect of saturation on impedance curves against speed :
dotted = unsaturable model solid = includes saturation
660 kW motor

The output from the simulation program IM_SIM.PAS was used to plot graphs of impedance variation with speed and current. These gave a clear picture of the significance of the large changes which occur in these quantities during starting. The program INSTART does not make these variables available for plotting and the main advantage of custom-made software such as the IM_SIM.PAS program is its ability to be modified to achieve particular research goals. Comparisons were made with various values of Isat and with the output of the saturable form of the equivalent circuit model. Graphs of impedance against current were also plotted as shown in Figure 8.3.6 and 8.3.7. It is noted that in the case of the rotor reactance it is subject to variation with slip, s which is changing simultaneously with the stator current. Similar graphs were plotted for the other motors studied to ensure that the internal models for leakage path saturation and skin effect were performing as expected. These models were incorporated as Turbo Pascal procedures in the program IM2.PAS which was based on the circuit model.

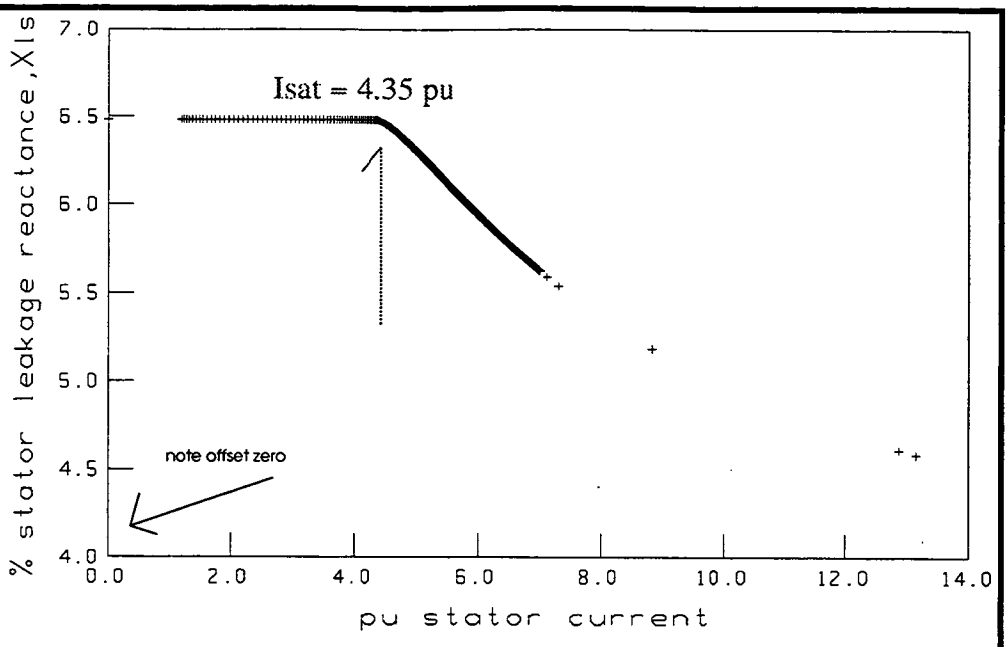

Figure 8.3.5 : Variation of stator referred leakage reactance with current for 8.2 MW motor (During run-up from rest)

The variation due to leakage path saturation can be clearly seen in Figure 8.3.5 with the initial saturation current of 4.35 pu.

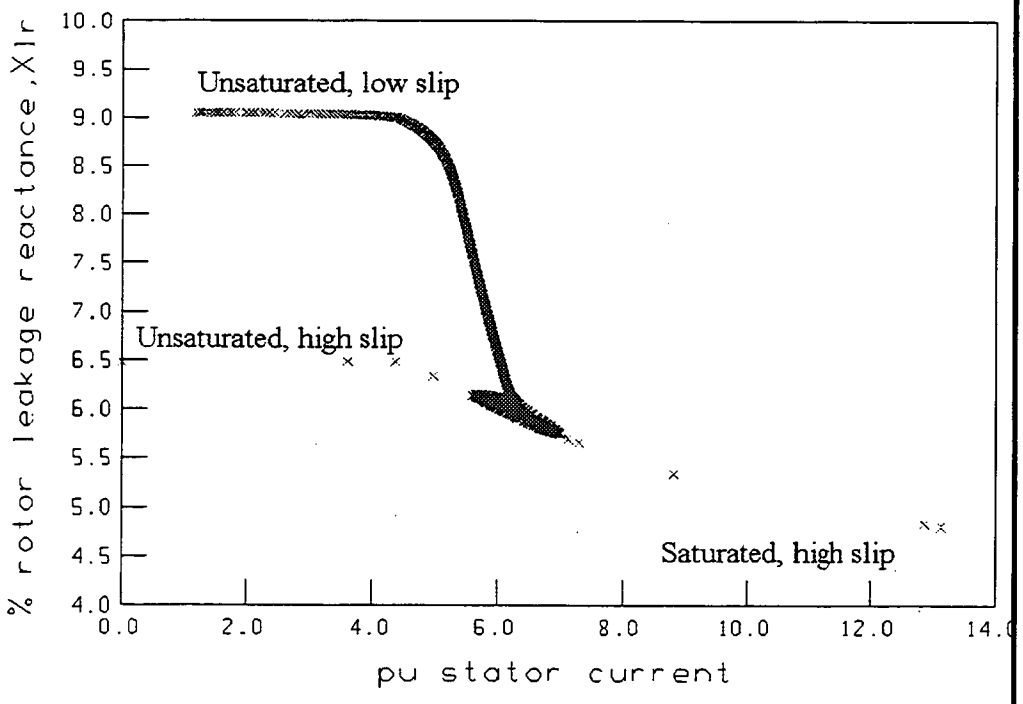

Figure 8.3.6 : Variation of rotor referred leakage reactances with current for 8.2 MW motor (During run-up from rest)

In the case of the rotor, the curve has two parts. The isolated crosses relate to the period of fast electrical transients where the slip, s is high.

8.3.4. The Effect Of Winding Temperature

The resistances of both the rotor and stator windings will vary with temperature. For purposes of comparison, the resistance values which related to the manufacturer's performance data were taken to be valid at a temperature of 115 ^{0}C. (Since the machines are likely to have Class F insulation where the performance is quoted at that temperature). The double-cage rotor resistance values when cold, (20 ^{0}C) were taken as 0.72 of the values at 115 ^{0}C. Other temperatures were also simulated with appropriate factors being used in each case. The results of these simulations are shown below in Figure 8.3.7 which indicates the importance of allowing for motor temperature if run-up times are required as simulation yields.

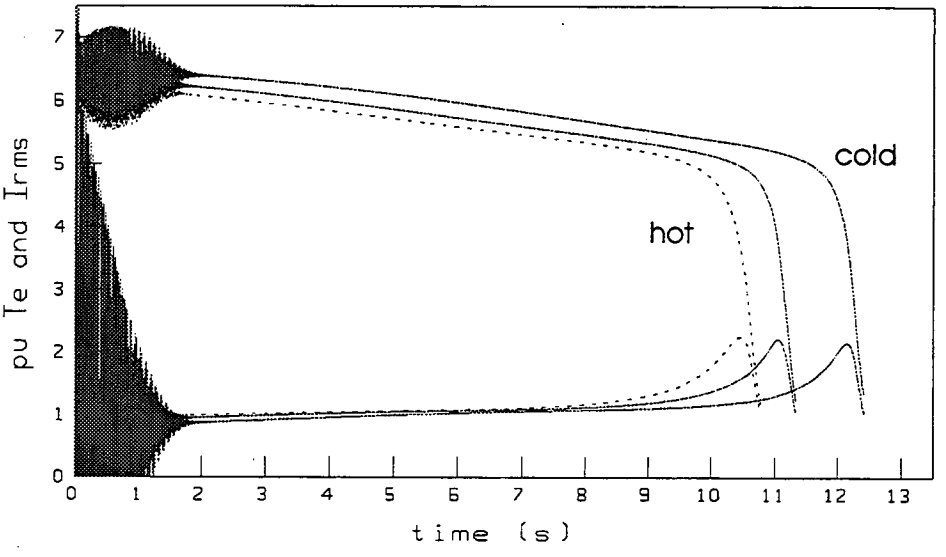

Figure 8.3.7 : Effect of temperature variation on performance of 8.2 MW motor at 120, 115 and 20 ^{0}C (from left to right)

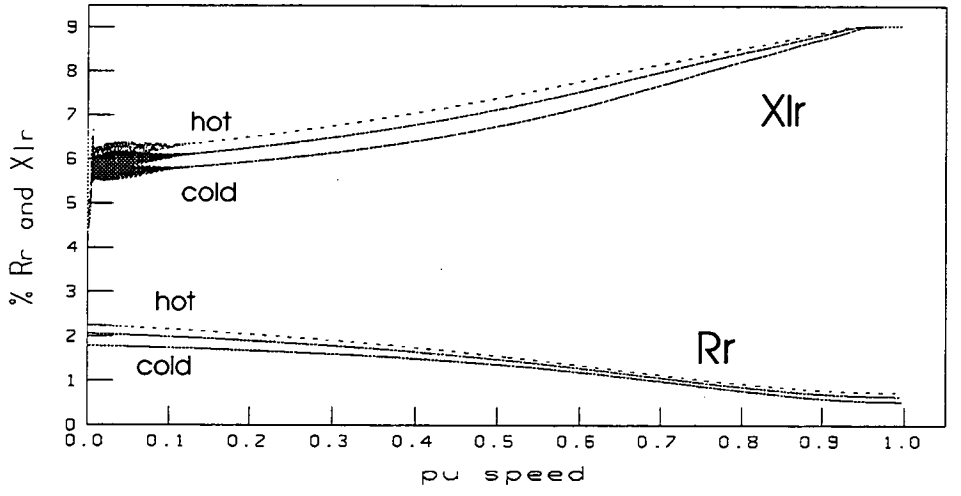

Figure 8.3.8 : Effect of temperature variation on parameters of 8.2 MW motor

From the results of Chapter 4 it was considered that the effect of changes in stator resistance, R_1 would be small (A factor of 234.5, was used for the copper stator winding compared with 225 for the aluminium rotor, but this was probably being pedantic). It was confirmed by simulation that the effect of variations in R1 was not significant. The small direct effect of temperature on the actual leakage reactance was not included but some variation arose in the referred rotor reactance due to resistance changes in the double cage model (See Figures 8.3.8 and 8.3.9).

Contrary to expectations, temperature did not have as much effect with the smaller motors as with some of the larger ones. Later, it will be seen that the effect on run-up times is in the opposite direction for the 37 kW motor. This was investigated by plotting the variation in referred rotor quantities with slip when hot and cold. In the case of the 8.2 MW motor there is a greater difference in the hot/cold starting values of rotor resistance and reactance than the difference between hot/cold at low slip. For the 37 kW motor the situation for resistance is reversed with the larger difference occuring at low slip but the reactance variation is the same as for the larger machines. This is due to the relative sizes of the components of the double-cage rotor circuit.

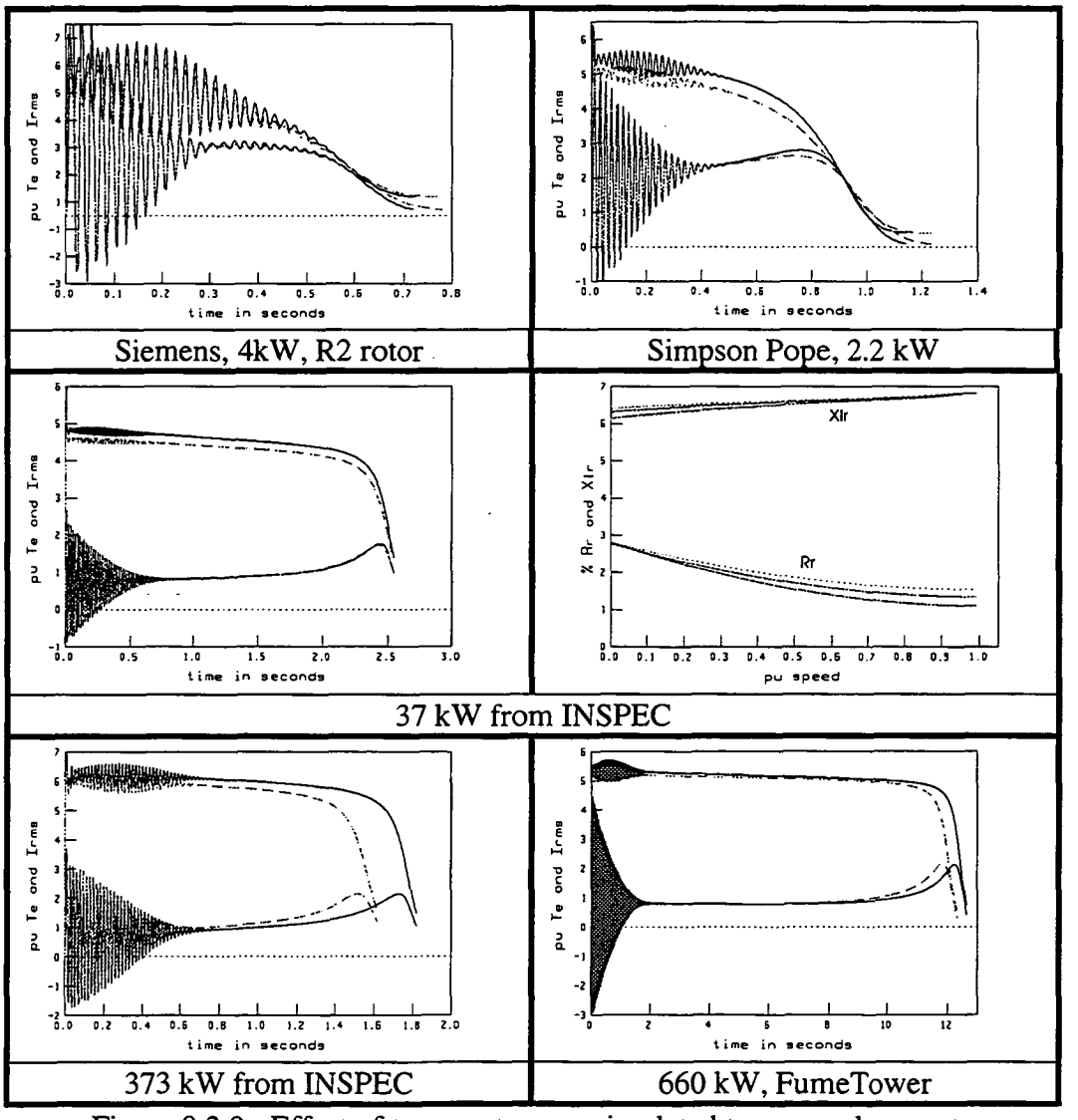

Figure 8.3.9 : Effect of temperature on simulated torque and current curves
Hot (115 ^{0}C) shown ---- Cold (20 ^{0}C) shown as a solid line

The fact that the rotor resistance is larger means that the maximum torque occurs at a higher value of slip. The extent to which this affects the run-up time depends on the nature of the load curve. In addition, the results of Section 5.4 showed that temperature affected the way in which the rotor resistance varied with slip in deep bar rotors (Figures 5.4.3 and 5.4.4). This is one reason why the effect is more pronounced with the larger motors. The shape of the rotor slot is also a factor. For example, Figure 5.4.3 for the W-Type bar shows a similar variation with temperature and slip as that for the 37 kW motor; ie with a larger difference at low slip in the resistive component and a vice-versa for the reactive part.

There was some concern about the validity of simply increasing the resistive part of the double cage circuit. If this is done then does it faithfully represent the variation in referred bar resistance and reactance with temperature? The VWB method introduced in Chapter 5 was used to confirm this. Simulated impedance variation was available from that work for several bar types as shown in Figures 5.34.2 to 5.4.5. Double-cage models were fitted to the sets {S} as defined in Section 5.2 for hot and cold bars and these were compared with each other and the variation produced by adjusting the double-cage circuit for the hot bar by a factor of 0.71 to allow for the temperature change from 120 °C to 20 °C. The process is shown in Figure 8.3.10. The graphs produced were identical, indicating that the effective bar impedance variation was well modelled simply by multiplying the resistive components by an appropriate temperature compensating factor. It is not possible to derive the simulated {S} for the cold bar directly from that for the hot bar using a simple multiplying factor.

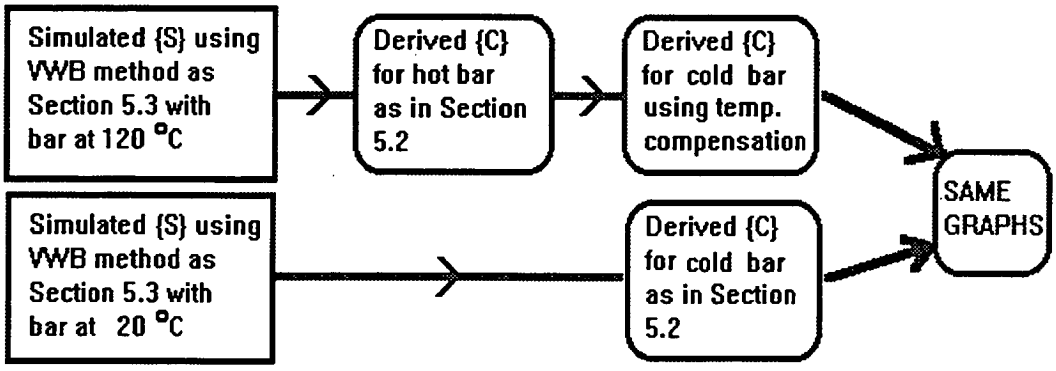

Figure 8.3.10 : Process by which the treatment of temperature variation in double-cage bars by linear increase of the resistive components was verified.

Whilst the effect on the torque/speed curve was small, the accumulative effect on the motor was such that the variation in run-up times shown above were created. The small effect on the torque/speed curve for the 8.2 MW motor is shown in Figure 8.3.11. This degree of change would arise from other causes; eg with the permitted variation in mains supply voltage. It was surprising how small a change in predicted torque is needed to achieve a significant, (10%) increase in predicted run-up time. On reflection this was seen to be due to the integration of the torque difference over the run-up time.

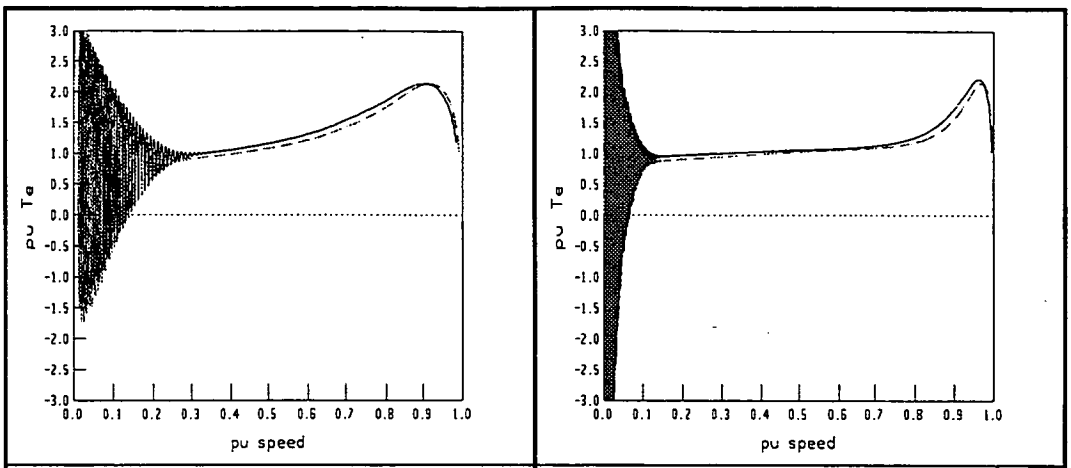

Figure 8.3.11 : Effect of temperature on the torque/speed curves
Hot (115 °C) shown as a solid line Cold (20 °C) shown ----

8.3.5. Systematic Evaluation Of The Effect Of Variations

Once an overview of the effect of the variation in the factors mentioned above was obtained by a reasonable number of simulations, it was decided to approach the problem in a more systematic manner. The factorial method used in Chapter 4 was again brought to bear but this time the complete factorial analysis was performed rather than following a fractional plan. This was justified because, with five factors, the number of treatments was only 32.

The five factors varied were identified by letters to form a pattern of systematic variation from the nominal (JSFNH) to the extreme case (KUIRC) as defined in the chart of Section 8.3.8. This was done because it was easier to remember than the binary code usually used in factorial analysis.

factor	nominal		variation	
total inertia constant	1.0s ,	J	0.8s,	K
leakage saturation	saturable,	S	unsaturable,	U
pu line impedance	nominal value,	F	reduced impedance,	I
load curve	nominal,	N	reduced,	R
Temperature	hot (115 °C),	H	cold (20 °C),	C

Table 8.3.3 : Description of range of treatments in the systematic factorial study

For example, the treatment, JUFNC, (which is normally designated 01001 in factorial analysis) is the case with nominal values of inertia, bus-finiteness and load but with adjusted values of saturation and temperature. ie

J	0	Inertia constant = 1.0s,	as nominal
U	1	Unsaturable parameter values	variation from nominal
F	0	V=0.85 in equation (8.3.1)	as nominal
N	0	Nominal load as Table 8.3.4	as nominal
C	1	Cold motor resistances.	variation from nominal

8.3.5.1. Definition of the variations in the factors

The five factors were varied in the following way :

8.3.5.1.1. Inertia

The total inertia constant of the motor and load was set to 1.0s for the nominal case (J) and this was reduced to 0.8s for the variation (K). This simulated the effect of the 10% tolerance allowed in AS1359.69 to both the motor and load.

8.3.5.1.2. Saturation

The equivalent circuit data for the unsaturable models as determined by program INSPEC are given in Section 8.3.9. It was noted above that different values of design ratio were necessary in order to reduce the error in calculated maximum torque and that, for the small motors, a reasonably accurate unsaturable model could not be determined. These motors were therefore omitted from the systematic study.

8.3.5.1.3. Line Impedance

The line impedance was set using $$X_{line} = \frac{(1-V)}{VI_{st}} \qquad (8.3.1)$$

with I_{st} being the per-unit starting current at rated voltage and V being taken as 0.85 for the nominal case and 0.95 for the reduced impedance. The nominal and reduced line impedances for each motor are given in Section 8.3.9 below

8.3.5.1.4. Load Curve

For comparison purposes, the load curve constants were set during the systematic study as in Table 8.3.4 for all motors.

Load Curve	kt1	kt2	kt3	kt4
Nominal load, (N)	0.1	0.1	0.8	10
Reduced load, (R)	0.08	0.08	0.64	10

Table 8.3.4: Nominal and reduced load torque/speed curves for all motors

Skin effect was omitted from this systematic study because it was apparent that, for the machines used, if it were omitted it would be impossible to develop a model which was consistent with the quoted performance data. The two items of additional data required to determine the double cage rotor model (ie Isat and m) could be determined by an iterative method as described in Chapter 6.

8.3.5.2. Result of applying all 32 treatments

When all thirty two possible treatments were applied, the simulation yields (as defined in Chapters 4 and 6) were computed and stored in files of the form xx.A** , with ** taking a value from 1 to 32. and xx being RS, FT,I1 or I2 to identify the motor being studied. ie RS for 8200 kW ..and. I2 for 37 kW). Four examples of the definition of particular treatments (combinations of factors) are given in Table 8.3.5

Case	Treatment		description of treatment
1	00000	JSFNH	nominal case
2	00001	JSFNC	as above but cold
6	00101	JSINC	as above but reduced line impedance and cold
27	11010	KUFRH	reduced inertia, unsaturable model, reduced load

Table 8.3.5 : Four examples of the interpretation of the definition of treatments.

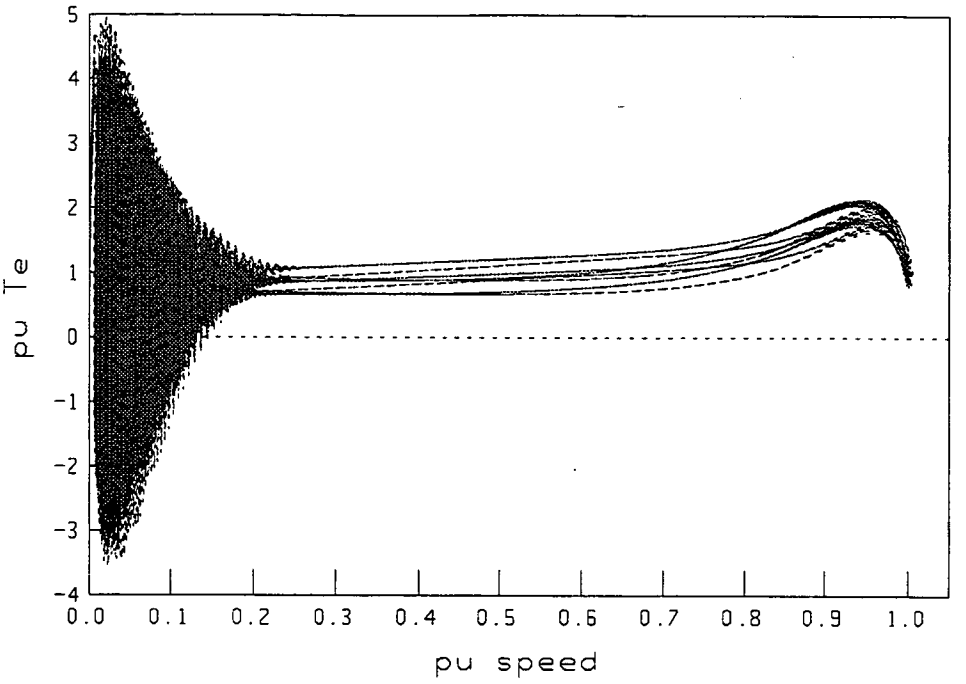

Figure 8.3.12 : Torque/speed curves for all 32 treatments for 660 kW motor

Graphs for all 32 cases were plotted on the same axes in order to show the uncertainty introduced in the simulated output by the selected variations. Figure 8.3.12 shows the range of variation of the torque/speed curve for the 660 kW motor. It can be seen that the curves are all within a fairly narrow envelope. The most important differences arise in the pull up torque which occurs at about 0.5 pu slip. For loaded motors this affects the available accelerating torque significantly and leads to the large differences in run-up times which are shown in Figure 8.3.13.

rating	Simulations runs in order from longest to shortest run-up times, t6															
8200	**10**	12	2	26	4	9	14	28	11	16	1	**18**	3	20	25	30
	13	32	27	6	15	17	8	19	29	5	22	7	31	24	21	23
660	1	9	3	2	**10**	11	12	4	17	25	19	**18**	5	26	13	27
	7	20	15	28	14	6	16	8	21	29	23	31	30	22	32	24
373	2	4	**10**	**18**	1	12	20	26	3	9	17	6	28	14	11	8
	19	16	25	5	22	30	7	27	13	24	32	15	21	23	29	31
37	2	4	1	**18**	**10**	3	20	17	12	6	26	19	9	8	5	28
	11	14	7	22	16	25	24	21	13	27	30	23	15	32	29	31

Table 8.3.6 : Treatments in order from longest to shortest run-up times, t6

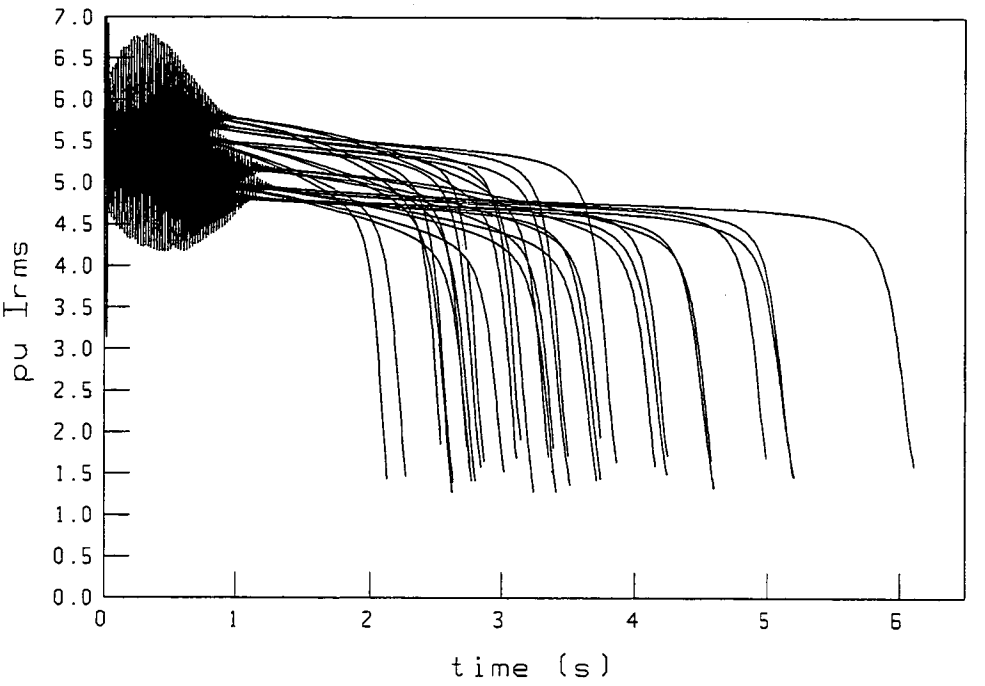

Figure 8.3.13 : Current/time curves for all 32 treatments for 660 kW motor

Table 8.3.6 shows how the various treatments as defined in Section 8.3.9 affected the run-up time, t6. In some cases the conclusions are obvious, eg that the 10th case, JUFNC takes longer than the 12th, JUFRC. In others, useful information may be obtained. For example the relative positions of the 10th and 18th (KSFNC) cases is an indication of the effect of saturation on the torque speed curve relative to an decrease in inertia. These usually affect the run-up time in opposite senses. The unsaturated high inertia case (JU) takes much longer for the 8200 kW motor with the gap narrowing as motor size reduces until finally for the 37 kW motor the saturation effect is more significant than the decrease in inertia.

8.3.5.3. Statistical analysis of yields

The yields as determined by program IM_SIM.PAS were analysed using some of the routines developed in Chapter 5. The results for the 660 kW motor are shown in Table 8.3.7.

Yield	Nominal	Min.	Max.	Mean	Std. Dev.	Cv	% R
t3	5.037	2.018	5.994	3.4516	0.92796	0.27	80.0
t5	5.048	2.024	5.967	3.4473	0.92152	0.27	80.0
t6	5.231	2.139	6.162	3.5963	0.94005	0.26	80.0
t8	5.229	2.137	6.160	3.5948	0.94005	0.26	80.0
t9	2.735	1.178	2.778	1.9127	0.43235	0.23	80.0
IT1	37	20	43	31.06	6.6235	0.21	90.0
t7	0.765	0.419	0.885	0.6436	0.13427	0.21	90.0
t1	0.034	0.034	0.054	0.0366	0.00671	0.18	90.0
TST	0.689	0.482	0.864	0.6962	0.10980	0.16	95.0
t2	0.045	0.045	0.065	0.0592	0.00913	0.15	95.0
TPN	-2.691	-3.695	-2.684	-3.077	0.32487	-0.11	95.0
TPM	4.069	4.032	5.240	4.4697	0.35576	0.08	99.5
TPS	1.813	1.631	2.142	1.8956	0.15342	0.08	99.5
CP2	4.712	4.711	5.530	5.1149	0.32321	0.06	99.5
CP1	9.174	8.577	10.077	9.356	0.4691	0.05	99.5
SP3	0.946	0.936	0.964	0.9514	0.00839	0.01	99.5
Sm	0.994	0.994	1.007	0.9999	0.00306	0.00	99.5

Table 8.3.7 : Results of statistical analysis of simulation yields for 660 kW motor.

8.3.5.4. Comments on systematic variation of factors

In Table 8.3.7 the yields are arranged in descending order of the absolute value of the coefficients of variation, C_V . This means that the yields at the top of the table are associated with greater variability over the range of treatments. If a simulation is intended to determine these yields it is more important to acquire specific information about the five factors rather than to make estimates based on comparison with the performance of other motors.

On the other hand, the simulation yields TPN, TPM, TPS, CP2, CP1, SP3 and Sm are associated with small standard deviations and so an estimate of a particular case may be made more reliably based on type-test data or design rules which may not assign the correct values to one or more of the factors.

Coefficients of performance were computed using the method described in Chapter 4. They may be used as a guide to the relative significance of the various factors on the simulated performance of a particular motor. Coefficients of performance are negative when a change from the nominal factor causes a lower yield. They are shown in Section 8.3.6 in tabular form with the complete experimental plan being given in Section 8.3.8. (These last Sections form an appendix to Chapter 8).

When the results of Tables 8.3.9 and 8.3.10 are considered it can be seen why it is essential to consider the effects of inaccuracy in system data as well as motor data.

For example, for the two smaller motors, the 20% reduction in load torque had as much effect on the predicted time to reach 0.5 pu speed, t9 as neglecting leakage saturation and only half as much effect as ignoring a winding temperature change from 115^{0}C to 20^{0}C.

It is noted that, for the 37 kW motor, temperature affected most yields in the opposite sense. This was thought to be due to the reduced effective bar depth for the smaller motor which meant that the effect of temperature directly on rotor resistance was more prominent than its effect on the referred bar impedance with frequency.

The experience gained in the simulation work presented in this chapter was used as the basis for the Expert System algorithm which is described in Chapter 9.

The relative significance of the five factors is summarised in Table 8.3.8 where, for example, it is shown that the variation in load model used had little effect on most of the yields. This was because both the load curves used were comfortably within the capabilities of the motors so that in no case were the available accelerating torques reduced to such small values that the motors nearly failed to start. Obviously for more extreme variation in the factors, the relative significance might well change. It is considered that the ranges used here were representative of the uncertainties which arise in practical motor studies.

From the results of the work reported in this Section, the order of priorities seems to be Bus, Temperature, Saturation, Total Inertia, Live load Curve.

Yield	most	->	->	->	least
TPM/TPN	Temp	Sat.	Bus	Inertia	Load
CP1	Sat.	Temp	Bus		
IT1/t7	Temp (not 37 kW)	Sat/Bus	Inertia	Load	
TPS	Bus	Temp	Sat.		
SP3	relatively	unaffected	by all	factors	
t3	Bus	Inertia	Temp/Sat	Load	
CP2	Bus	Temp (All)	Sat.		
t9/t5/t6	Bus	Inertia	Temp/Sat.	Load	

Table 8.3.8 : Relative significance of the five factors for each yield

8.3.6. : Coefficients Of Performance For Systematic Study

rating (kW)	**TPM**	Inertia	Saturation	Finite bus	Load	Temperature
8200	8.197	-0.88	-20.69	11.29	-0.12	-2.47
660	4.069	-0.93	-7.15	10.80	-0.17	7.37
373	2.739	-0.25	-6.57	14.02	-0.08	7.08
37	3.037	-0.05	-11.55	8.95	-0.01	28.44
rating (kW)	**TPN**	Inertia	Saturation	Finite bus	Load	Temperature
8200	-6.094	1.53	-15.71	11.12	0.25	12.97
660	-2.691	1.23	-6.40	8.22	0.24	21.08
373	-1.644	0.35	-6.94	9.19	0.11	25.20
37	-0.817	-0.11	-16.71	-5.43	-0.00	55.91
rating (kW)	**CP1**	Inertia	Saturation	Finite bus	Load	Temperature
8200	15.36	-0.01	-25.23	2.41	-0.00	10.05
660	9.174	-0.00	-5.73	2.60	-0.00	8.00
373	9.926	-0.00	-7.52	2.34	-0.00	9.06
37	6.661	-0.00	-0.36	2.05	-0.00	17.86
rating (kW)	**IT1**	Inertia	Saturation	Finite bus	Load	Temperature
8200	36	-8.68	23.61	-7.64	-2.43	38.19
660	37	-7.77	-5.41	-26.01	-3.38	19.93
373	44	-10.09	-6.11	-18.89	-4.97	16.05
37	36	-6.60	-43.75	-13.54	-1.04	-0.35
rating (kW)	**t7**	Inertia	Saturation	Finite bus	Load	Temperature
8200	0.595	-8.75	23.03	-9.12	-3.18	38.50
660	0.765	-7.53	-5.52	-25.56	-3.28	19.39
373	0.760	-9.59	-6.36	-18.07	-4.64	15.47
37	0.648	-6.22	-45.07	-13.20	-0.93	-0.41

Table 8.3.9: Coefficients of Performance for the transient run-up period

rating (kW)	**TPS**	Inertia	Saturation	Finite bus	Load	Temperature
8200	2.189	-3.05	0.28	14.25	-1.52	-8.48
660	1.813	-2.78	2.10	15.06	-1.78	-6.44
373	1.935	-2.73	10.57	18.37	-1.38	-4.15
37	2.027	-1.62	-3.09	16.88	-0.72	8.43
rating (kW)	**SP3**	Inertia	Saturation	Finite bus	Load	Temperature
8200	0.956	-0.17	0.72	-0.85	-0.09	1.13
660	0.946	-0.09	0.71	-0.55	-0.09	1.51
373	0.936	-0.08	0.61	-0.70	-0.03	1.81
37	0.921	-0.13	0.47	-1.09	-0.07	1.80
rating (kW)	**t3**	Inertia	Saturation	Finite bus	Load	Temperature
8200	2.304	-16.21	14.91	-23.51	-5.13	17.16
660	5.037	-14.06	-16.30	-24.75	-7.38	11.77
373	5.353	-16.28	-9.38	-30.17	-8.96	20.15
37	2.945	-15.75	-0.97	-21.75	-4.40	-4.37
rating (kW)	**CP2**	Inertia	Saturation	Finite bus	Load	Temperature
8200	6.595	0.01	-9.32	13.94	0.05	6.09
660	4.712	-0.01	0.52	13.06	-0.00	3.69
373	5.205	-0.01	1.91	14.69	-0.00	2.96
37	4.876	-0.00	-2.82	13.45	0.00	11.67
rating (kW)	**t9**	Inertia	Saturation	Finite bus	Load	Temperature
8200	1.315	-15.06	18.69	-21.39	-3.30	23.79
660	2.735	-13.61	-10.35	-22.79	-4.12	8.78
373	3.428	-15.94	-7.22	-27.76	-6.71	15.95
37	1.741	-15.31	-2.50	-20.13	-2.75	-7.81
rating (kW)	**t5**	Inertia	Saturation	Finite bus	Load	Temperature
8200	2.294	-16.10	14.61	-23.04	-5.05	16.54
660	5.048	-13.98	-16.50	-24.47	-7.31	11.19
373	5.381	-16.22	-9.51	-29.88	-8.92	19.58
37	3.005	-15.66	-1.10	-21.10	-4.42	-5.31
rating (kW)	**t6**	Inertia	Saturation	Finite bus	Load	Temperature
8200	2.416	-15.95	13.80	-22.46	-4.97	16.22
660	5.231	-13.94	-16.20	-24.05	-7.22	11.00
373	5.537	-16.11	-9.64	-29.37	-8.78	19.09
37	3.143	-15.62	-0.59	-20.72	-4.69	-5.27

Table 8.3.10 : Coefficients of Performance for period after transients have decayed

8.3.7. : Data For Unsaturable Motor Models

ID		8.2 MW	660 kW	373 kW	37 kW
Isat	A	9999	9999	4400	9999
X1	Ω	0.29227	1.1004	0.0557	0.44585
R1	Ω	0.02141	0.2349	.0206	0.5367
Xm	Ω	15.585	33.4	2.286	18.42
Ra	Ω	0.1260	0.386	0.0150	0.3046
Xab	Ω	0.2515	0.997	0.0519	0.3394
Rb	Ω	0.03979	0.1879	0.0148	0.1359
Xb	Ω	0.2984	1.1488	0.0298	0.4404
Ist	A	6430	839	2901	290
Tst	pu	1.50	1.01	0.705	1.22
Tmax	pu	3.5	2.6	3.033	2.42
m		0.556	0.5	1.0	1.0

Table 8.3.11 Data for unsaturable models for larger motors

For the smaller motors it proved impossible to fit the performance data (particularly the pull-out torque) with an unsaturable model which produced the quoted starting torque and current. (See Figure 8.3.5 and Section 8.3.30).

The impedance connected between the supply system bus and the motor terminals was set as shown in Table 8.3.12 for the finite bus (F) and less finite (I).
(See Section 8.3.5.1.3)

ID		8.2 MW	660 kW	373 kW	37 kW
F	pu	0.0312	0.042	0.0425	0.041
I	pu	0.0093	0.0125	0.0127	0.012

Table 8.3.12 Supply line reactance for Finite bus (F) and less Finite bus (I) models

8.3.8. Plan For Complete (Non-Fractional) Factorial Study.

Inertia	Sat.	Bus	Load	Temp.	No.	Treatment
J	S	F	N	H	1	00000
				C	2	00001
			R	H	3	00010
				C	4	00011
		I	N	H	5	00100
				C	6	00101
			R	H	7	00110
				C	8	00111
	U	F	N	H	9	01000
				C	10	01001
			R	H	11	01010
				C	12	01011
		I	N	H	13	01100
				C	14	01101
			R	H	15	01110
				C	16	01111
K	S	F	N	H	17	10000
				C	18	10001
			R	H	19	10010
				C	20	10011
		I	N	H	21	10100
				C	22	10101
			R	H	23	10110
				C	24	10111
	U	F	N	H	25	11000
				C	26	11001
			R	H	27	11010
				C	28	11011
		I	N	H	29	11100
				C	30	11101
			R	H	31	11110
				C	32	11111

9. AN ALGORITHM FOR MODEL SELECTION

This chapter describes the development of an Expert System-based algorithm for the selection of a method for modelling the performance of induction motors. Section 9.1 discusses the reasons for using an expert system to perform this task. Section 9.2 documents the organisation of the knowledge obtained as described in the earlier chapters of the thesis into a format suitable for use as an Expert System. Section 9.3 gives some examples of the use of the expert system to select a system model which is appropriate for a particular application. The final section, Section 9.4, gives some reflections on the Leonardo expert system shell, discusses its limitations and makes suggestions for any future development work.

9.1. Reasons For Using An Expert System

When the work described in this thesis was begun the use of Expert Systems was not common. Whilst the consistent goal of the work has been to present the experience gained in the form of a structured set of rules for attaining the objective, the tools for doing this were not selected until fairly late in the process.

Initially it was thought that the algorithm would take the form of a conventional program written in a language such as Turbo-Pascal. This program would evaluate the available data in terms of the simulation objectives and advise the user on the best simulation model for a given situation. This could have been made to work but it would have been awkward to generate appropriate textual messages to the user and to devise suitable logic paths.

The conventional programming methods were rejected in favour of an Expert System developed within the Leonardo Expert System shell mainly because of the following features of the Expert System :

- A facility for proceeding in a non-sequential manner through a set of rules, ie backward chaining as well as the more normal forward path.
- The ability to develop the rule set by gradually adding more rules as the knowledge increased.
- The ability to ask for additional information and to explain why certain choices were made along the path to the final selection of the best available simulation model.

These features will be demonstrated in Section 9.3 where examples are given of the use of the Expert System.

9.2. The Structure Of The Algorithm In The Form Of An Expert System

The first task in the development of an Expert System is to organise the available data so that it becomes information which can later be structured to become knowledge. The overall structure of the Expert System is shown in Figure 9.2.1. Further diagrams are introduced later in order to expand on the basic structure outlined in this initial overview. The initial sub-goal, (goal4) is to establish that all the essential motor data is available. This condition may be satisfied by either having the required performance data in the specified data file or by having both the equivalent circuit data and some performance points in the region of interest. This topic is discussed further in Section 9.2.1.

In order to establish which data items are needed, the purpose of the simulation is first defined by asking the user a series of questions. This is used to establish the ideal simulation model which is then compared with the available model. If the "available simulation model" is as least as good as the "ideal simulation model" then the second sub-goal, (goal 3) of the Expert System is completed.

When both goal3 and goal4 are completed the algorithm advises the user of the situation with comment on the suitability of the available system model with warnings on any deficiencies in it.

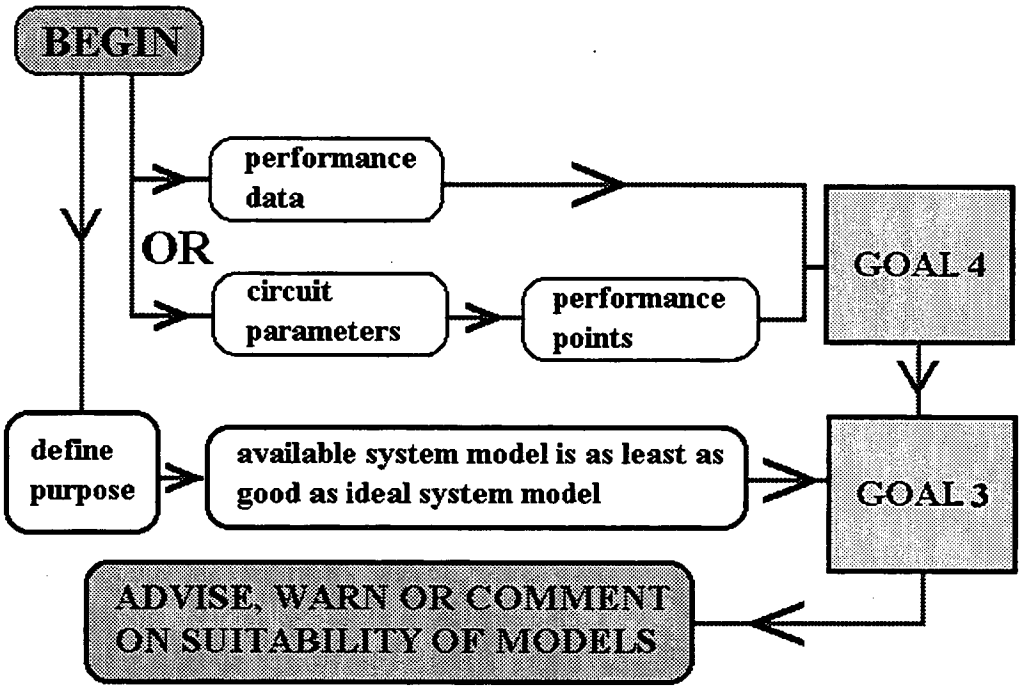

Figure 9.2.1 : Overall Structure of the Expert System to select an appropriate method for modelling induction motors in simulation studies.

9.2.1. Data Needed For Various Models

Figure 9.2.2 shows the process used in the first part of the Expert System where either goal1 or goal2 is sought. In this part of the algorithm, the objective is to establish that all the essential data is either available or can be evaluated using data from the file.

In order to establish the state of goal1, the system reads the specified file and uses data redundancy to assign values to unknown items. In some cases the data supplied in manufacturer's catalogues is not self-consistent. The system checks for this, warns the user and if possible, uses data redundancy to suggest alternative data values.

If redundancy fails to determine a value for a missing item, then the user is questioned during the running of the program. If this fails to obtain an answer that is within a sensible range then the sub-goal, (goal1) is not achieved and the alternative path, (goal2) via the circuit parameters is sought.

The use of quoted circuit parameters without at least a few performance points in the region of interest is not recommended by the algorithm. Either single or double cage parameters are sought depending on the motor size and required range of operation. In the absence of circuit parameter values, NEMA type values are accepted as a fall-back position but a warning is given and this is taken into account when the rest of the system is modelled. If some performance curves are available (eg a torque/speed curve) but not all the data defined as essential, then the unknown items may be approximated initially by NEMA type data and an optimisation method used to assign better values.

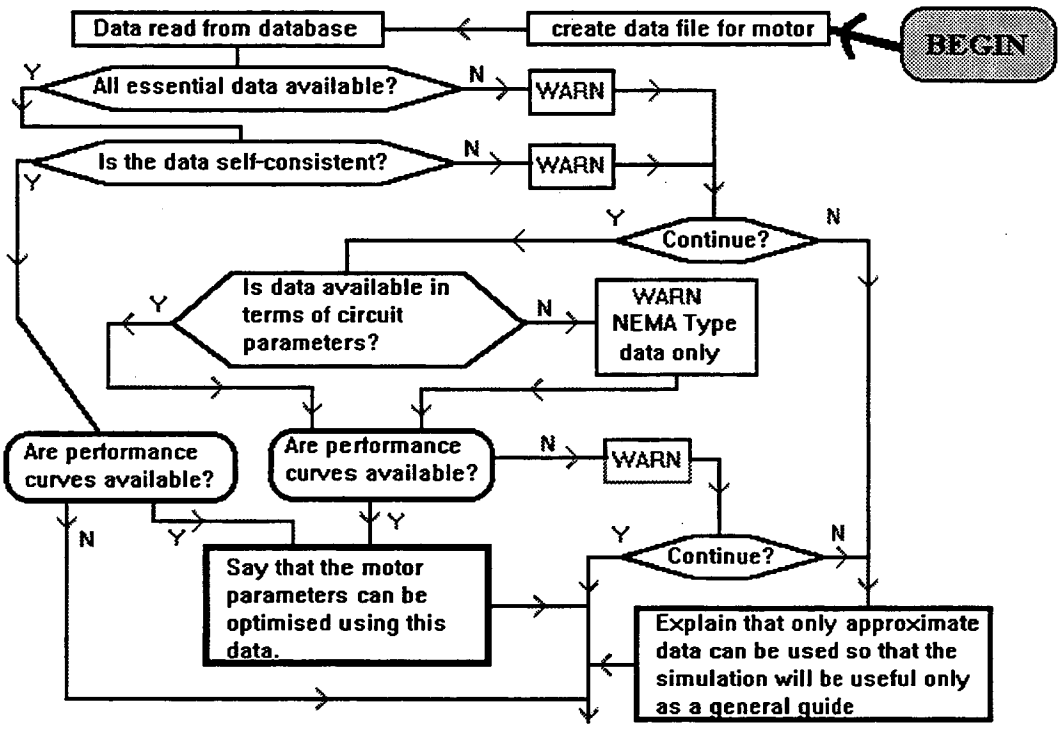

Figure 9.2.2 : Over-view of the Expert System : checking of data for completeness and consistency

The basic data is that which is essential for the derivation of the equivalent circuit parameters as in Chapter 6. The need to complement this basic data with additional performance data is stressed. This is because the performance data is associated with an uncertainty due to manufacturer's tolerances which can be large. There are two ways to overcome this; either by insisting on performance data with tighter tolerances than allowed for in the AS1359 standard or by including additional performance data points in the expectation that averaging will take place. In practice a combination of these is the most likely. The uncertainty will be reduced if the additional performance data is chosen to be in the region of slip/current which is of interest in the simulation.

9.2.1.1. Sorting of essential and non-essential motor data

Some of the motor data which is available is desirable but not as important as other data items. A list was made of the data which might be needed. Data importance was estimated by considering the application of the methods described in Chapter 6 and the results of Chapter 4. Several Venn diagrams were drawn of

the form of Figure 9.2.3 to indicate the dependence of each motor circuit parameter on the performance data.

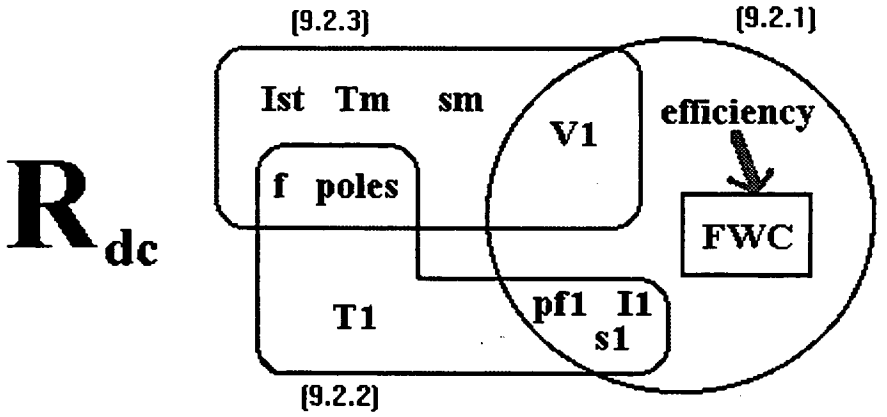

Figure 9.2.3 : The dependence of motor circuit parameters on performance data. (dc value of rotor referred resistance ; brackets refer to equations below)

In the diagram of Figure 9.2.3, items which are related by a common rule are included in a particular set. For example, equation (9.2.1) is represented in the diagram by the circle.

The diagram for R_{dc} can be related to the following relationships :

$$R_{dc} = \frac{V_1}{I_1}\frac{\eta_1(1+FWC)s_1}{(1-s_1)pf_1} \qquad \text{[Rogers and Shirmohammadi, 1987]} \quad (9.2.1)$$

$$R_{dc} = \frac{s_1 T_1 \omega_s}{I_1 pf_1} \qquad \text{[Ansuj et al, 1989]} \quad (9.2.2)$$

$$R_{dc} = s_m\sqrt{\left(R_1^2 + \left[X_{dc} + X_1\right]^2\right)} \qquad \text{[Fitzgerald, Kingsley and Umans, 1983]} \quad (9.2.3)$$

Some relationships have within them the need for other circuit parameters. For example, equation (9.2.3) requires the dc value of the rotor reactance, X_{dc} and stator leakage reactance, X_1. The equation for X_{dc} needs data for X_1 (and R_1 for small machines where the resistance is comparable with the reactance). These items can be derived from performance parameters using the equations presented in Chapter 6 or as equation (9.2.4).

$$X_{dc} = \sqrt{\left(\frac{3V_1^2}{2\omega_s T_m} - R_1\right)^2 - R_1^2} - X_1 \qquad \text{[Fitzgerald, Kingsley and Umans]}$$

$$X_{dc} \approx \frac{3V_1^2}{2\omega_s T_m} - X_1 \qquad (9.2.4)$$

This process imposes a sequence on the search for data and yields a hierarchy of dependence. This sequence is followed in the algorithm so that if the data is

insufficient for the determination of the equivalent circuit parameters then an early decision to warn the user can be made.

Similar Venn diagrams were constructed for other circuit parameters in order to structure the knowledge contained in the available equations. It was found that one of the main side effects of the choice to use a Expert System approach was that it forced the author to adopt a high level of organisation of the available knowledge and consequently led to more compact summaries that would probably have been produced within a free environment such as Turbo Pascal.

The analysis of the data need allows a decision to be made as to the usefulness of continuing the proposed simulation. If the required data is unavailable, the user is asked to decide between

Halting the algorithm in order to to make an attempt to locate the missing data items.

OR

Accepting the best available approximation for the motor parameters and continuing with the assessment of the system model.

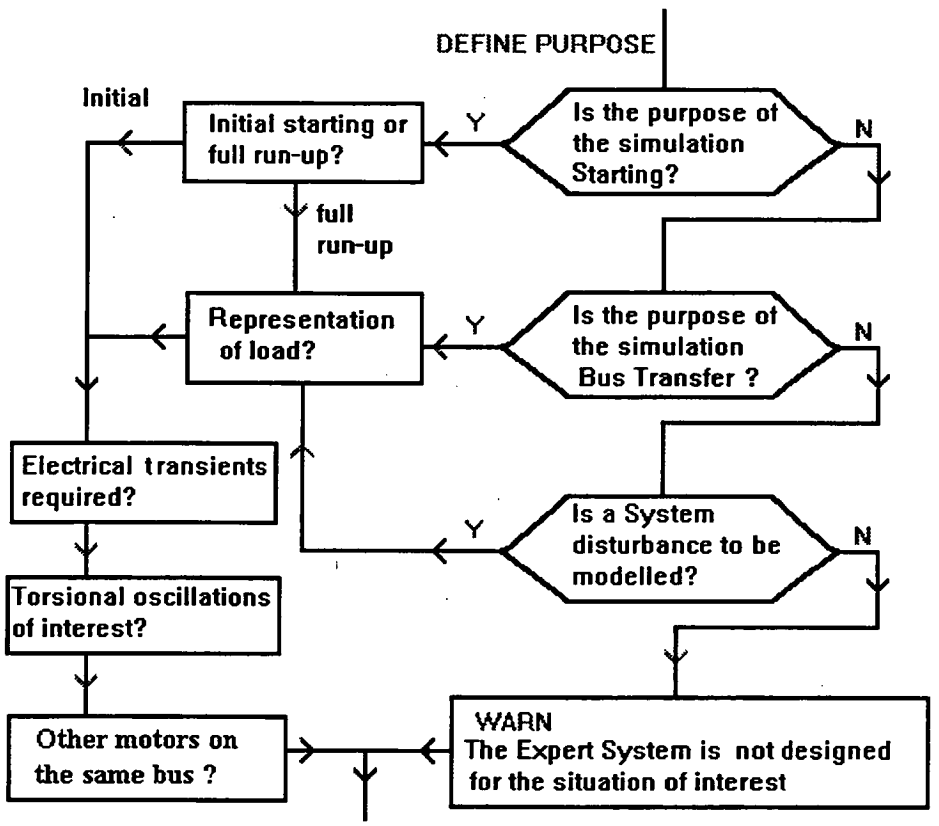

Figure 9.2.4 : Over-view of the Expert System : Definition of purpose of simulation

9.2.2. Defining The Purpose Of The Simulation

The second part of the expert system tries to determine the purpose of the simulation. Some of these purposes may overlap. For example, it is possible for the study to be concerned with starting and electrical transients (at the same time).

The same is not true of starting and bus-transfer because one would take place after the other and the same model may not be needed for both parts of the simulation (conditions are quite different). A flow diagram for this part of the expert system is shown in Figure 9.2.4.

The definition of purpose achieved by querying the user is not final because some purposes may be included in the established set of purposes on the basis of available data. For example, if the motor is large and the complete run-up time is to be simulated with particular interest in the pull-out torque, (yield, TPS) then the requirement for the inclusion of transients will be adopted automatically. This ensures that the reduction in TPS due to the interaction of rotor and stator transients is not missed, (see Figure 8.2.2).

9.2.2.1. Purposes other than starting

In addition to starting, some advice is given for the supply disturbance and bus transfer conditions. For power supply disturbances, the criterion of Krause and others, [1979] was adopted for determining when to advise the use of reduced-order (transient stability) model for the induction motor. This criterion was expressed in terms of performance data rather than as circuit parameters. That is, the criterion as stated is that $R_1 R_2 / X_l^2 < 0.2$. Using equations (6.1.3) and (6.1.5) the criterion was expressed as :

$$\frac{\eta' s_1}{(1-s_1)}\left[1-\frac{\eta'}{(1-s_1)}\right] I_{st}^2 < 0.2 \qquad (9.2.5)$$

The expression for rotor resistance used in deriving (9.2.5) was that for the low slip operation because this is most appropriate to small system disturbances for which the criterion is applicable. All the data for equation (9.2.5) is available in the basic set required for determining the circuit parameters and described in Section 9.2.1.

The conclusions of Richards, [1988] regarding the effect of load inertia and the type of model to be used for bus transfer studies, were included in the algorithm. If there are other motors connected to the same or adjacent bus bars then references are given at an appropriate point to the use of aggregate load models, [Rogers et al, 1984] and [IEEE Task Force, 1995].

The modelling of VSD systems was excluded from the algorithm. If the user does not select one of the above purposes, then reference is made to the work of Slemon, [1989] on VSD models.

9.2.3. Attributes Of A Model For Induction Motor Simulation

The first task was seen as to define the required outcome, ie to create a definition of each possible model type. Computational models were defined according to six main criteria :

- Mathematical Model of Motor in terms of Equations
- Supply System Representation
- Skin-Effect Modelling
- Leakage Path Saturation Model
- Operating Temperature
- Load Model

Each of these basic categories was further divided into logical alternatives. These are shown in Figure 9.2.5. For the selection of the ideal model the six choices may be made independently, creating six sub-models; eg it is possible to use an equivalent circuit representation of the motor with either an infinite bus or multi-bus representation of the supply. With the categorisation given, there are 972 possible system models.

MOTOR		Equivalent Circuit 1		Transient Stability, 2		Full Stator/rotor Transients, 3	
BUS		Infinite Bus, 1		Single Bus 2		Multi-Bus 3	
PARAMETERS	Skin Effect	Fixed, low slip, 1		Fixed, High slip, 2		Double-Cage 3	
	Leakage Saturation	Fixed 1	Cprop 2	UNS 3	ML 4	Lee 5	DF 6
	Temperature	Hot, 1		Cold, 2			
LOAD		unloaded, 1		inertia, 2		polynominal, 3	

Figure 9.2.5 : Definition of model attributes

In practice, it may not be possible to use the ideal sub-model for a particular aspect of the system. In such cases, a less than satisfactory model must be used. The best available simulation model for the purpose in hand will consist of a combination of the best available sub-models. However, if it is necessary to use any one sub-model which is less than the ideal, then the estimated degree of approximation of the simulation is increased and it becomes less important to achieve accuracy in the other sub-models. For example, if due to lack of data the power system must be considered as an infinite-bus, then there is little point being overly concerned that modelling of leakage path saturation can only be done by the Corrected Proportional method.

The Expert System algorithm uses information from the data-base to determine the availability of each of the sub-models. In some cases additional information would help to refine the model. The user is asked if this is available and in some cases for actual values. If the requested data is said to be unknown, then an explanation is given of the effect of using the best available system model/data.

In some cases the available sub-model is deemed inadequate for the defined purpose. In the initial version of the algorithm, the program would then terminate. This meant that the user would be left with an incomplete assessment of the whole system model. This early experience with the use of the Expert System, led to a decision to leave the final choice to the user with the algorithm simply warning that an approximate system model was all that was available and explaining which part of the system model needed to be upgraded. The user was then requested to opt either to continue with the assessment of the rest of the system model or to terminate the algorithm.

On the other hand, it may some times be convenient to use a model which is more sophisticated than absolutely necessary. For example, if the user needs to determine the run up time on a weak bus, then it is clear from Figure 8.2.2 that the equivalent circuit model will be adequate. If the engineer has, and is familiar with, a software package which includes all transients, it may be much quicker in practice to use this familiar software than to search for, or try to write, a program based on the simpler model. The algorithm indicates to the user that the more detailed/sophisticated model may be used in preference but also states the simplest model that is consistent with the purpose and level of approximation in the other models.

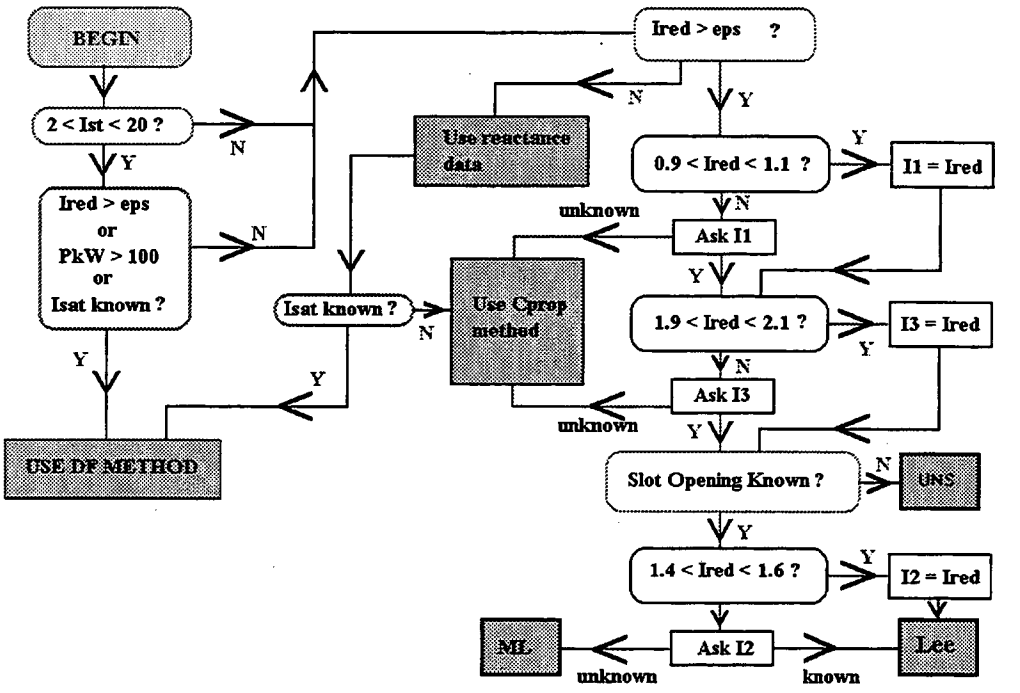

Figure 9.2.6 : Determination of the available model for leakage path saturation

9.2.3.1. Determination of the available model for saturation

Figure 9.2.6 shows how the available model for leakage path saturation is determined. This is consistent with, and derived from, Section 5.1 but was written in the form of a flow chart to assist programming of the Expert System. Similar diagrams were drawn for many of the other logical choices but the example below is given because it is somewhat more complex than the others.

The preferred method for the representation of leakage path saturation in simulation programs is the DF method. This is because, for large motors, it can be made to work well with only one locked rotor test result, the value of Isat being determined by iteration as described in Chapter 6. Because the value of Isat arrived at in this way may be different from the value which is determined from a locked-rotor test, there may be a small difference in the separation of leakage reactance into saturable and unsaturable parts. Any discrepancy is compensated for by slight variation of the double cage circuit so that in practice a reasonable agreement is achieved over the full range of the steady-state operating curves.

For small motors a separate reduced-voltage locked rotor test must be used either to determine the reduced voltage starting current, Ired or to apply another method, such as the UNS method. It is stressed that an unsaturable model which fits the quoted performance data is unlikely to be able to be derived for motors under about 25 kW in rating or for motors fitted with a single cage model; (See Figure 8.3.4 and comments accompanying Table 8.3.11).

The likely reduction in the probable error which may be gained by supplying additional data so that Lee's method may be used is indicated by the Expert System algorithm. If the available reduced-voltage locked-rotor test point, Ired is close to one of the values in Table 5.1.1 then it is not requested from the user. The limits around I1, I2 and I3 in Figure 9.2.6 are empirical and are needed because the sophisticated logarithmic methods, such as Lee's Method, were not found to work well with reduced-voltage test points which were significantly different from those specified in Table 5.1.1, (See Section 7.6.1.2).

Values for Ist outside of the range, $2 < Isat < 20$ are considered invalid. For the case where both the Ist and Ired values are outside the required range and hence considered unknown, the only recourse is to use quoted or NEMA circuit data. If the parameters are accurate and a suitable value of Isat is available, then the former will give good results with the DF method. In other cases, the Corrected Proportional method must be adopted. It is significant that provided that some form of saturation modelling is available it doesn't seem to matter much which method is used. Figure 5.1.13 demonstrates this.

9.2.3.2. Determination of the available accelerating torque

The data files contained slots for three points on the manufacturer's torque/speed curve. These were the starting torque at rated voltage, T_{st} the pull-up torque, T_{pu} (minimum) and pull-out torque, T_m (maximum) together with their respective slip values, S_{pu} and S_m. These were used in conjunction with the given load representation in the form of a polynomial to confirm that there was an 0.1 pu margin between the calculated motor torque and the load torque. Since the motor torque is sensitive to the supply voltage and frequency, an estimate of these was made using the approximate methods of Section 3.3 and the torque adjusted. If the margin was not achieved then a warning was given that this aspect should be examined more closely.

9.3. Justification Of The Algorithm

This part of the work was the subject of much thought and soul searching. The reason for this is that during the course of the whole project many papers were read which attempted to justify methods by presenting one or two selected cases to demonstrate that the proposed method was good. On closer inspection many of these were unconvincing because of one or more of the following :

- The comparisons were in fact of two different simulations so that unwanted (and un-modelled) effects were excluded.
- No comparisons were made with practical measurements in the area of interest.
- No comparisons were made with previously published methods used for simulating the behaviour of interest.
- The method worked well for the motor/system demonstrated but failed when applied to different data.

Because the early version of the Expert System algorithm was developed into the final version by correcting its errors it is clear that at the end of this process there would be no errors left to detect. Any test case which was tried which did reveal errors would lead to those errors being corrected. By definition, the end of this process was reached when a wide range of motor data was used and for each case the algorithm gave recommendations which were consistent with the results of the earlier chapters of the thesis. Of what then could justification of the algorithm consist? The only valid conclusion that could be reached by presenting a few test cases, is that the Expert System algorithm worked well for these particular sets of data.

It is impossible to guarantee that the algorithm will always give a result which agrees with the recommendations of all project engineers. In fact it is possible that the experts themselves will differ in marginal cases. Some confidence was obtained by the experience of applying the algorithm to additional cases which were not used during its development. In practice, the Expert System algorithm developed during the project would serve as a tool to assist the project engineer rather than an absolute guide. It is likely that during use the algorithm would be further developed to include conditions not envisaged during its initial construction. The structure of an Expert System readily allows this to be done by adding to the rule set or knowledge base.

Even though it was realised that it was impossible to rigorously justify the Expert System, it was considered desirable to make an attempt to convince the reader that the algorithm did in fact work, by presenting the results of four test cases. The four cases which were selected to demonstrate the working of the Expert System algorithm were :

- A motor starting study for a 220 kW motor
- Starting of the 8200 kW motor used previously
- A supply disturbance problem for a set of 12, 1417 kW pump motors
- A protection study for a 1.6 MW pump motor.

The algorithm was also run successfully for several motors rated below 100 kW. The recommendations and advice appeared obvious and it is likely that an Expert System would not really be useful for small motors unless the power systems were also small and/or the applications engineer relatively inexperienced. For both large and small motors the algorithm served to remind the user of the various aspects which need to be covered in modelling induction motor performance and to reduce the likelihood of gross errors due to neglecting certain aspects of the system.

The Expert System algorithm contained procedures for assessing the relative kVA rating and inertias of the motor and power supply based on the criteria established in Section 3.3. These were considered acceptable for the purposes of the thesis even though it was recognised that an accurate determination of the supply system response would require more sophisticated system models. The principle adopted was that a simple model should be used first, with a broad safety margin. If this model indicated that there might be a problem, say with a failure to start, then the more complex model would be needed (but also more reliable data).

In all cases the program echoed the data from the specified data file to the screen so that the user could exit the procedure if an error were spotted. In addition, checks were made on data consistency. These are demonstrated in Section 9.3.1.1.

In the following sections the response of the Expert System is given within a double lined box an example of which is shown below :

Because the manufacturer's performance curves are unavailable it is possible that the simulated Torque/Speed curve will not fit precisely to the actual curve in the mid-slip region. A data point for the minimum (pull-up) torque would be helpful.

The introductory screen message was as shown below :

The program will help you to select an appropriate model for certain induction motor simulation problems. In particular, it focuses on direct on line starting bus transfer power system disturbances Data will be read from the data file to be selected. If this data is incomplete then the program will attempt to derive the missing values from data already held. The program will also check that the data is consistent. eg if the power = torque * speed. This is a check for gross errors in data entry. First the purpose of the study is defined and this establishes the need for additional data. This data is then requested. The Expert System will ask if you have any motor simulation software packages and are and familiar with them. The aim of the program is to advise the selection of a suitable model for the problem in hand.

9.3.1. Case 1 : 220 kW WEG Motor Starting

The objective of the study was to confirm the successful starting of the motor when started direct on line from the nominal 415 V bus with significant line reactance. The minimum acceleration and maximum current occurring during the starting period was also desired.

	P1	N1	poles	f1	V1	T1	I1	H
SI units	220000	1480	4	50	415	0	375	0.6
	pf1	E1	s1	FWC	**Ist**	Tst	Ired	Vred
per-unit	0.87	0.93	0	0.022	**0.0**	1.4	3.4	0.48
	kl2	kl3	Tpu	spu	Tm	Sm		
per-unit	0.10	0.90	1.1	0.5	2.0	0.026		

Table 9.3.1 : Basic data for 220 kW WEG motor ; File DF1.DAT

Before using the algorithm, the data file DF1.DAT was created containing the basic data for this motor as given in Table 9.3.1. For this example, the starting current at rated voltage was deliberately made zero in order to demonstrate the use of saturation models other than the describing function method. (The actual value was 8.8 pu).

The initial questions established the purpose of the study as starting from rest to final speed with interest in the modelling of torque, current and run-up time. No particular interest was expressed in the modelling of transients. The only available software was said to be the equivalent circuit model. The load curve was available in the form of a polynomial with constants entered in the data file.

The algorithm confirmed that all the necessary data was available to allow a double-cage circuit model to be constructed.

Once the purpose of the simulation was determined, the conclusion that the software model was inadequate was reached and the message below was displayed.

> The recommended motor software model is Full_DE but the best available software is Equivalent Circuit.
>
> This means that the maximum torque will be over-estimated and the run-up time will be shorter than in reality by about 1s.
>
> Select OK if you wish to proceed to examine the other aspects of the system model.

On receiving the instruction to proceed, information was sought regarding the system fault level, system kVA and inertia constant of the supply. If values for these were too small, then a warning was given. Based on the methods of Section 3.3, an estimate of the probable voltage and frequency dips was given . For example if the fault level was given as 40 pu (on a motor base) and the inertia constant of the supply as 15 s then a flashing box appeared with estimates of the supply voltage and frequency droops as 0.18 pu and 2 Hz respectively.

For the leakage saturation sub-model, the response of the algorithm was to request data for the locked rotor test at currents of 1 and 2 pu. When these were given it requested the type of rotor slot opening :

> What kind of rotor slot opening is there?
> If the slot opening type is unknown, then select Not_known.
>
> If the slot is known to be closed then a logarithmic proportional method can increase the probability that the error in predicted current is less than 6% from 75 to 90%.

The slot opening was said to be unknown and therefore agreement to proceed was sought as follows :

> The simulation of Starting in a 220 kW motor requires
> a good saturable model for leakage reactance.
> This must be based on more than one locked rotor test.
>
> Since the system is far from infinite there will be complex interactions between supply voltage, line current and leakage reactance during starting.
>
> Knowledge of the rotor slot opening type will improve the reliability of the current estimate.
>
> You may select OK to continue with the algorithm or NOK to quit and try to obtain more locked-rotor test data or rotor slot type from the manufacturer.
>
> Since some approximations have already been made
> Select OK to accept the approximate model.

The final recommendation of the algorithm was :

> The ideal model can be compared with the available model below.

IDEAL MODEL		AVAILABLE MODEL
Full DE	Motor Software	Equivalent Circuit
Single Bus	Bus Model	Single Bus
Double-Cage	Skin Effect	Double-Cage
Describing Function	Leakage Saturation	UNS
Polynomial	Load Model	Polynomial

The following messages were given :

A more sophisticated motor model is needed in order to study Starting of the 220 kW motor because you have expressed an interest in modelling All_Variables over the complete run-up period. The leakage saturation model is less than ideal but since the motor software is non-optimum then this should be corrected first.

The above conclusions agree with the experience detailed in earlier chapters. In particular, it is clear from Figures 8.2.2 and 8.3.4 that a saturable differential equation model is required with a 220 kW motor in order to predict the run-up time. Although the errors are not large, the effect on run-up time will be large. The algorithm suggested that there would be no problem in starting this motor.

9.3.1.1. Inconsistent data

A modified form of file DF1.DAT was used to demonstrate the response of the algorithm to inconsistent data. This was called DF5.DAT. For this file, the value of the rated torque and speed yielded an output of 213 kW and this was sufficient to trigger a highlighted warning box. The torque was recalculated to be 1424 Nm and the algorithm proceeded. The results were much the same as for file DF1.DAT except that the DF method was available since the Ist value was included. The following warning was given at the conclusion :

Because the data in the file is inconsistent the conclusions are not definite. Please check the data file and re-run the program.

9.3.1.2. Incomplete data

File DF6.DAT has rated speed, torque and slip all unspecified. The algorithm requests these in that order from the user. If an acceptable value was entered for any one of them, the others were calculated. If all three were entered as unknown, the user was asked first for the double-cage circuit parameters and then for performance data to optimise these. In the particular example these were also said to be unknown and a warning was given that the default type data is all that was available. The user was then asked to confirm that the program should proceed with estimated data.

At the end of the program run, the data in file DF6.DAT was repeated to allow checking by the user.

The performance data as read from the file DF6.DAT was incomplete.
The following are essential : items given as zero are unknown.
rated power 220.0 kW **speed 0.0 rev/min**
poles 4.0 frequency 50.0 Hz
415.0 V 0.87 power factor
375.0 A efficiency 0.93 pu
Torque 0.0 Nm **rated slip 0.0 pu**
Inertia constant of motor and load is 0.6 s

These items are optional
Constant losses: Friction, Windage & Core loss, 0.02 pu of total loss
Starting current at rated voltage is 8.8 pu
at reduced voltage of 0.48 pu it is 3.4 pu
Starting torque is 1.4 pu

The equivalent circuit data was not available
and could not be derived from the incomplete performance data

Experience shows that circuit impedance values quoted by manufacturers need to be checked against performance data.

The manufacturer's performance curves could not be used to optimise the circuit parameters because the curves were unavailable.

In addition, the following warning was given.

The motor model used is based on the circuit data given and may not be accurate.

The rest of the system may be modelled as given below.

For a motor of rating 220.0 kW it is better to model the variation of rotor parameters due to skin effect by using a double-cage circuit.
Ignoring skin effect can lead to large errors in predicted starting conditions.

A double cage model could not be used with any confidence because only type data was available.

Clearly the algorithm expected better data than was available before modelling could proceed. If inconsistent data were used without checking, then the conclusions of the Expert System algorithm would depend on the particular decision path chosen. For example, the various relationships in Figure 9.2.3 would lead to different R_{dc} values so that decisions based on the magnitude of R_{dc} may conflict.

9.3.2. Case 2 : 8.2 MW Motor Starting Time

This was based on the familiar pump motor used in previous chapters. The simulation was for a direct-on-line start from a weak bus. The objective of the study was to determine the peak electrical torque after the electrical transients had died away and the time at which it occurred. This case was chosen to demonstrate that the Expert System algorithm correctly identified that modelling of saturation, whilst important, is secondary to some of the other factors such as the accuracy of the voltage droop at the bus and the assumed temperature of operation.

Before using the algorithm, the data file DF2.DAT was created containing the basic data for this motor which was taken from Table 8.1.4. The available model for leakage path saturation was restricted to the Corrected Proportional method by excluding the locked rotor test data from the File DF2.DAT. When asked, it was said that the temperature of the motor was unknown and the full differential equation simulation software were available. The algorithm concluded that the available system model was acceptable with the recommendations of

Full DE software, single bus system model, double-cage circuit, describing function model for saturation and a polynomial fit for the load curve. In addition, it gave the following comments :

> The leakage saturation model is less than ideal but since the motor temperature is uncertain this probably is unimportant.
>
> You are advised to confirm the operating temperature because this will affect the results of the simulation quite significantly.

This is a reasonable conclusion in the light of the simulation work presented in Chapter 8.

9.3.3. Case 3 :Supply Disturbance Problem For 1417 kW Pump Motors

This problem was the subject of a load rejection study at a nuclear power plant, [Rogers, Beaulieu and Hajagos, 1995]. There were a total of 12 motors split between two bus bars. On load rejection, the plant operated in island mode, frequency rose and the high motor/load inertia prevented the motor speed from tracking the frequency. As slip increased, so did the motor currents reducing the 4.16 kV bus voltage and further reducing the available torque. This led to stalling of some motors especially when they were unequally distributed between the two bus bars.

The characteristics of the system which caused the problem were high motor inertia, low generator inertia and high transformer impedance. Because the supply disturbance is sufficient to cause the motor to move away from the normal slip range, modelling of skin effect and saturation are necessary. The fact that the motor is large means that the pull-out torque cannot be determined from the equivalent circuit model.

	P1	N1	poles	f1	V1	T1	I1	H
SI units	1417000	0	4	60	4160	0	236	6.25
	pf1	E1	s1	FWC	Ist	Tst	Ired	Vred
per-unit	0	0	0	0	8.8	1.77	0	0
	kl2	kl3	Tpu	spu	Tm	Sm		
per-unit	0.10	0.95	1.7	0.75	3.1	0.03		

Table 9.3.2 : Basic data for 1900 hp pump motor; File DF3.DAT

The starting point for the modelling process was the performance parameters but these were not published. The circuit parameters derived using INSPEC were given in full.
The algorithm concluded that the data in the file, DF3.DAT was insufficient for the calculation of the double cage circuit parameters. When the missing performance data items were declared to be unknown, the circuit parameters and performance points were sought. These were confirmed to be available.

The purpose of the simulation was declared to be "Power Supply Disturbance" with the presence of "Other Motors". A warning was given that errors in pull-out torque would arise with a motor of this size if transients were not included. Questions were asked regarding the supply kVA and inertia. It was confirmed that the data for each bus was available enabling a multi-bus model to be used.

The Expert System concluded that the motor was "Large" and hence anticipated considerable speed variation. This was achieved within the algorithm by comparison of the total motor and load inertia constant with that of the representative supply generator which was estimated from the known frequency rise curve from the load rejection test.

A warning was given that for a supply disturbance with a motor of this size the polynomial load model was required which fitted the test data in the region of slip between $0 < s < 0.5$ pu. That is, errors in modelling the load curve in the region of starting were not important.

IDEAL MODEL		AVAILABLE MODEL
Full DE	Motor Software	Full DE
Multi Bus	Bus Model	Multi Bus
Double-Cage	Skin Effect	Double-Cage
Describing Function	Leakage Saturation	Describing Function
Polynomial	Load Model	Polynomial

The critical features of this study were the modelling of the supply frequency disturbance, the load and the accurate estimation of the pull-out torque. Reducing the terminal voltage to 0.82 pu as was done after load rejection would significantly reduced the available torque. If a rise in frequency, were added to this, then the torque would be reduced further. Clearly the load curve is a significant determinant of the system stability outcome. The square law model used by Rogers et al, led to rapidly increasing load torque with increasing motor speed at a time when the available torque was already low due to the decreased main flux (V/f ratio).

Two key questions arose in the assessment of this simulation example. First, could the motor modelling be performed satisfactorily using an equivalent circuit? Secondly, could the multi-bus representation of the supply be replaced by an equivalent single bus?

The full differential equation as selected by the algorithm is needed with this large motor because the need to accurately represent the behaviour in the region of pull-out torque, (See Section 8.2).

The single bus supply model could be used if the following assumptions were made :

- All the motors on one bus behaved in a similar manner, allowing symmetry to be used.
- The main generator was such that the voltage and frequency varied during the simulation period in the manner indicated by the test curves.
- The only significant impedance between the motor and the bus was that of the transformer.

With the above assumptions, an indication that there might be a problem with motor stalling was given by a simulation based on a single bus model for the power system and an equivalent circuit model for the motor. Interpretation of the results of this model required recognition that it was optimistic since it over-estimated the available pull-out torque under transient conditions. This simulation confirmed the choice of the full DE software by the Expert System, though a preliminary study based on a simpler model would not be a bad idea.

The above assumptions would still leave the problem of assessing the effect of distributing the 12 motors into two groups of either 8/4 or 7/5. Since this question was central to the simulation, the need to use a multi-bus model seems unquestionable.

9.3.4. Case 4 : 1.6 MW Pump Motor Protection Study

This motor was the subject of an unpublished study by the Tasmanian Hydro Electric Commission (HEC). The problem which occurred was that the motor tended to trip during starting due to overcurrent. Whilst this could be overcome by increasing the current setting slightly, it was considered desirable to identify the cause.

The problem was found to be the presence of significant and sustained dc offset currents due to the switching instant being away from a voltage zero-crossing, (as in Figure 8.2.4).

	P1	N1	poles	f1	V1	T1	I1	H
SI units	1600000	741	8	50	11000	0	106	1.0
	pf1	E1	s1	FWC	Ist	Tst	Ired	Vred
per-unit	0.85	0	0	0.025	4.06	0.7	0	0

Table 9.3.3 : Basic data for 1.6 MW pump motor ; File DF4.DAT

The load data was excluded from the data file. For the purposes of the algorithm, the motor was said to be started from cold.

When the data was presented to the algorithm the conclusions were that

IDEAL MODEL		AVAILABLE MODEL
Full DE	Motor Software	Full DE
Single Bus	Bus Model	Single Bus
High Slip	Skin Effect	Double-Cage
Describing Function	Leakage Saturation	Describing Function
Inertia	Load Model	Inertia

It was commented that the skin effect model which was available was better than necessary. The algorithm recommended the DF method because it is the preferred method and is available with the data given in file DF4.DAT. The motor was modelled satisfactorily by HEC engineers using the ATP4 program with a single cage rotor model with motor parameter values appropriate to the high slip condition and a single bus model for the power supply. Leakage path saturation was not included in the HEC model but the values used in the simulation were the saturated reactances.

It is considered that the recommendations of the algorithm were appropriate.

9.4. Some Reflections On The Leonardo Expert System Shell

With hindsight, the decision to use the Leonardo Expert System Shell was unfortunate. At the time it was the only Expert System development tool available but it suffers from several limitations which make it unsuitable for commercial use (at least in the DOS Version 3.24). These limitations reflect its age and were that :

- It does not allow easy documentation of the process by importing screens into other PC applications.
- It is unable to link with programming packages without requiring a large amount of memory and slowing to an unacceptable speed.
- It has an extremely unfriendly text editor which does not allow significant cut and paste operations nor the use of a mouse.

The difficulties experienced in the writing of Section 9.3 emphasised the problems which would occur in trying to maintain an acceptable Quality Assurance program in a consulting environment with such software. This would require traceability of the decision process. There is a limited log in the Leonardo software but whilst it records the user responses it does not indicate the corresponding PC screens which indicate why the response was made.

The ability to link with packages such as Turbo Pascal would have allowed significantly more assessment of the numerical data, leading to quantitative comparisons of different models. For example, it would have been possible in Case 1 to use a comparison of the polynominal representation of the load curve with the available motor torque to confirm that the motor would start correctly . The algorithm could, with difficulty be used to prepare data files for programs such as IM_SIM.PAS described in Chapter 3 but in practice it was easier to rewrite the data, (although this introduced the possibility of typographical errors in the new data file).

The limited editor facilities would hamper future development of the Expert System which would inevitably be required after some commercial use.

These problems did not encourage the development of a commercial version of the Expert System software. It is more likely that the experience gained in the writing of this package will be used to develop a similar system based on newer Expert System shells, (such as LEVEL5 OBJECT, by Microsoft). The file for the Leonardo-based Expert System is contained in the pocket at the back of the thesis together with the data files and a text file version of the algorithm in Word 2 format.

10. CONCLUDING REMARKS

The examples of Chapter 9 bring the thesis to an end and it is appropriate at this point to summarise what has been done and to indicate the uses to which it may be put.

The original major goal of the thesis was to summarise the available knowledge about induction motor modelling into a structure which allowed a user, who was inexperienced in the field, to select a simulation model which would be appropriate for the problem in hand. This has been achieved.

In order to achieve the original major goal it was necessary to perform other tasks. The most significant part of the whole work which led up to the thesis, was the systematic review of all the factors which might affect the outcome of a numerical simulation of an induction motor under direct-on-line starting conditions. This review led to some new insights and methods for the modelling of the skin effect in the rotor and leakage reactance saturation in both stator and rotor. These methods were introduced and discussed in Chapter 5. A better understanding of the relationships between the established methods for modelling these parameters enabled comparisons to be made between them. This in turn allowed recommendations to be made regarding the circumstances in which a particular sub-model might be improved and the extent to which this was necessary.

The use of manufacturer's quoted performance values as starting points for the simulation process was adopted. In consequence, it was necessary to investigate the effect of data uncertainties due to permitted tolerances. This problem has been ignored previously. It was shown in Chapter 6 that if the full range of permitted tolerances were used, then in some cases, the simulation results can be grossly unrealistic. It proved necessary to check data consistency and to confirm that the proposed motor model fitted the quoted performance data with as small an error as practical. It was found that the RMS error over several data points could be reduced to less than 5%. It was pointed out that the claims of some authors to achieve consistently better than this are unrealistic due to the fact that the performance parameters themselves have associated uncertainties greater than this.

One result of the work which led to the thesis was the identification of the need to review the broad performances tolerances permitted by AS1359 and IEC34. For some motors, if these are applied simultaneously, then they lead to unrealistic values for the model parameters; ie it is impossible to model the quoted performance over the full operating range using a single model with positive impedance values. This is the reason why numerical optimisation methods did not work consistently well when used to determine circuit parameter values from performance specifications. It is recommended that these tolerances be reviewed and that in the interim, manufacturers quote more realistic tolerances which recognise that the performance parameters are not truly independent, eg starting torque and current are not both free to vary in either direction.

The significant effect of motor operating temperature on the outcome of numerical simulations has been demonstrated in Chapter 8. This has not been previously appreciated, especially for large motors.

Although it is impossible to make definitive conclusions without the data pertaining to a particular case, it may be helpful to summarise the results of the systematic study in Chapter 8 as follows :

- The process of simulation has two components; the system model and the data. A considerable amount of work has been done to develop accurate models with the result that the main limitation on the ability to accurately predict performance is likely to be the reliability or unavailability of the input data.

- Since the reliability of the simulation output depends on the level of uncertainty in the data input, it is important to confirm the actual tolerances in the data used. In some cases the tolerances allowed by AS1359 are too large and combinations of tolerances lead to impractical motor designs.

- The most important aspect of the simulation model is correct modelling of the bus voltage and frequency during the period of interest. The detailed response of the generator governor is usually unimportant since the frequency depression is unlikely to be larger than that which may arise during normal operation. The modelling of the voltage depression requires accurate data for the supply reactance and leakage path saturation in the motor.

- It is especially important to include leakage path saturation with small machines where the change in reactance cannot be included by other means. For large motors, the overall reactance change can be modelled fairly well by an unsaturable double cage model, (See Chapter 8).

- The inclusion of motor temperature was a surprisingly important determinant of the output of the simulation. Temperature should not be omitted from worst-case studies. It may easily be included by adjusting the resistance values in the equivalent circuit. The appropriate assumption is that the circuit parameters as derived are valid at normal operating temperature, (115 ^{0}C to AS1359).

- The equivalent circuit model may be used with reasonable accuracy as a first attempt to modelling the problem in hand. For small motors (< 100 kW) it is likely to give good results. The additional data required to derive the double-cage circuit model is not excessive and so this is recommended. The newer version of the INSPECT program is probably the best way of determining the circuit parameters.

The construction of the Expert System algorithm was in itself a very interesting and useful process. The algorithm was demonstrated to work correctly in four test cases. The format in which it exists imposes limitations on its use in industrial consulting situations. The important contribution of this part of the work was the formalisation of the relationships between the variables and the definition of sub-models which could be combined to create an overall system simulation model. It is envisaged that this structure will be retained in the future development of the Expert System algorithm in a commercial consulting engineering environment. As it stands, the algorithm is to be regarded as a prototype which needs to be developed by further application to practical case studies before being relied upon for commercial work.

A1. APPENDIX : PROGRAM IM_SIM.PAS

This appendix relates to the induction motor simulation program IM_SIM.PAS. The program uses a 4th Order Runga-Kutta method to solve the state equations derived in Chapter 3. It was used to produce the results shown in Chapter 8. An earlier version of it was used in the factorial study of Chapter 4. This earlier version is a subset of the default version and may be reproduced by setting appropriate values in the control data file DSU. (See Section A1.3 below).

Section A1.1 explains how to run the default version of the program and view the simulation results. If modifications to the default version are required, then these may be done along the lines indicated by the rest of the chapter.

The program was written in Turbo Pascal version 7 and ran on an IBM compatible 386 PC with or without a numerical co-processor.

A1.1. Use Of The Default Version Of The Program

When the program is run, the user is asked to confirm the default mode by pressing the RETURN key four times. The default mode is :
Graphs plotted on base of motor speed to the PC screen for a motor at normal operating temperature (115 ^{0}C). Alternatively, options may be selected by responding as shown in Table A.1.

The default output variables are defined in the program procedure ASGN in unit PART7.PAS. These are saved to a text file, may be graphed and are :

- time in seconds
- per-unit motor speed
- per-unit value of the RMS stator phase current (not the instantaneous current)
- per-unit electrical torque on a base of rated power and synchronous speed
- per-unit value of the RMS terminal voltage at the motor terminals
- percentage effective rotor referred resistance per phase
- percentage effective rotor referred leakage reactance per phase
- percentage effective stator leakage reactance per phase

This large number of variables can make the screen rather cluttered but since they are also saved to a text file they can be accessed by other packages and plotted individually if required. The simplest way to change the plotted (and saved) variables is to edit (and re-compile) the procedure ASGN in the unit PART7.PAS. This would only be necessary if simulation variables other than the above were required to be plotted or saved.

The program will perform numerical simulation of the run up to steady-state for each machine in the file A1.DAT in order. The default name of the text file for the simulation output for the nn th motor simulated is QQ.Ann. The QQ prefix can be changed by editing the file DSU or creating a new file similar to DSU as described below.

The standard configuration gives :

- simulation with leakage path saturation included
- skin effect treated using a double-cage circuit model
- polynomial motor load
- supply treated as a finite bus

These options can be overridden by editing the file DSU. Constants for each of the above configuration items are read from the data file A1.DAT for each motor. ie the values of Isat, double-cage circuit parameters in ohm, load curve fit constants and bus model data.

Simulation yields for all the motors as defined in Chapters 4 and 6 are stored in a text file called QQ.YLD.

Message To Screen	Response	Result Of Choice
Normal Temperature ?	RETURN C or c	Machine at normal temperature, 115 °C. Cold machine is simulated
Graphs plotted?	RETURN N or n	Graphical output is plotted, in format as defined below. Graphs are not plotted and the rest of the questions are not asked. This is a diagnostic option not normally used. It requires the HGRAPH units to be available. If the HGRAPH units are unavailable then use IM0_SIM.PAS.
Enter P for graphs to Printer or Archive	RETURN P	Graphical output is directed to screen. Question below is asked
enter 0=screen 3=printer ↑ 4=printer →; > 4 for Archive	0 3 4 >4 RETURN	Graphical output is directed to the screen Graphs plotted to printer (portrait) Graphs plotted to printer (landscape) Graphs saved to HGRAPH archive file Ignores and waits for a value as above
Enter T for graphs against time	RETURN T or t	Graphs plotted against pu speed Graphs plotted against time

Table A.1. Alternatives to the default mode which can be set at run time from the keyboard

A1.2. Structure of the Main Program Segment

Control of the way in which this program operates is effected in three different ways:

- The use of constants set within the main program segment CONST statement.
- Setting variables read in from data file, DSU.
- Information requested from the keyboard at run time.

It was recognised that this might make the program less user friendly but it was not the primary intention to develop software for others, eg commercially. The strategy adopted had the advantage of reducing the amount of explanation and interactive questioning at the keyboard prior to each simulation. It allowed the user to run the

program in the default mode without needing to know how the complete program worked. It also allowed the way in which the program worked and the complexity of the simulation model used to be changed fairly easily without editing the program units, merely changing the control data file used.

The CONST declaration statement of the main program segment defines the constants shown in Table A.2.

Name	Purpose	Default Value
YLD.OUT	Destination file for simulation yields	QQ.YLD
DSUN	name of the control file which contains the variables as described below	DSU.
RE_START	If TRUE then the RK4 initial conditions are read from file RESTART.DAT ELSE the initial conditions are assumed to be zero, (motor de-energised).	FALSE
over_plot	If TRUE then graphs from all simulations in this program run are plotted on the same axes ELSE the user must press RETURN to initiate the exiting from the plot routine and starting of the next simulation.	FALSE
keep_track	If TRUE then a graph of pu torque is plotted point by point during the simulation	TRUE

Table A.2. CONST declaration statement of the main program segment

A1.3. The Control Data File DSU.

The first three lines of this file control the scale of the graphical output to the screen during the simulation.

0.00 10.0	Horizontal axis range
-4.0 10.0	Vertical axis range
1.00 2.00	Variables xdiv and ydiv for axis interval marks

A1.3.1. Diagnostics and definition of the case to be simulated

The next five variables control the diagnostics requirement and range of motors simulated.

Variable KBD controls the output of data to the screen prior to the start of the graphical display. Setting KBD = 0 leads to printing out of the data as input and with applied tolerances as described later. Also output are the Runge-Kutta interval lengths and step sizes. This diagnostic feature is not normally used.

DATA IN FILE			DATA ITEM NAMES		
1	11		KBD		KMCMAX
6	10	2	KMC1	KMC2	KMC3

KMCMAX sets the number of lines of motor data in the file. The example above shows a data file which is expected to contain data from 11 motors. Simulation is performed for the KMC1 th motor in the data file and then the (KMC1+KMC3) th until the (KMC2) th. ie for the values shown, there are 11 sets of motor data and simulation is performed for the 6th, 8th and 10th motors only.

A1.3.2. Various treatments which may be applied

The simulation may be performed with the model varied, for each set of motor data, according to the format described below. For normal use this is not required and the variables are set to 1. For all 32 treatments this line would be set as :

```
1  32  1 ,     (ie 1 to 32 in steps of 1)
```

This generates treatments in the following format : Five integers are read in to set the states of variables which control the model type :

LKG Set = 1 for variation of leakage reactances with current according to the describing function method and the value of Isat read in from the motor data file. If LKG is set = 0 the pu value of Isat is set at a very large value so that no saturation occurs. (Note this is not the same as using an unsaturable model whose parameters have been optimised with saturation neglected; see Chapter 8).

SKEFFSet =1 for a full double cage model. If SKEFF is set =0 then a single cage model is used based on the double cage parameters in the data file but with values appropriate to either low frequency or high frequency depending on the setting of the next variable. LF.

LF If SKEFF is set =1 then this parameter has no effect. If SKEFF is set =0 then LF does the following : If LF is set =1 then the low frequency values of rotor impedance are used throughout the simulation. If LF is set =0 then high frequency values are derived based on the double cage circuit in the data file and these are used for the whole simulation.

FWload If FWload is set =1 then the load torque is applied to the motor as defined by the parameters in the motor data file. If FWload is set = 0 then no shaft load is applied. ie inertial loading only.

FIN If FIN is set = 1 then the finite system model described in Section 3.3 is applied so that the supply voltage and frequency will dip during the motor run-up. FIN = 0 sets an infinite bus system.

Combinations of the above five parameters may be applied to any given motor in a systematic way. This is called a "Treatment" and was useful in assessing the effect of each of the models on program output. The technique of factorial analysis is discussed at length in Chapter 4. Treatments are defined using an array, the first four rows of which are given as :

LKG	SKEFF	LF	FWload	FIN	Treatment	Output file ID
					1 1 0 1 0	
					0 0 0 1 1	
					0 0 1 0 1	
					0 0 1 1 1	

This means that in the third case there is no modelling of leakage path saturation, skin effect in the rotor is ignored and the low frequency value of the rotor impedance is used in a single cage rotor circuit. There is an inertia load only and the voltage dip due to the supply system transient reactance is included in the model.

The next three lines in the file DSU. give the names of variables as shown in Table A.3.

VARIABLE NAME	DEFAULT VALUE	
DRIVNMS	empty line, ie local directory	The drive in which data files are to be found and to which output files are written
MFS	A1	The data file containing motor data
PIDS	QQ	The initial two letters of the text file(s) used to save the variables plotted on the screen. Additional letters are automatically added by the program to identify the particular motor and treatment as defined above. For example, the fourth treatment of the third motor in data file A1.dat the graphical output will be saved in file ZZ.C04. This feature was added to avoid overwriting output in multiple runs.

Table A.3 : Setting of input and output file names and directories

The rest of the file is optional text used for recording information about the file itself.

A1.4. The Motor Data File A*.DAT

The first line of the data file contains an identification of the file's purpose.
The next two items are constants which specify the number of state variables, and the number of system constants to be read in.

Data for program IM_SIM.PAS
8 25

The next 25 lines contain the names of the system constants which are set out below in horizontal tabular form with corresponding values for the 50 hp motor from the INSPEC data base. These values are not included at this stage in the file. These constants are defined in Table A.7 below.

On each subsequent line, appropriate values are repeated for each motor in the file, but not the variable names. A space is used as the variable separator.

H	X1	Rb	Kz	Kj	Ke	Kt	f	Vll	R1	Xm
0.5	0.55469	0.13141	4.5E-02	200	1.0	0.1	60	575	0.53740	19.8638

kt2	kt3	kt4	kt1
0.8	0.8	0.2	0.25

Pout	PP	PHI	Kd	Ra	Xab	Xb	Il	Isat	Ks
3.73E+04	1.0	0.0	0.0	3.07E-01	0.41706	0.43850	48	249	0.5

Table A.4 : Sample of constants for 50 hp (37 kW) INSPEC motor

A1.5. The Program Units PART1, PART3 AND PART5

The main function of unit PART1.PAS was to define global variables and constants and to read in data from the control the data file DSU.

Unit PART3.PAS was used to read in data from the file A1.DAT.

Unit PART5.PAS was used to estimate the run-up time, the pull-out torque and to calculate the system mechanical and electrical time constants. These were used to set the interval lengths and integration steps for the subsequent RK4 procedure. The following base quantities were defined :

```
IBASE := C[23]=I1;          FBASE :=C[8] = f ;
PBASE := C[16] = Pout;      WBASE := FBASE*2.0*PI;
TBASE := C[16]*C[17]/WBASE; ZBASE := C[9]/(SR3*IBASE);
```

These were used to convert reactances at nominal frequency to inductances. The inertia constant was used to calculate the rotational inertia, J which appears in equation (3.2.7).

The facility was created to vary the input data according to a predetermined pattern as described in Chapter 4. This meant that a second array D was created of the same size as C and whose elements differed from those of C only when the required tolerances were applied.

Some frequently appearing quantities were computed and stored in an array, R as shown in Table A.5.

Array R	Definition in Section 3.2.2
R[1]	Stator self-inductance, Ls=Ll+Lm
R[2]	Rotor electrical time constant
R[3]	Mechanical time constant
R[4]	$L_r L_s - L_m^2$
R[5]	1 pu torque at motor synchronous speed
R[6]	Free axis angular velocity, ω_e
R[7]	Rotor self-inductance, Lr=L2+Lm
R[8]	Unsaturated stator leakage inductance, Ll
R[9]	Unused
R[10]	1 pu line current on power, Vline base
R[11	Finite supply angular frequency, ω_s
R[12]	Finite supply line voltage, V_s
R[13]	Magnetising inductance, Lm in Henry
R[14]	Effective referred total rotor cage resistance, R_r
R[15]	Polar moment of inertia, J

Table A.5 : Quantities computed and stored in array, R

A1.6. Unit PART7.PAS : The Main RK4 Segment

For programming convenience the variable names were assigned aliases and stored and manipulated as components of arrays. The 'e' superscript used to designate the synchronous reference frame was dropped since it can be taken that all state variables are referred to the freely rotating reference frame. The state variables and their differentials were identified with the arrays Q and F as Table A.6.

Section 3.2.2	Program IM_SIM		Section 3.2.2	Program IM_SIM
Ψ_{dr}	Q[1]		$p\Psi_{dr}$	F[1]
Ψ_{qr}	Q[2]		$p\Psi_{qr}$	F[2]
Ψ_{ds}	Q[3]		$p\Psi_{ds}$	F[3]
Ψ_{qs}	Q[4]		$p\Psi_{qs}$	F[4]
ω_r	Q[5]		$p\omega_r$	F[5]
E_f	Q[6]		pE_f	F[6]
ω_v	Q[7]		$p\omega_v$	F[7]
T_{pm}	Q[8]		pT_{pm}	F[8]

Table A.6 : Program aliases for state variables

This led to the expression of the system differential equations in terms of rotor and stator flux linkages which were solved by an RK4 method. The complete simulation period was broken down into up to five sub intervals with different integration step sizes. The simulation was terminated when either the maximum simulation time as set in file DSU. was reached or the load torque was equal to the motor torque.

The 25 system constants were read in from a data file as elements of array C defined in Table A.7.

Subscript	Name	Description	
1	H	Inertia constant, $H = \frac{1}{2} J\omega^2 / (ratedVA)$	
2	X1	Per phase leakage reactance of stator at freq. f	
3	Rb	Resistance of lower rotor cage	
4	Kz	Impedance factor	Used for modelling finite supply as discussed in Section 3.3
5	Kj	Inertia factor	
6	Ke	Excitation factor	
7	Kt	Prime mover torque factor	
8	f	Nominal frequency, used for all reactance data	
9	Vll	Rated line voltage	
10	R1	Stator AC resistance per phase in Ohm.	
11	Xm	Magnetising reactance referred to the stator	
12	kt_2	Load torque representation as a polynominal : function of per-unit speed, N with T_{base} defined in terms of rated power and synchnonous speed. $T_{load} = T_{base}\left[kt_1 + kt_2(1-N)^{kt4} + kt_3 N^2\right]$	
13	kt_3		
14	kt_4		
15	kt_1		
16	Pout	Rated power output in watts	
17	PP	Number of pole pairs in stator winding	
18	PHI	Phase angle at which starting occurs	
19	unused		
20	Ra	Resistance of rotor upper cage in Ohm	
21	Xab	Mutual reactance between upper and lower cages	
22	Xb	Leakage reactance of lower rotor cage	
23	Il	Rated line current in amperes	
24	Isat	Per-unit stator current at which saturation starts	
25	Ks	Unsaturable leakage reactance/ total leakage reactance, Xt0 / Xtl (see section 2.2.4.1)	

Table A.7 : Definition of the system constants in array C

BIBLIOGRAPHY

1) Abu-Elnaga MM and Alden RTH, "Dynamic performance of a synchronous generator - fourth order microcomputer model", IEEE power Engineering Society, Summer Meeeting, Portland Oregon, July 1988, IEEE paper No. 88 SM 533-2.

2) Adkins B and Harley RG, "The General Theory of Alternating Current Machines, application to practical problems", Chapman and Hall, 1975, pp 240-253.

3) Agarwal and Alger PL, "Saturation factors for leakage reactance of induction machines", Trans AIEE, Pt. III, 1960, Vol. 79, pp 1037-1042.

4) Ager, R, "Transient overspeeding of induction motors", AIEE Trans., Vol 60, 1941, pp1030-1032

5) Alger PL, "The Nature of Polyphase Induction Machines.", John Wiley, 1951.

6) Alger PL, "Induction Machines, Their Behavior and Uses", Gordon & Breach, 1965, pp 265-270.

7) Andria G, Dell'Aquila A , Salvatore L and Savino M, "Improvement in modeling and testing of induction motors", IEEE Trans. Energy Conv., Vol, EC-2, No.2, June 1987, pp 285-293.

8) Ansuj S, Shokooh F and Schinzinger R, " Parameter estimation for induction machines based on sensitivity analysis", IEEE Trans. Indus. App. Vol. 25, No. 6, 1989, pp 1035-1039.

9) Arneaud J, "Comparison of models for the DOL starting of the induction motor from a finite system.", Australasian Universities Power and Control Enginering Conference, Monash University, October 1991, pp 109-114.

10) Arneaud J, "Deep-Bar and Double-Cage Models for Cage Induction Machines", Australian Universities Power Engineering Conference 1993, University of Wollongong, Vol. 2., pp 502-507.

11) Arneaud J, 'The Effect of Manufacturer's Performance Tolerances on the Simulated Performance of Induction Machines', International Power Engineering Conf. Singapore, March 1995, pp 578-583.

12) Arneaud J, "Modelling of leakage reactance saturation in induction motor simulation studies", Australasian Universities Power Engineering Conference, Nedlands, WA Sept. 1995, pp 410-415.

13) Arneaud J and Lagman R, "Induction motor starting current", Electrical Energy Conference, Adelaide, Sept. 1995, pp 203-208.

14) AS 1359 1974, Part 69 , Tolerances, Table 69.1.

15) Barber DE, "Effects of motor loads on generating sets", Petbow Limited Technical Reprint, 1982.

16) Belmans R, Findlay RD and Geysen W, "A circuit approach to finite elemet analysis of a double squirrel cage induction motor", IEEE Power Engineering Society, Summer Meeting, Mineapolis, Minnesota, July 1990, IEEE Paper No. 90 SM 287-3 EC.

17) Bengiamin NN and Holcomb FH, "PC-Based Power Systems Software: Comparing FUnctions and Features", IEEE Computer Applications in Power, Jan. 1992, pp 35-40.

18) Bourne R, "Electrical rotating machines testing", Ilisse, London, 1969.

19) Brown JE and Grantham C, "Determination of the parameters and parameter variations of a 3-phase induction motor having a current-displacement rotor." Proc. IEE, Vol. 122, No. 9, Sept. 1975, pp 919-921.

20) Brown JE, Kovacs KP and Vas P, "A method of including the effects of main flux path saturation in the generalised equations of ac machines", IEEE Power Engineering Society Winter Meeting 1982, IEEE Paper No. 82 WM 239-2.

21) Cathey JJ, Cavin RK and Ayoub AL, "Transient load model of a induction motor", IEEE Trans. PAS-92, No.4, Jly/Aug 1973, pp 1399-1406.

22) Chalmers BJ and Mulki AS, "Design Synthesis of Double-Cage Induction Motors", Proc. IEE, Vol. 117 No. 7, July 1970, pp 1257-1263.

23) Concordia C, "Steady-state stability of synchronous machies as affected by voltage-regulator characteristics", Electrical Engineering (Trans AIEE), Vol. 63, May 1944, pp 215-220.

24) Dally JW, Riley WF and McConnell KG, "Instrumentation for engineerig measurements", Second Edition, John Wiley, 1984, pp 533-538.

25) Daniels AR, "Introduction to electrical machines", Macmillan, 1976

26) de Mello FP and Walsh GW, "Reclosing transients in induction motors with terminal capacitors", AIEE Trans. on Power App. Syst., Vol. 80, Feb 1961, pp 1206-1213.

27) Diana G and Harley RG, "Transient behaviour of induction motor flux and torque during run-up", IEEE Trans. on Energy Conv., Vol. EC-2, No. 3 , Sept 1987, pp 465-469.

28) Field AB, "Eddy currents in large slot-wound conductors", Trans. AIEE, Vol. 24, 1905, pp 761-788.

29) Fitzgerald A E, Kingsley C, and Umans S D, "Electric Machinery", 4th Ed., McGraw-Hill, 1983.

30) Foulkes J, "Induction Motor Modelling", Undergraduate thesis report, University of Tasmania, 1994.

31) Gol Ö, "Induction machine models for design.', Int. Conf. on evolution and modern aspects of induction machines., Torino, Italy, 1986.

32) Gosbell V J and Dalton PM , "Measurement of Induction Motor Parameters for Control Purposes", IE Aust. & IREE Aust. Vol. 11 No. 2 June 1991 pp 134-139.

33) Grantham C, "Determination of induction motor parameter variations from a variable frequency standstill test", Electrical Machines and Power Systems, 10:239-248, 1985, pp 239-248

34) Grantham C, "Rapid parameter determination of machines", Elec. Energy Conf. 1987, Adelaide, 6-9 Oct 1987, pp 418-422.

35) Gunaratnam N and Novotny, DW, "The effects of neglecting stator transients in induction machine modeling", IEEE Trans. PAS, Vol. PAS-99, No. 6, Nov/Dec 1980, pp 2050-2059.

36) He YK and Lipo TA, "Computer simulation of an induction machine with spatially dependent saturation", IEEE Trans. on Power Apparatus and Systems, Vol. PAS-103, No. 4, April 1984, pp 707-714.

37) Healy C and Lang R, "Transient motor studies", Electrical Enginer, Feb. 1992, pp 40-44.

38) Ho S, Mayhew G and Arneaud J, "The slip measurement of induction machines", Australasian Universities Power Engineering Conference, Univ. of Adelaide, Sept. 1994. pp 238-243.

39) Holley HJ, Higgins TA, Young PL and Snider WL, "A comparison of induction motor models for bus transfer studies", IEEE Trans. on Energy Conversion, Vol. 5, No. 2, June 1990, pp 310-318.

40) IEC34 - 1, Section 9, Table X, Item 8, 1983

41) IEEE Committee Report, "Computer representation of excitation systems", IEEE Trans. on Power Apparatus and Systems, Vol. PAS-87, No. 6, Jun 1968, pp 1460-1464.

42) IEEE Standard 112, Test procedure for polyphase induction motors and generators, 1988, Form F1.

43) IEEE Standard #399, "The Brown Book", 1980

44) IEEE Task Force on Standard Load Models for Power Flow and Dynamic Performance Simulation", IEEE Trans. on Power Systems, Vol. 10 No. 3, Aug. 1995, pp 11302-1313.

45) IEE of Japan, "Calculating method of starting current in induction motors", Technical Report No. 131, Sept. 1980, (in Japanese).

46) Johnson BK and Willis JR, "Tailoring induction machine analytical models to fit known motor performance characteristics and satisfy particular study needs", IEEE Trans. Power Systems, Vol. 6, No. 3, Aug. 1991, pp 959-965.

47) Jones CV, "The unified theory of electrical machines", Butterworth, 1967

48) Klaes NR, "Parameter identification of an induction machine with regard to dependencies on saturation", IEEE Trans. Indus. App. Vol29, No. 6, Nov/Dec 1993, pp 1135-1140.

49) Klingshirn EA and Jordan HE, "Simulation of polyphase induction machine with deep rotor bars", IEEE Trans. on Power Apparatus and Systems, Vol. PAS-89, No. 6 Jly/Aug 1970, pp 1038-1043.

50) Kopilov IP, Ilyinski NF and Kuznetsov NL, "Application of experimental planning methods to electrical machine analysis and synthesis problems", Elektrichestvo, 1970, (2), pp 24-27.

51) Kostenko M and Piotrovsky L, "Electrical Machines", Part II, Foreign Languages Publishing House, (undated), pp 522-527.

52) Krause, PC, "Analysis of Electric Machinery", McGraw-Hill, 1987 , pp 189-197.

53) Krause PC, Nozari, F , Skvarenina and Olive, DW, "The theory of neglecting stator transients", IEEE Trans. on Power Apparatus and Systems, Vol. PAS-98, No.1 Jan/Feb 1979, pp 141-148.

54) Kron G, "The application of tensors to the analysis of rotating electrical machinery", General Electric Review, Schenectady, NY, 1942, pp 202-206.

55) Lastman GJ and Siha NK, "Microcomputer-based Numerical methods for Science and Engineering", Saunders College Publishing, 1988.

56) Lauw H.K and Scott Meyer W, Universal machine modelling for the representation of rotating machinery in an electromagnetic transients program. IEEE Trans. Indus. App. Vol IA-18, No. 4, 1982, pp 393-399.

57) Lee L, "Determination of starting current in three-phase induction motors", IEEE 1989 PES Summer Meeting, Long Beach California, Jly 1989 IEEE Paper No. SM 740-2 EC.

58) Levine SJ, "An analysis of the induction motor", Electrical Enginering, May 1935, pp 526-529.

59) Lindsay JF and Barton TH, "Parameter Identification for Squirrel Cage Induction Machines", Trans. IEEE, PAS, Vol 92 , 1973, pp 1287-1291.

60) Lipo TA and Consoli A, "Modelling and simulation of induction machines with saturable leakage reactances", IEE Trans Indust. Appl., Vol 20, No. 1, 1984, pp 180-189.

61) Maginniss FJ and Shultz NR, "Transient performance of induction motor", Trans. AIEE, Sept. 1944, Vol 63, pp 641-645.

62) Melik G, "Simple but accurate method of induction motors modelling", Elec. Energy Conf. 1987, Adelaide, 6-9 Oct 1987, pp 641-647.

63) Melkebeek JAA, "Magnetising-field saturation and dynamic behaviour of induction machines", IEE Proc. Vol. 130, Pt. B, No. 1, Jan 1983, pp1-17.

64) Mouillet A, Ille JL, Akroune M and Dami MA, "Magetic and loss characteristics of nonoriented silicon-iron under unconventional conditions", IEE Proc- Sci. Meas. Techology, Vol. 141, No. 1 Jan 1994, pp 75-78.

65) Natarajan R and Misra VK , "Starting transient current of induction motors without and with terminal capacitors." , IEEE Trans. Energy Conv., Vol. 6, No. 1, March 1991, pp 134-139.

66) National Bureau of Standards, Applied Mathematics Series 48. U.S. Dept. of Commerce, "Fractional Factorial Experimental Designs for Factors at Two Levels.", 1957 Plan 4.8.32, pg 22.

67) Naunin D, The calculation of the dynamic behaviour of electrical machies by space phasors", Proc. of Int. Conf. on Elec. Machines, Brussels, Belgium, Sept. 1978, pp T/5.1 - T/5.11.

68) NEMA Standard MG1, Part 12, Sections MG1 - 12.35 - 12.36, 1987.

69) Osama M, Sakkoury K and Lipo TA, "Transient behaviour comparison of saturated induction machine models", Proc. of the IMACS-TCI '93 conference '

Computational Aspects of Electromechanical Energy Converters and Drives", Ecole Polytechnique de Montréal, July 1993, pp 577-580.

70) Park RH, "Two-reaction theory of sychronous machines, generalised method of analysis I", AIEE Trans., Vol. 48, July 1929, pp 716-730.

71) Pereira L, "Induction generators for small hydro plants", Water Power and Dam Construction, November 1991, pp 30 -34.

72) Power Technologies Inc, "PSS/E Program Application Guide, Dec. 1994, pp 13_56 -13_60.

73) Richards GG, "Reduced order models for an induction motor-group during bus transfer", IEEE, PES Summer Meeting, Paper No. 88 SM 685-0, Portland, OR, July 24-29, 1988.

74) Rogers, GJ, . *INSPEC & INSTART*. Cherry Tree Scientific Software, Colbourne, Ont. Canada. 1993.

75) Rogers GJ, Beaulieu RE and Hajagos LM, "Performance of Station Service Induction Motors Following Full Load Rejection of a Nuclear Generating Unit", IEEE Trans. of Power Systems, Vol 10, No. 3, Aug. 1995, pp 1314-1320.

76) Rogers GJ and Benaragama DS, "An induction motor model with deep-bar effect and leakage inductance saturation", Archiv. Fur Electrotechnik 60, 1978, pp 193-201.

77) Rogers GJ , Di Manno, JD and Alden RTH, "An aggregate load model for industrial plants", IEEE Trans. on Power Apparatus and Systems, Vol. PAS-103, No. 4, April 1984, pp 683-690.

78) Rogers GJ and Shirmohammadi D, "Induction machine modelling for electromagnetic transient program", IEEE Trans. Energy Conv., Vol. EC-2, No. 4, Dec. 1987, pp 622-628.

79) Sastry KPR and Burridge RE, "Investigation of a reduced-order model for induction machine dynamic studies" IEEE Trans. PAS-95, No. 3, May/Jun 1976, pp 962-969.

80) Say MG , "Alternating Current Machines", 4th Ed .Pitman (1976), pg 302 & pp53-59.

81) Sen Gupta DP and Lynn JW , "Electrical Machine Dynamics" , Macmillan, 1980

82) Silvester P, "Dynamic resistance and inductance of slot-embedded conductors", IEEE Trans on Power Apparatus and Systems, Vol. PAS-87 No. 1, Jan 1968, pp201-207.

83) Sivokobylenko VF and Kostenko VI, "Mathematical modelling of deep-slot asychronous machies", Electric techology in USSR, No. 2 ,1980, pp 11-21

84) SKM Systems Analysis Inc, "Power Tools, Electrical Engineering Software", Box 3376, Manhattan Beach, CA, FAX (310) 372-2171, 1995.

85) Skvarenina TL and Krause PC, "Accuracy of Reduced Order Model of Induction Machines in Dynamic Stability Studies", IEEE Trans. on Power Apparatus and Systems, Vol. PAS-98, No. 4, Jly/Aug 1979, pp 1192-1197.

86) Slater RD and Wood WS, "Constant-speed solutions applied to the evaluation of induction-motor transient torque peaks", Proc. IEE, Vol. 114, No. 10 , Oct. 1967, pp 1429-1435.

87) Slemon GR, "Circuit models for polyphase induction machines", Electrical Machines and Power Systems, Vol. 8, July/Oct 1983, pp 369-379.

88) Slemon, GR, "Modelling of induction machines for electric drives", IEEE Trans. on Indust. Appl. Vol. 25, No. 6, Nov/Dec 1989, pp 1126-1131.

89) Smith IR and Hamil B, "Effect of parameter variations on induction-motor transients", Proc. IEE, Vol. 120, No. 12, Dec 1973, pp 1489-1492.

90) Smith IR and Sriharan S , "Transient performance of the induction motor.", Proc. IEE , Vol. 113, No. 7, July 1966, pp 1173-1181.

91) Smith JR, Rogers GJ and Buckley GW, "Application of induction motor simulation models to power station auxiliary pump drives", IEEE Trans. on Power Apparatus and Systems, Vol. PAS-98, No. 5, Sept/Oct 1979, pp 1824-1830.

92) Stanley HC, "An analysis of the induction machine", AIEE Trans. Vol. 57, 1938, pp 751-757.

93) Swann SA and Salmon, Effective resistance and reactance of a solid rectangular conductor placed in a semi-closed slot.", Proc. IEE, Vol. 110 C, 1963, pp 1656-1662.

94) Tabatabaei-Yazdi H and Grantham C, "A DSP based scheme for the on-line monitoring of performance and parameters determination of three phase induction motors.", Seventh International Conference on Electrical Machines and Drives, 11-13 Sept. 1995, University of Durham, IEE Con. Pub. No. 412 , pp 166-170

95) Waters S and Willoughby R ,"Modeling induction motors for system studies", IEEE Trans. on Indust. Appl., Vol. IA-19, No. 5, Sept/Oct. 1983, pp 875-878

96) WEG Electric Motor Manual, Catalog 512.04.0881.PE, 1986

97) Williamson S and Flack TJ, "Effect of radial rotor ventilation ducts on cage motor equivalent circuit parameters", IEE Proc- Electr. Power Appl. Vol 141, No. 3, May 1994, pp155-161.

98) Zhu JG and Ramsden VS, "Core loss modelling in rotational electrical machines", Proc. ICEMA Conference, Adelaide, Sept 14-16 1993, pp 52-57.

INDEX OF REFERENCES

Author(s)	Year	Thesis page
IEE of Japan	1980	5,56
Johnson BK and Willis JR	1991	130
Jones CV	1967	7,26,29,31
Klaes NR	1993	14,110,117,130, 145
Klingshirn EA and Jordan HE	1970	16
Kopilov IP, Ilyinski NF and Kuznetsov NL	1970	44
Kostenko M and Piotrovsky L	undated	17,19,22
Krause	1987	29,141,179
Krause PC, Nozari F, Skvarenina and Olive DW	1979	33,213
Kron G	1942	26
Lastman GJ and Siha NK	1988	130,153
Lauw H.K and Scott Meyer W.	1982	26
Lee L.	1989	12,56
Levine SJ	1935	26
Lindsay JF and Barton TH	1973	19
Lipo TA and Consoli A	1984	79,159
Maginniss FJ and Shultz NR	1944	26
Melik G	1987	14,19,55
Melkebeek JAA	1983	32
Mouillet A, Ille JL, Akroune M and Dami MA	1994	9
Natarajan R and Misra VK	1991	23
National Bureau of Standards	1957	42
Naunin D	1978	185
NEMA Standard MG1	1987	71,145
Osama M, Sakkoury K and Lipo TA	1993	34,38,120
Park RH	1929	26,31
Pereira L	1991	118,121
Power Technologies Inc	1994	29
Richards GG	1988	213
Rogers GJ	1993	2,27,137
Rogers GJ, Beaulieu RE and Hajagos LM	1995	223
Rogers GJ, Di Manno, JD and Alden RTH	1984	213
Rogers GJ and Shirmohammadi D	1987	2,5,10,12,16,19, 27,90,121,137, 211
Sastry KPR and Burridge RE	1976	46
Say MG	1976	15
Sen Gupta DP and Lynn JW	1980	22,46
Sivokobylenko VF and Kostenko VI	1980	11
SKM Systems Analysis Inc	1995	28
Skvarenina TL and Krause PC	1979	29,216
Slater RD and Wood WS	1967	23,183
Slemon GR	1983	22
Slemon GR	1989	213
Smith IR and Hamil B	1973	7,44,46
Smith IR and Sriharan S	1966	23,183,185
Smith JR, Rogers GJ and Buckley GW	1979	13,14

Author(s)	Year	Thesis page
Stanley HC	1938	26,31
Swann SA and Salmon	1963	17
Tabatabaei-Yazdi H and Grantham C	1995	145
Waters S and Willoughby R	1983	28,121,130
WEG Electric Motor Manual	1986	100
Williamson S and Flack TJ	1994	6
Zhu JG and Ramsden VS	1993	6,119